JORGE FILIPE RODRIGUES PONTES

Dry powders: Developing tools to study the impact of inhalation over respiratory epithelium

UNIVERSIDADE DO ALGARVE

FACULDADE DE MEDICINA E CIÊNCIAS BIOMÉDICAS

2023

JORGE FILIPE RODRIGUES PONTES

Dry powders: Developing tools to study the impact of inhalation over respiratory epithelium

PhD in Mechanisms of Disease and Regenerative Medicine

Work developed under supervision of Prof. Doctor Ana Margarida Moutinho Grenha and co-supervision of Prof. Doctor Rui Miguel da Silva Coelho Borges dos Santos

UNIVERSIDADE DO ALGARVE

FACULDADE DE MEDICINA E CIÊNCIAS BIOMÉDICAS

2023

This page was intentionally left in blank.

Dry powders: Developing tools to study the impact of inhalation over respiratory epithelium

Declaração de autoria de trabalho

Declaro ser o autor deste trabalho, que é original e inédito. Autores e trabalhos consultados estão devidamente citados no texto e constam da listagem de referências incluída.

_____

(Assinatura do Autor)

This page was intentionally left in blank.

This work was performed at:

Drug Delivery Laboratory
Centro de Ciências do Mar do Algarve (CCMAR)
Universidade do Algarve, *Campus* de Gambelas
Faculdade de Ciências e Tecnologia, Edifício 8, Laboratório 2.22
8005-139 Faro, Algarve
PORTUGAL

With the collaboration of:

Laboratoire d'Automatique, de Génie des Procédés et de Génie Pharmaceutique (LAGEPP) – UMR CNRS 5007 & Centre Technologique des Microstructures – CTμ
Université Claude Bernard – Lyon 1
43 Boulevard du 11 de Novembre 1918
69622 Villeurbanne Cédex

University of Alberta, Department of Mechanical Engineering
10-203 Donadeo Innovation Centre for Engineering
9211 116th Street NW, Edmonton, Alberta, T6G 1H9, Canada

Departamento de Farmácia Galénica e Tecnologia Farmacêutica
Faculdade de Farmácia, Universidade de Lisboa, *Campus* do Lumiar
Estrada do Paço do Lumiar, 22, Edifício F, R/C
1649-038 Lisboa, Portugal

This work was supported by National Portuguese funding through FCT – Fundação para a Ciência e Tecnologia, through the scholarships PD/BD/137064/2018 and COVID/BD/152626/2022, the PESSOA Program project (5116/FCT, 2019-2021) and projects UIDB/04326/2020, UIDP/04326/2020 and LA/P/0101/2020.

This page was intentionally left in blank.

Ao meu Avô Joaquim e ao meu Tio Custódio,
que estarão algures a olhar por mim.
Que esta conquista os deixe orgulhosos
onde quer que eles estejam.

It takes as much energy to wish as it does to plan.
Eleanor Roosevelt

You will reach your destination even though you travel slowly.
Icelandic Proverb

Education is the most powerful weapon which you can use to change the world.
Nelson Mandela

This page was intentionally left in blank.

TABLE OF CONTENTS

ACKNOWLEDGMENTS

We often think that a PhD journey is as lonely as it can be, but, after all these years, every single life we touched remained with us, alongside their lessons, smiles, tears, failures, and victories.

First and foremost, I would like to thank my supervisors, Prof. Ana Margarida Grenha and Prof. Rui Borges dos Santos. I know that words cannot seem to gather all that we have achieved together, both personally and professionally, but know that I have grown so much, and I am a better man and a better researcher because of you.

To my fellow laboratory colleagues that, in a way, kept me (in)sane for all these years: Susana, Filipa, Noelia, Ana Macedo, Inês Torquato, Inês Rocheta, Miguel Rodrigues, Joana Cruz, Dinis and Joana Silva. We all worked together to give a shiny life to our dear Drug Delivery Laboratory, our 2.22. I could not close this group without include Inês Santos, that despite not being part of our lab, she was always a warm presence and a close friend in these years of PhD. For all the meals shared together, the smiles, laughs, frustrations, and companionship, you were all awesome and I carry you all in my heart.

To my other Academic acquaintances and friends spread all over the world: Prof. Ana Costa, Prof. Eusébio Conceição, Prof. Hermínio Diogo, Prof. Manuela Gaspar, Prof. Pedro Fonte, Prof. Reinhard Vehring, Hui Wang, Mani Ordoubadi, Eride Quarta, Luba Slabyj, David Barona, Dr. Giovanna Lollo, Dr. Annalisa Rosso, and Dr. Luís Spencer from Paralab. In these 5 years of the PhD, you played an important part in my journey. For all those moments shared, the help that you provided, the scientific and personal discussions, and the enlightenment that you helped achieve, I give you my sincere thanks.

To the ProRegeM family and, especially, to the 2018 class: Ana Chegão, Ana Pina, Andreia Oliveira, João Charneca, Margarida Rasteiro e Sara Pestana. These last few years were crazy (to say the least), and we stayed together through hours of paper reading and discussion, presentations, shared anxiety, and love. I could not

think of a better class to go through this PhD journey. We understand and support each other, and I can only wish we continue to do so in our next stages of life.

To Culture, in the forms of music, radio, podcasts, and games. I have discovered the beauty of listening (without talking), of smiling when inspiration kicked in, of thinking more and better, of writing while the energy of music engulfed my body, and of playing to get out of a not-so healthy mental environment. A special thanks goes to my radio-friends at Antena3. Although we are more than 300 km apart, radio waves made sure to reach Algarve onto my ears and soul. Without you, these last five years wouldn't have been as bearable as they were. Your music, your humour, and all your knowledge about everything were and are still one of the best parts of my day, and I will be sure to take with me all that we have shared. Thank you for being there all these days, thank you for changing my life for the better.

At a more personal level, I cannot forget all these beautiful people: Pedro Canelas, Vanda, Inês, Jerome, Ricardo Nunes, Catarina Almeida, Diana, Catarina Sardinha, Priscila, Pedro Pinheiro, Rui, Ricardo Dias, Ana Advinha, Bruna, Verónica, Tiago, João "Figas", João Sousa, Leonardo e Renato. And from the ProRegeM 2018 class, Catarina Carvalho, João Lopes e Leonardo Silva. You were all there, every day, to listen to me, to my frustrations and my joys, to lift me up when I needed, to smile and to laugh, to cry and to scream. There is no gift nor prize that I can give you other than my smile and my sincere thanks for your presence in one of my most difficult times in my life.

To all I have not personally mentioned here but entered my life at any point. Each one of you shared something with me, allowing for both of us to learn together and grow. Thank you for being there!

To my family, that despite not knowing the full scope of what a PhD really entails, they were always there for emotional support and stability, two of the most important elements for a mindful PhD period. Despite our hardships, I am here, today, thanks to you.

To Daniel, my rock in these last few months. Without your support and company through the final part of my PhD, your words of encouragement and your sweetness, I think this thesis could not have become what it is today. You were my lighthouse in those moments when I could only see darkness (and they were a lot). Thank you for being my lucky shiny charm, and for being my guide, not allowing me to give up and making me stay on the right path even when the struggle was impossible to win.

Finally, my last acknowledgement goes to myself. I would not be here without my failures, my tears, my smiles and my fights to go through all the obstacles the PhD put in front of me. I know me now better than I did back in 2018. I know my limits, and I know what I need to do to be happy and to go after my dreams. This is for me, for all those times I wanted to give up. This is proof that I can do everything, that I can change the world, even if for a bit, and that I can leave the world a little better than it was on the day before.

Thank you all for being unforgettable.

This page was intentionally left in blank.

ABSTRACT

The lung is responsible for the gaseous exchange of carbon dioxide (CO_2) with oxygen (O_2). Furthermore, within the lung there is an equilibrium that is maintained by a great number of mechanisms that filter the air, making it free of materials that can induce damage. The knowledge of the different lung physiological processes helps understand diseases and promote adequate and efficacious therapies. Additionally, the study of the physics and mechanics of the lungs can work favourably when lung is used as a route of administration for drugs. Nowadays, there is a myriad of marketed inhalers that are mainly used in the therapy of asthma and chronic obstructive pulmonary disease. These essentially include metered dose inhalers and dry powder inhalers, the latter currently observing increased popularity. Research on the topic of inhalable dry powders is intense, with many formulations being proposed in the literature. After the intrinsic characterisation of formulations, their study continues focusing on behaviour aspects, particularly addressing the interactions with biological structures, such as cells, tissues or animals. These studies require the existence of methodologies and tests that generate reproducible data for a potential approval by the competent authorities. These methodologies can be divided in three categories: *in vivo*, *ex vivo* and *in vitro* tests. When the study of dry powders is focused, it is easier to replicate data in *in vivo* platforms, not only because animals are used after a careful selection of the best model and subsequent documentation for validation of an experimental setting, but also because dry powders are used and delivered as such. However, in *in vitro* assays, it is not easy to mimic the lung environment and inhalation itself, as the delivery of powders over cells cultured on an air-liquid interface is required for the drawing of robust conclusions. Often, cell-based *in vitro* assays entail testing of dry powders in suspension, meaning that the powder is added to the liquid media where cells grow, and the exposure is provided with the mediation of the media. Regrettably, this does not mimic the occurrences in the lung, as the organ is devoid of abundant liquid. *In vitro* platforms allowing to comply with realistic conditions are relatively scarce and those existing are expensive and technically complex, which is not feasible in early stages of research. The design and development of an affordable and simple *in vitro* platform capable of testing dry powders, ensuring reproducible experimentation and data, would be highly helpful.

This PhD project proposed the development of tools to improve lung delivery research using dry powders. The development of a device that allows the delivery of dry powders onto cell surfaces, thus simulating more appropriately the lung environment, was envisaged. Moreover, a quartz crystal microbalance was used to establish a technique enabling the determination of dry powder deposition profiles. In parallel, the determination of the viability of respiratory cells after the insufflation of a dry powder using the developed device was performed.

Locust bean gum (LBG) is a polysaccharide that has been proposed as excipient in several drug formulation strategies. It has been included in drug delivery systems such as microparticles and nanocarriers, but regrettably LBG does not have the best features for this end, with a low solubility in cold water, the high viscosity of solutions at concentrations above 1% (w/v), and the neutral character, hinder its use. Chemically modified LBG could be a strategy to overcome these limitations. A sulphated derivative of LBG was thus prepared and used in the production of lipid nanocapsules (LNC) by a technique of solvent displacement. Despite adequate properties of the carriers (size around 200 nm, PdI < 0.2, highly negative ζ-potential), encapsulation of the model drug rifabutin failed to achieve satisfactory loadings (< 2%). Moreover, the conversion of LNC into inhalable microparticles by spray-drying using mannitol as carrier matrix, was also not successful, resulting in a negligible amount of powder being recovered. The focus on the formulation used in this PhD project shifted, and the establishment of a spray-drying protocol permitting the production of LBG-based microparticles suitable for lung delivery purposes was investigated. In parallel, an exhaustive study of LBG characteristics, relevant for its role as matrix material, was performed. LBG from three different suppliers was tested, along with a range of spray-drying inlet temperatures, varying between 103 ºC and 160 ºC. The various dry powders were prepared and observed to have similar aspect from a macroscopical visualization. Considering the yields obtained for different temperatures, the chosen formulation was that prepared with an inlet temperature of 130 ± 1 ºC. This temperature ensured a compromise with an inlet temperature that is intermediate and an acceptable production yield around 55-60%. The geometric diameters of the microparticles were determined to vary within 3.8 and 4.5 µm. Further chemical characterisation of LBG was performed (Fourier-transform infrared spectroscopy (FT-IR), molecular weight distribution by High

Performance Size Exclusion Chromatography (HPSEC), thermogravimetric analysis (TGA) and differential scanning calorimetry (DSC)), evidencing that the heating cycles (for solubilisation and processing in the spray-dryer) might induce LBG depolymerization to a certain extent. However, additional tests are required to confirm these observations, and aerodynamic characterisation of the different LBG-based microparticles is also considered necessary. Notwithstanding, an LBG-based microparticle formulation was chosen to advance to cell-based and *in vivo* assays. The former relied on cell viability determination, where a concentration-dependent effect was observed. In fact, as concentrations increment, so does the viscosity of LBG, impacting negatively on cell viability. However, testing of LBG did not induce the disruption of the cell membrane and, thus, the release of the cytoplasmatic enzyme lactate dehydrogenase (LDH). As for the *in vivo* assays, no allergic reaction was initiated in the sequence of the inhalation of LBG microparticles, thus constituting a strong indication of LBG safety for lung drug delivery applications, although more studies, addressing different indicators, are needed. This work demonstrated that a thorough characterisation of polymers works favourably in the process of preparing dry powders, its optimisation and subsequent biological risk assessment.

The design and development of a device enabling the insufflation of dry powders onto cell supports followed the successful preparation of LBG-based microparticles. After several optimisations concerning the model, the method by which the dry powder is weighed and loaded into the device and the air insufflation mechanism, a final model comprised of a funnel and a weighing accessory was conceived. Different 3D printing techniques were also tested to obtain the device (fused deposition modelling and stereolithography), as well as several air pumps. An air compressor was selected as air pump, being tested at different outlet air pressures and using several polysaccharide-based dry powders, but the insufflation yields generally did not go beyond 20-30%, signalling this as a feature requiring future optimisation.

Alveolar epithelial cells were cultured on a petri dish and exposed for 24 h to LBG microparticles, insufflated with the developed device. No significant effect was found on cell viability (always > 70%) and the same was observed after pumping air,

indicating potential safety of LBG microparticles and of the proper insufflation method. Future assays assessing other parameters are anyway required to further support these findings.

An application of the device was further explored by means of inclusion of a Quartz Crystal Microbalance (QCM) into the experimental setting, which permitted evaluating the deposition profile of different dry powders in real time, allowing for a more thorough analysis of the device performance. The use of the QCM in cell-based tests, where cells are cultured over the crystal, using the developed device can provide more insight into the real interaction between cells and dry powders. Overall, the inclusion of this technology in experimentation, especially concerning the *in vitro* analysis of dry powders, can provide more precise data when compared with conventional techniques. In dry powder formulation development, it is advantageous for choosing the most adequate excipients that translates into the best deposition profile. At more advanced stages, the quantification of interactions between cells and particles will be certainly crucial, as the determination of the best excipients for formulations will help on the improvement of the therapeutic approaches. Further developments concerning this PhD project are envisaged, but all that was achieved and the discussion that followed, will certainly guide future endeavours in aerosol research.

Keywords: Aerosol, biorelevance, dry powder, insufflation, lung drug delivery, polysaccharide

RESUMO

O pulmão é um dos órgãos essenciais à vida, sendo responsável pelas trocas gasosas de dióxido de carbono por oxigénio. Para que este processo decorra, existe um equilíbrio que é mantido por diversos tipos de células e diferentes mecanismos, que filtram o ar atmosférico de substâncias que podem danificar o pulmão. O conhecimento dos diferentes processos fisiológicos deste órgão permite compreender as doenças a ele associadas. Além disso, o estudo da física e dos processos mecânicos que ocorrem no pulmão ajudam ao desenvolvimento de terapêuticas mais adequadas e eficazes quando este órgão é usado como via de administração. Atualmente, encontram-se disponíveis no mercado um conjunto de dispositivos, usados na terapêutica da asma e da doença pulmonar obstrutiva crónica, como por exemplo, os inaladores pressurizados com válvula doseadora e os inaladores de pó seco. Estes últimos têm visto, nos últimos anos, um incremento da sua popularidade. Além disso, e em paralelo, a investigação científica no que aos pós secos para inalação diz respeito é profícua e intensa, com diversas formulações a serem propostas na literatura. Após a caracterização intrínseca destas estratégias terapêuticas, o seu estudo prossegue, concentrando-se nas interações com estruturas biológicas como sejam células, tecidos ou animais. Os estudos de desenvolvimento de formulação requerem diversos métodos experimentais e testes, que geram dados reprodutíveis, que serão utilizados pelas autoridades competentes no processo de aprovação de novas terapêuticas. Os métodos experimentais podem ser divididos em três categorias distintas: *in vivo*, *ex vivo* e *in vitro*. Num contexto *in vivo*, quando se procura caracterizar uma formulação para ser administrada através do pulmão, gerar e replicar dados é uma tarefa relativamente simples, já que se utilizam modelos animais, que foram rigorosamente escolhidos, assim como o método experimental, previamente estudado e validado, usando-se o pó seco como tal. Contudo, nos ensaios *in vitro*, a mimetização do ambiente pulmonar e do processo de inalação é difícil, já que é necessária a insuflação de pós secos sobre células, que se encontram em cultura numa interface ar-líquido, para que se obtenham conclusões robustas. Atualmente, ensaios de células *in vitro* requerem experimentação com os pós secos em suspensão, isto é, estes são adicionados ao meio líquido onde as células estão a crescer, e a exposição é mediada por este meio líquido. Contudo, apesar de serem ensaios com peso

económico baixo, esses ensaios, tal como estão desenhados atualmente, não mimetizam as condições do pulmão, porque este não tem líquido abundante associado à sua fisiologia. As plataformas *in vitro* que permitam mimetizar de forma mais realista o ambiente pulmonar são escassas, sendo esta uma necessidade urgente e que precisa de ser suplantada. De facto, esta falta fomenta o uso de alternativas mais caras e complexas, que são inadequadas em estadios mais preliminares de investigação e desenvolvimento. Assim, uma possível solução é o desenho e o desenvolvimento de uma plataforma capaz de ser usada em testes *in vitro* de pós secos para administração pulmonar, assegurando experimentação reprodutível e, para esse efeito, dados robustos.

O trabalho desenvolvido durante o projeto de doutoramento discutido neste documento propôs o desenvolvimento de ferramentas que melhorem a investigação e o desenvolvimento na área pulmonar, utilizando pós secos. Neste caso particular, foi previsto o design e o desenvolvimento de um dispositivo que permite a aerossolização de pós secos sobre um suporte celular, com o intuito de mimetizar o ambiente pulmonar. Além disso, uma microbalança de cristal de quartzo foi utilizada para desenvolver e estabelecer um método experimental para a determinação dos perfis de deposição dos pós secos testados. Paralelamente, a viabilidade celular após insuflação de ar com e sem pós secos com a ajuda do dispositivo foi determinada.

A goma de alfarroba é um polissacárido que tem vindo a ser proposto como excipiente em diversas formulações para veiculação de fármacos, tendo sido incluída em trabalhos em que micro- e nanopartículas foram estudadas. Porém, a goma de alfarroba não possui as características químicas mais adequadas para a sua fácil manipulação: baixa solubilidade em água fria, requerendo sempre temperaturas altas para a sua dispersão, a elevada viscosidade quando a concentração da goma é maior do que 1% (m/v) e a ausência de carga. Uma das possíveis soluções para ultrapassar estas limitações é a utilização de uma goma de alfarroba quimicamente modificada. Neste sentido, após a sua purificação e posterior sulfatação, o derivado foi usado na produção de nanocápsulas lipídicas por um processo de deslocamento de solvente. Apesar das características físico-químicas adequadas (tamanhos de cerca de 200 nm, índice de polidispersão < 0.2,

e um potencial zeta fortemente negativo), a encapsulação de um fármaco de interesse, a rifabutina, foi inefetiva, não tendo sido atingidos valores de *drug loading* satisfatórios (< 2%). Além disso, a conversão das nanocápsulas lipídicas em micropartículas inaláveis por um processo de atomização, usando o manitol como matriz, não teve o êxito esperado. A massa de pó seco obtido para esta formulação foi baixa e, por essa razão, a estratégia de formulação de pós secos pensada para o projeto de doutoramento teve de ser ajustada. Assim, procedeu-se à otimização de um protocolo de atomização, que permitisse a produção de micropartículas à base de goma de alfarroba, com características adequadas à sua inalação. Além disso, e em paralelo foi realizado um estudo mais profundo sobre as características físico-químicas da goma de alfarroba. Assim, este polissacárido obtido de três fornecedores diferentes foi usado para este efeito, tendo sido feito um varrimento de temperaturas inlet, entre 103 ºC e 160 ºC. Após a preparação dos respetivos pós secos, uma análise macroscópica preliminar evidenciou características semelhantes entre todos os pós. Assim, considerando os rendimentos de atomização para as diferentes temperaturas inlet testadas, a formulação escolhida foi aquela que foi produzida a 130 ± 1 ºC. Esta temperatura assegura um compromisso entre uma temperatura inlet intermédia e um rendimento de atomização aceitável, entre os 55-60%. Os diâmetros geométricos para as micropartículas produzidas a 130 ºC, com goma de alfarroba de três fornecedores distintos, foram determinados, variando entre 3.8 e 4.5 µm. Uma caracterização química adicional foi realizada (espectroscopia de infravermelho com transformada de Fourier (FT-IR), distribuição de pesos moleculares por cromatografia de exclusão por tamanho de alta performance (HPSEC), análise termogravimétrica (TGA) e calorimetria de varrimento diferencial (DSC)), em que se detetou que sucessivos ciclos de aquecimento (para a solubilização da goma e as altas temperaturas decorrentes do processo de atomização) podem induzir algum grau de despolimerização. Contudo, são necessários mais testes para confirmar esta hipótese, assim como a caracterização aerodinâmica das micropartículas à base de goma de alfarroba. Não obstante, a formulação que havia sido escolhida anteriormente foi utilizada em ensaios com células (*in vitro*) e animais (*in vivo*). Os ensaios *in vitro* evidenciaram um efeito dependente da concentração, ou seja, à medida que a concentração de goma de alfarroba testada aumenta, a sua viscosidade também incrementa, o que impacta negativamente a viabilidade celular. Adicionalmente, experiências com a

goma de alfarroba não induziram a disrupção da membrana celular e como tal, a libertação da enzima citoplasmática lactato desidrogenase (LDH). Com respeito aos ensaios *in vivo*, nenhuma reação alérgica foi iniciada na sequência da inalação de micropartículas à base de goma de alfarroba, sendo esta uma forte indicação de que a goma de alfarroba é segura para administração pulmonar. Este trabalho demonstrou que uma caracterização minuciosa e rigorosa de polímeros facilita a preparação de pós secos, a sua otimização e subsequentes testes de determinação de risco biológico.

O design e o desenvolvimento de um dispositivo que permita a insuflação de pós secos sobre suportes celulares foi o passo seguinte, após a preparação de micropartículas à base de goma de alfarroba. Após diversas otimizações relativas ao modelo, ao método através do qual o pó seco seria pesado e colocado dentro do dispositivo e ao mecanismo de insuflação que seria aplicado, um modelo final foi produzido, sendo este composto por um funil e por um acessório de pesagem. Diferentes técnicas de impressão 3D foram testadas para a obtenção do dispositivo (modelação por deposição fundida e estereolitografia), assim como diversas estruturas de injeção de ar, das quais se elegeu o compressor de ar. Este último foi posteriormente testado com diferentes pressões de saída de ar e diversos pós secos à base de polissacáridos previamente preparados, mas os rendimentos de insuflação não foram além dos 20-30%, um parâmetro que foi assinalado como sendo necessário otimizar no futuro.

Células epiteliais alveolares foram colocadas em cultura numa caixa de petri e expostas, por um período de 24 h, a micropartículas de goma de alfarroba, que foram insufladas com o dispositivo desenvolvido. Os ensaios, de maneira geral, evidenciaram que a insuflação de ar e de pós secos sob uma interface ar-líquido não impactaram negativamente a viabilidade celular, que se manteve em todos os ensaios acima dos 70%, tendo-se obtido resultados semelhantes quando unicamente ar foi insuflado. Estes resultados indicam um perfil de segurança tanto para as micropartículas à base de goma de alfarroba como para o método de insuflação utilizado. Apesar destes resultados, ensaios futuros necessitarão da determinação de outros parâmetros além da viabilidade celular para dar suporte aos resultados obtidos.

Uma possível aplicação do dispositivo na análise de pós secos *in vitro* foi estudada, quando a microbalança de cristal de quartzo foi integrada nas experiências, o que permitiu a avaliação do perfil de deposição de diferentes pós secos em tempo real, permitindo uma análise mais rigorosa do desempenho do dispositivo. Neste sentido, o uso da microbalança de cristal de quartzo em testes celulares futuros poderá providenciar dados importantes a respeito da interação real entre células e pós secos. De uma maneira geral, a inclusão desta tecnologia em experiências, mais concretamente, na análise *in vitro* de pós secos, mostrar-se-á útil na obtenção de dados mais precisos quando comparados com aqueles gerados por equipamentos mais convencionais. O desenho de formulações de pós secos poderá ver vantagens nesta tecnologia, já que o QCM permitirá a escolha de um polímero que resulte numa formulação com um perfil de deposição muito bom. Além disso, em estadios mais avançados de investigação, a quantificação das interações entre células e partículas será crucial, já que esta determinação permitirá escolher os excipientes mais adequados para serem usados em formulações, com vista ao melhoramento das estratégias terapêuticas atuais. Tal como estas experiências futuras, outros desenvolvimentos focados na melhoria do dispositivo estão previstos, indo além do que foi inicialmente proposto para este projeto de doutoramento. De qualquer maneira, tudo o que foi aqui concretizado e discutido permitirá futuros avanços importantes na investigação e desenvolvimento de aerossóis.

Palavras-chave: Aerossol, biorrelevância, insuflação, polissacáridos, pó seco, veiculação de fármacos por via pulmonar

This page was intentionally left in blank.

LIST OF THE DIFFERENT OUTPUTS GENERATED AND PUBLISHED DURING THE PhD PERIOD (2018-2023)

International Patent Application

- **Pontes, Jorge F.**; Diogo, Hermínio P.; Conceição, Eusébio; Santos, Rui M.B.; Grenha, Ana. Portable Device to Study the Exposure of Cells to Dry Powders. World Intellectual Property Organization, application n.º PCT/IB2022/060464 (PT 117541), deposited on **31/10/2022** (patent pending).

Distinctions

- Honourable Mention for the project "AIR: Aerosol Invitro Respirator" in Ideias em Caixa 2021 - 7th Edition promoted by Universidade do Algarve through CRIA - Divisão de Empreendedorismo e Transferência de Tecnologia pertaining to the evaluation of potential business ideas.

Publications

- **Pontes, Jorge F.**; Grenha, Ana. Multifunctional nanocarriers for lung drug delivery. *Nanomaterials*, **2020**, 10. DOI: 10.3390/nano10020183.
- **Pontes, Jorge F.**; Guerreiro, Filipa; Rosso, Annalisa; Alves, Ana D.; Rodrigues, Susana; da Costa, Ana M. Rosa; Lollo, Giovanna; Gaspar, Maria Manuela; Grenha, Ana. Toxicological profile of Locust Bean Gum (LBG) for inhalation: Excipient characterisation and biological evaluation. (working manuscript)

Meeting Abstracts

- **Pontes, Jorge F.**; Braz, Luis; Guerreiro, Filipa; da Costa, Ana M. Rosa; Almouazen, Eyad; Lollo, Giovanna; Grenha, Ana. Sulphated locust bean gum-coated lipid nanocapsules as potential lung delivery carriers. *Journal of Aerosol Medicine and Pulmonary Drug Delivery* **2020**, *33*, A15-A15, doi: 10.1089/jamp.2020.ab01.abstracts.
- **Pontes, Jorge F.**; Diogo, Hermínio P.; Conceição, Eusébio; Musacchio, Flávia; Santos, Rui M.B.; Grenha, Ana. Development of a prototype of an aerosolisation device for dry powders to improve *in vitro* cell-based assays in the context of lung

delivery. *Journal of Aerosol Medicine and Pulmonary Drug Delivery* **2022**, 35:2, A20, DOI: 10.1089/jamp.2022.ab01.abstracts.

Oral communications (Pre-Recorded)

- **Pontes, Jorge F.**; Duarte, Emanuel; Flórez-Fernández, N.; Rico, João; Cruz, Joana; Lollo, Giovanna; Grenha, Ana. Fucoidan-coated lipid nanocapsules encapsulating a model drug for lung drug delivery. Drug Delivery to the Lungs (Online), 9th to 11th of December of 2020, Edinburgh, United Kingdom.

Pontes, Jorge F.; Diogo, Hermínio P.; Conceição, Eusébio; Musacchio, Flávia; Santos, Rui M.B.; Grenha, Ana. Development of a prototype of an aerosolisation device for dry powders to improve *in vitro* cell-based assays in the context of lung delivery. Drug Delivery to the Lungs (Online), 8th to 10th of December of 2021, Edinburgh, United Kingdom.

Poster presentations

- **Pontes, Jorge F.**, Braz, Luís, Costa, Ana M. Rosa da, Almouazen, Eyad, Lollo, Giovanna, Grenha, Ana, Development of nanocapsules using a locust bean gum sulfate derivative, 22nd International Symposium on Microencapsulation, 25th to 27th of September 2019, Salvador, Brazil
- **Pontes, Jorge F.**, Braz, Luís, Costa, Ana M. Rosa da, Almouazen, Eyad, Lollo, Giovanna, Grenha, Ana, Sulphated locust bean gum-coated lipid nanocapsules as potential lung delivery carriers, Drug Delivery to the Lungs, 11th to 13th of December 2019, Edinburgh, United Kingdom
- **Pontes, Jorge F.**, Braz, Luís, Costa, Ana M. Rosa da, Almouazen, Eyad, Lollo, Giovanna, Grenha, Ana, Stability evaluation of sulphated locust bean gum-coated lipid nanocapsules, XIIIth Spanish-Portuguese Conference on Controlled Drug Delivery, 22nd to 24th of January 2020, Santiago de Compostela, Spain

Other works

- **Pontes, Jorge F.**, Flórez-Fernández, Noelia, Afonso, Carolina, Cruz, Joana, Alsayyed, Rahaf, Grenha, Ana. Será o mar a próxima grande fonte de biomateriais? In *UAlgoritmo – A Ciência Trocada por Miúdos*, 3(2), 22-28, **2021**.

LIST OF FIGURES

LIST OF TABLES

ABBREVIATIONS

ACI: Andersen Cascade Impactor
ANOVA: Analysis of Variance
BALF: Bronchoalveolar Lavage Fluid
BSA: Bovine Serum Albumin
CAD: Computer Assisted Design
CCM: Cell Culture Media
CFTR: Cystic Fibrosis Transmembrane conductance Regulator
COPD: Chronic Obstructive Pulmonary Disease
COVID-19: Coronavirus disease
CRG: Carrageenan
Cryo-TEM: Cryogenic Transmission Electron Microscopy
DOTAP: 1,2-dioleoyloxy-3-trimethylammoniumpropanchloride
DMEM: Dulbecco's Modified Eagle's Media
DMF: Dimethylformamide
DMSO: Dimethylsulfoxide
DPI: Dry Powder Inhaler
DS: Dextran sulphate
DSC: Differential Scanning Calorimetry
EDTA: Ethylenediaminetetraacetic Acid
FBS: Fetal Bovine Serum
FDA: Food and Drug Administration
FESEM: Field Emission Scanning Electron Microscopy
FTIR: Fourier-Transformed InfraRed (spectroscopy)
HPSEC: High Performance Size Exclusion Chromatography
IF: Industrial Farense
IgE: Immunoglobulin E
INH: Isoniazid
KGM: Konjac glucomannan
LBG: Locust bean gum
LBG Su: Locust bean gum sulphate
LDH: Lactate dehydrogenase
Leu: Leucine

LNC: Lipid nanocapsules

Man: Mannitol

MDI: Metered Dose Inhaler

MP: Microparticle(s)

MTT: Thiazolyl blue tetrazolium bromide

NSCLC: Non-Small Cell Lung Cancer

PADDOCC: Pharmaceutical Aerosol Deposition Device On Cell Cultures

PBS: Phosphate Buffer Saline

MDI: Metered Dose Inhaler

QCM: Quartz Crystal Microbalance

RFB: Rifabutin

SARS-CoV 2: Severe Acute Respiratory Syndrome Coronavirus 2

SCLC: Small Cell Lung Cancer

SDS: Sodium Dodecyl Sulphate

SEM: Scanning Electron Microscopy

SMI: Soft-Mist Inhaler

TGA: Thermogravimetric Analysis

VEE: (Keysight) Visual Engineering Environment

WHO: World Health Organisation

XG: Xanthan gum

CHAPTER 1:

GENERAL INTRODUCTION

The information contained in this chapter was partially included and published in the following publications:

Pontes, Jorge F.; Grenha, Ana. Multifunctional nanocarriers for lung drug delivery. *Nanomaterials*, **2020**, 10. DOI: 10.3390/nano10020183

Pontes, Jorge F.; Guerreiro, Filipa; Rosso, Annalisa; Alves, Ana D.; Rodrigues, Susana; da Costa, Ana M. Rosa; Lollo, Giovanna; Gaspar, Maria Manuela; Grenha, Ana. Toxicological profile of Locust Bean Gum (LBG) for inhalation: Excipient characterisation and biological evaluation. (under preparation)

This page was intentionally left in blank.

1.1. Overview

The human body is a very complex structure comprised of cells, organs, mechanisms, and barriers that allow life as it is today. Together with evolution, humans have improved their existence, their ways to maintain life, to cure diseases and, most of all, to strive in very harsh environments [1]. This capacity to adapt allows for continuous improvement [2], but despite all scientific advancements, scientists still struggle to alter the course of certain diseases, efficiently and effectively [3,4]. Notwithstanding, the convoluted array of biological processes can still be manipulated to turn what could be a damaging feature into something beneficial.

1.1.1. Physiology and barriers of the lung

The study of the different organs and the way they intertwine has still many mysteries to uncover, but all are important in homeostasis. The lung is responsible for the gaseous exchange of carbon dioxide (CO_2) with oxygen (O_2) [5]. The first is a by-product of cell metabolism that needs to be expelled due to its toxicity. The exchange occurs deep within the lung, and its rate is dependent on the individual's activity state, being more rapid and intense if any physical activity is being made [6]. In any case, the lung is one of the few structures that is in constant contact with the environment. Atmospheric air with oxygen and many other components enters through the nose and mouth, passes through the nasal cavity and several more passages to reach the alveolar sacs, where the gaseous exchange occurs [7]. But, as simple as it may sound, breathing is a process involving a great number of cells and mechanisms that filter the air of materials that can have a damaging effect on the human body. A depiction of the lungs and their branching can be seen in Figure 1.1.

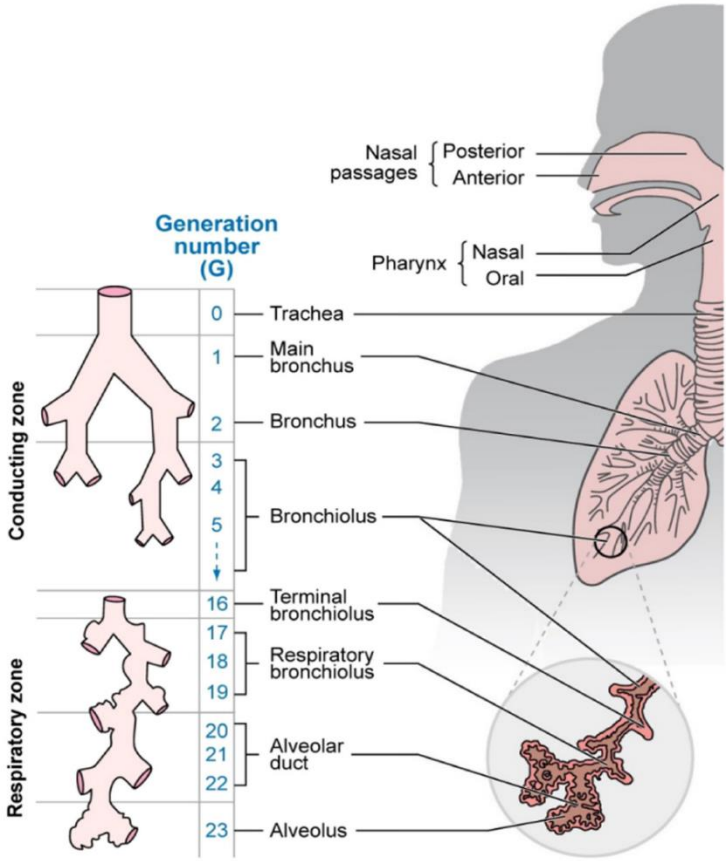

Figure 1.1 – The structural organisation of the lung and its branching, in accordance with the Weibel model [8]. Adapted from [9].

Figure 1.1 shows the complex structure of an adult human lung, an organ that had its embryonic development studied greatly elsewhere [5,10,11]. The respiratory system can be divided into two different regions: (1) the upper airways, consisting of all the structures going from the nasal cavity until the larynx; and (2) the lower airways, that further divide into the conducting zone, comprised by the trachea, the bronchi, and the terminal bronchioles and the respiratory zone, having the respiratory bronchioles, the alveolar ducts, and the alveolar sacs. This macro structure was simplified in one of the first descriptions of this tree-like architecture made by Weibel, back in 1963 [8]. This model divides the lung into 24 generations, to which generations 0 through 16 correspond to the conducting zone, and the remaining generations (17 to 23/24) are attributed to the respiratory zone. Although simplistic, this is a very useful model of the lung. Additionally, it helps researchers estimate the aerodynamic parameters of potential therapeutic particles.

The adult human lungs are comprised of two soft tissue units, one on the left and one on the right side. These units exhibit three lobes on the right and two lobes on the left, which are enveloped by a membrane called pleura. The lungs are delimited by the diaphragm, separating the thorax from the abdominal zone [12]. At a more mechanistic and cellular level, the lung is a complex environment with a great number of components, each taking an important role in lung defence, as depicted in Figure 1.2.

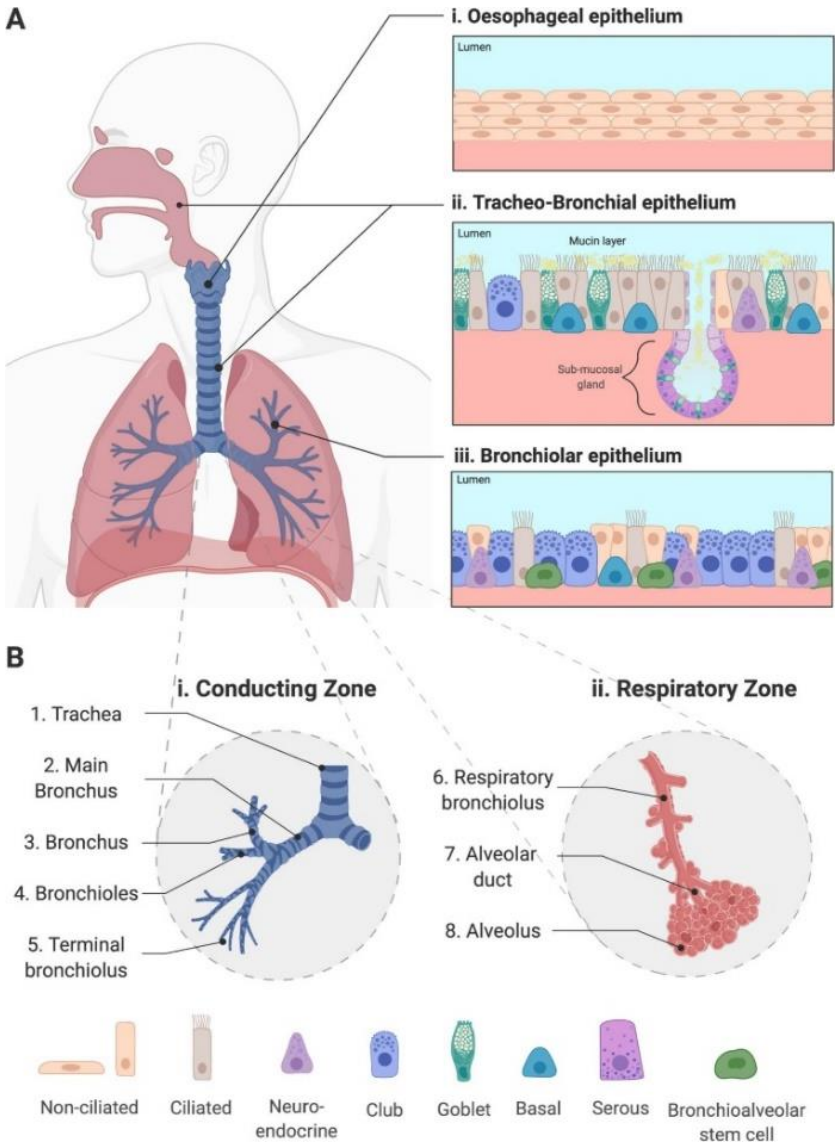

Figure 1.2 – Overview of the lungs and the respective sectional cuts of the bronchial epithelium and of the alveolar barrier, containing various types of cells and physiological barriers [13].

Like any other structure inside the human body, lungs are populated by cells that differ depending on the zone of the respiratory tree, as detailed in Figure 1.2. The access to the lungs is given by the nose and the oesophageal region, that is comprised of a multi-layered squamous non-keratinising epithelium [14,15]. Going deeper into the tree, the next region to be considered is the tracheae, and the bronchi. Here, there is a pseudo-stratified epithelium containing a mixture of non-ciliated, basal [16], ciliated [17], and secretory cells (club [18] and goblet [19]). The latter are responsible for the production of mucin and other substances that, together with other proteins coming from a sub-mucosal gland containing serous cells [20], form the mucus. This is one of the defence mechanisms of the lung, as the mucus' catches particulate matter and microorganisms, being expelled from the lungs helped by the movement of the cilia, in a process called mucociliary clearance [17,21]. The bronchiolar epithelium comes next, bearing the same pseudo-stratified epithelium comprised also by a mixture of non-ciliated, basal, ciliated, secretory, and neuroendocrine cells [22,23]. The next region comprises the alveoli, which are comprised by a thin layer of alveolar epithelial cells , also known as pneumocytes (type 1 and 2) [24], that are covered, on the basolateral side, by a network of capillaries. Type 1 alveolar cells cover around 95% of the alveoli and are flattened squamous cells responsible for the CO_2 - O_2 gas exchange [25,26]. Type 2 alveolar cells cover the remaining 5% of the alveolar surface, being responsible for the production of lung surfactant, a key component preventing pulmonary collapse [27], and for maintaining lung homeostasis by playing an important role in immunity [26,28]. Additionally, in the alveoli, there is a very small amount of liquid called lung lining fluid, which is useful for the non-desiccation of the organ spread across [29]. Important to mention is the presence of alveolar macrophages, another important defence mechanism [30]. In addition to this complex variety of cells and organisational structure, there are also other types of tissue, including the muscular and cartilage, which are present in the trachea and bronchi [8,12].

Altogether, the homeostasis within this organ is a delicate equilibrium that is achieved by the many cellular components, some discussed herein, which find a more detailed explanation, alongside their genetic characterisation, elsewhere [31]. Some imbalances are far too critical and can result in diseases that negatively

influence not only the lung, but also the overall balance in the human body. Some of the most common or relevant lung diseases will be discussed next.

1.1.2. Pathophysiology of lung diseases

In the previous section, the lung was discussed from the perspective of the absence of disease. However, due to the intricate equilibrium the lung requires to be always in, the presence of a disease alters the physicochemical dynamics of the cells [32] and the capacity of the lung to be used as a route for drug delivery [33,34]. The importance of the lung goes beyond its physicochemical traits, and the 2020 report published by the World Health Organisation (WHO), concerning the top leading causes of death is proof of that. Globally, chronic obstructive pulmonary disease (COPD), lower respiratory infections and trachea, bronchus and lung cancers are positioned in third, fourth and sixth places as to being the diseases that have the highest number of deaths (in millions) [35]. In Portugal, the situation is similar, with lower respiratory infections, trachea, bronchus and lung cancers and COPD taking the fourth, fifth and seventh places as to being the diseases causing more deaths *per* 100 000 inhabitants [36]. These alarming statistics evidence the importance of lung health, and the relevant impact lungs have on everyday life. Although this document does not intend to be an index of lung disease, it is important to describe some of these physiological disturbances.

Lung pathology can be divided in two major categories: infectious and non-infectious diseases. Tuberculosis and the most recent coronavirus disease (COVID-19) are two examples of diseases that are included in the first category. In these two cases, there is an external agent, either a bacterium (*Mycobacterium tuberculosis*) or a virus (severe acute respiratory syndrome coronavirus 2 or SARS CoV-2, in short), that accesses the lung through contaminated droplets. These are left in suspension in the air by an infected person, after a sneeze or cough, and are afterwards breathed by a healthy individual, leading to a probable development of the corresponding disease. In most cases, the lung defences protect the host, and the disease does not manifest. However, when it does, different mechanisms can be observed. In the case of pulmonary tuberculosis, after the bacterium enters the nose and goes through all the respiratory tree, it reaches the alveoli where it is taken up by the

alveolar macrophages. After that, either it remains contained or develops into an active disease [37], as depicted in Figure 1.3.

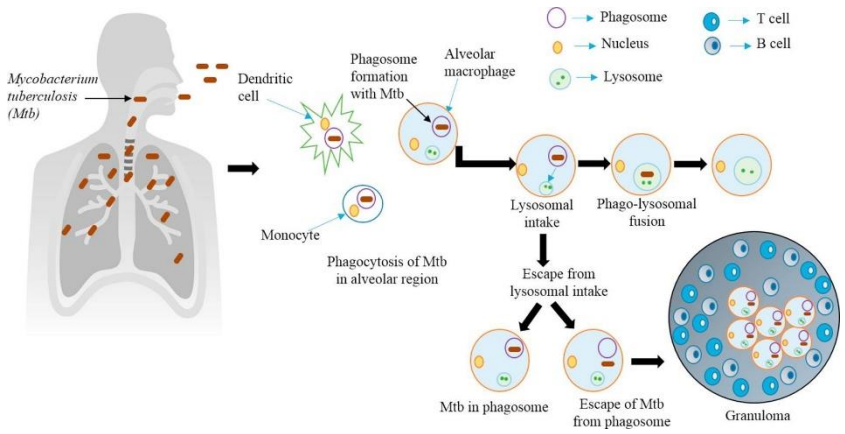

Figure 1.3 – *Mycobacterium tuberculosis* infection mechanism. If the bacterium reaches the alveolar zone, it is phagocyted by an alveolar macrophage and either two possible paths can follow: (1) degradation inside a phagolysosome, resulting from the fusion between the phagosome and the lysosome or (2) escape from the phagosome and after a series of inflammatory events, the formation of the granuloma [38].

As for COVID-19, the virus goes through the same path as the bacterium, reaching the alveoli, but the final target changes and it interacts with host target receptor angiotensin-converting enzyme type 2, leading to the subsequent replication of the virus and the development of the disease [39]. This results in a myriad of symptoms, that greatly differ from person to person without a pattern, but that, in a long-term scenario, might leave the patient with sequelae (increased mucus production, cough, tiredness, alteration of lung respiration capacity) [40]. Despite the numbers of infected individuals for tuberculosis have been incrementing for the past few years [41], and the numbers for COVID-19 are, nowadays, highly dependent on the dominant variant and its inherent transmissibility, infectious diseases still have a lower dominance in developed countries. Even so, other lung infections such as influenza infection and pneumonia are also worth of mention. The former is known by the community as the common cold, and the spike of infections usually spawns through winter, caused by the propagation of the influenza virus in aerosols from infected persons [42]. As for pneumonia, this is a more complex disease because, not only it can be caused by both bacteria and virus, but it is also a disease difficult to spot. It is required to know

the etiology of the microorganism causing pneumonia to establish an adequate treatment, otherwise resulting in long-term complications that can hinder the overall quality of life of a patient [43,44]. Despite this scenario, in developed countries, the prevalence of non-infectious diseases is still larger, thus requiring a larger budget investment and take a great toll on the national health systems.

One of the most relevant examples is asthma, a chronic airway inflammatory disease, that is highly prevalent in the world. A variety of symptoms can be associated with this disease, such as, wheezing, shortness of breath, cough and limited expired airflow, thus negatively influencing patients quality of life [45]. Even if it is triggered by allergens, infections or airway irritants, asthma is a reversible disease, meaning that, with adequate therapy, the typical acute symptomatic episodes either do not occur or, when they do, the lung returns to its normal state [46]. The same cannot be said about COPD, being also an inflammatory airway disease that leads to increased mucus production and thickening of the airways [47]. Due to the constant inflammation of the lungs, ultimately, it can lead to the destruction of the tissue (also called emphysema), fibrosis and loss of function. Symptoms such as cough, breathlessness, and increased mucus production are the most reported by patients [48]. Despite the approved therapeutic guidelines, COPD is irreversible, especially if there is emphysema already occurring. The chronic inflammation of the lung, that is observed in COPD patients, can also play a pivotal role in another troubling disease: lung cancer. This disease can be classified into two major groups: small cell lung cancer (SCLC) and non-small cell lung cancer (NSCLC), the latter subdivided into adenocarcinoma, squamous cell carcinoma and large cell carcinoma [49]. The high heterogeneity seen in this classification relates to the different genetic backgrounds and histological patterns lung cancer presents [50]. One of the main differences between SCLC and NSCLC is the aggressiveness, with the former being the most destructive [51]. SCLC is a neuroendocrine tumour characterised by its fast-growing rate and early metastases, resulting in a late diagnosis and a very diminished survival rate [52]. Fortunately, this type of lung cancer is the least common, NSCLC being reported in approximately 85% of all cases [53]. NSCLC evidences slower growth and is characterised by an heterogeneity of genetic mutations, resulting in neoplasia with different histological subtypes that must be determined upon diagnosis [54]. Due to the slow growing profile, NSCLC has a long-term healthcare

impact, and guidelines for the determination of cancer stage and the best possible therapeutic approach were proposed, as to lead the medical community to the best possible outcome [55]. Notwithstanding, both neoplasia require a quick action, corresponding to the total removal by surgery and/or radiation and/or chemotherapy to avoid metastasis, and even then, the prognosis is still uncertain.

Despite lung cancer being discussed herein as a single disease, it can be the terminal consequence of idiopathic pulmonary fibrosis, a debilitating and progressive lung disease [56] that is characterised by an irreversible alteration of the tissue going from a normal epithelium to a fibrous one. The latter results in a loss of function, which ultimately leads to respiratory failure. This disease is triggered by many factors, such as particles and virus, that result in an inflammation and a series of healing events, leading to an excessive accumulation of fibrous components. Regrettably, no treatment options are available to cure this disease and the life expectancy does not go beyond 5 years [57,58]. In fact, the quality of life and the number of years yet to live for a patient with any type of lung disease is a complex matter and a major issue in cystic fibrosis, the last lung condition to be debated in this section. This is a genetic disease caused by a mutation in the cystic fibrosis transmembrane conductance regulator (CFTR) protein. This protein is a chloride channel located in the epithelial cells, that is responsible for the flow regulation of chloride ions [59]. This flow is impaired in cystic fibrosis patients, that experience a major alteration on the lung mucus (Figure 1.4) [60].

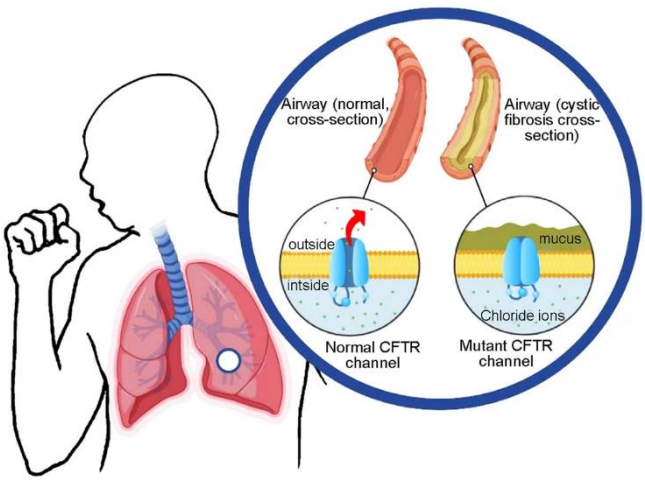

Figure 1.4 – Differences in the airways in a healthy and in a cystic fibrosis patient, the latter having a mutant CFTR channel. Adapted from [60].

In these patients, the produced mucus is very thick, thus blocking several ducts and constituting a favourable environment for the proliferation of bacteria [60,61]. These patients must constantly take antibiotics, which can lead to multidrug-resistant species, that can further hinder their health [62]. Although detected early in a patient's life, understanding the CFTR mutation of patients is the priority upon diagnosis. There are several CFTR mutations, which are grouped in seven different categories, each corresponding to a specific impairment of the receptor [63]. The F508del mutation belonging to class II ("impaired trafficking") is the most frequently found in European patients (82.4%) [64], but despite research and the therapeutic guidelines enabling life without major lung events [65,66], there is no cure for cystic fibrosis.

As seen, lung diseases tend to share a similar symptomatic pattern. In most cases, the mucus production is increased, breathlessness and/or modification of breathing patterns occurs and inflammation develops. All combined result in the loss of lung tissue function and its progressive destruction, further leading to respiratory failure and, ultimately, death. Understanding these diseases and the underlying mechanisms allows for better guidelines and therapeutic strategies. For some illnesses, treatments can only act on the symptoms, whilst others go even further and can help return patients to their healthy state. These strategies will be discussed later, but it is a proof that the compilation of information, its integration in a bigger picture and the multidisciplinary approaches will enable all to give hope to patients and a better quality of life in long-term care.

1.1.3. Studying the lung

The study of the lung has seen great advancement in the last years. In fact, despite being one of the organs that most contacts with the environment, accessing and assessing it is not easy. *In vitro* approaches may include the use of cell lines with lung origin, such as A549 (alveolar) and Calu-3 (bronchial) cells [13], that may be used to enable a first perception of the interaction of samples with structures of the lung [67,68]. Better replication of the lung environment involves culturing the cells at an air-liquid interface in order to allow the development of features of a cell barrier, although it is only possible with certain cell lines (e.g. Calu-3 cells) [69]. Cells can also be grown to form organoids, which are 3D structures resembling the lung [70] and will be discussed later. Finally, a third strategy called "lung-on-a-chip", is a more

complex approach requiring microfluidics, but it can be helpful as it incorporates an analogous breathing mechanism into the growth of cells [71], also detailed later. Despite these strategies, *in vitro* approaches are generally considered to not fully mimic the lung. Notwithstanding, these strategies are advantageous and useful, and a handy approximation for the biological characterisation of drugs and formulations.

Regardless of these living systems, in parallel, technology advanced and made other options available. This is the case of 3D printing, an additive manufacturing strategy, because it builds a device by adding a material layer-by-layer, thus resulting in a 3D object [72]. The first description a 3D printing method was reported by Hull et al., in the 1980s [73], and it all starts with a computer-assisted design (CAD) software to develop the idea [74]. Since then, several methods have been described to obtain the diversity of devices and parts that are designed [75]. One of the most common methods is the fusion deposition modelling, a technique requiring the melting of a polymer filament, that goes through a nozzle onto a heated bed. The printer builds the piece considering the spatial position of the model contained into the file that was loaded into the 3D printer [76]. A different kind of method is the one employed in stereolithography, as it uses the same file coming from the CAD software and build the object by discharging UV light onto a resin, causing it to harden [77]. Whichever method used, this technology enables the exploration of several new approaches in science, as it allows researchers to create specific objects for experimentation that otherwise could not. This same consideration can be applied to lung drug delivery. It is true that, nowadays, (micro/nano)cameras allow the inspection of certain zones of this organ, but it is almost impossible to go deeper in the lung without causing damage to the patient. It is, at this point, that these additive manufacturing strategies come in handy, because they enable the design and creation of models of certain areas of the human body (*e*. *g*. lungs), without the need for invasive procedures. One of the earliest cases reported belongs to Minocchieri and his team, in which they describe a premature-infant nose throat aiming at the study of aerosol delivery at this age [78]. The team used images of the respiratory system of the infant obtained from magnetic resonance imaging, which were afterwards compiled to prepare a real-life model by 3D printing. In line with this use of medical imaging, Bücking and collaborators propose this same use to prepare a 3D-printed model of the thorax [79] for a general medical use. In line with these authors, throat models can also be 3D

printed, as seen elsewhere [80]. Despite their use being outside the medical field, these structures may be relevant in inhalation experimentation that will be discussed in later sections.

In the age of personalised medicine, 3D printing can also find its place, and in a lung-related area, it is specifically applicable in cases of cystic fibrosis. As mentioned before, cystic fibrosis is a genetic disease encompassing several mutations that differ from patient to patient, resulting in different pathological outcomes [63]. In this regard, Mirza *et al.* reported the use of a radiograph and computed tomography data of a cystic fibrosis patient to create and print a 3D model of the afflicted lungs. The authors state that the use of 3D printing in these patients helps on the characterisation of the disease for each individual, the education of both patient and their medical team, and on the improvement of the treatment plan [81]. Within the scope of making models of organs, the works of Zhang and Galliger and their respective teams are also important [82,83]. The former uses the technology for the bioprinting of tissues [84], that is the same layer-by-layer deposition method using biological materials or cells. The authors refer not only to this process but also the use of bioinks [85], functionalised high-molecular polymeric mixtures encapsulating cells, that will be very useful in tissue regeneration. As for Galliger, they propose this method of bioprinting and bioinks to produce organs for transplantation. Although this bioprinting technology applied to this medical scenario still needs to respond to various concerns, it can be a viable option, in the future, to overcome the lack of organ donors throughout the world [86].

The advancements that are made in science and technology everyday allow for researchers to go further in the proposals of solutions for day-to-day problems and for medical procedures. Since the discovery of 3D printing and going from the most common polymeric filaments to the most recent ones mixing biological components [87], the interdisciplinary network between engineering, healthcare and the most fundamental biology pose a viable solution for the current limitations the world faces [88-90]. The study of the lung encompasses several points of view, and the scenario would be incomplete if only the pathophysiology, its mechanics and innovative ideas were discussed. In the next section, a more detailed look into the current therapeutic approaches involving lung delivery will be given, as well as new delivery strategies

that have been studied, culminating with aerosols, one of the major approaches on the approved guidelines.

1.2. The lung as a viable route of administration

1.2.1. Therapies into and through the lung: inhalation and other (new) strategies

Inhalation has been used since ancient times for the delivery of vapours and gases, as described in several manuscripts [91]. At that time, people did not know that the architecture-like structure of the lungs and the presence of an epithelium throughout the organ endowed the lung of an enormous surface area. This enables the contact of the components of the gases and vapours with a great number of cells, throughout the respiratory system, in a vast surface area. Furthermore, the high capillary density allows for an easier access to the bloodstream [92], avoiding the first-pass effect, a metabolic effect that can greatly influence the circulating concentration of the active principle. These advantages can work in favour of local drug delivery, such as the dry powders in asthma and COPD [93], and systemic approaches for treatments, such as the work developed with inhalable insulin for diabetes management, which started with Exubera® [94] and has evolved to the currently marketed formulation Afrezza® [95].

The design and development of drug delivery approaches for lung applications has seen a lot of advancement in the last years. Despite the number of approved excipients for this route of administration being small, the scientific community has been making an effort into the proposal of several new strategies for lung diseases, as debated elsewhere [96]. Inhalable formulations for the treatment of tuberculosis [37] are a sound example, finding diverse approaches in the literature. In some cases, carriers of the antitubercular drugs were prepared with polysaccharides containing mannose residues that are recognized by the mannose surface receptor on the alveolar macrophages, the hosts of the bacteria. This recognition facilitates the internalisation of drug carriers bearing these residues on their composition and, thus, the co-localisation with the bacteria, with a possible benefit on the therapeutic effect [97,98]. Still in infectious diseases, COVID-19 has been part of society's life for the past three years, changing many behaviours and highlighting the importance of the lung for human health and vaccination [99]. Other viral infections such as

influenza are also important to note, especially because, before COVID-19, their impact in healthcare systems was already huge. In the past, therapies for the common cold focused on treating the symptoms but research has been contributing with new antivirals [100], to stop transmission of the virus in the community, thus protecting those frailer. Moreover, to avoid complications in the winter months, governments put out vaccination campaigns, so that risk populations are immunised against the dominant influenza strain circulating in that year. Formulation development also occurs in vaccines, to improve their overall efficacy, pharmacokinetic aspects and release profile, as discussed by Masjedi in his most recent work [101]. The same immunisation seen for viral infections can also find its usability in diseases caused by bacteria, as it is the case of pneumonia and one of its main microorganisms, *Streptococcus pneumoniae*. The scientific community has discussed the feasibility of spray-dried pneumococcal membrane vesicles, which were successfully prepared and showed promising results in terms of immunogenic potential, still requiring an *in vivo* and clinical step up [102].

In the domain of non-infectious diseases, asthma has been known for a long time, and despite the myriad of pharmaceutical options [103], much work has been done to improve what is already on the market. One of the innovative approaches towards asthma is the proposal of a non-phospholipid nanovesicular carrier called novasome to increment the bioavailability of terbutaline sulphate, a bronchodilator used in asthma patients [104]. As for COPD, nowadays, there is even more knowledge as to its intrinsic mechanisms of disease. Although the current therapy is effective in giving patients a better quality of life, an overall improvement would be beneficial, which has been proposed to be possible through the use of nanotechnology platforms [105,106]. The case of lung cancer is more complex, as it is the most heterogenous disease of the lung. Treatment guidelines often involve chemotherapy, which, under certain circumstances, can result in pharmacological resistance. Understanding the molecular mechanisms behind this, enables a better use of the drugs and therapeutic alternatives [107]. It is this heterogeneity that allows many different research approaches, especially in terms of nanotechnology and the development of drug-loaded carriers [108], as well as the delivery of biologics [109]. Despite the more critical prognosis of lung cancer, treatment options are available, which is not the case for idiopathic pulmonary fibrosis. In this disease, the best that can be done is to

control the symptoms. Nevertheless, some authors have highlighted the advantages of gene therapy in this disease, to control the fibrous events [110]. As for cystic fibrosis, and the many complications associated with this disease, innovative drug delivery systems have also been explored [111]. Another approach that has been reported is the analysis of the resistome, which is the analysis of the lung microorganisms aiming at discovering possible antibiotic resistances to improve treatment possibilities [112].

Formulation development still holds many hopes for future therapies, and many proposals have been suggested [113-115]. Multifunctional strategies have also been widely studied, employing modifications in the polymers or even endowing them of chemical moieties that are stimuli-responsive [96,116-118]. Additionally, 3D printing has also found its place in lung drug delivery, in the development of carriers using this technology, by tailoring the aerodynamic parameters of the particles [89]. Different formulation strategies have also been proposed under the name of aerogels. These are solid materials with very low density, high porosity, high surface area, and high versatility as to the materials that can be used for their production and the components that can be associated with them [119]. One of the applications found for these aerogels in lung drug delivery is the work of Obaidat and their team, that successfully prepared a chitosan-based aerogel loaded with salbutamol, a drug used often in asthma patients [120]. One final approach worth of mention is the one proposed by McVey and their team. Despite not being a formulation in its entirety, the analysis of extracellular vesicles that encapsulate molecules and components coming from cells might be one of the future targets, to determine if there are any signs of disease in a person, contributing to yet another mechanism to better detect and diagnose, and to effectively guide treatment options [121].

Lung research has been giving a great contribution to the improvement of guidelines and current therapy of known lung diseases. The efforts made to look at the lung as a viable route of administration are being successful, and further advancements, especially the ones concerning excipients [122], drug repurposing [123] and the use of medicinal chemistry [124], enable new therapeutic ventures.

1.2.2. The case of aerosols

Inhalation is the corner stone of lung therapy, and formulations used for that endeavour are called aerosols. However, their use in lung drug delivery is a delicate subject because there are aerodynamic requirements that need to be met for an efficient delivery and an efficacious therapy.

1.2.2.1. Aerodynamic parameters of inhalable formulations

Particle engineering and particle deposition are two fundamental topics when lung drug delivery is referred. While the former focuses on the formulation, the latter relies on the bio- and physicochemical aspects of the different parts of the respiratory tree [125]. Despite being two different approaches, both particle engineering and particle deposition are intertwined, influencing the efficacy of a lung formulation. Tailoring particles has been one of the focuses in the last years within the research community, especially in terms of size, and although not exclusively, it can influence the region where the particle will deposit upon emission, as shown in Figure 1.5 [126].

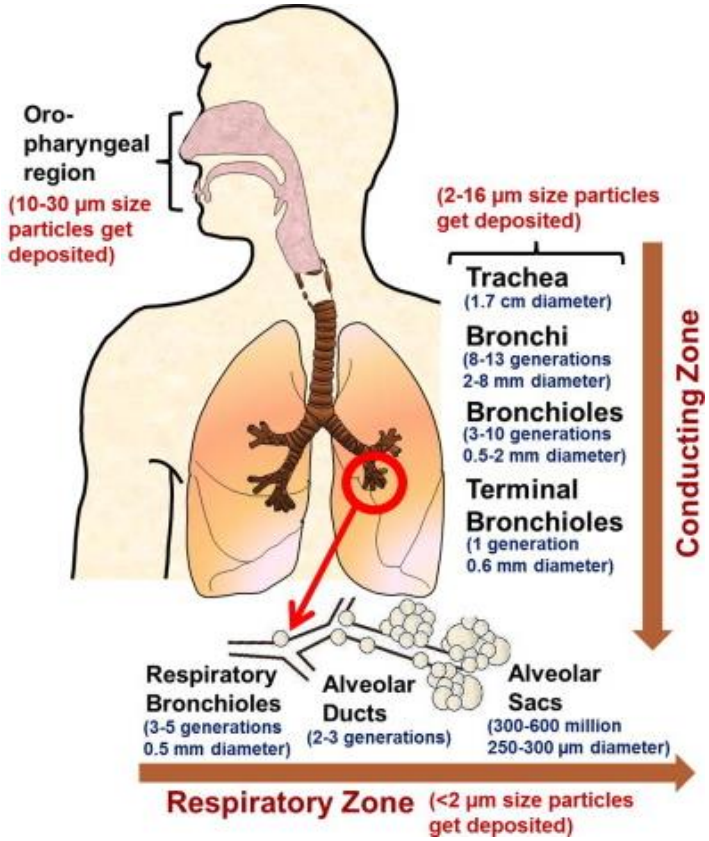

Figure 1.5 – The size dependent deposition of the particles in the different parts of the lung. Adapted from [126].

The size of these particles can be characterised by two parameters: the geometric size also known as Feret's diameter (d_F), and the aerodynamic diameter (d_{aer}). Both refer to the diameter of a sphere, but d_F is considered an approximation of the real size, because its determination is made by the manual measurements of the diameters of the particles by optical microscopy [127]. As for the d_{aer}, it is a parameter closer to the real diameter of the particle, defined as the diameter of a sphere with unit density and a similar velocity as the studied particle [128], and it can be calculated using Equation 1.1,

$$d_{aer} = d_F \sqrt{\frac{\rho_{particle}}{\rho_0 \chi}} \qquad \text{(Equation 1.1)}$$

where d_F corresponds to the geometric size of the particles, $\rho_{particle}$ refers to the density of the particles, ρ_0 specifies the unit density ($1\ g/cm^3$) and χ is the shape factor, that varies between 1 (spherical) and 2 (irregular) [129]. In parallel, the mass median aerodynamic diameter (MMAD) refers to the mean size of particles that reach the respiratory tree, excluding the ones that deposit in the throat [128], and it can be calculated using Equation 1.2,

$$MMAD = d_{50} \sqrt{\frac{\rho_{particle}}{\rho_0 \chi}} \qquad \text{(Equation 1.2)}$$

where d_{50} corresponds to median diameter of the particle size distribution. Moreover, parameters such as the Fine Particle Dose (FPD) and the Fine Particle Fraction (FPF) aid on further characterising an aerosol. The former characterises the mass of formulation/drug with a d_{aer} between 1 and 5 µm [130], an interval of sizes that ensures particles fly into deeper parts of the lung. The FPF refers to the percentage ratio of the FPD that is recovered from the emitted dose, which is the amount of formulation/drug released from the inhaler upon activation [131]. These parameters can be determined experimentally using an Andersen Cascade Impactor (ACI) or a Next Generation Impactor (NGI) [132]. These two apparatuses are crucial in lung research because they allow for the aerodynamic characterisation of aerosols for lung applications (Figure 1.6) [133].

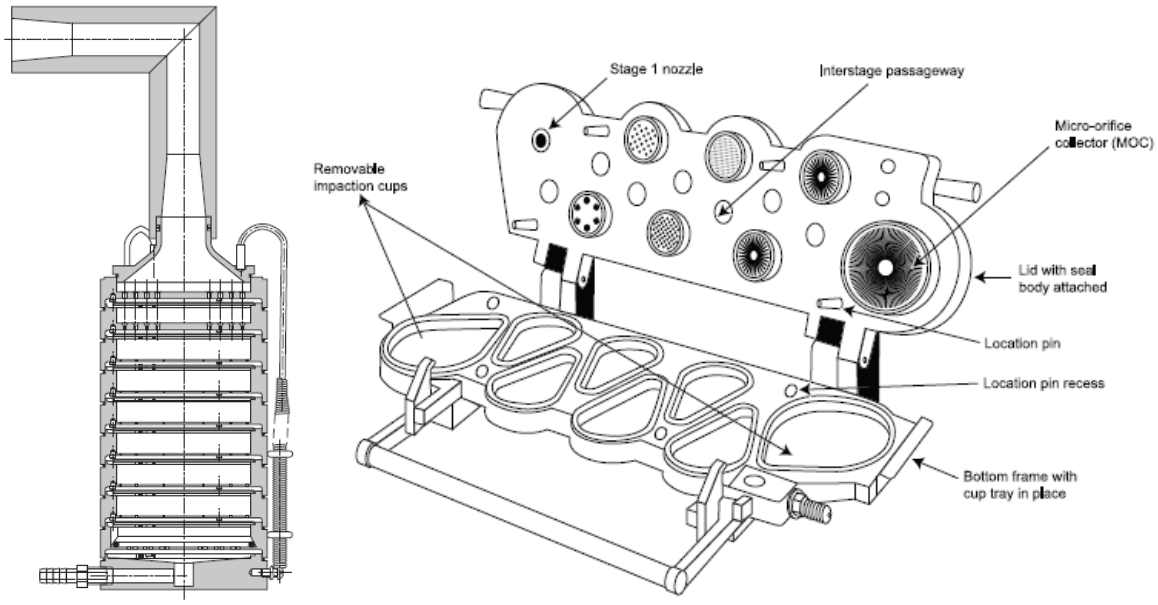

Figure 1.6 – Schematic representations of the apparatuses for the experimental determination of aerodynamic parameters of dry powders: on the left, the Andersen Cascade Impactor (ACI) and on the right, the Next Generation Impactor (NGI) [133].

Figure 1.6 shows the structures of the ACI and the NGI, historic apparatuses created to mimic the respiratory tree at a laboratory scale [133,134]. The different regions of the lung are presented in the form of stages with orifices that have narrower diameters for the levels either closer to the bottom on the ACI or on the right part of the NGI. Data obtained from tests performed with either the ACI or the NGI provide useful information for the optimisation of a lung formulation, making it easier to predict where the deposition will occur inside the lung (Figure 1.7) [135].

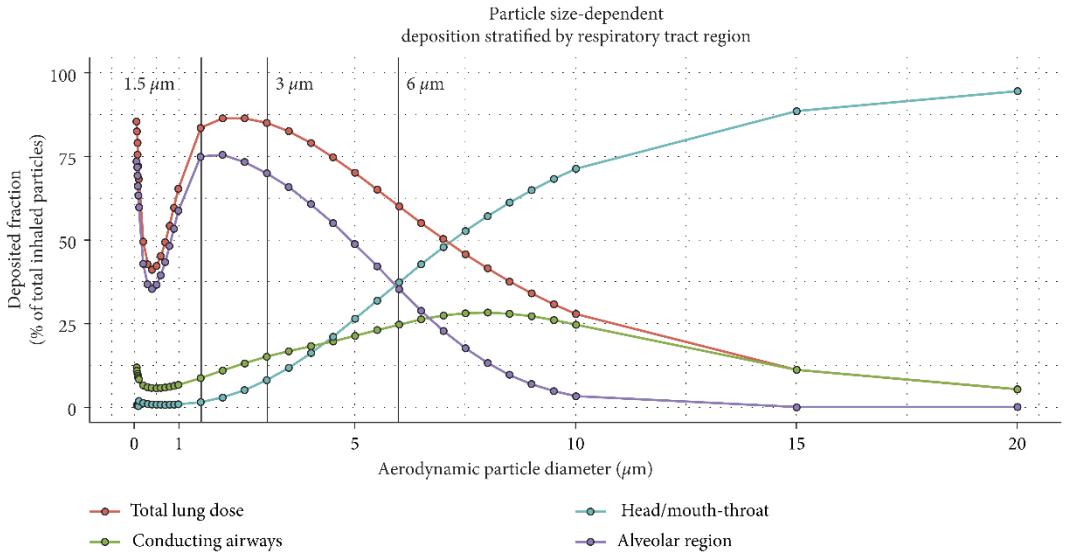

Figure 1.7 – Size-dependent particle deposition in the different parts inside the lung. Adapted from [135].

Figure 1.7 details the deposited fraction of inhaled particles in function of their d_{aer} and the target region of the lung. There are three main particle size-dependent lung deposition processes: inertial impaction, sedimentation and diffusion [9]. The first occurs in the tracheal region, for particles bigger than 5 µm. For particles with sizes between 2 and 5 µm, a process of sedimentation governs its deposition pattern along the bronchiolar region. Particles with sizes between 0.5 and 2 µm have a deposition pattern that is dominated by Brownian motion, allowing for the random diffusion inside the alveolar region [130]. Furthermore, other mechanisms such as turbulent mixing, electrostatic precipitation, and interception contribute to particle deposition and are discussed elsewhere [136,137]. The many aerodynamic requisites that are needed for a formulation to be suitable for lung applications is challenging, but in all cases, all information converge to obtain optimised products and successful therapies. These strategies will be discussed next.

1.2.2.2. Types of aerosol devices

Lung research has evolved greatly in the past years but aerosols and their corresponding devices are still one of the essential strategies by which asthma and COPD patients, as well as others, manage their disease [138]. In this great group of

aerosols, there are four main types of devices: the metered dose inhalers (MDIs), the dry powder inhalers (DPIs), the nebulisers and the soft-mist inhalers (SMIs).

MDIs first appeared in the second half of 1950s [139], and their technology has not changed much ever since. It is a simple system, in which the patient activates the device by pressing the cannister and the dose is released from a reservoir onto a metering chamber. At this point, the drug and a propellant mix in either a homogeneous solution or a micronized suspension. Finally, this mixture is released into a mouthpiece, thus contacting with the patient taking the medication [140]. It is required that, upon activation, the patient takes a deep breath so that the drug enters the respiratory tree, hold for some seconds, and then exhale. This process maximizes the contact between the drug and the lung tissue, so that it can be absorbed and exert the therapeutic effect. The easiness of use, multi-dose capacity, high reproducibility in dosing, among others, make this a desirable approach in therapy [141]. The process that makes it so easy to use is, at the same time, one of the limitations. Due to que requirement of coordination between inspiratory movements and device activation, for some patients, this task can be difficult. For that reason, two alternatives were developed: (1) the use of a spacer, in which the device is activated first, with a subsequent diffusion of the cloud containing the drug inside it; afterwards, the patient just breathes the dose [142] and (2) the breath actuated inhalers, where the device is activated only when the patient breathes, permitting an easier patient compliance with the therapy [143]. Several other improvements were described elsewhere, such as valve innovations and alternative cannister designs [144], but that is out of the scope of this section. Another limitation concerning the MDIs is related with environmental sustainability [145,146], as their carbon footprint is high due to the propellants used. When the MDI devices were developed, they used chlorofluorocarbons (CFC) as propellants. Regrettably, due to the enormous impact that CFC have on the ozone layer, they were replaced by hydrofluoroalkenes (HFA), a safer alternative [141]. Nowadays, the most used HFA are the HFA 134a and HFA 227ea [147,148], but there are others being studied such as HFA 152a [149] and HFO 1234ze [150], with a carbon footprint that is equivalent to the DPIs.

The latter constitute an alternative to MDIs [151], and are the second type of device to be discussed in this section. The fundamental difference between an MDI and a DPI is that, while the former uses a propellant to disperse the drug or drugs, the latter is a dry powder formulation, which can use an excipient to help with its dispersion [152]. Moreover, another difference is that the aerosolisation of the dry powder in the DPI is only dependent on the patient's inspiratory flow, thus not requiring the coordination between the activation of the device and the patient's breathing. This feature is one of the three aspects that are used to categorise the DPI devices, and it is called the activation mechanism of the DPI. The mechanism can be either active, requiring a battery or other external source of energy that causes the deagglomeration of the dry powder as the patient inhales, or passive, the most common mechanism that relies on the patient's inspiratory flow to cause the deagglomeration of the dry powder particles upon inhalation [153]. Besides this one, it is also considered the number of doses the device carries, which can be single-unit dose (capsule), multi-unit dose (blister) and multi-dose reservoir [154], and the device resistance that can be low, medium or high [155] being closely linked to the patient's inspiratory flow [156]. Adding to this, the type of formulation used on the DPI can also be a factor, because it can be carrier-free or carried-based. The former entails only micronized particles of the drug, which have been subject of intense research concerning particle engineering [157], while the latter is comprised of a mixture of micronized drug and carrier particles, usually lactose [158]. The categorisation of the DPI devices is complex, and a detailed inventory of the marketed devices can be consulted elsewhere [159]. Fluticasone propionate is an example of an active pharmaceutical ingredient that is currently part of the asthma Portuguese guidelines described by the Direcção Geral de Saúde [160]. This carrier-based formulation is a mixture of the drug with lactose and it is included in a multi-unit dose (blister) device with a passive mechanism (breath-actuated), being the given commercial name of Flovent® Diskus [159,161]. The choice of a DPI is dependent on the patient, the progression of the disease, the therapy that is currently prescribed and the proper training of the patient towards the device [162]. The advantages of the DPI are closely related to the formulation being a dry powder, because the production is facilitated as well as its transport, ultimately having an impact on the marketing-associated costs. Additionally, in terms of drug compatibility, the adsorption of drugs to a solid carrier is easily understood, as no requirement of solubility in a liquid propellant is needed [103]. However, despite being

an advantage, the administration of dry powders can result in cough reflexes more frequently than in MDIs, in which the propellant could help on the wettability of the dosed powder, thus making it easier to breathe. Nevertheless, the use of DPIs has been increasing for the past few years, even among children [163], aiming at improving current formulations and devising new ones aided by particle engineering [164], while decreasing the health economic burden and the environmental impact associated with inhalers [165].

Nebulisers are the third approach to be mentioned in this section. Contrary to MDIs and DPIs, these devices aerosolise liquid solutions and suspensions by a myriad of methods [153]. They are comprised of three basic parts: an energy source, a container and a mouthpiece [166]. Due to the nature of the device, they do not require propellants, as the vehicle of aerosolisation is the one comprising the solution/suspension, that will create the droplets and drag the active pharmaceutical ingredient and excipients. The droplets are tailored to have a certain aerodynamic diameter, to reach the required target zone within the lungs, and it is a viable approach for nanoscale treatments and for patients unable to work with both MDIs and DPIs [167]. Nebulisers can be divided into three different categories: pneumatic/jet, ultrasonic and mesh, depending on the type of source used to form the aerosol. The energy source can be an air compressor or a piezoelectric crystal producing either a high-frequency (1-3 MHz) or low-frequency (100-200 kHz) acoustic waves [168], respectively. The energy created by these sources will interact with the vehicle, thus forming the aerosol that will be inhaled by the patient. Despite being technologically more advanced than MDIs and DPIs and providing a viable therapeutic approach, nebulisers are expensive devices [169,170], and still fail to be as portable as the MDIs and the DPIs [171]. Notwithstanding, the choice of the device continues to be centred around the patient and is often influenced by the respiratory capacity of the user, an important feature that must be evaluated with the patient's medical team [172].

The last type of device worth of mention corresponds to the soft-mist inhalers. There is only one marketed formulation called Respimat®, approved since 2003 [173]. This type of device was developed for two main reasons: (1) to improve the mechanisms already marketed for a better patient compliance and (2) to create an optimised

single-breath inhalable aerosol from a solution containing the active pharmaceutical ingredient [174]. This device simplifies patient manipulation, requiring only the twisting of the base of the device at 180º. The twist will induce tension on a spring inside the device, forcing the solution to go through an array of filters and nozzles. This mechanical mechanism forms the aerosol that will be inhaled after it is released upon pressing the dose-release button [175,176]. The delivery of the aerosol is performed at a slow velocity, which coupled with an optimised droplet diameter given by the array of nozzles, it increases the fine particle dose and maximizes lung deposition [177]. Despite these improvements, the soft-mist inhalers are more expensive than MDIs, DPIs and nebulisers, which can impact the decision-making process of patients upon choosing their therapy [175]. Moreover, the soft-mist inhalers require a basic assembly and priming before the first use. The latter is a process that ensures that every dose results in a reproducible ready-to-inhale aerosol, requiring a certain dexterity that is often lacking in older patients [178].

Considering all that was discussed until now, going from a more pathophysiological approach of the lung to the many therapeutic strategies and respective innovations, lung research should be straightforward. However, that is not the case, and for the approval of dry powders and aerosols to be used in therapeutics, thorough studies must be conducted to guarantee safety and to determine the toxicological profile. This is easier when researchers investigate the methods at their disposal and use *in vivo* models, as they are the closest to a human living system, enabling robust conclusions and correlations. However, at a more fundamental level, *in vitro* assays can also give strong inputs, which requires ensuring biorelevance of the assay conditions. This concept entails testing in an experimental setting that allows robust *in vitro-in vivo* correlation, with the aim of waiving the need for animal models [179]. In the next section, various methods for aerosol research will be discussed as potential biorelevant *in vitro* approaches in lung research.

1.3. Aerosol research in lung delivery

The importance of the lung has been discussed, in previous sections, as to its role in the overall health maintenance. It is a structure that allows the exchange of gases [180,181], thus implying an interaction with atmospheric air. The air is subject to many changes related to temperature, pressure, relative percentages of gases and

particulate matter in suspension, and all these can have an important impact (either positive or negative) in the act of breathing [182]. It is natural that this close contact with externalities would induce evolution to develop several protective mechanisms to safeguard the organ from any kind of aggression [183,184]. Although advantageous for the maintenance of life, the protective mechanisms can hinder lung drug delivery applications, requiring formulations to comply with several aerodynamic requirements to efficiently deliver drugs through the lungs.

The use of the lung as a route of administration for drugs has been discussed within the scientific community [138,185]. The development of a formulation requires several methods and tests that generate reproducible data for a potential approval by the competent authorities. These can be divided into three categories: *in vivo*, *ex vivo* and *in vitro* tests. In lung applications, producing and replicating data *in vivo* requires an evaluation of the best animal model to use and the validation of an experimental setting [186]. *In vitro* assays, in turn, do not make mimicking the lung environment an easy task. Therefore, drawing conclusions concerning the behaviour of formulations from an *in vitro* assay can be severely hindered as they fail to be as robust as the conclusions obtained in *in vivo* assays. After the development of a medicinal formulation, an inhalable one in the case, the characterisation of its behaviour becomes a need. At initial stages of development, many of the envisaged assays are to be performed with cells. When the inhalable formulation comprises a dry powder, it should be tested as a dry powder. However, nowadays, the most common cells assays performed, test dry powders in suspension. This means that the powder is added to the liquid media where cells grow, which is followed by a waiting period to enable contact between the dry powder and cells. Regrettably, although being cost-effective, this is a strategy that does not mimic lung conditions, because the lung does not have abundant liquid [29]. Moreover, international guidelines foster the reduction of animal experimentation [187] and, thus, *in vitro* approaches that may replace *in vivo* studies while helping building robust conclusions, are highly needed. *In vitro* platforms enabling the assessment of dry powders in cell-based studies are scarce. The existing ones are expensive and technically complex, not feasible for early stages of research. The identified limitation still requires a more permanent solution.

The existing approaches evidencing a possible application in the evaluation of inhalable dry powders are detailed subsequently. Firstly, the *in vivo* methods will be looked into, followed by the new *ex vivo* techniques, and finishing with the *in vitro* strategies employed in lung drug delivery.

1.3.1. *In vivo* methods

The use of animals in experimentation, often referred as *in vivo* assays, has been subject of controversy. Although they are the most reliable method of establishing behavioural correlations and conclusions, ethical questions concerning the life and safety of the animals are making scientists rethink experimentation, particularly in early stages of formulation development. Furthermore, European legislation has been getting tighter concerning the use of animal models [188]. Despite this context, *in vivo* assays are still crucial for the approval of new medicines, especially if lung drug delivery is concerned. The lack of adequate alternatives (*ex vivo* and *in vivo*) impairs a much-needed transition, particularly in early stages of formulation development.

The first approach is an insufflator developed by PennCentury™ (Figure 1.8) [189]. Conceived for *in vivo* assays [190,191], it was later adapted for *in vitro* tests [192,193], a use that will be detailed and discussed later.

Figure 1.8 – PennCentury™ insufflation device (model DP-4M) conceived for *in vivo* assays [189]. Its core use was for the insufflation of dry powders onto the lungs of mice (*in vivo*), but it could be adapted for the same type of assays on cell culture supports containing grown lung-derived cell lines (*in vitro*).

The device shown in Figure 1.8 was designed for *in vivo* assays, as the metal cannula is used to enable an oral gavage and the direct insufflation of dry powders onto the lungs of the mice [190,191]. It is a tool that is comprised of three parts. Looking at the figure and going from left to right, there is a first tube that will enable the connection of a syringe to serve as a point of entry for the air, redirecting it to the remainder of the tool. The middle part, which has a black line, is comprised of a series of membranes, that help on the weighing of the powder and function as a collection chamber. The final part, more on the right, is the cannula, which goes into the mice onto the lung. Its small diameter endows the powder of enough velocity to simulate an insufflation, thus enabling its dispersion inside the organ. Although being practical, this device doesn't consider the breathing of the animals. In fact, in the process of breathing, there is always loss of powder/active principle, thus delivering almost all the powder directly into the lung possibly can lead to biased conclusions. This one limitation was surpassed by an apparatus proposed in a patent called "Laboratory Animal Pulmonary Dosing Device" [194]. This apparatus requires the animals to be contained in side chambers that will be connected to a main chamber. To the latter, there will be a nebulizer connected, enabling the generation of an aerosol, that will be accumulated in the main chamber, and then breathed by the animals. This second approach can be considered an improvement of the first, considering the breathing of the animals for the intended analysis. A third approach is yet another improvement of the PennCentury™ device, a recent invention designed and created by AptarPharma called "Powder Administration Device for Animal". It resembles an automatic pipette, that has on its end a compartment for 1-20 mg of powder and a cannula, much like the Insufflator DP-4M (Figure 1.8). Each time this device is used by pressing the button on top of it, it releases around 200 µL of air that drags the powder into the cannula, and afterwards into the lungs of mice [195].

One last approach worthy of note is a setup mentioned elsewhere [98,196] corresponding to an unofficial device, as several parts were put together to achieve the intended purpose. In brief, mice were restrained in a 50 mL Falcon tube with a hole pierced in the bottom. Using a baby bottle teat, the 50 mL tube was connected to a 15 mL tube, also pierced on the bottom, where the dry powder/sample (30 mg) was weighed. The connected holes allow the dispersion of the powder to the mouse,

by means of a plastic pump connected to the upper part of the 15 mL tube, that creates a turbulent air stream. The animals would have to inhale the formulations for 2 min, a timeframe ensuring that the dose of the weighed powder is breathed by the animals. Similar approaches relying on adaptations, adjustments of parts of other apparatuses or even one specific design [197] occur not only *in vivo*, but in the alternatives that will be discussed next. Ultimately, some of those devices or solutions were built to help achieve a certain goal and, in parallel, to avoid more complex, expensive and unreachable strategies, but the limitations still remain for early stage formulation development.

1.3.2. *Ex vivo* approaches

One of the possible solutions to bypass concerns regarding *in vivo* assays, is the use of *ex vivo* platforms, which are considered a bridge between *in vivo* and *in vitro* assays, as they combine advantages of both. In brief, *ex vivo* assays conserve the organ intended to study, maintaining its 3D-structure and microenvironment, but at a laboratory scale [198]. Precision cut lung slices and isolated perfused lungs are two proposed models. The former refer to sections that are collected from lung tissue immediately after the death of an animal, which are infused with low-melting agarose in buffer or tissue culture media, solidifying at low temperature and retaining their physiognomy and physiology [199,200]. Despite the higher reproducibility of the platform for therapeutic efficacy and drug toxicity, there is a lack of significant translation of data to clinical applications, and dosing problems [201]. The latter model entails the isolation of the lung of a rodent in a thoracic chamber, at physiological conditions, while a perfusion buffer is administered to mimic pulmonary circulation [202]. This strategy allows the determination of aerodynamic and pharmacokinetic parameters, being a viable option to better come near a real scenario, permitting a robust and stronger clinical translation [13]. Nevertheless, these *ex vivo* approaches still require animals to provide the organs, which does not comply with international guidelines, thus requiring the development of adequate and accurate *in vitro* methodologies.

1.3.3. *In vitro* methods

In the specific application of lung delivery, *in vitro* assays show a limitation regarding the adequate mimicking of the respiratory conditions. Apparatuses and other viable

strategies developed in this context have been trying to overcome this key limitation. The first set of *in vitro* platforms deserving a mention are (1) cell culture in air-liquid interface [203], (2) organoids [204] and (3) lung-on-a-chip [205].

The cell culture in air-liquid interface is the simplest of all the techniques to be discussed in this section. It has been studied for many years, and a detailed description can be found elsewhere [69]. It can be resumed to an insert, over a well of a cell support, in which a monolayer of lung epithelium grows. After that, sedimentation of a sample, a dry powder for example, occurs by aerosolizing it onto the system. The subsequent analysis focuses on permeation, toxicity, or other aspects [206,207]. Although the simplest, the air-liquid interface is a feature that will take part in many other approaches of increased complexity, that will be detailed later. The second platform, pertaining to the organoids, is an improvement of the first, because it entails the growth of cells in an immature organ, a shape that acquires a 3D structure instead of the 2D cell monolayer, and which is important for disease modelling [70]. Moreover, these organoids can be paired with microfluidic systems, which will produce an environment to study drug diffusion, an analogous strategy to understand what occurs in a human lung [208]. The third and final platform refers to the lung-on-a-chip strategy. This consists of microfluidic devices populated with cultivated cells that grow by slowly infusing medium and by cyclic movements provided by the device resembling the mechanism of breathing [71]. The imposed modifications of air pressure and flow induce differentiation and proliferation, which, ultimately, contribute for the interaction between the living systems and the test sample [209]. This platform seems to be the most competent in establishing a potentially biorelevant *in vivo* environment by itself, allowing for a more translational approach concerning lung drug delivery experimentation.

Other more complex strategies have been proposed that can better mimic the respiratory system. Overall, these require high investments that are not feasible for many research groups. Formulation development for lung drug delivery involves, many times, creative investments to reach a certain goal, due to the scarcity of funds and the need to allocate those that exist in alternatives, especially in more preliminary approaches. One of these proposals is an apparatus called Pharmaceutical Aerosol Deposition Device On Cell Cultures (PADDOCC) that was

built by Hein *et al*. [210,211]. The three-component tool can be seen, in a drawing, in Figure 1.9.

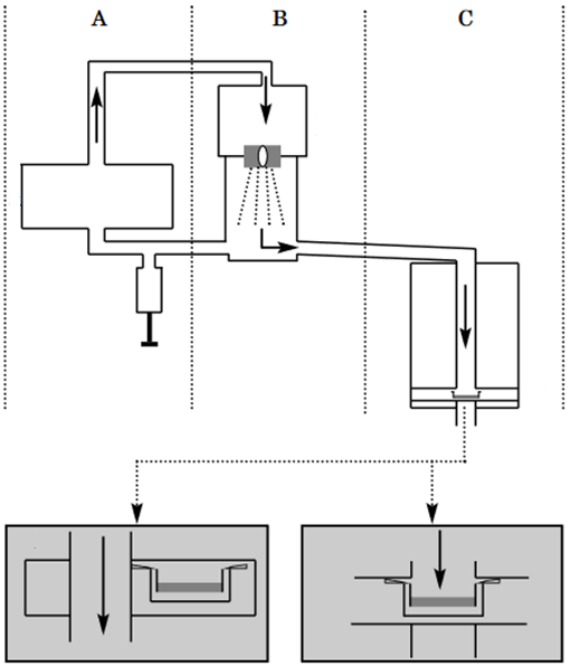

Figure 1.9 – The PADDOCC system: A represents the air-flow control unit, B depicts the aerosolisation unit and C illustrates the deposition unit. The left grey panel shows a drawing of a blank assay, in which air is going through the system and the right grey panel is a depiction of an assay with cells waiting for the dry powder to deposit on top of them. Adapted from [210].

The authors describe this ingenious device as having three different parts: A represents the air-flow control unit, B depicts the aerosolisation unit and C illustrates the deposition unit. The latter is a disk comprised of several holes, that alternate between the ones receiving samples and the others that are for ventilation only. Thus, the PADDOCC system has two modes to generate data: the first is the ventilation mode, in which, only air passes through the device, whereas on the sampling mode, air and the dry powder are aerosolised, as mentioned previously.

The next apparatus that is worth mentioning is protected by two patents. It is named as “device for measuring superfine particle masses” and it is comprised of a platform with six sampling units, with one or more containing a Quartz Crystal Microbalance (QCM) [212]. In brief, this technology allows for the detection of masses by the

variation of frequency of a vibrating quartz crystal. The QCM technology has been investigated for the past years as a biosensor [213,214] but its application as measuring balance in this context was just proposed. In the case of these inventions, the aerosols were thought to be emitted onto deposition surfaces (the QCM), for subsequent analysis. Differences in the frequencies are studied by comparing the oscillating crystal with the other crystals that are not moving but are incorporated into the platform. Although permitting the study of the insufflation of powders, the introduced complexity is reflected on the price, which hinders a more preliminary use in formulation development. However, other similar technologies are in the market, such as the VITROCELL® equipments, which also use the QCM technology to generate data concerning aerosol deposition. One apparatus that was first documented elsewhere [215,216], was comprised of a box covering six sampling holes. On top of this, there was a nebulizer that received a liquid solution or a particle suspension, and upon formation of a cloud, it deposited on top of the QCM and the necessary analytical information was assessed. Despite making use of a nebulizer, this method can be useful for the evaluation of the impact of droplets on cells cultured in inserts placed on the sampling holes and, in parallel, understand its mechanism. An improvement of this device was proposed some years later as the VITROCELL® Powder Chamber, using the same QCM technology, and enabling deposition of dry powder aerosols on cells at an air-liquid interface [217]. Firstly, the dry powders are loaded into the device by means of an adapter and then, the sedimentation tubes are filled with these powders. The final step is the rotation of the tray, enabling the exposure of the inserts to dry powders, in which cells are being grown in a monolayer, resembling what occurs in the lung.

Still in the *in vitro* domain, there is a simpler approach that is worth mentioning. It is a device used for dry powder dispersion proposed by Asai *et al*. [218], which can be seen in Figure 1.10.

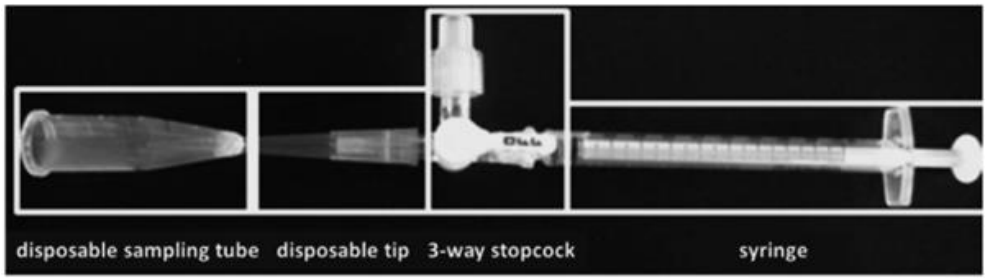

Figure 1.10 – Apparatus for dry powder dispersion. From left to right: an Eppendorf tube functioning as a disposable sampling tube, connected to a 3-way stopcock by a disposable tip, and on the right end, a 1 mL syringe. From [218].

These authors developed a very simple device, with an eppendorf tube, a 3-way valve and a 1 mL syringe, enabling the insufflation of powder over an air-liquid interface. They had also an alternative sampling mechanism for liquid, consisting of using the cannula of the PennCentury™ insufflator inside an eppendorf tube much like in Figure 1.6, coupled with a metal syringe, responsible for introducing air into the system and enable the insufflation over cultured cells.

Another adaptation made by our research group at Universidade do Algarve resulted in using the PennCentury™ tool for *in vitro* assays, instead of its normal *in vivo* use, as described elsewhere [219-222]. Figure 1.11 depicts this repurposing, that will respond to the need of a tool enabling dry powder insufflation over cultured cells.

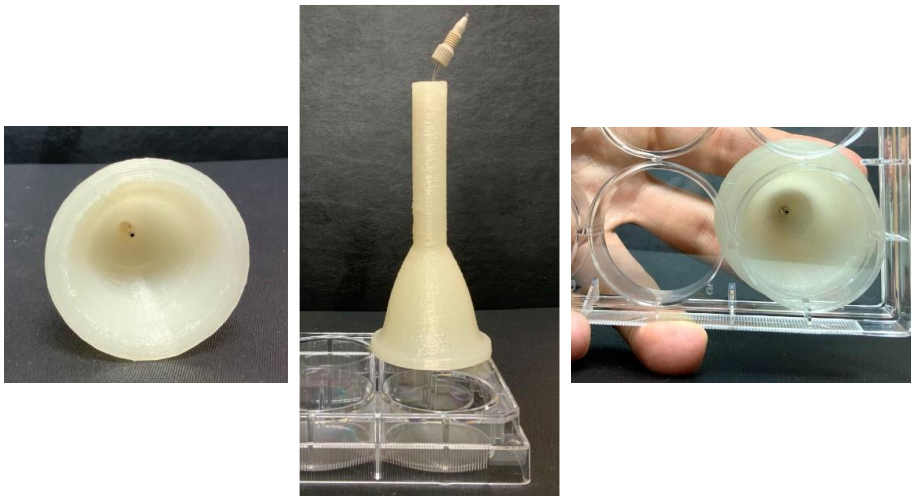

Figure 1.11 – Schematic of how the insufflator and the funnel work as devised. From left to right: the cannula of the PennCentury™ tool inside a funnel, the home-made funnel on top of a 6-well plate and a bottom view of the placement of the funnel.

For the insufflator to be used in this repurposing experimental method, the design and development of an accessory to direct the insufflated dry powders towards a specific area, a cell support containing grown lung-derived cell lines, was required. The best solution was to draw and use 3D printing to obtain a funnel that would be placed on top of the cell support. This funnel would be fit to secure the cannula of the PennCentury™ device, so that the cells grown in the cell support underneath would interact with the insufflated dry powder (Figure 1.11). However, the dispersion of the powder on the cell support was far from optimised, because upon insufflation, the sample would fall off predominantly on the centre of the well. As optimisation was being conducted, the news about PennCentury™ closing its doors broke out, meaning that they would stop selling this device and other tools [223]. This decision left the market lacking a solution that, although not ideal, provided a way to conduct important experiments at a lower cost.

These simpler strategies were left to last because they concentrate the many issues and limitations concerning the apparatuses used for *in vitro* testing in lung drug delivery. This section intended to give a broader view on the mechanisms and apparatuses that are used for *in vivo*, *ex vivo* and *in vitro* assays related with lung delivery. Although simpler approaches were discussed, the need that arose from PennCentury™ closure is still not fulfilled. Or, better yet, this need is partially taken care of for a selected number of research groups that can gather the necessary funds to invest and are able to justify said investment long-term. Moreover, if all propositions herein discussed are considered, all *in vivo* and *ex vivo* seem to be more robust, completed and developed, showing that higher funds were applied here. Although there is a confidence conferred by these assays concerning lung drug delivery, nowadays, *in vitro* methods becoming more popular, and positioning themselves as cost-effective. In the next and final section of the Introduction, these implications will be discussed culminating in what this PhD project proposes to achieve.

1.4. Lung-related economy

Nowadays, Earth is experiencing very delicate circumstances concerning the environment [224]. Airborne diseases are systematically posing some sort of threat to the way humans live [225,226]. The last one was COVID-19, caused by SARS-CoV-2, a virus that is easily transmissible through droplets with origin in the nose and mouth of infected people [227], with a recurrent negative impact on individuals [228]. With the air quality throughout the world decreasing, and the probability of developing respiratory diseases increasing [229], the lung should be paid more attention. Lung-related economy translates all the aspects concerning respiratory health impacting daily life, thus requiring constant surveillance and, in parallel, scientific advancements [230] to improve therapeutics. This can only be achieved with the correct tools, ultimately resulting in the prevention of diseases at earlier development stages [31,231]. The use of technology to develop and tailor devices was discussed in the previous section, and the current massification of the 3D printing devices stimulated even more creativity in experimentation. Although 3D printing is still finding its way to be incorporated in scientific methods and laboratories, the development of lung delivery formulations can possibly benefit of the technology regarding the design of new assessment devices, tailored to the needs. The feasibility of the inclusion of 3D printing in lung drug delivery was evaluated through a SWOT analysis [232] to provide a wider view (Table 1.1).

Table 1.1 – SWOT analysis [232] integrating the concepts of 3D printing and lung drug delivery at a laboratory scale.

Strengths	Weaknesses
- Versatility and low-cost associated with 3D printing and easiness of implementation in research groups with limited funds - Coverage of many scientific areas with 3D printing technology - Easiness on the adaptation of the technique to rapidly respond to a necessity	- Lung delivery being a niche research topic, meaning that it is for specific market - Questionable long-term sustainability to translate from the laboratory to the industry - Longer learning curve to work with design programs and 3D printing
Opportunities	**Threats**
- Market gap - Inclusion of 3D printing at a laboratory scale, increasing the potential and versatility of scientific experimentation - Design and development of other types of personalised devices/equipments/apparatuses	- Few funding opportunities - Development of simpler products and/or a cheaper portfolio of products that can compromise ideas/patents at a laboratory scale

The inclusion of 3D printing in the experimental method widens the applicability of this technology in the scope of scientific experimentation [89]. In fact, despite the many options in the market for devices/equipments/apparatuses, the economic limitations frequently experienced in science and some niche scientific domains without support, hinder much needed advancement [233]. The incorporation of these most recent technologies enables the development of more specific tools for experiments, which would not be feasible to be built at a large-scale endowing projects with new capabilities [234,235]. Notwithstanding, and despite 3D printing answering to a necessity, those are often niche problems, presenting a questionable long-term viability. In parallel, simplifications of commercialized devices are an opportunity for companies to build a cheaper portfolio of products, which can turn the concept at a laboratory scale completely unfeasible. However, despite the weaknesses and threats that can come with these ideas and technologies, all have proven to benefit science in some way, and that should be taken into consideration in the years to come.

This page was intentionally left in blank.

CHAPTER 2:

MOTIVATIONS AND OBJECTIVES

This page was intentionally left in blank.

Exploring new ways for the delivery of drugs has been one of the aims of pharmaceutical research, so that more effective treatments can be achieved, and current guidelines improved. Lung drug delivery has been getting a lot of attention, nowadays, especially concerning the local treatment of certain diseases, and to reach systemic delivery of the drugs. The production of dry powders, that can be used in these scenarios, has been evolving greatly and drug-loaded microparticles pose a viable strategy in this regard. Besides the internalisation of the drug itself, the encapsulating matrix can also play an important role in the treatment, as it can potentiate favourable interactions between cells, drug carriers, and the proper drugs. However, the study of dry powders in an *in vitro* setting proves to be challenging. Assays involving cells should require the insufflation of dry powder (instead of previous suspension in liquid) and apply conditions mimicking the air-liquid interface of the lung, in presence or absence of mucus depending on the desired therapeutic effect. There is a narrow range of apparatuses that can be used for dry powder insufflation over cell layers, but they are very expensive and translate into complex mechanics, often not suitable for more preliminary approaches. Despite that, it is recognizable that some applications would benefit from a tool that allows quantifying the interaction/affinity of particles towards the cells of interest.

The need to overcome the described limitation of cell-based *in vitro* assays involving testing dry powders was the driving force of the present PhD project. The development of tools to improve research on lung delivery using dry powders was proposed. In this case, it is envisaged the development of a device that allows the delivery of dry powders onto cell surfaces, thus simulating more appropriately the inhalation as a process, while quartz crystal microbalance (QCM) will be used to establish a technique enabling the determination of a dry powder deposition profile. Microparticles composed of locust bean gum will be used as model dry powders. The determination of the viability of respiratory cells after the insufflation of air with and without dry powder using the developed device will be performed. The concept of the project is depicted in Figure 2.1.

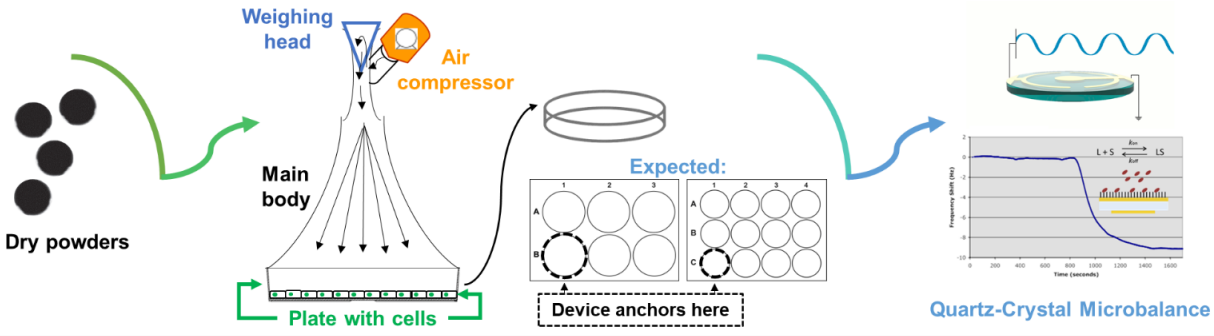

Figure 2.1 – Scientific diagram of the idea of the project. From left to right: dry powders containing microparticles are loaded into the weighing head (blue piece of a 3D-printed device), that is assembled to a main body placed on top of a cell support. Air coming from an air compressor will drag the powder down, and the deposition profile of the tested dry powders will be determined with the help of a Quartz-Crystal Microbalance (QCM). Additionally, the impact of air insufflation will be assessed in cell-based assays with and without dry powders. In future endeavours, the cell support will be interchangeable.

To accomplish the main objective, several partial goals were established, which are described below:

1) To develop a locust bean gum-based drug delivery platform, either a nano-in-micro formulation or a microparticle formulation;

2) To characterise the toxicological profile of locust bean gum as a matrix material and as a drug delivery platform;

3) To develop a device that enables the insufflation of dry powders over cultured cells;

4) To use the QCM to study the dosimetry of the developed device and ensure replicability;

5) To use the QCM for the determination of the deposition profile of several dry powders insufflated with the developed device;

6) To test the device in proof-of-concept assays of cell cytotoxicity.

In summary, the aim is to develop tools that can potentiate the reliability of *in vitro* assays by providing biorelevant conditions of the pulmonary conditions, while fostering their use in substitution of *in vivo* assays, whenever it is applicable.

CHAPTER 3:

DRY POWDER-BASED FORMULATIONS USING LOCUST BEAN GUM

The information contained in this chapter was partially included in the following publication:

Pontes, Jorge F.; Guerreiro, Filipa; Rosso, Annalisa; Alves, Ana D.; Rodrigues, Susana; da Costa, Ana M. Rosa; Lollo, Giovanna; Gaspar, Maria Manuela; Grenha, Ana. Toxicological profile of Locust Bean Gum (LBG) for inhalation: Excipient characterisation and biological evaluation. (under preparation)

This page was intentionally left in blank.

3.1. Introduction

Locust bean gum (LBG) has been proposed as a viable excipient in several drug formulation strategies. In fact, the Food and Drug Administration (FDA) has approved its use in oral dosage forms, as it is stated in the Inactive Ingredients Database [236]. Although the oral route is not the subject of this memory, it is important to say that several less explored materials are being considered (and used) to enable viable alternatives to current therapies [122]. LBG has been used in more conventional formulations as a thickener [237], but it can find uses in other formulation-based strategies. The inclusion of LBG in drug delivery systems such as microparticles and nanocarriers has been considered elsewhere [98,238]. Nevertheless, the eventual feasibility of application in nanocarrier formulation is relevant, as LBG may not display the best features for this end. In fact, solubility difficulties, requiring dispersion in hot water, the high viscosity if concentrations above 1% (w/v) are aimed, and the neutral character, hinder its usability [239,240]. Often, the methods for nanoparticle production make use of the charges provided by the chemical composition of the involved components, promoting the interaction between opposite charges with the consequent formation of nanocarriers [219]. A possible solution to overcome these limitations would be a change in LBG's chemical structure, by endowing it of certain chemical groups, that would promote these interactions [241].

The use of different LBG derivatives and even other polymers could constitute an interesting branching of polymer chemistry. In fact, the versatility provided by these chemical entities could resolve the complicated profiles of certain drugs, molecules that violate the Lipinsky's rule of five [242,243] and, complementarily, are in groups II-IV of the Biopharmaceutical Classification System [244]. Additionally, other types of formulations that rely on a two-phase system could link the polymer derivatives and the drugs, resulting in a viable approach towards therapy. In this section, LBG will be chemically modified and used in the preparation of lipid nanocarriers that will be characterised regarding physicochemical parameters. Afterwards, one of the formulations will be chosen and embedded in a mannitol matrix, so that a dry powder is obtained to be used in the upcoming tasks concerning the project herein explored.

3.2. Locust bean gum (LBG) to be used in nanoparticulate drug delivery systems

3.2.1. Materials and methods

3.2.1.1. Materials

LBG was a kind gift from Industrial Farense (LBG IF, Portugal), and its purified form was used throughout the works herein detailed. Chlorosulfuric acid ($HClSO_3$), dimethylformamide (DMF), potassium bromide (KBr) and D-mannitol were also purchased from Sigma-Aldrich®. 1,2-dioleoyloxy-3-trimethylammoniumpropanchloride (DOTAP) was a kind gift from Lipoid® (France). Rifabutin (RFB, $C_{46}H_{62}N_4O_{11}$, M_w 847.00 g/mol) was supplied from CHEMOS (Germany). Acetone was purchased from Labchem (Laborspirit, Portugal), ethanol 96% (v/v) was acquired from AGA (Portugal) and Miglyol® 812 from Acofarma (Spain). Ultrapure water (Milli-Q, Millipore, Watford, UK) was used throughout. All other chemicals were reagent grade.

3.2.1.2. Locust bean gum (LBG) purification

The presence of about 7% of proteins and impurities may hinder the subsequent uses of the polymer. Therefore, a purification step was required, which was based on a protocol reported elsewhere [241]. In brief, an amount of LBG was dispersed in ultrapure water heated at 85 ºC, for 1 h. After cooling of the dispersion to room temperature, it was centrifuged at 22 000 x g, 20 ºC for 20 min, and the supernatant precipitated in an equal volume of ethanol. With the help of a stainless-steel sieve, the precipitate was collected and separated into small threads, and dried in a vacuum oven at 30 ºC, for 72 h.

3.2.1.3. Synthesis of locust bean gum sulphate (LBG Su)

A sulphate derivative of LBG was prepared, in accordance with a previously reported protocol [241]. In brief, purified LBG was dispersed in water, precipitated with ethanol, and added do DMF at 60 ºC for 30 min. Afterwards, the SO3.DMF complex, previously prepared [245], was added to the mixture and left stirring for 4 h. After cooling to room temperature, sodium hydroxide 30% (m/v) solution was added to neutralize the mixture and induce the precipitation of a residue. Further concentration was achieved by evaporating the organic solvents. Subsequently, dialysis and freeze-drying were performed, to obtain LBG Su in its dry form.

3.2.1.4. Fourier-Transformed Infrared (FT-IR) spectroscopy for locust bean gum sulphate (LBG Su) analysis

For a characterisation purpose and to confirm the occurrence of the expected chemical reaction, LBG Su was analysed by FT-IR, as performed in [241]. To do so, a sample was blended with KBr in a mortar and compressed into a disc. The spectrum was collected by means of a 37-scan interferogram, in transmittance mode, in the 4000 to 400 cm^{-1} region, with a 4 cm^{-1} resolution (Bruker Tension 27, Bruker OPTIK GmbH, Germany). An OPUS software (version 6.5) was used for data acquisition and analysis.

3.2.1.5. Preparation of lipid nanocapsules (LNC)

The preparation of lipid nanocapsules (LNC) is often done using a solvent displacement technique [246], promoting the interaction between opposite charges of the involved components, resulting on the nanocarrier. In this work, an adaptation of the technique was used to prepare the LNC [247]. In brief, an organic phase comprised of 1,2-dioleoyloxy-3-trimethylammoniumpropanchloride (cationic lecithin – DOTAP), medium chain triglycerides (Miglyol® 812), ethanol and acetone was prepared and poured over the aqueous solution of LBG Su. The nanocapsules were formed upon contact of both phases, under intense magnetic stirring. Organic solvents were removed by evaporation, reaching a final volume of 10 mL. Different concentrations of DOTAP (0.05% and 0.1%, w/v) and LBG Su (from 0.2% to 2%, w/v) were tested to verify their effect on LNC characteristics.

3.2.1.6. Characterisation of lipid nanocapsules (LNC)

3.2.1.6.1. Morphology

LNC with and without LBG Su-coating were visualised using cryogenic transmission electron microscopy (Cryo-TEM), according to a protocol described elsewhere [248]. In brief, diluted samples were dropped onto a 300-mesh holey carbon film (Quantifoil R2/1) and quench-frozen in liquid ethane using a cryoplunge workstation (made at Laboratoire de Physique des Solides-LPS, Orsay, France). Afterwards, these meshes were placed on a precooled Gatan 626 sample holder, transferred into the microscope (Phillips CM120) and observed at an accelerating voltage of 120 kV.

3.2.1.6.2. Physicochemical characterisation

Following the successful preparation of LNC, the carriers were characterised, regarding their size and zeta potential, by diluting the samples in deionised water and a 0.1 mM potassium chloride solution, respectively (Zetasizer Nano ZS, Malvern Panalytical, UK).

3.2.1.6.3. Stability evaluation

The stability of LNC was evaluated based on the physicochemical characteristics, which were evaluated upon storage at 4 ºC, for a period of 90 days. At the various timepoints, aliquots of the samples were taken and prepared for measurement as detailed in the previous section.

3.2.1.7. Thermophysical characterisation of lipid nanocapsules (LNC) and their components

3.2.1.7.1. Differential Scanning Calorimetry (DSC)

The thermal behaviour of the materials was evaluated using a differential scanning calorimeter (DSC Q200, TA Instruments, Germany). Each sample was weighed (5 - 15 mg) into aluminium pans, which were sealed, and their lids pierced. Measurements were performed between -80 °C and 220 °C with various heating rates (10 °C/min and 20 °C/min), under a nitrogen atmosphere.

3.2.1.7.2. Thermogravimetric Analysis (TGA)

The thermal stability of all the materials was evaluated via Thermogravimetric Analysis (TGA 209-F1 Iris®, Netzsch, Germany). The samples (up to 15 mg) were heated from 20 °C up to 1000 °C, at a heating rate of 10 °C/min, under a nitrogen atmosphere.

3.2.1.8. Association of rifabutin to lipid nanocapsules (LNC)

The association of a hydrophobic antitubercular drug, RFB, was carried out before mixing the organic and the aqueous phase (section 3.2.1.5). A stock solution of RFB was prepared by dissolution in ethanol 96% (v/v; 13.2 mg/mL), under magnetic stirring for 10 min, at room temperature, protected from light. Several dilutions of the stock solution were prepared depending on the desired drug loading (0.5-10%, w/w).

RFB solutions in ethanol were added to the organic phase prior to pouring over the aqueous phase.

3.2.1.9. Spray-drying of lipid nanocapsules (LNC)

A solution of mannitol (4%, w/v) was prepared in ultrapure water and mixed with the LNC before spray-drying. Both unloaded and RFB-loaded LBG Su-based LNC were processed. In all cases, microparticles of mannitol/LNC = 85/15 (w/w) were prepared using a Buchi B-290 laboratory mini spray-dryer (Buchi Labortechnik AG, Switzerland) equipped with a high-performance cyclone. A spray flow rate of 473 L/h was set, along with an inlet temperature of 103 ºC, aspirator at 100% and flow rate at 4.3 mL/min. The yield of spray-drying process was calculated by gravimetry, using Equation 3.1:

$$Yield\ (\%) = \frac{Weight\ of\ microparticles\ (g)}{Total\ amount\ of\ solids\ (g)} \qquad \text{(Equation 3.1)}$$

3.2.1.10. Dry powder characterisation

The obtained microparticles were characterised regarding morphology by field emission scanning electron microscopy (FESEM Ultra Plus, Zeiss, Jena, Germany). Samples were placed onto metal plates and a 5 nm thick iridium film was sputter-coated (model Q150T S/E/ES, Quorum Technologies, Lewes, UK) on the dry powders before viewing. Microparticle geometric size was estimated as the Feret's diameter and was directly determined by the manual measurement of 300 microparticles on the photographs obtained by FESEM.

3.2.1.11. Statistical evaluation

A two-way analysis of variance (ANOVA, Dunnett's test) with the pairwise multiple comparison procedure was used to compare results obtained for the stability assay. Two different sets were analysed: (1) size, polydispersity index and ζ-potential obtained in days 15, 30, 45, 60, 75 and 90 were compared with the data obtained on day 1 to evaluate any time-dependent effect, and (2) size, polydispersity index and ζ-potential obtained for different formulations, where the amount of the materials varied, were compared with each other to ascertain the existence of a concentration-dependent effect. All analyses were run using the GraphPad Prism® statistical

program (GraphPad Software, version 9.4.0.673), differences being considered significant at a level of $p < 0.05$.

3.2.2. Results and discussion

3.2.2.1. Preparation of the locust bean gum (LBG) derivative

Prior to its use, the commercially obtained LBG underwent a process of purification. The purified LBG was afterwards used to perform the chemical modification necessary to obtain the sulphate derivative, following the protocol detailed in [241], which was used to produce the lipid nanocarriers. Figure 3.1 shows the chemical structures of both the purified LBG (LBG IF) and the LBG Su, along with a FTIR spectra of both.

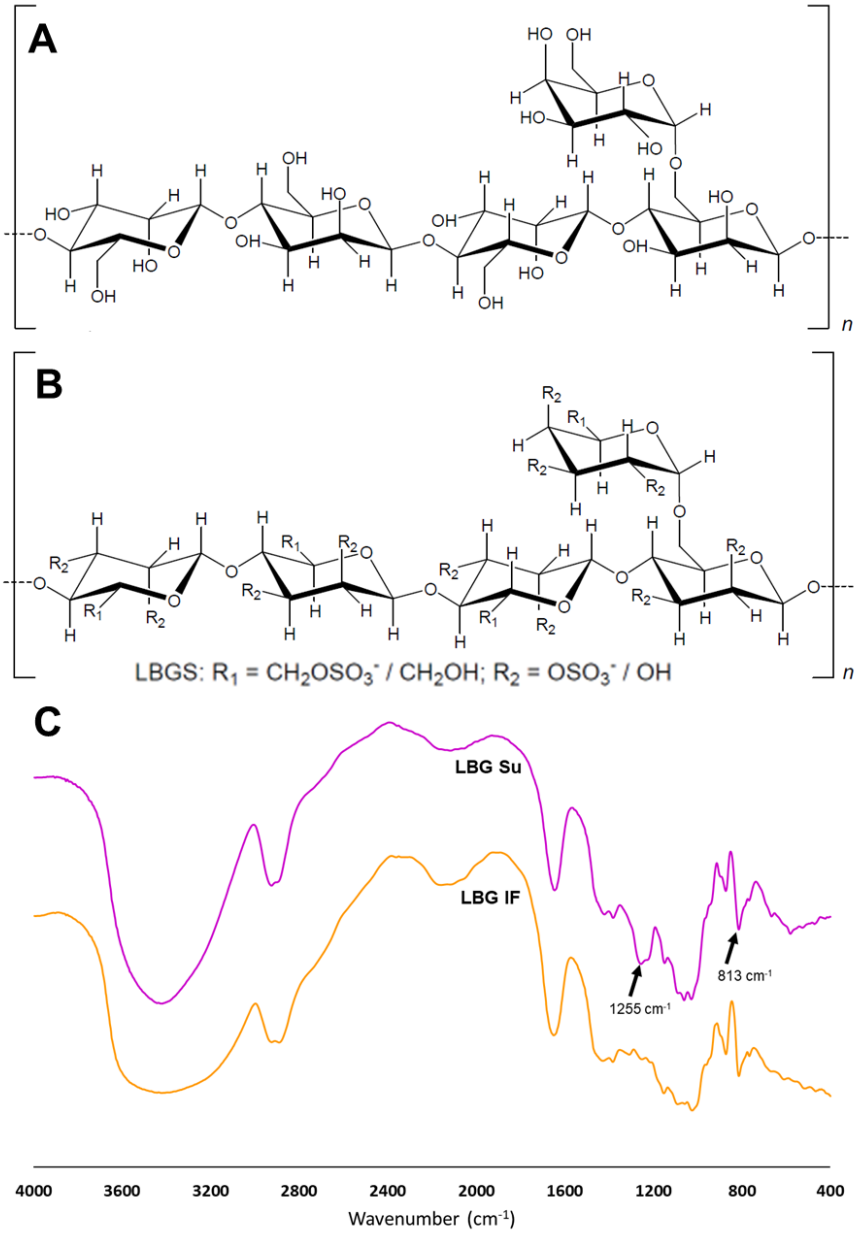

Figure 3.1 – From top to bottom: chemical structures of purified LBG from Industrial Farense (A, LBG IF) and of its sulphate derivative (B, LBG Su), and their respective FTIR spectra (C): orange for LBG IF and purple for LBG Su (●●, Table B.I and B.III in Annex B). Arrows indicate bands characteristic of sulphate groups.

The FTIR spectrum for LBG Su has two bands approximately at 1255 cm^{-1} and 813 cm^{-1} corresponding to the stretching of S=O and C-O-S bonds. These two bands indicate the presence of sulphate groups and confirm that the reaction was successful. In fact, the referred bands are absent in the spectrum of purified LBG, only appearing in that of LBG Su.

3.2.2.2. Preparation and characterisation of lipid nanocapsules (LNC)

Overcoming the obstacles associated with drug solubility remains in certain cases as one of the most challenging aspects of formulation work. Following the preparation of a LBG derivative, three different formulation strategies were considered to prepare nanocarriers: (1) LNC, (2) lipid nanoparticles and (3) nanoemulsion, Nevertheless, only the first method revealed successful in generating viable carriers, without any sign of precipitation of materials and breaking of the formulation. For that reason, all data presented in this section are related to the production of LNC using the technique of solvent displacement. The produced carriers consist of a core composed of a mixture of medium chain triglycerides (Miglyol® 812) and DOTAP, expected to load any drugs being associated, and the LBG Su provides a coating of the carrier. The concentrations of both LBG Su and DOTAP used in the formulation were varied and the obtained results depicted in Table 3.1.

Table 3.1 – Physicochemical characteristics of LBG Su-coated lipid nanocapsules (mean ± SD, n = 3).

LBG Su/DOTAP (%, w/v)	Size (nm)	PdI	Z-potential (mV)
0.2/0.05	210 ± 5	0.089 ± 0.029	-73 ± 4
0.2/0.1	228 ± 13	0.119 ± 0.019	-72 ± 3
0.5/0.05	217 ± 9	0.106 ± 0.040	-84 ± 4
0.5/0.1	207 ± 5	0.081 ± 0.035	-80 ± 3
1.0/0.05*	194	0.039	-77
1.0/0.1*	183	0.046	-77
2.0/0.05*	231	0.194	-79
2.0/0.1*	194	0.103	-82

Note: Formulations presenting an asterisk (*) were only prepared once, thus no standard deviation was determined (n = 1).

The sizes of the various formulations of LNC prepared were quite similar, varying roughly between 180 and 230 nm. Moreover, low polydispersity index was transversally obtained, indicating monodisperse populations (PdI < 0.2 and in most cases ≤ 0.1). The ζ-potential varied between -72 and -84 mV, results that can be attributed to the high negative charge density of the LBG Su coating of the LNC.

Despite the presence of the positive charge density of DOTAP, it is not sufficient to counter the negative charge density provided by the LBG Su, resulting in an insignificant contribution to the overall ζ-potential of the nanocarrier. Additionally, the variation of the LBG Su concentration did not influence the surface charge of the particles in all prepared formulations, resulting always in negatively charged nanocarriers. These observations suggest that the variation of the amount of both LBG Su and DOTAP does not have a pronounced effect on the physicochemical parameters of the formulations. Considering these data, and the time and economic constraints, it was decided to continue the assays with the LNC composed by lower amounts of LBG Su and DOTAP. The experimental method used to obtain LBG Su is a very slow process, often resulting in insufficient amounts to adequately compensate the time investment. Moreover, DOTAP is an extremely expensive reagent and highly sensitive to degradation, which justifies the use in limited amounts. For these reasons, LNC comprised of 0.2% (w/v) and 0.5% (w/v) of LBG Su and of 0.05% (w/v) and 0.1% (w/v) of DOTAP, in a total of four formulations, were selected to pursue further experimentation. A stability evaluation was performed at 4 ºC, monitoring size, polydispersity index and ζ-potential of the LNC for 3 months. Figure 3.2 shows the variation of the parameters.

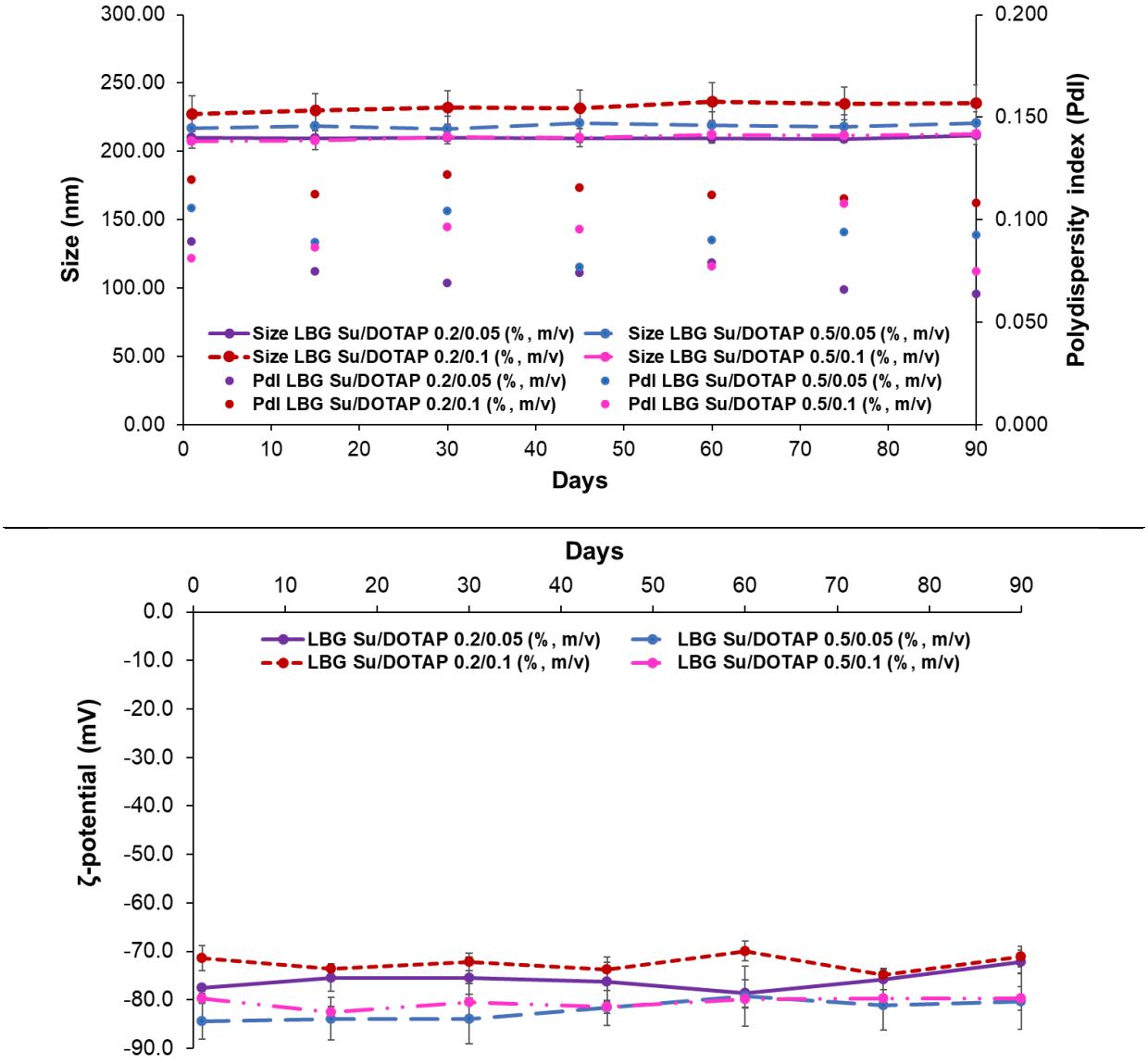

Figure 3.2 – Evolution of size and polydispersity index (top) and ζ-potential (bottom) of LBG Su-coated lipid nanocapsules (●●●●, Table B.II in Annex B), upon storage at 4 ºC, over the course of 90 days. Data represent mean ± SD, n = 3.

Regarding the size of the formulations, upon storage at 4 ºC and considering the measurement at day 1 as a reference, the size ratio (comparison of final size with the initial size) was maintained at 1.0 for all formulations, which indicates the stability of this parameter for the analysed interval. As for the polydispersity index, no statistical difference was noticed in the analysis performed, which can be an indication of the maintenance of the homogeneity of the formulations, suggesting no major aggregation of the nanocapsules and an indication that the populations

remained monodisperse. Concerning the ζ-potential, again no statistical difference was observed for the comparisons between different days. Small differences found are too spread between formulations, which hinders a definitive conclusion about the impact of the charges of the polymer in this parameter. Notwithstanding, after the screening herein discussed, the chosen formulation was LBG Su/DOTAP (0.5/0.1, % m/v). This will be used in the subsequent assays, regarding encapsulation of a model drug and its conversion into a dry powder by means of spray-drying, which will be discussed later.

While formulating, a need to deepen the understanding of the structure and physicochemical aspects of these LNC became evident. For that matter, thermal behaviours were characterized by DSC and TGA. The former allows the possibility to determine the crystallinity of a polymer, its melting and crystallisation temperatures and the discovery of the glass transition temperature, an important parameter in lyophilisation processes [249]. On the other hand, TGA requires the samples to go through a range of temperatures to understand a product's stability threshold. Their integrity is measured by means of loss of mass throughout the process. Additionally, TGA allows the understanding of the maximum temperatures the polymers can withstand, and it is a complementary technique to DSC, helping the latter to be more efficient [250]. Figures 3.3 and 3.4 show the diagrams obtained for several materials used in the production of these nanocarriers by DSC and TGA, respectively.

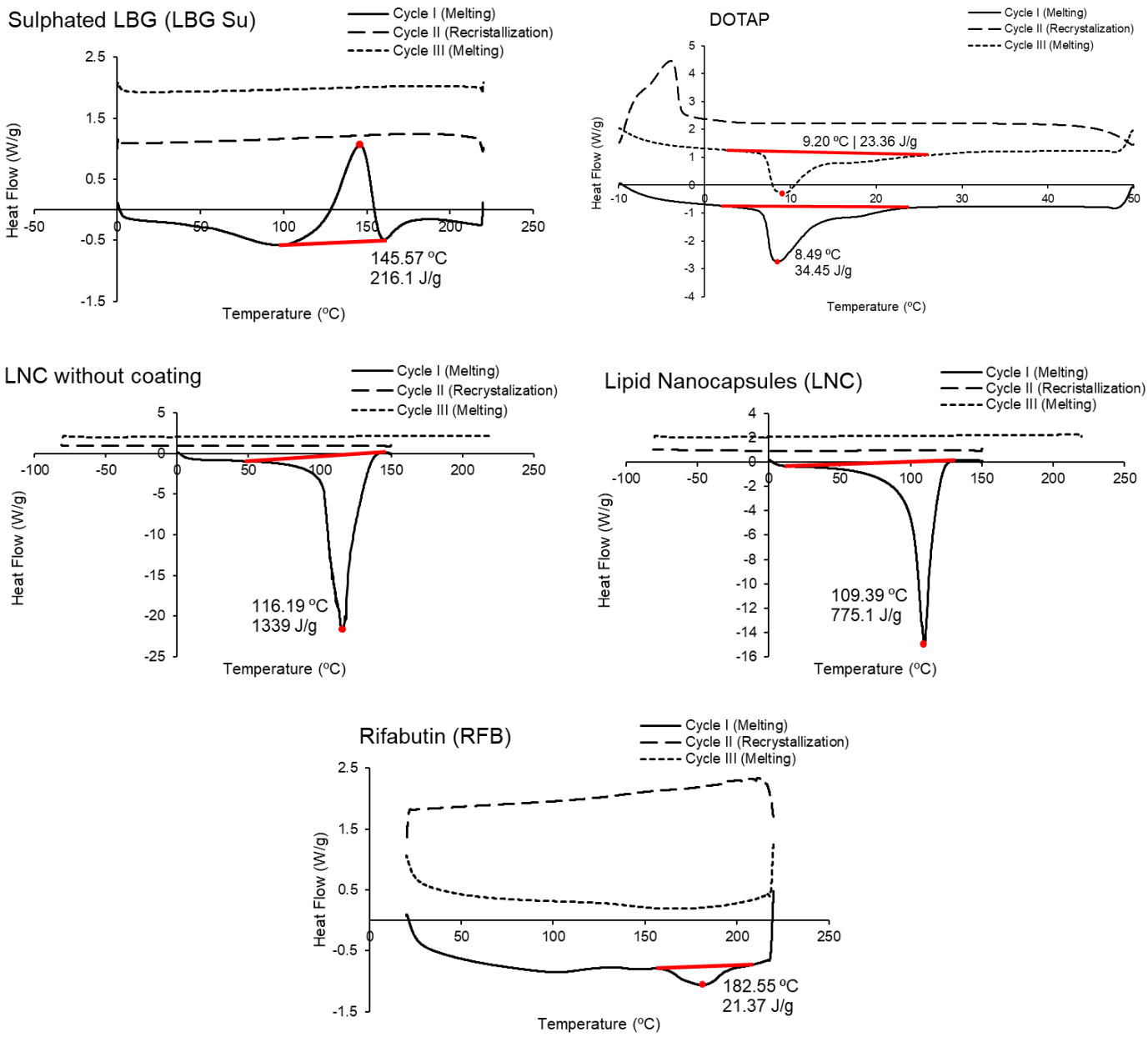

Figure 3.3 – Differential scanning calorimetry curves for A) LBG Su, B) cationic lecithin – DOTAP, C) LNC without coating, D) LBG Su-coated LNC and E) rifabutin (RFB).

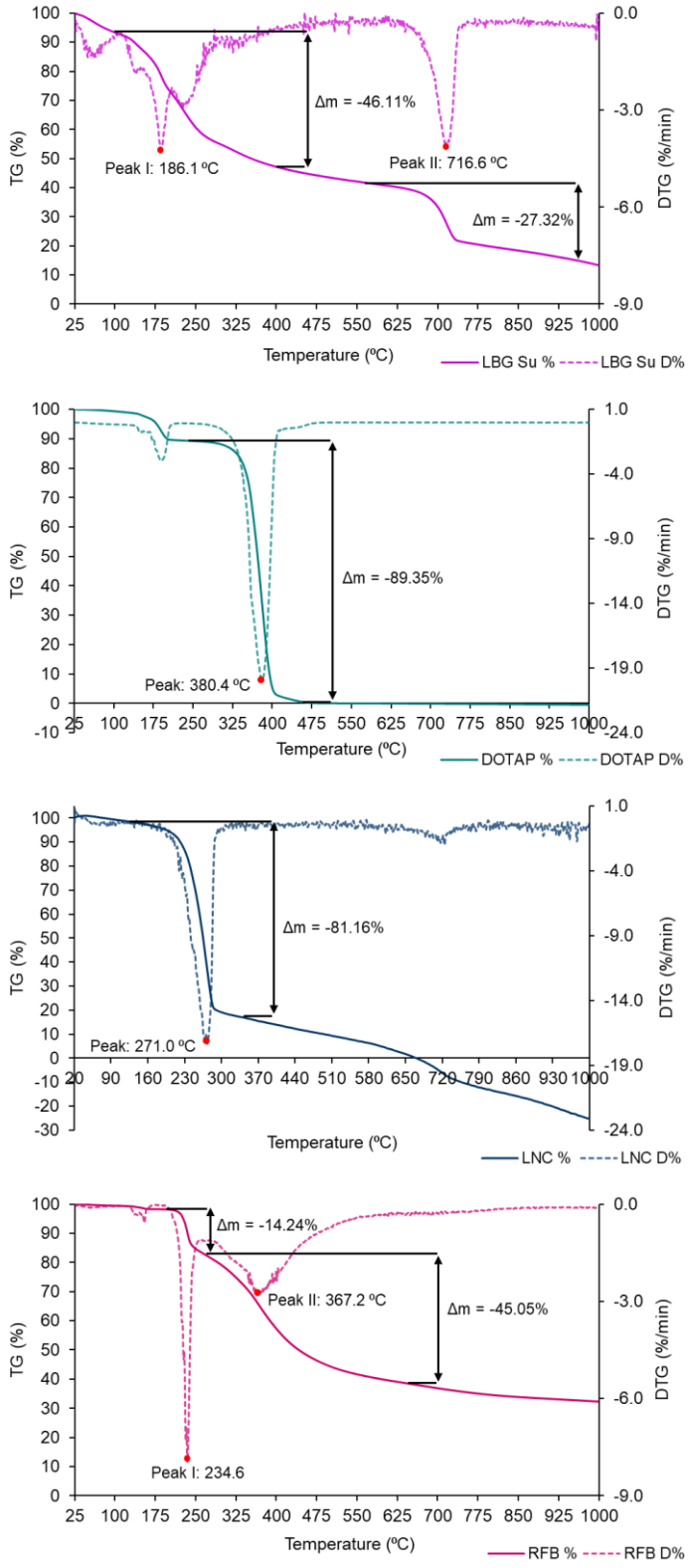

Figure 3.4 – From top to bottom, thermogravimetric curves for LBG Su, cationic lecithin – DOTAP, LNC and rifabutin (RFB) (●●●●, Table B.I in Annex B). The continuous lines refer to the variation of mass of the polymers throughout the process (TG, %), and the dashed lines are the respective derivatives (DTG, %/min).

Figure 3.3 shows different DSC diagrams of the materials used in the production of the LNC. The DSC diagram for LBG Su was unexpected, as no peak related to either melting or recrystallisation could be detected. There is one exothermic peak at 145 ºC, which so far could not be attributed to any event. The second graphic refers to DOTAP, with a clear melting point around 8-9 ºC, which is in accordance with what is found in the literature [251]. The next two graphs, which are related to the uncoated LNC (no LBG Su present) and the LBG Su-coated LNC, both show an endothermal peak around 100 ºC, which is attributed to the evaporation of the water during the heating phase of the DSC cycle. In fact, in the next cycles of recrystallisation, no other peaks are shown (dashed lines). Lastly, the graph concerning RFB suggests that this drug is crystalline, showing a melting peak around 183 ºC, a result comparable to the works of Upadhyay and their team [252], but a bit above what was reported by Gaspar *et al.* [253]. As no other peaks were detected in the analysis of the mentioned compounds, the glass transition temperature (T_g) could not be detected in any of them.

Continuing the analysis of the thermal behaviours of the LNC components, the TGA diagrams are shown in Figure 3.4. Concerning LBG Su, much like the DSC graph, its behaviour is somewhat erratic, as it starts to lose mass at lower temperatures, having a first peak at 186 ºC. Another loss of mass occurs at higher temperatures (716 ºC), but further testing should be performed to ascertain the thermal behaviour of this derivative. DOTAP showed two important variations of mass: one at 190 ºC of 10% (not shown), and the major loss at 380 ºC. By the end of the analysis, no DOTAP remained in the pan, which is also true for the LNC formulation, that lost around 81% of its total mass at 271 ºC. For RFB, there were two main events of mass loss: one at around 235 ºC of about 15% and the second is a more progressive event resulting in a total loss of 60% by the end of the assay, a behaviour observed elsewhere [252].

The thermal characterisation of components used in formulation development is crucial. Often, the use of lipids in formulations require experimental methods that rely on the use of temperature. One of those examples is the phase-inversion temperature (PIT) method, that uses the change in solubility of surfactants at different temperatures, to obtain other types of lipid-based carriers, such as

nanoemulsions [254] and solid lipid nanoparticles [255]. The knowledge of the adequate temperature interval helps on the establishment of an adequate protocol and its further optimisation, thus preventing unwanted and unforeseen degradation of the components used.

Following the thermal behaviours, the selected LNC were also characterised using cryo-TEM. This is a technique derived from TEM, in which it is required the rapid freezing of fresh sample in liquid ethane prior to the observation [256]. The observations were made for: 1) the LBG Su-coated LNC and 2) the uncoated LNC, and the corresponding microphotographs are illustrated in Figure 3.5.

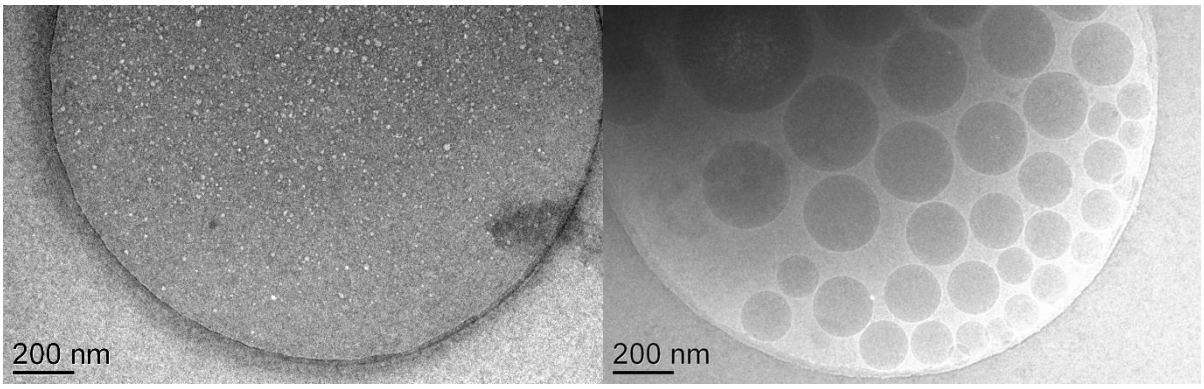

Figure 3.5 – Cryo-TEM photographs of uncoated LNC (left) and LBG Su-coated LNC (right).

From the obtained photographs, it is suggested that the polymeric coating plays a pivotal role in the stability and integrity of the LNC. On the left part of Figure 3.5, the LNC without the polymeric coating render unstable systems that do not survive the sample preparation process, thus, the grids seem plain. On the right part of Figure 3.5, the LNC with the polymeric coating are very well defined, showing various sizes. The smaller particles are closer to the border of the grid, while larger ones are more central. This finding suggests that, despite the polydispersity being smaller than 0.1 (on a scale of 0 to 1), as determined by DLS, there is still some heterogeneity of sizes for the lipid nanocarriers. In fact, results obtained by DLS measures refer to averages concerning the distribution of the physicochemical parameters for a given formulation. Cryo-TEM, as evidenced in Figure 3.5, enhances the LNC particles individually. However, despite the different sizes observed in the photographs, the

LNC can be considered as homogeneous. Moreover, both techniques (DLC and Cryo-TEM) can be considered complementary, providing different data that result in an thorough characterisation of these lipid systems.

After the steps of optimisation and characterisation of the LNC, the conditions to associate a drug were achieved. For several years, an intense work in the context of tuberculosis therapy involving the development of a dry powder containing antibiotic-loaded polymeric microparticles has been performed by the research group, where RFB was used as antibiotic. For this reason, RFB was chosen as a model drug, to continue the assays. Several amounts of RFB that correlate with a specific theoretical drug loading were tested, which can be found in Table 3.2.

Table 3.2 – Screening of the different amounts of rifabutin (RFB) tested with the respective theoretical drug loading.

LBG Su-based LNC with RFB							
RFB (mg)	0.33	0.66	1.32	1.98	2.64	3.30	6.60
Theoretical drug loading (%)	0.5	1.0	2.0	3.0	4.0	5.0	10

The first attempt was the encapsulation of 6.6 mg of RFB, corresponding to 10% of theoretical drug loading. This percentage was chosen to maximise the use of the RFB and the characteristics of the LNC. Moreover, similar concentrations were tested elsewhere [196], being helpful on corroborating testing this higher amount. There were no solubility limitations, as RFB is added to the organic phase prior to the LNC formulation. However, this production was halted as it can be seen in Figure 3.6.

Figure 3.6 – Round-bottom flask with the remains of the LNC formulation and RFB precipitated in the laterals.

The figure shows the precipitation of RFB all around the flask, which is not suitable. Similar behaviours were obtained when amounts of RFB corresponding to theoretical drug loadings as low as 3% were tested. Successful encapsulation was only possible for the lower amounts of RFB (between 0.5% and 2% drug loading) as depicted in Figure 3.7.

Figure 3.7 – LNC formulations containing different amounts of RFB. From left to right, LNC with 0.5, 1.0 and 2.0% of theoretical drug loading.

After obtaining the optimised RFB-loaded LNC, the objective was to endow the formulation with suitable characteristics for an application in inhalation. On a first approach, the unloaded optimised LNC were used to that end. To do so, spray-drying was performed using mannitol (4%, w/v) as an embedding matrix, with the

parameters detailed in Section 3.2.1.9. A morphological analysis was performed afterwards by FESEM, and representative microphotographs of the microparticles are shown in Figure 3.8.

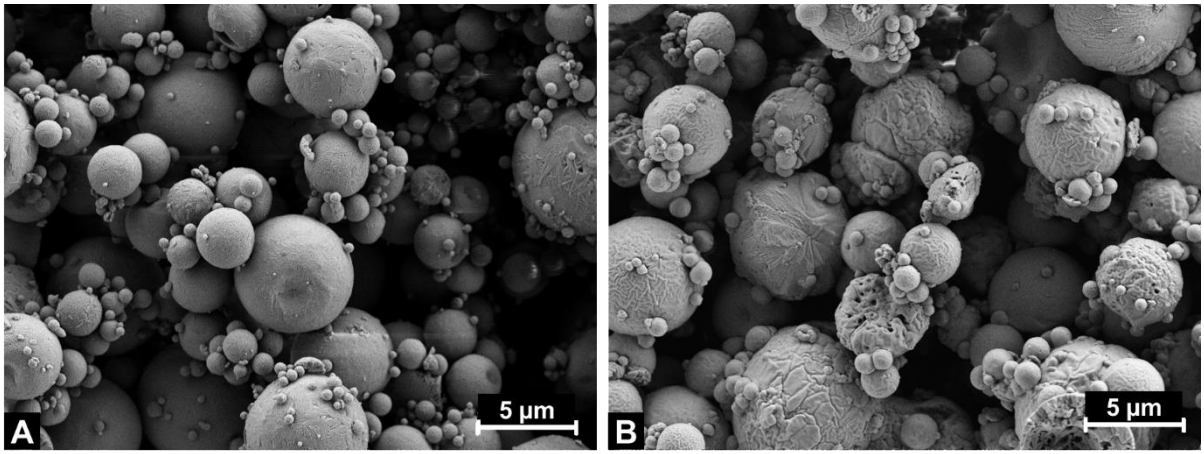

Figure 3.8 – Representative microphotographs of microparticles composed of (A) mannitol and (B) mannitol/unloaded lipid nanocapsules (85/15, w/w) obtained by field emission scanning electron microscopy (FESEM).

A yield of 84% was obtained for mannitol microparticles, while microparticles containing unloaded LNC (mannitol/LNC = 85/15, w/w) resulted in 73% yield. Furthermore, their Feret's diameter was determined to be 2.6 ± 1.8 µm and 3.1 ± 1.9 µm, respectively. The obtained microphotographs evidence a spherical shape for both formulations, as depicted in Figure 3.8. A closer look on the surface of microparticles shows needle-shaped crystals, which are present in both mannitol and mannitol/unloaded LNC microparticles (Figure 3.9).

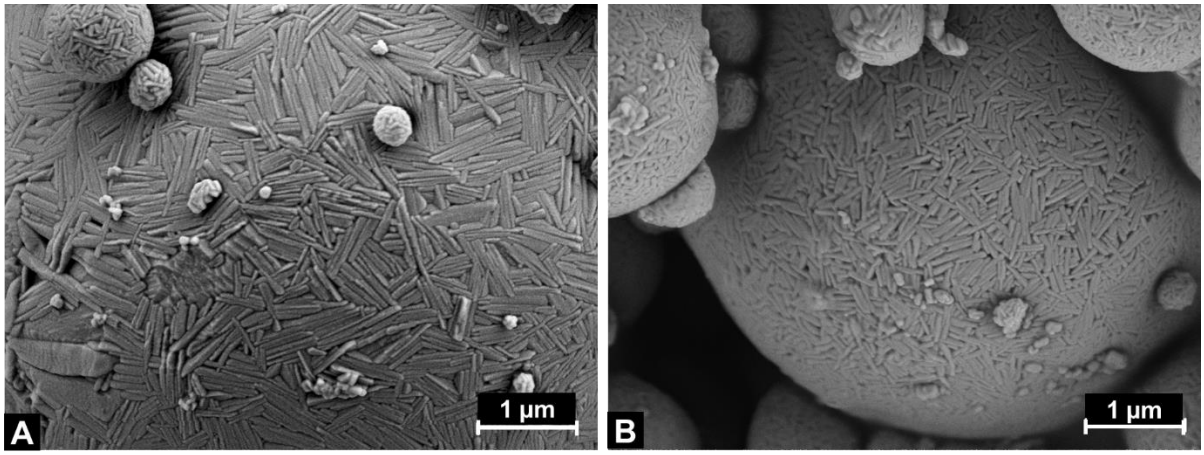

Figure 3.9 – Representative microphotograph of the surface of mannitol (A) and mannitol/LNC (85/15, w/w) (B) microparticles obtained by scanning electron microscopy (SEM).

These findings have already been reported in the context of the spray-drying of mannitol [257-259]. The crystals are attributed to mannitol, which suggests, in this case, that the lipid nanocapsules are inside the particle, thus a successful encapsulation taking place. The following stage was aimed at obtaining an inhalable dry powder containing the drug-loaded LNC (Figure 3.10). The LNC were mixed with mannitol to obtain a mannitol/LNC ratio of 85/15 (w/w).

Figure 3.10 – Photographs showing the production of microparticles containing rifabutin (RFB)-loaded LNC.

For a total amount of solids of 416.19 mg, only 43 mg were collected after the process, resulting in a yield of 10.33%. Contrary to what was observed with the unloaded LNC formulation, this latter test was not successful. One possibility that could explain this occurrence relates to the interaction between RFB and the other components of the formulation, leading to a possible break of the LNC and the appearance of an oily layer on the high-performance cyclone. Another possible explanation relates to the formation of the droplets at the end of the injector. Due to the hydrophobic character of the oil, it tends to escape from the water by accumulating on the surface of the droplet. In turn, while the water evaporates, the droplet shrinks in the opposite direction, towards the centre. This could influence the migration of mannitol, and its subsequent process of establishing a sturdy solid structure to efficiently encapsulate the lipid carrier (as seen in Figure 3.8), which ultimately leads to unsuccessful formation of microparticles.

Considering all the data herein discussed, concerning significantly low amounts of RFB being encapsulated and the negligible amount of powder recovered after spray-drying, a decision to not pursue this formulation further was made. A new approach, involving optimisation, is required, being a possibility for future projects.

3.3. Locust bean gum (LBG) matrix in microparticulate drug delivery systems

Up to this point, lipid nanocarriers were the focus of the formulation section of the project. However, due to the unexpected limitations concerning its transformation into a dry powder, the focus had to shift. Despite the reported uses of LBG as inhalable microparticle matrix, in previous works of the research group [219,220], the developed formulation involved the use of hydrochloric acid as a means to decrease the viscosity of the gum and enable a more favourable drying process. Even if the impact on cell viability was minimal [219], it was recognised that the formulation could benefit from an even further optimisation. The objective herein was, thus, to perform a deeper study of LBG characteristics and establish a spray-drying protocol permitting the production of microparticles suitable for lung delivery purposes.

3.3.1. Materials and methods

3.3.1.1. Materials

Three LBG raw materials were obtained from different sources: one was acquired from Sigma-Aldrich® (polymer origin: Italy) and the other two were kind gifts from Industrial Farense® (Faro, Portugal; polymer origin: Portugal) and C.E. Roeper® (Germany; polymer origin: Mediterranean region, unspecified). Sodium azide (NaN_3) was purchased from Sigma-Aldrich®. Ultrapure water (Milli-Q, Millipore, Watford, UK) was used throughout.

3.3.1.2. Locust bean gum (LBG) purification

The purification of LBG was performed as detailed in Section 3.2.1.2, being applied to the samples from the three suppliers.

3.3.1.3. Fourier-transform infrared spectroscopy (FT-IR)

The FTIR method used to characterize the three different purified LBG samples was already described in Section 3.2.1.4.

3.3.1.4. Spray-drying to obtain locust bean gum (LBG)-based microparticles

Purified LBG corresponding to the three different samples was used to produce microparticles by a technique of spray-drying (Buchi B-290 laboratory mini spray-dryer, Buchi Labortechnik AG, Switzerland). An amount of LBG was weighed and

dispersed in ultrapure water (1%, m/v) at 85 ºC for 1 h for solubility enhancement [239]. After cooling to room temperature, the dispersion was left under mild stirring overnight. The next day, the LBG dispersion was heated again (85 ºC) before spray-drying, to decrease its viscosity. The apparatus was equipped with a high-performance cyclone and the conditions were as follows: spray flow rate of 473 L/h, inlet temperatures varying between 103 ºC and 160 ºC, aspirator at 100% and feed flow rate set at 1.0 mL/min. The yield of the process was calculated using equation 3.1, as described in section 3.2.1.9.

3.3.1.5. Characterisation of locust bean gum (LBG)-based microparticles

The morphology of the microparticles was determined by field emission scanning electron microscopy (FESEM; FESEM Ultra Plus, Zeiss, Oberkochen, Germany), using a protocol detailed in [260]. The size of the microparticles was determined as the Feret's diameter by the manual measurement of 300 particles, registered from the photographs obtained by FESEM.

3.3.1.6. Molecular weight distribution

High Performance Size Exclusion Chromatography (HPSEC) with a refractive index detector (Knauer K-2300, Berlin, Germany) was used to analyse commercial and purified LBG from three different suppliers, as well as the LBG-based microparticles. Two columns OHpak SB-806M HQ of 300 × 8.0 mm were used in series with a 50 × 6.0 mm OHpak SB-G 6B guard column (Shodex, Tokyo, Japan). Ultrapure water with 0.02% NaN_3 was used as mobile phase at a flow rate of 1 mL/min. Samples were dissolved in the solvent used as mobile phase at a concentration of 1 mg/mL and filtered through a 0.45 µm size-pore filter (VWR, Portugal). Pullulan standards were injected and used to draw a calibration curve, as used elsewhere [260-262]. Results were analysed using a commercially available chromatography software (Clarity, version 8.8.0, DataApex). The equation for the analysis model (Equation 3.2) is as follows:

$$y = 0{,}00022x^3 - 0{,}02579x^2 + 0{,}06427x + 10{,}18816 \qquad \text{(Equation 3.2)}$$

The model presented above was employed in the chromatogram of the materials analysed for the calculation of molecular weight results (M_n = number-average

molecular weight, M_w = average molecular weight). Furthermore, the broadness of the peaks obtained in the chromatogram that translates into a polydispersity index can be calculated using the former parameters [263] in Equation 3.3:

$$PDI = \frac{M_w}{M_n} \quad \text{(Equation 3.3)}$$

3.3.1.7. Thermophysical features of locust bean gum (LBG) and locust bean gum (LBG)-based microparticles

3.3.1.7.1. Thermogravimetric analysis (TGA)

The thermal stability of all LBG-based samples (commercial LBG, purified LBG and microparticles) was evaluated via Thermogravimetric Analysis (TGA 209-F1 Iris®, Netzsch, Germany). The samples (up to 15 mg) were heated from 20 °C up to 1000 °C, at a heating rate of 10 °C/min, under a nitrogen atmosphere.

3.3.1.7.2. Differential Scanning Calorimetry (DSC)

The thermal behaviour of the various LBG samples was evaluated using a differential scanning calorimeter (DSC Q200, TA Instruments, Germany). Each sample was weighed (5 - 15 mg) into aluminium pans, which were sealed, and their lids pierced. Measurements were performed between -80 °C and 250 °C with a heating rate of 10 °C/min, under a nitrogen atmosphere, and for three cycles per sample.

3.3.2. Results and discussion

3.3.2.1. Purification and preparation of locust bean gum (LBG)-based microparticles

Polymer purification is one important step for formulation development. For LBG the situation is no different, as it retains around 7% of impurities and proteins, requiring removal. The purification step was performed prior to the use of LBG using a methodology involving ethanol precipitation, which is described elsewhere [241,264]. The yield of purification was 66% on average, for LBG from the three different suppliers. Henceforth, and unless stated otherwise, the LBG that will be used will be the purified one.

Previous works using LBG as a polymeric material for the preparation of spray-dried microparticles required the use of hydrochloric acid to reduce the viscosity of the gum and increase the polymer concentration to be used [219]. However, an optimisation was desired to avoid the use of the acid. A screening of inlet temperatures of the spray-drying process between 103 ºC and 160 ºC was performed, with the main objective of using the lowest possible temperature for the obtention of LBG-based microparticles, while obtaining a powder with good flow properties and a satisfactory yield of production. The screening of temperatures for microparticles prepared with LBG from Sigma-Aldrich® is shown in Table 3.3.

Table 3.3 – Screening of different temperatures used in the production of LBG microparticles composed of LBG from Sigma-Aldrich®. Data represent mean ± SD, n = 3.

LBG-based microparticles, Sigma-Aldrich®				
T_{inlet} (ºC)	**T_{outlet} (ºC)**	**Aspirator (%)**	**Feed flow (mL/min)**	**Yield (%)**
103 ± 1	66-72	100	0.88 ± 0.05	51.9 ± 3.1
110 ± 1	70-84		0.89 ± 0.01	54.9 ± 3.8
120 ± 1	73-79		0.90 ± 0.05	55.2 ± 2.2
130 ± 1	**81-88**		**0.90 ± 0.01**	**55.5 ± 3.1**
140 ± 1	88-93		0.86 ± 0.01	55.5 ± 2.4
150 ± 1	93-100		0.89 ± 0.01	60.5 ± 2.6
160 ± 1	98-105		0.89 ± 0.03	58.0 ± 4.2

The study continued and the screening of temperatures for microparticles prepared with LBG from Industrial Farense® is shown in Table 3.4.

Table 3.4 – Screening of different temperatures used in the production of LBG microparticles composed of LBG from Industrial Farense®. Data represent mean ± SD, n = 3.

LBG-based microparticles, Industrial Farense®				
T_{inlet} (ºC)	T_{outlet} (ºC)	Aspirator (%)	Feed flow (mL/min)	Yield (%)
103 ± 1	67-77	100	0.81 ± 0.01	51.1 ± 1.7
110 ± 1	72-80		0.79 ± 0.03	56.3 ± 0.8
120 ± 1	75-82		0.81 ± 0.02	56.2 ± 6.3
130 ± 1	**82-100**		**0.78 ± 0.03**	**57.8 ± 3.4**
140 ± 1	87-91		0.85 ± 0.05	57.2 ± 5.0
150 ± 1	94-102		0.91 ± 0.03	53.3 ± 3.8
160 ± 1	98-107		0.86 ± 0.04	58.6 ± 3.9

Lastly, the screening of temperatures for microparticles prepared with LBG from C. E. Roeper® is shown in Table 3.5.

Table 3.5 – Screening of different temperatures used in the production of LBG microparticles composed of LBG from C. E. Roeper®. Data represent mean ± SD, n = 3.

LBG-based microparticles, C. E. Roeper®				
T_{inlet} (ºC)	T_{outlet} (ºC)	Aspirator (%)	Feed flow (mL/min)	Yield (%)
103 ± 1	65-75	100	0.84 ± 0.03	54.1 ± 2.6
110 ± 1	71-76		0.84 ± 0.03	54.4 ± 2.3
120 ± 1	79-82		0.81 ± 0.04	57.3 ± 2.8
130 ± 1	**83-87**		**0.82 ± 0.02**	**60.4 ± 3.0**
140 ± 1	85-94		0.82 ± 0.04	60.4 ± 4.8
150 ± 1	93-107		0.80 ± 0.00	64.3 ± 3.4
160 ± 1	89-110		0.82 ± 0.05	66.4 ± 0.2

After the preparation of all dry powders, a macroscopic analysis was performed focusing on the overall aspect and the occurrence of visible aggregation. All the prepared powders seemed similar, and considering the yields obtained for different temperatures, the chosen formulation was the one with an inlet temperature of 130 ±

1 ºC. This temperature ensured a compromise with an inlet temperature that is intermediate and an acceptable yield of around 55-60% for all the tested materials.

Following the choice of the conditions to produce LBG-based microparticles, the need for a deeper understanding of the polymer characteristics and its behaviour while in a dispersion and as matrix to be used in drug delivery carriers, was identified. A morphological analysis performed by FESEM was carried out on each LBG-based microparticles and the respective photographs are displayed in Figure 3.11.

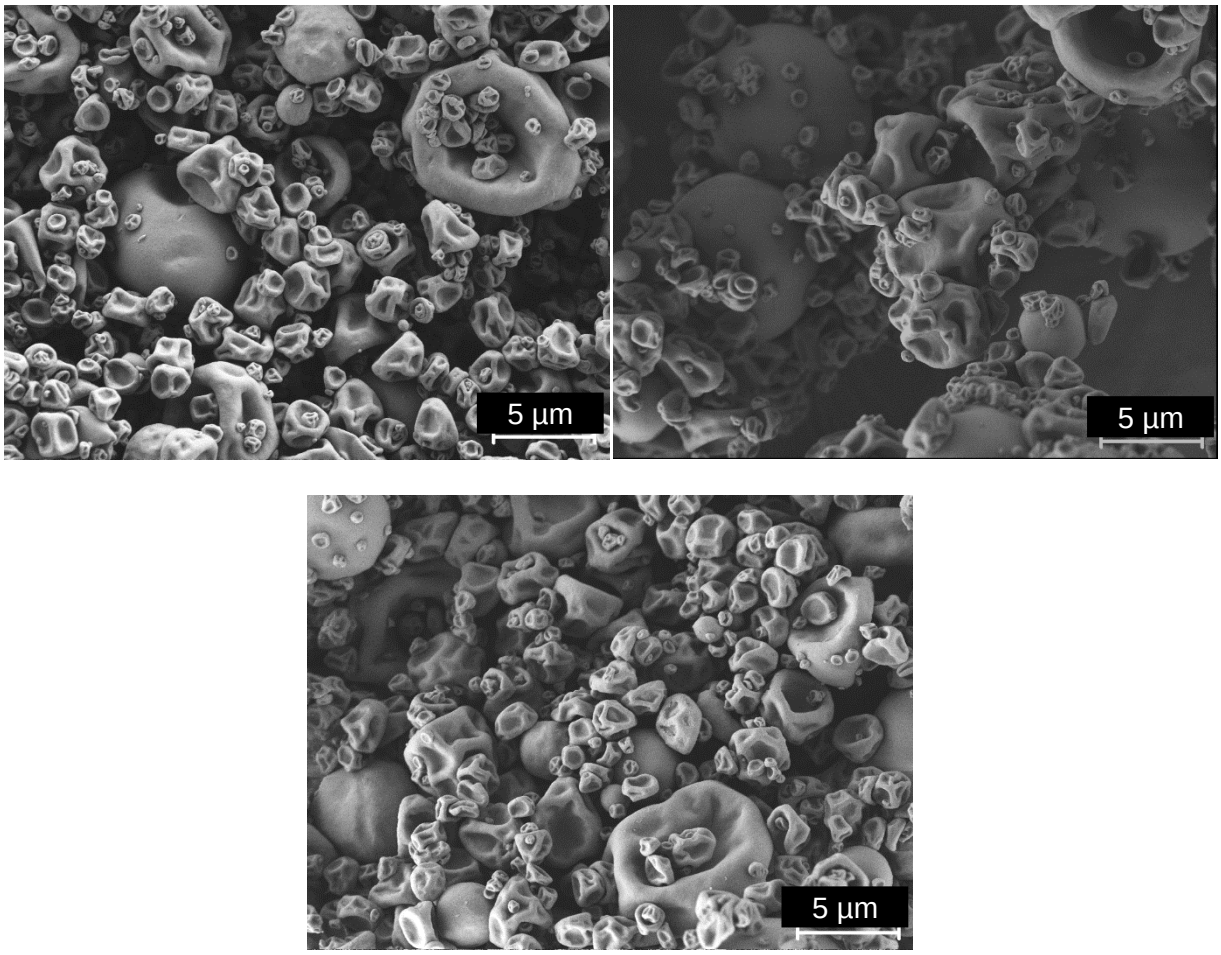

Figure 3.11 – Representative microphotographs obtained by field emission scanning electron microscopy (FESEM) of LBG-based microparticles produced (inlet temperature = 130 ºC, aspirator = 100%, feed flow = 0.8 – 0.9 mL/min) using LBG from Sigma-Aldrich® (A), Industrial Farense® (B) and C. E. Roeper® (C).

The microphotographs show irregular particles with convexities, which is theoretically beneficial for the flowing properties [128]. The resulting appearance can be explained through the concepts of particle engineering, an area of pharmaceutical technology that has been gaining a lot of attention for some years [265,266]. One of the fundamental aspects of polymers is that for the majority, their structure tends to be amorphous (with rare exceptions, *e. g.* D-mannitol [267]). Whenever a droplet is formed at the far end of the spray-dryer injector and considering that a single droplet results in one microparticle, the amorphous aspect leads to an uneven distribution of the polymer on the droplet. Upon drying, there is a migration of the polymer to the surface of the droplet called surface enrichment. Initially, it is suggested that this might function as a protective shield, but when water dries out, this protective cover collapses, resulting in the appearance shown in the FESEM photos [265]. Envisaging a lung delivery application, these microparticles are suggested to be better than spherical ones, as their surface area is higher leading to less air resistance upon flying and thus enabling reaching a deeper region of the lung [128]. However, morphology and shape factor are only one of the decisive factors for dry powder characterisation. Through FESEM images, the Feret diameters of the microparticles were determined, being those of 3.95 ± 4.25 µm for microparticles produced with LBG from Sigma-Aldrich®, 4.31 ± 4.39 µm for those prepared with LBG of Industrial Farense® and 3.76 ± 4.54 µm for those made with LBG from C.E. Roeper®. Regrettably, the aerodynamic characterisation of these LBG-based microparticles is lacking. On being solely composed of LBG, the typically used impaction methods (ACI, NGI) are hindered by the need to provide rigorous quantification (through HPLC or spectrophotometry [268]) of the polysaccharide. Naturally, mathematical calculations could provide theoretical predictions, but these are known to typically lead to underestimations.

3.3.2.2. Chemical and thermophysical characterisation of various forms of locust bean gum (LBG)

The following section is comprised of several results concerning the chemical and thermophysical characterisation of various forms of LBG. For reading and analysis purposes, and due to the use of three different LBG raw materials, the results are organised as follows:

- In-text mentions of LBG 0 correspond to the commercial form of LBG. As an example, LBG 0 Sigma, refers to the LBG raw material obtained from Sigma-Aldrich®.
- In-text mentions of LBG 1 correspond to the purified form of LBG. As an example, LBG 1 Sigma, refers to the purified LBG prepared from the raw material of Sigma-Aldrich®.
- In-text mentions of LBG 2 correspond to the microparticles prepared with the purified form of LBG. As an example, LBG 2 Sigma, refers to the microparticles prepared with the purified LBG prepared from the raw material of Sigma-Aldrich®.
- Table B.III in Annex B details the colour palette (●●●) used in the various Figures of this section.

3.3.2.2.1. Fourier-transform infrared spectroscopy (FT-IR)

Excipient characterisation is one of the important features when applications in formulation development are being considered. Infrared spectroscopy is a qualitative method to analyse the specific chemical bonds in the sample. Due to the importance of purification, the spectra of the three purified LBG prepared from the raw material of the suppliers is shown in Figure 3.12, below.

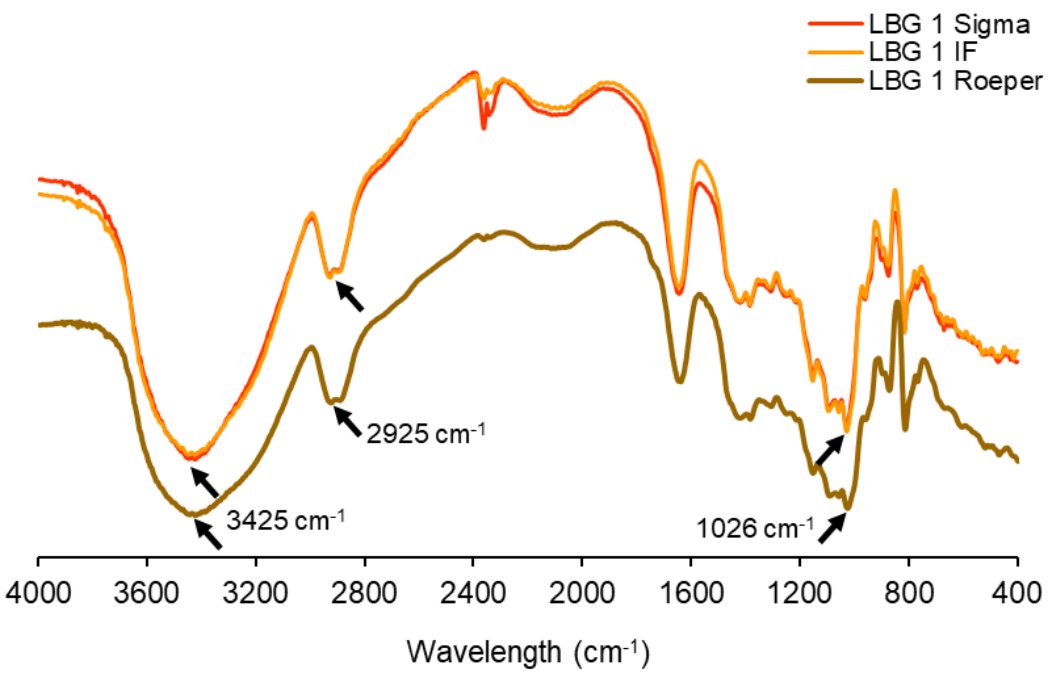

Figure 3.12 – FTIR spectra of purified locust bean gum (LBG 1) of three different suppliers: Sigma-Aldrich®, Industrial Farense® and C. E. Roeper®. Arrows indicate bands characteristic of certain groups present in the LBG molecules.

Three characteristic bands can be observed in the three LBG samples analysed. The first one is around 3425 cm^{-1}, which is related to the stretching of hydroxyl (O-H) groups. The other two bands, 2925 and 1026 cm^{-1}, can be associated with the C-H stretching of -CH and $-CH_2$ groups and the stretching of the C-O-H bond, respectively. These findings are in accordance with other reported LBG analyses [269-271]. Although some of these bands can be found in other compounds, the fact that the three spectra are very similar to each other, shows the resemblance of the samples, and suggests that the purification removes any possible interferent, that could contribute to other bands or the masking of the indicated ones.

3.3.2.2.2. High Performance Size Exclusion Chromatography (HPSEC)

Continuing the characterisation of the various forms of LBG, a HPSEC analysis was performed to ascertain the molecular weight of all samples. Figure 3.13 depicts the distribution graphs for the commercial forms of LBG from the three different suppliers.

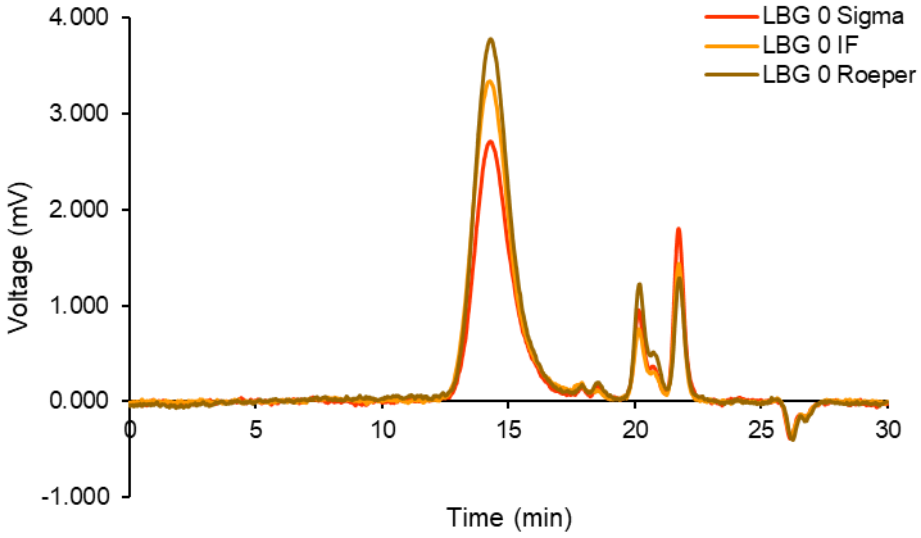

Figure 3.13 – HPSEC chromatograms of commercial locust bean gum (LBG 0) from three different suppliers.

Three main peaks can be detected in the chromatogram: the first appears between 14.20 and 14.30 min, the second around 20.15 min and the third between 21.70 and 21.80 min. The three commercial gums seem to be very similar, as the chromatograms overlay with each other, with the peaks being at around the same retention times, even if the areas under the curve vary. These peaks translate into molecular weight results (M_n and M_w) using the calibration curve shown in Equation 3.2. Moreover, the respective polydispersity index was calculated using Equation 3.3. All these results can be seen in Table 3.6.

Table 3.6 – HPSEC analysis of commercial locust bean gum (LBG 0) from three different suppliers. The different parameters are as follows: M_n = number-average molecular weight, M_w = average molecular weight, PdI = polydispersity index.

		Commercial: LBG 0 Sigma	Commercial: LBG 0 IF	Commercial: LBG 0 Roeper
M_n (Da)*	**Peak 1**	1388296	1470436	1430526
	Peak 2	428	584	387
	Peak 3	39	44	33
M_w (Da)*	**Peak 1**	3371771	3871341	3572181
	Peak 2	567	661	532
	Peak 3	48	49	46
PdI	**Peak 1**	2.4287	2.6328	2.4971
	Peak 2	1.3241	1.1324	1.3741
	Peak 3	1.2323	1.0996	1.3861

The results concerning the molecular weight (M_w) for the commercial samples of LBG were as follows: 3.37 x 10^6 Da for the one from Sigma-Aldrich®, 3.87 x 10^6 Da for the one from Industrial Farense® and 3.57 x 10^6 Da for the one from C. E. Roeper®. These results vary, upon comparison with what is found in the literature, which reports lower values: 0.92 x 10^6 Da [272], 7.4 x 10^5 Da [273], 2.08 x 10^6 Da [274], 0.86 x 10^6 Da [275]. These differences can be linked to the place where the tree/pods grew and the abiotic factors influencing their growth, which ultimately affects the composition of LBG. Moreover, the extraction method used to obtain the gum (acid hydrolysis) can also affect its composition, which translates into different M_w, given the depolymerisation occurring upon contact with the acid. Despite that, all three gums have a similar M_w, as they are within the same range, and similar results were found in the work of Lazaridou *et al*., with LBG from the Greek islands: 2.18-3.94 x 10^6 Da [276].

After analysing the commercial gums, the purified forms of LBG were also characterised and results are depicted in Figure 3.14.

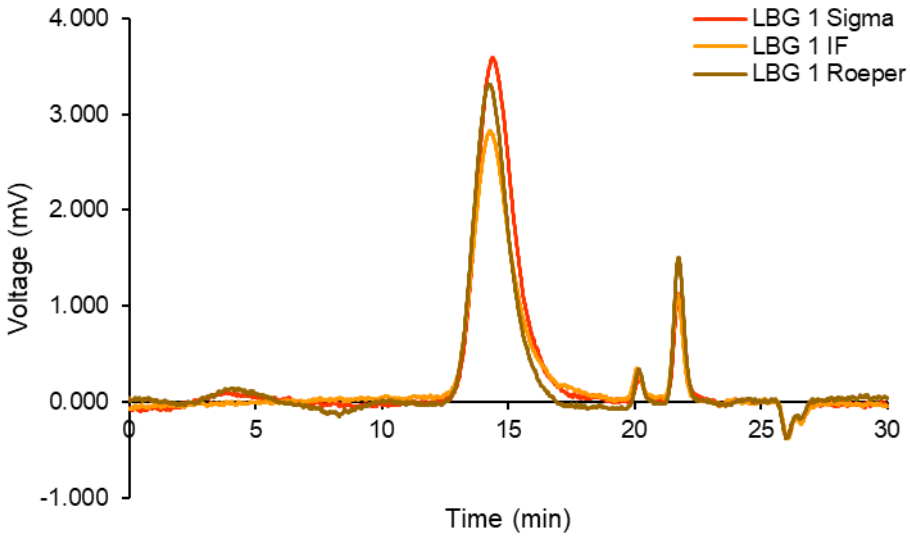

Figure 3.14 – HPSEC chromatograms of purified locust bean gum (LBG 1) from three different suppliers.

As observed with the commercial samples, the purified LBGs have similar retention times: (1) 14.2-14.4 min, (2) 20.1-20.2 min and (3) 21.7-21.8 min. Although the area under the curve is closer with these samples, there was an event that was unexpected. The second peak has a lower height than its counterpart in the commercial samples, and the opposite, being that of a higher peak, occurs with the third one. A first look into the commercial chromatograms and the subsequent analysis of Table 3.6 suggested that these two peaks can be associated with degradation products of LBG, which appear during the purification process. In fact, this process requires LBG to be dispersed in heated water (at 85 ºC) and its subsequent precipitation with ethanol, which can be the cause of some degree of degradation [273,277], thus reflecting on the height and on the area under the curve of these two peaks.

The same method of converting the peaks into quantifiable results of molecular weight and was performed for these samples (Equations 3.2. and 3.3), and they can be seen in Table 3.7.

Table 3.7 – HPSEC analysis of purified locust bean gum (LBG 1) from three different suppliers. The different parameters are as follows: Mn = number-average molecular weight, Mw = average molecular weight, PdI = polydispersity index.

Polymer		Purified: LBG 1 Sigma	Purified: LBG 1 IF	Purified: LBG 1 Roeper
M_n (Da)*	Peak 1	1173729	1400104	1590226
	Peak 2	628	705	652
	Peak 3	44	48	46
M_w (Da)*	Peak 1	3038912	3398325	3574440
	Peak 2	662	748	697
	Peak 3	49	53	50
PdI	Peak 1	2.5891	2.4272	2.2478
	Peak 2	1.0547	1.0608	1.0696
	Peak 3	1.1067	1.1105	1.1051

The calculations for the molecular weight of the purified samples of LBG resulted in the following data: 3.04 x 10^6 Da for the one from Sigma-Aldrich®, 3.40 x 10^6 Da for the one from Industrial Farense® and 3.57 x 10^6 Da for the one from C. E. Roeper®. These results are within the same range as those obtained for the commercial samples. Information concerning the molecular weight of this polysaccharide is scarce, and the data that exists elsewhere varies greatly in between samples: 1.8 x 10^6 Da [278]. In fact, in this case, while the molecular weight for LBG is reported to be in between 3 x 10^5 and 3,6 x 10^5 Da [279], the one obtained here is 10 fold higher. A very similar chromatogram was reported elsewhere [280], detailing similar elution times, also showing two peaks and alerting for the presence of other sugars upon elution of LBG samples. This is a good argument for the theory that heat might induce some sort of degradation of LBG, especially because of the decrease in M_w of LBG 1 Sigma and LBG 1 IF, when compared to the commercial samples.

HPSEC analysis was also applied on the corresponding LBG-based microparticles, produced with a composition based only on the polymer, using the purified LBG. The chromatograms are depicted in Figure 3.15.

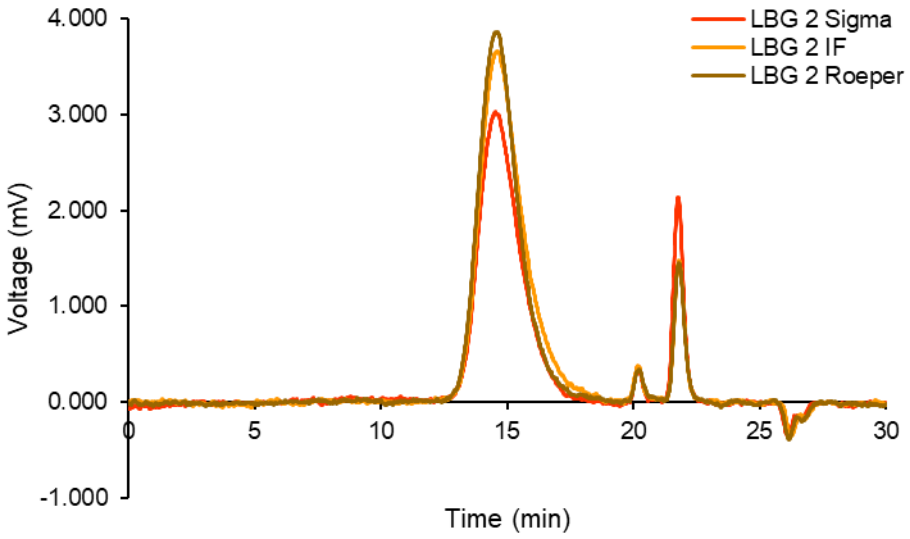

Figure 3.15 – HPSEC chromatograms of locust bean gum-based microparticles (LBG 2) from three different suppliers.

Much like in the unprocessed polymers, the LBG-based microparticles showed similar retention times: (1) around 14.60 min, (2) 20.10-20.30 min and (3) 21.70-21.90 min. The area under the peaks changed once more. The height of peak 2 was similar or lower than the samples in Figure 3.14, whilst peak 3 showed a slight increase. The process used to produce microparticles requires another cycle of heating, to better disperse the LBG in water. But this might hinder the integrity of the LBG, as it is suggested to induce further depolymerisation [273,277].

As previously mentioned, a relevant outcome of the use of HPSEC is the possibility to calculate the molecular weight of the analysed samples, using the calibration curve (Equation 3.2) and the corresponding PdI for the peaks (Equation 3.3). The results of these parameters are shown in Table 3.8.

Table 3.8 – HPSEC analysis of locust bean gum (LBG)-based microparticles (LBG 2) from three different suppliers. The different parameters are as follows: Mn = number-average molecular weight, Mw = average molecular weight, PdI = polydispersity index.

Polymer		Microparticles: LBG 2 Sigma	Microparticles: LBG 2 IF	Microparticles: LBG 2 Roeper
M_n (Da)*	Peak 1	911325	825211	995914
	Peak 2	622	633	595
	Peak 3	43	40	40
M_w (Da)*	Peak 1	2458674	2377731	2568461
	Peak 2	661	671	634
	Peak 3	47	45	45
PdI	Peak 1	2.6979	2.8814	2.5790
	Peak 2	1.0615	1.0600	1.0663
	Peak 3	1.1080	1.1020	1.1180

The results for the molecular weight of the LBG-based microparticles are as follows: 2.46 x 10^6 Da for the one from Sigma-Aldrich®, 2.38 x 10^6 Da for the one from Industrial Farense® and 2.57 x 10^6 Da for the one from C. E. Roeper®. These results of molecular weight further corroborate the theory that additional cycles of heating (for solubilisation and possibly inside the spray-dryer) might induce LBG depolymerization [273,277], thus leading to a decrease in the M_w comparing with the commercial and purified counterparts.

All in all, these chromatograms follow the distributions observed with other LBG samples [281]. Moreover, the progression of LBG from their commercial form to the production of microparticles, which requires heating throughout, might affect the overall chemical stability of the gum, thus a deeper comprehension of LBG behaviour is required to understand the data herein presented.

3.3.2.2.3. Thermogravimetric analysis (TGA)

One of the possibilities to ascertain how LBG behaves depending on the temperature is to use TGA. This technique allows the determination of a temperature threshold, meaning that, it gives an indication at which point the sample starts to

degrade. The curves obtained for all LBGs are compiled in Figures 3.16, 3.17 and 3.18.

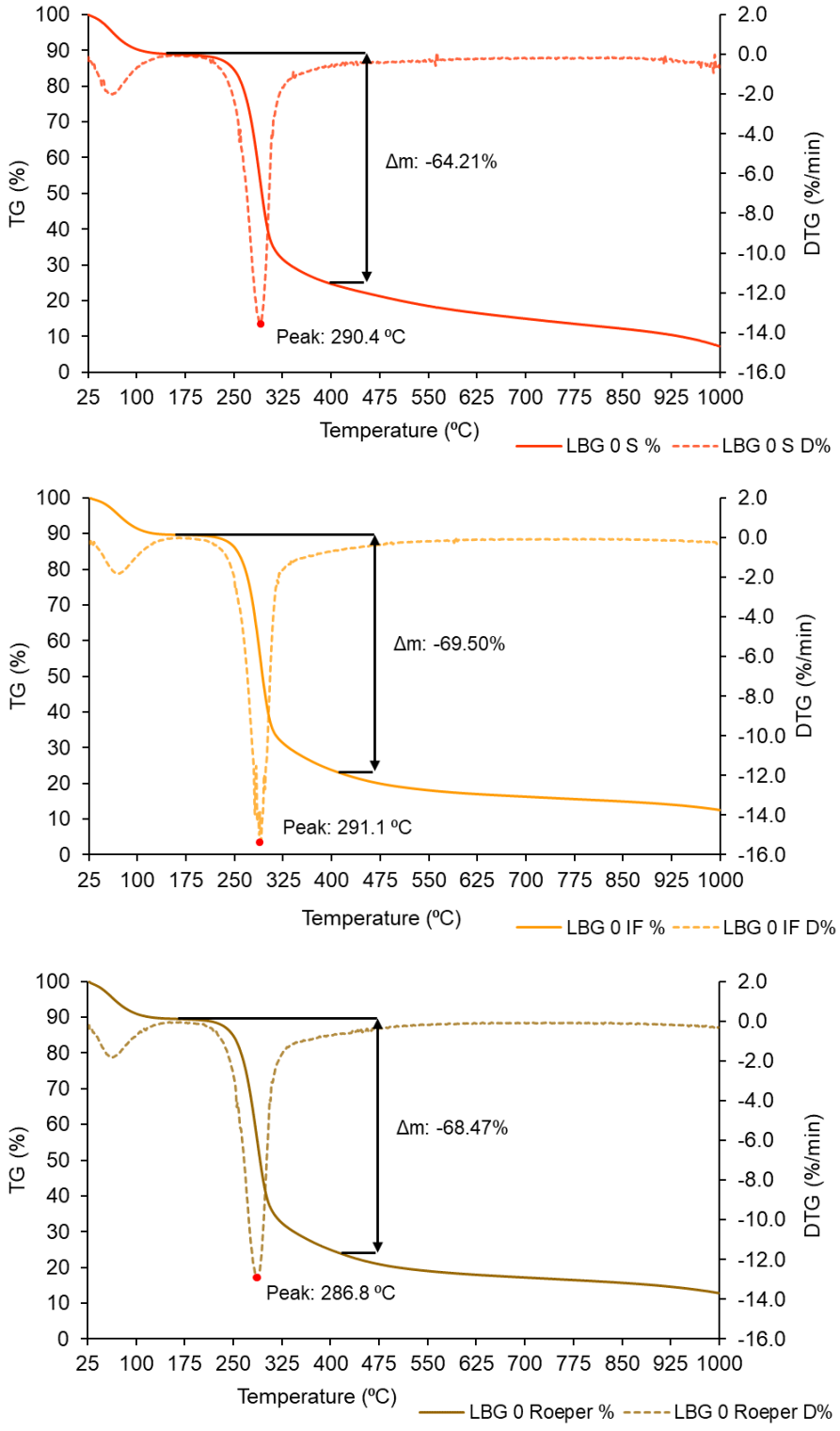

Figure 3.16 – Thermogravimetric analysis (TGA) curves for commercial locust bean gum (LBG) samples from three different suppliers. From top to bottom: LBG from Sigma-Aldrich®, Industrial Farense® and C. E. Roeper®.

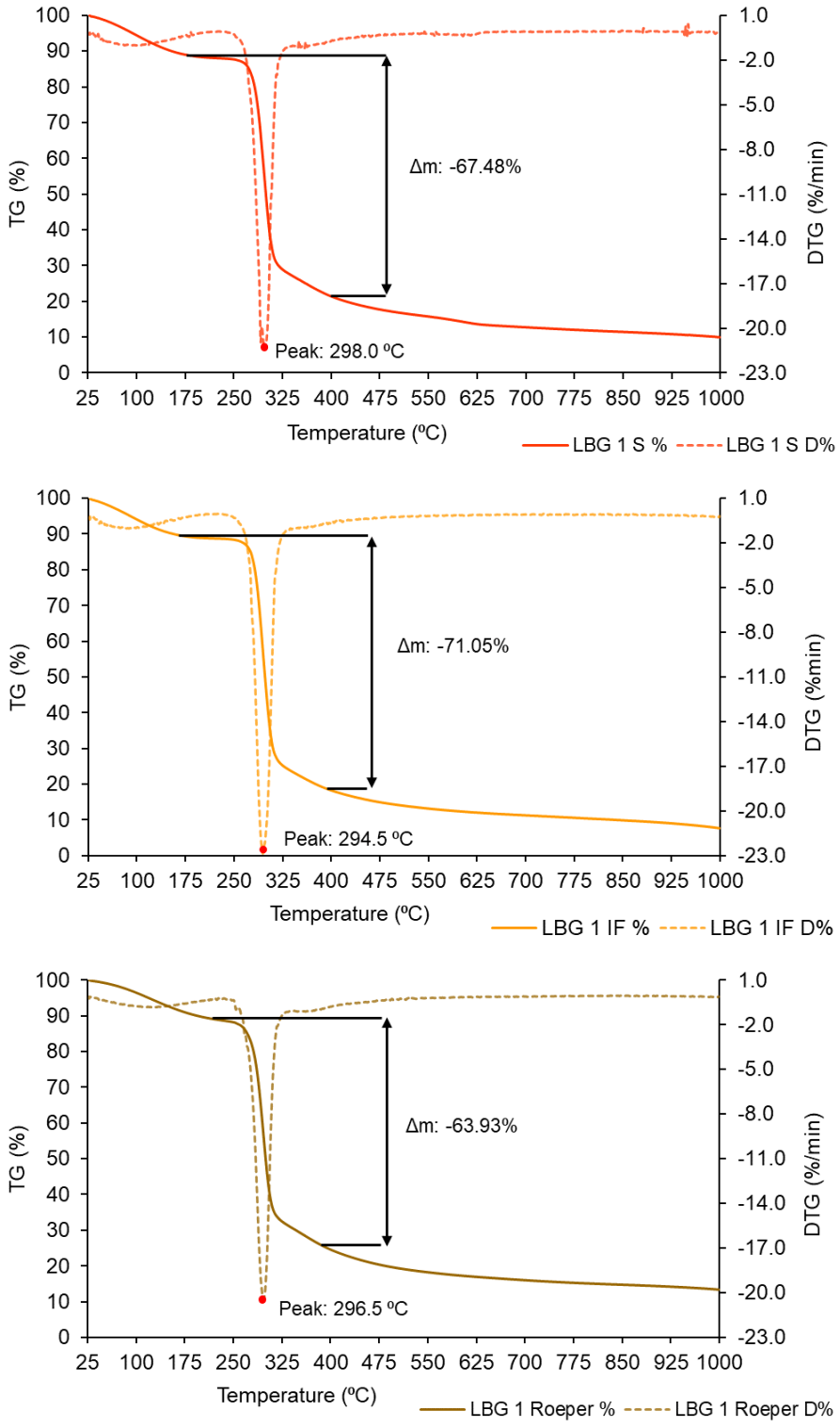

Figure 3.17 – Thermogravimetric analysis (TGA) curves for purified locust bean gum (LBG) samples from three different suppliers. From top to bottom: LBG from Sigma-Aldrich®, Industrial Farense® and C. E. Roeper®.

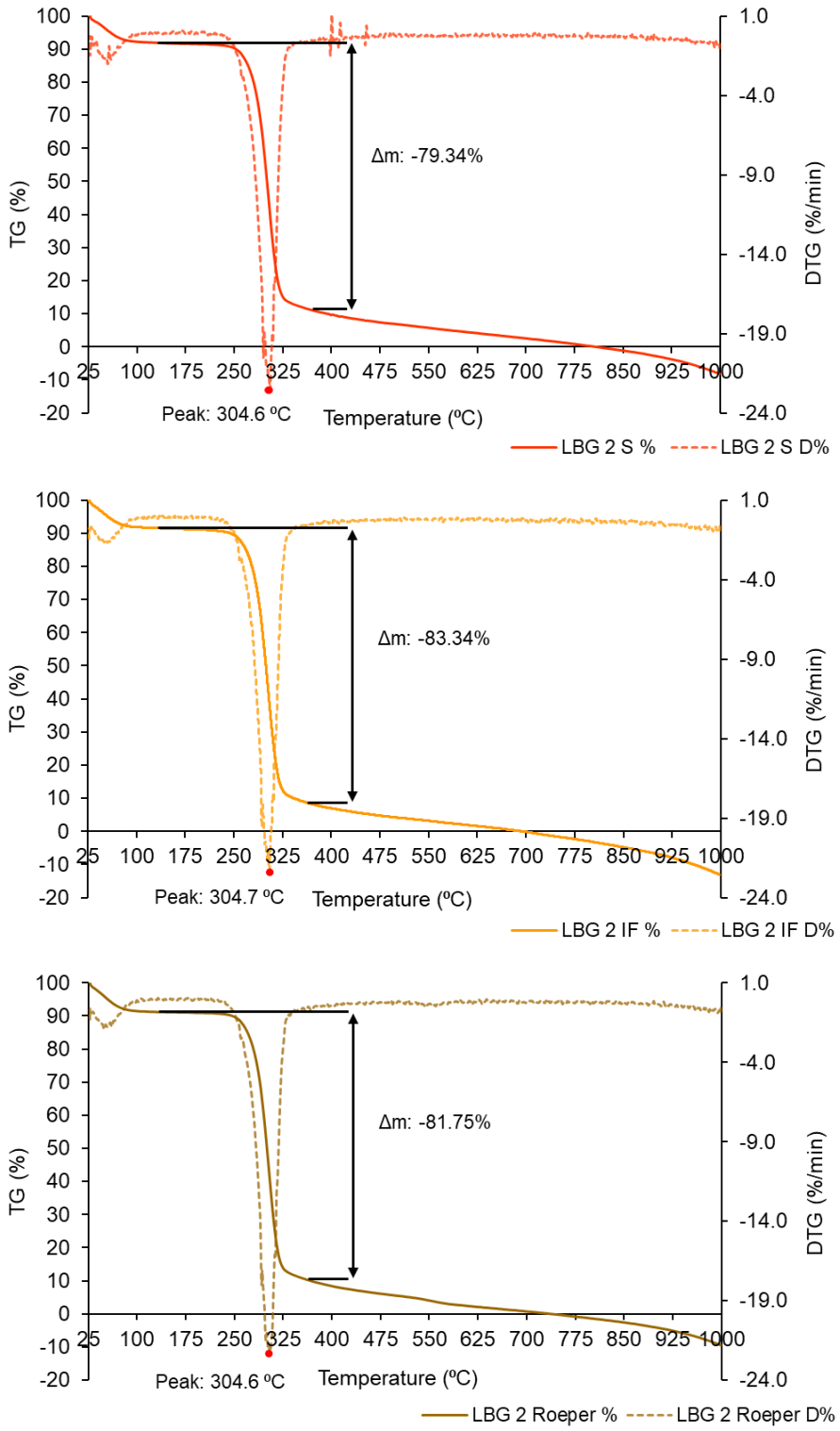

Figure 3.18 – Thermogravimetric analysis (TGA) curves for LBG-based microparticles samples from three different suppliers. From top to bottom: LBG from Sigma-Aldrich®, Industrial Farense® and C. E. Roeper®.

Overall, the TGA curves present two different peaks: one at an earlier temperature (< 100 ºC) and another very intense event at a higher temperature. The first one can be attributed to the loss of water that is associated with the sample, although the temperature at which it evaporates varies significantly. In the purified samples (LBG 1), these losses of mass occur around 100 ºC, whilst lower temperatures were registered for the other cases. Despite these differences, all show this same behaviour. As for the more intense event, that can be associated with the degradation of LBG, occurring around 300 ºC, as observed elsewhere [282]. Clarifying these aspects prove essential in defining a DSC protocol. This is even more important when there are samples that are still relatively unknown. In this specific case, the DSC method, detailed in section 3.3.1.6.1., could not be set at temperatures higher than 300 ºC, because if it did, the tentative measures to determine crystallinities or the glass transition temperatures would be biased. This analysis continues in the next sub-section.

3.3.2.2.4. Differential Scanning Calorimetry (DSC)

After ascertaining the temperature at which LBG degrades, a DSC protocol could be set. Figures 3.19, 3.20 and 3.21 present the corresponding curves for the commercial and purified forms of LBG, as well as the LBG-based microparticles.

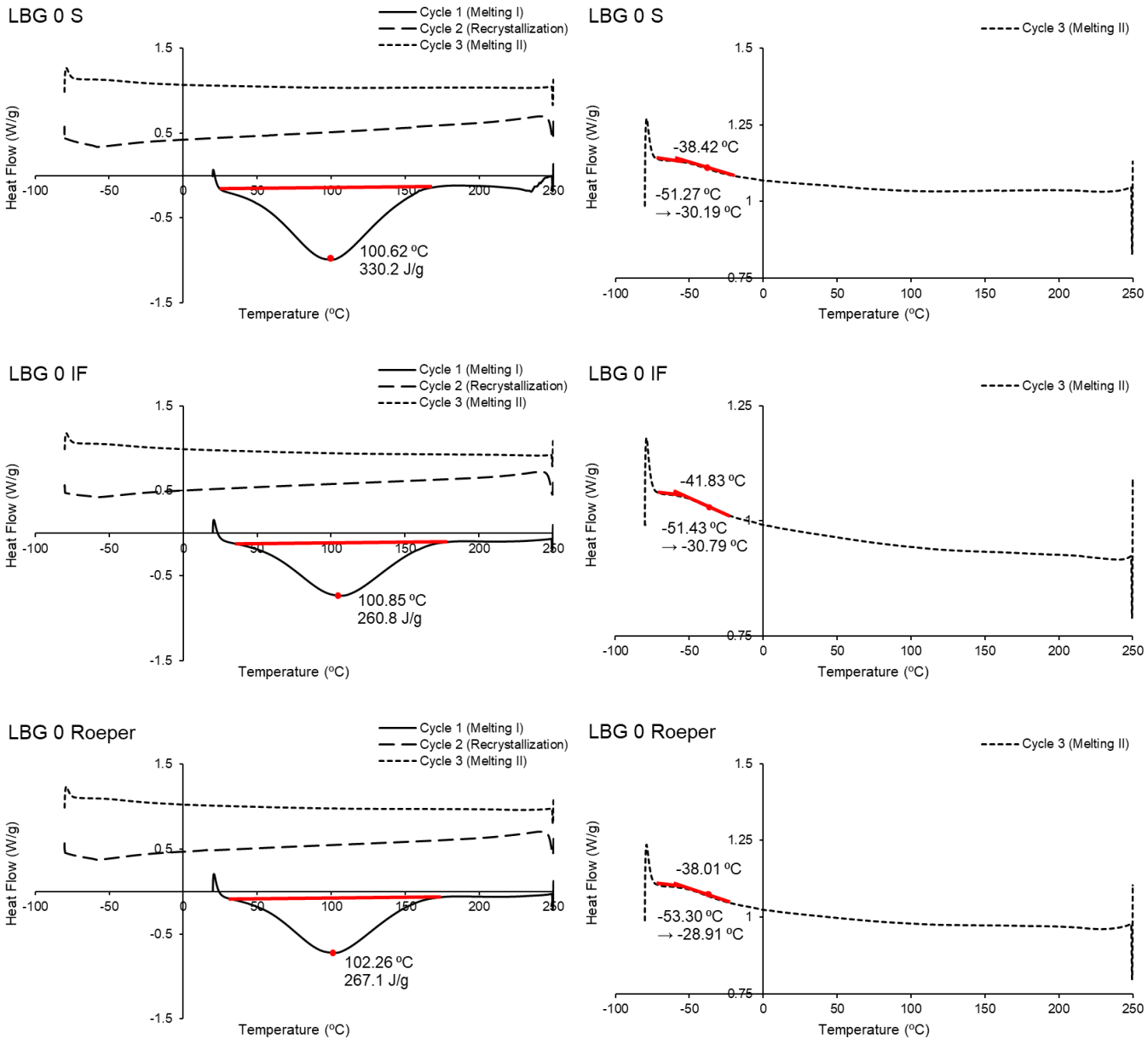

Figure 3.19 – Differential Scanning Calorimetry (DSC) curves for commercial locust bean gum (LBG 0) samples from three different suppliers. The left panels show the thermal behaviour of the samples, and the right panels detail the glass transition temperature (T_g) found for the respective samples.

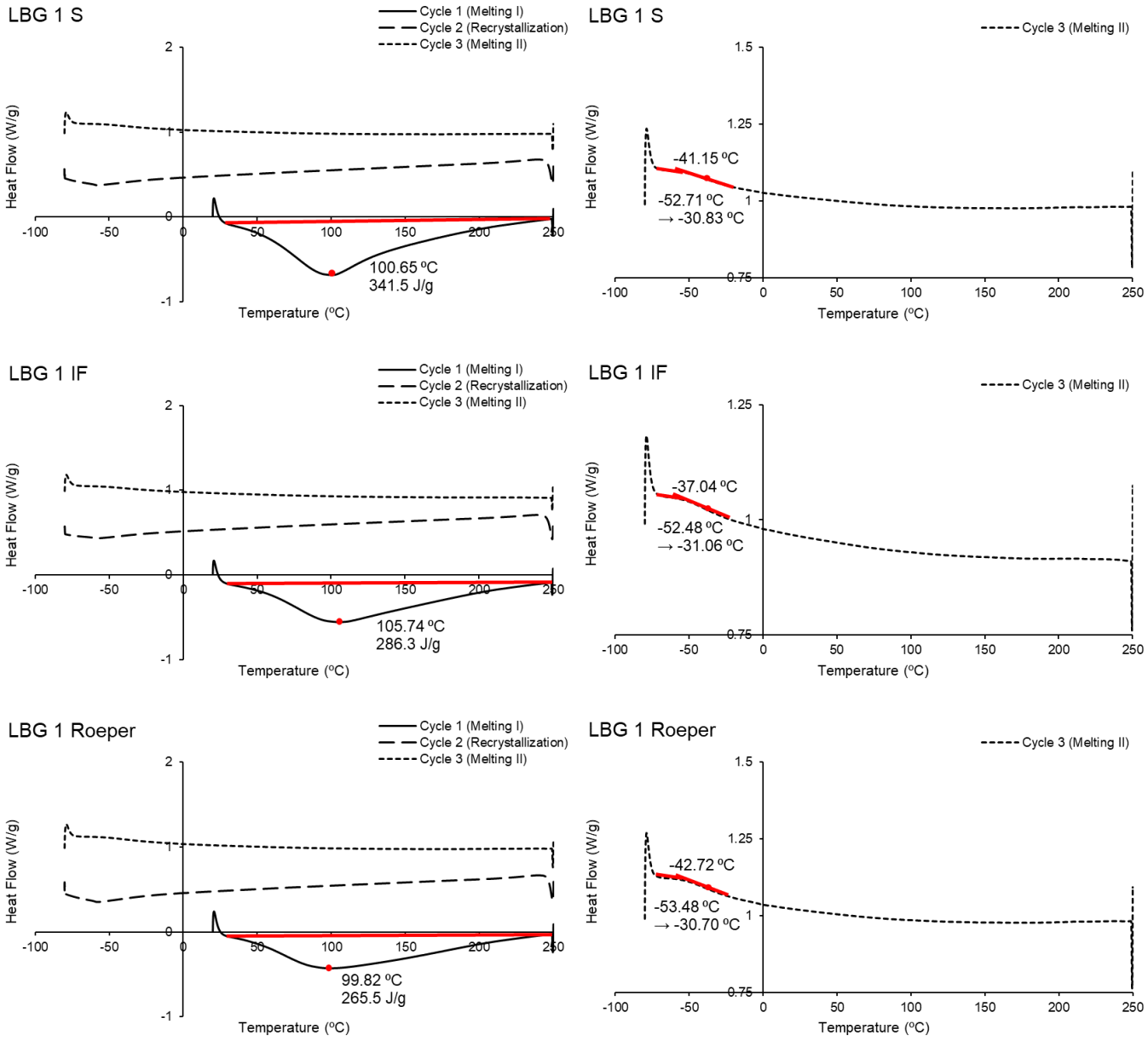

Figure 3.20 – Differential Scanning Calorimetry (DSC) curves for purified locust bean gum (LBG 1) samples from three different suppliers. The left panels show the thermal behaviour of the samples, and the right panels detail the glass transition temperature (T_g) found for the respective samples.

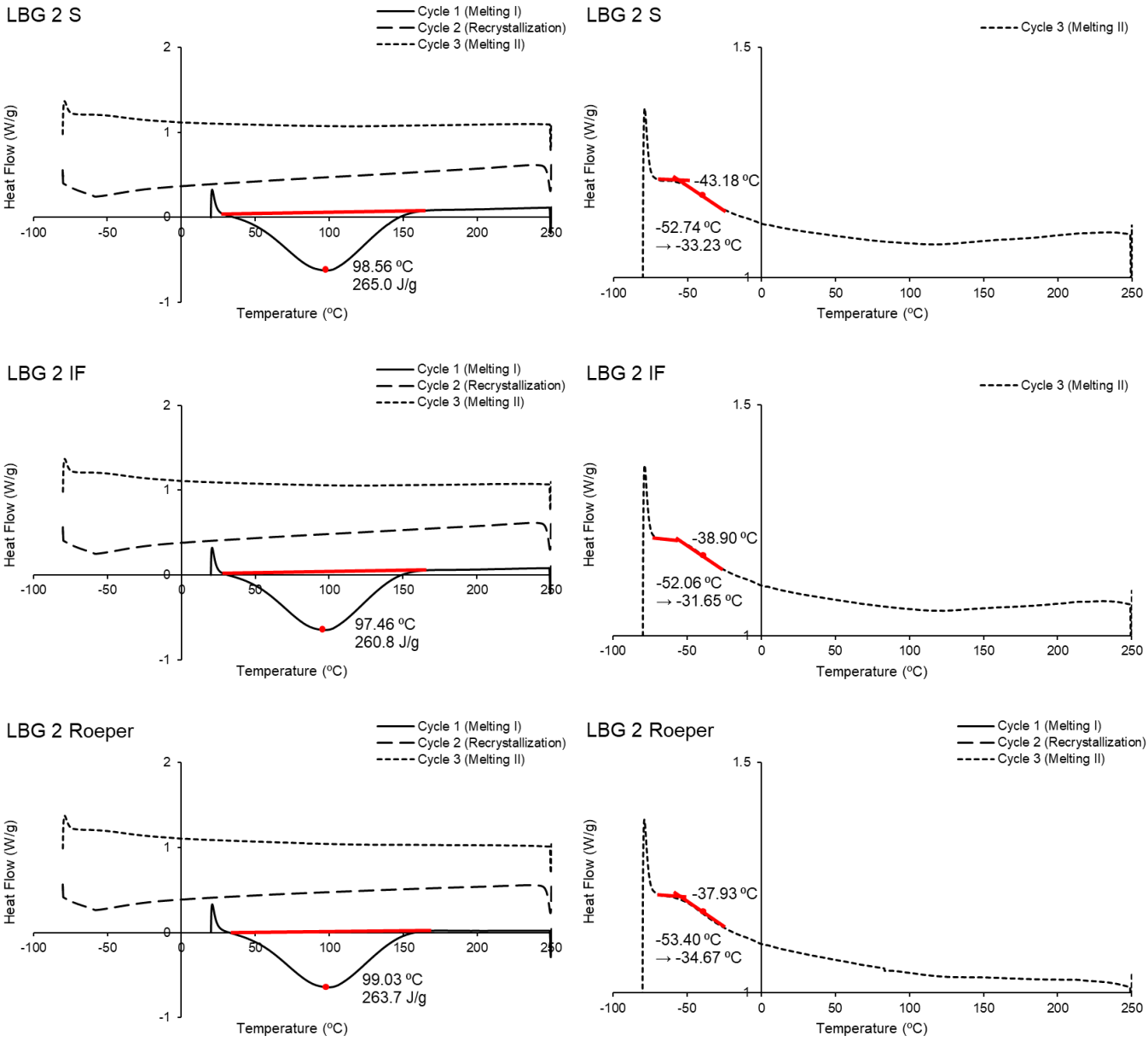

Figure 3.21 – Differential Scanning Calorimetry (DSC) curves for locust bean gum (LBG)-based microparticles samples from three different suppliers. The left panels show the thermal behaviour of the samples, and the right panels detail the glass transition temperature (T_g) found for the respective samples.

The protocol set for DSC cannot go beyond the temperature of 300 ºC, previously determined by TGA, to guarantee the fidelity of the analysis. In the left panels of Figures 3.19, 3.20 and 3.21, the first heating cycle of each of the samples show an endothermic peak around 100 ºC. This peak is associated with the loss of water that

is bonded to the various forms of LBG, which does not appear in the subsequent cycles, as seen elsewhere [282]. The second cycle is one of cooling, thus it enables the search for a temperature that induces a recrystallisation, if the sample is indeed crystalline. In the case of LBG, all its forms do not show a recrystallisation temperature, suggesting that they are all amorphous. The third cycle, which is a second heating, intends to look for a melting temperature, if the sample is crystalline, or for a glass transition temperature (T_g). In the case of the various LBGs, the T_g seems to be between 37.04 and 43.18 ºC, an observation that was also discussed elsewhere [283], although other temperatures were observed that greatly differ from what is reported here [284].

Considering all the data herein discussed, the characterisation of LBG still requires much attention. A thorough profile of polymers is, nowadays, one of the crucial aspects in formulation development for a potential approval by the competent authorities. All those aspects can have a decisive implication in the methods used and in the choice of co-excipients. LBG is not different, as the application of this polymer as matrix material in inhalable microparticles should take into consideration all the physicochemical aspects of the molecule. This thorough characterisation works favourably in the process of preparing dry powders, as well as in its optimisation. Ultimately, all data converges in the determination of the aerodynamic properties of the resulting dry powders, thus influencing further experimentation and applicability in lung delivery scenarios. In the next chapter, the biological risk associated with LBG will be evaluated, further gaining a wider perspective onto how it behaves in living systems.

This page was intentionally left in blank.

CHAPTER 4:

BIOLOGICAL RISK ASSESSMENT OF MATERIALS

The information contained in this chapter was partially included in the following publication:

Pontes, Jorge F.; Guerreiro, Filipa; Rosso, Annalisa; Alves, Ana D.; Rodrigues, Susana; da Costa, Ana M. Rosa; Lollo, Giovanna; Gaspar, Maria Manuela; Grenha, Ana. Toxicological profile of Locust Bean Gum (LBG) for inhalation: Excipient characterisation and biological evaluation. (under preparation)

This page was intentionally left in blank.

4.1. Introduction

Nowadays, the characterisation of materials proves to be a relevant feature in formulation development when an approval for general use is envisaged. As discussed in the previous chapter, the comprehension of materials behaviour can help on the prediction of interactions that can be used in subsequent experimental analyses. In this chapter, that knowledge on material characterisation is complemented with a biological risk assessment, which pertains to the evaluation of the impact of the materials in living systems. In the context of *in vitro* assays, cytotoxicity is one of the most commonly studied parameters to evaluate the impact of a certain material or sample on the cell function and, namely, metabolic activity, as described in the guideline ISO 10993-5-2009 [285]. That guideline establishes that for a material or sample to be safe, the cell viability determined after exposure to the material should not be lower than 70%. However, the small scale of most *in vitro* assays does not allow to fully grasp the effects of the samples in a way that can be correlated to more complex living systems. Despite the many alternatives discussed in Chapter 1, *in vivo* assays still play the most important role in formulation development. Considering the above, an *in vitro* evaluation of various samples of LBG (commercial, purified and spray-dried microparticles) from different suppliers, as well as an *in vivo* test of the microparticles, were performed. The aim of these assays was to assess the behaviour of LBG as excipient for an application in inhalation.

4.2. Materials and methods

4.2.1. *In vitro* safety evaluation

4.2.1.1. Materials

LBG was obtained from three different suppliers, one was an acquisition from Sigma-Aldrich® and the other two were kind gifts from Industrial Farense® and C. E. Roeper®. L-glutamine solution (200 mM), non-essential amino acids solution and penicillin/streptomycin (10000 units/mL, 10000 g/mL), trypsin-EDTA solution (2.5 g/L trypsin, 0.5 g/L EDTA), trypan blue solution (0.4%), thiazolyl blue tetrazolium bromide (MTT), sodium dodecyl sulphate (SDS), dimethylformamide (DMF), Triton-X 100, phosphate buffered saline (PBS) tablets pH 7.4 and dimethyl sulfoxide (DMSO) were acquired from Sigma-Aldrich (Germany). Lactate dehydrogenase (LDH) kit was obtained from Takara Bio (Tokyo, Japan) and fetal bovine serum (FBS) from Gibco

(Life Technologies, USA). Ham's F-12 and RPMI 1640 media were from Lonza Group AG (Switzerland). Ultrapure water (Milli-Q, Millipore, Watford, UK) was used throughout. All other chemicals were reagent grade.

4.2.1.2. Cell culture

Human lung epithelial adenocarcinoma cells (A549) were provided by the American Type Culture Collection (ATCC, USA) and used in passages 20-38. Cells were cultured in flasks (75 cm^2), at 37 °C, in an incubator with 5% CO_2/95% humidified atmospheric air. Cell culture media (CCM) was Ham's F-12, supplemented with L-glutamine 200 mM (1%, v/v), non-essential amino acids (1%, v/v), penicillin/streptomycin at 1% (v/v) and FBS at 10% (v/v). CCM was exchanged two to three times per week.

4.2.1.3. Samples tested in *in vitro* and *in vivo* assays

For *in vitro* assays, a stock solution of 2 mg/mL of commercial and purified LBG, as well as of LBG-based microparticles was prepared for the three polymers obtained from different suppliers: Sigma-Aldrich®, Industrial Farense® and C. E. Roeper®. In brief, each LBG sample (commercial, purified and LBG-based microparticles) was dispersed in ultrapure water (Milli-Q, Millipore, Watford, UK), previously heated at 85 ºC, for 1 h under constant magnetic stirring. After that, four dilutions were prepared with CCM, in the laminar flow hood and using a vortex for homogeneisation, to reach concentrations of 0.1 mg/mL, 0.25 mg/mL, 0.50 mg/mL and 1 mg/mL. The dispersions were used immediately after preparation, being mixed in the vortex before their load into the 96-plate.

For *in vivo* assays, LBG-based microparticles prepared with the polymer from Sigma-Aldrich® were used in the insufflation assays that will be detailed and discussed in the next sections. In brief, purified LBG from Sigma-Aldrich® (1%, m/v) was dispersed in ultrapure water (Milli-Q, Millipore, Watford, UK), previously heated at 85 ºC, for 1 h under constant magnetic stirring. Afterwards, the dispersion was spray-dried (Buchi B-290 Mini Spray Dryer; Buchi Labortechnik AG, Switzerland) at an inlet temperature of 130 ºC and a flow rate of 0.9 ± 0.01 mL/min, with the aspirator set at 100% and the spray flow rate at 473 L/h.

4.2.1.4. Determination of cell metabolic activity

The metabolic activity of A549 cells after exposure to the various LBG samples (commercial, purified and microparticles) from different suppliers and varied concentrations was determined. A stock solution of each LBG was dispersed in ultrapure water and diluted in CCM without FBS at several concentrations between 100 and 1000 µg/mL. The cells were seeded in 96-well plates at $1x10^4$ cells/well, incubated overnight, and exposed to the samples after that. CCM and SDS at 2% (w/v) were used as controls. After 3, 24 and 48 h of exposure, the samples were removed and replaced by 30 µL of MTT (5 mg/mL in PBS pH 7.4), which remained under incubation for 2 h. After that, 50 µL of DMSO were added to each well to solubilise the formazan crystals. The absorbance was read by spectrophotometry (Infinite M200; Tecan, Austria) at 540 nm, with background correction at 640 nm. The cell viability was calculated using Equation 4.1:

$$Cell\ viability\ (\%) = \left[\frac{A-S}{CM-S}\right] \times 100 \qquad \text{(Equation 4.1)}$$

where A is the absorbance obtained upon exposure to each example, S represents the absorbance measured for SDS 2% and CM is the absorbance read for the cells incubated in CCM. The assay was performed at least 3 times, with 3 replicates for each tested concentration.

The obtained data allowed the calculation of the half maximal inhibitory concentration (IC_{50}), which was calculated for samples reaching less than 50% of cell viability in the conditions of the study. IC_{50} values were determined by sigmoidal fitting of the data in the GraphPad Prism statistical program (GraphPad Software, version 9.4.0.673, USA).

4.2.1.5. Cell membrane integrity test

Cell membrane integrity was assessed by the quantification of the cytoplasmic enzyme LDH on the supernatant of A549 cells after 24 h and 48 h exposure to various LBG samples at concentrations of 500 and 1000 µg/mL. CCM was used as negative control and Triton X-100 (1:100 dilution) as positive control of LDH release. Supernatants were centrifuged (16000 x *g*, 5 min) and then, 75 µL of sample were

inserted in the wells of a 96-well plate, to which 75 µL of the LDH reagent were added, after preparation following the indications of the supplier (TaKaRa, Tokyo, Japan). Absorbances were measured in a spectrophotometer (Infinite M200, Tecan, Grödig, Austria) at 490 nm and the background was corrected at 690 nm. The LDH release (%) was calculated using Equation 4.2:

$$LDH\ release\ (\%) = \frac{A-CCM}{L} \times 100 \qquad \text{(Equation 4.2)}$$

where A is the absorbance for the samples corrected with the background, CCM is the absorbance obtained for cell culture media (negative control) and L is the absorbance obtained for Triton X-100 (positive control). The assay was carried out at least three times with three replicates for each tested concentration.

4.2.1.6. Statistical analysis of *in vitro* data

The results were analysed considering three different groups, pertaining to the three different suppliers of LBG. Within the same group, data were analysed considering two different approaches: a time- and concentration-dependent analysis. For MTT, the data were analysed using a one-way ANOVA using the Tukey's multiple comparisons test. As for the LDH, the data were analysed by means of an ANOVA using the Dunnett's multiple comparisons test, taking into consideration the control column attributed to the CCM data. All analyses were run using GraphPad Prism® statistical program (GraphPad Software, version 9.4.0.673), and differences were considered significant at a level of $p < 0.05$.

4.2.2. *In vivo* safety evaluation

4.2.2.1. Animals

Male BALB/c mice (21-27 days) were obtained from Charles River (France). The animals were maintained in standard hygienic conditions with access to commercial chow and acidified drinking water *ad libitum*. All the experiments performed with the animals were approved by the ethical committees of the Faculty of Pharmacy of the University of Lisbon in accordance with the European Union Directive (201/637EU) and Portuguese laws (DL 113/2013, 2880/2015, 260/2016 and 1/2019) for the use and care of animals in research.

4.2.2.2. Lung administration

Animals (6-8 weeks; 22-28 g) were divided in three groups, naïve (control), LBG 1x and LBG 10x, with six animals each. The groups LBG 1x and 10x were exposed, respectively, to a single dose (acute exposure) and to ten doses (subacute exposure) of microparticles composed solely of LBG over a period of 2 weeks. The naïve group corresponded to untreated animals which received no LBG microparticles. The administration of the powder was performed using a homemade apparatus. Mice were restrained in a 50 mL tube and their nose positioned in a small hole in the bottom of the tube to promote the inhalation of the powder. In parallel, LBG powder was weighed in a 15 mL tube, the powder being then administered using a small pump connected to the upper part of the tube, creating an air stream. The air stream facilitated the insufflation of the powder and subsequent entry through the mice' nose. Previous experiments revealed that circa 10% of the powder is inhaled by the animals, thus the administered dose was, approximately, 240 mg/kg [98]. Each dose corresponded to 60 mg of LBG-based microparticles, and mice were exposed to each dose for 2 min. The weight of the animals was registered before each administration.

One day after the last administration, animals from all groups were anesthetised with isoflurane (IsoVet® 1000 mg/g, Piramal Healthcare, UK). Then, blood was extracted from the retinal blood vessels (retro-orbital bleeding technique) and stored in vials containing ethylenediaminetetraacetic acid (EDTA) to prevent blood coagulation. The animals were sacrificed by cervical displacement under anaesthesia and the bronchoalveolar lavage fluid (BALF) and organs such as liver, spleen, lung, and kidneys were collected, weighed, and stored for further analysis.

4.2.2.3. Bronchoalveolar lavage (BAL)

BALF was collected following the protocol proposed by Van Hoecke *et al* [286], with adaptations. After animal sacrifice, 700 µL of PBS (pH 7.2) containing 100 µM of EDTA were delivered to the lung through intratracheal instillation, and then recovered to a 15 mL tube, which was placed on ice. This protocol was repeated three times. BALF was centrifuged for 7 min at 400 x g at 4 ºC, and the supernatant collected and stored at -80 ºC for further analysis.

4.2.2.4. Biochemical and histological analysis

4.2.2.4.1. Leucocyte count and differentiation

Blood samples were collected from mice of all groups and divided into two fractions: one was sent to DNAtech (Lisbon, Portugal) to determine the leukocyte count and differentiation and the other was used in the analyses described below.

4.2.2.4.2. Immunoglobulin E (IgE) evaluation

The determination of immunoglobulin E (IgE) levels was performed in both plasma and BALF samples. The blood volume fraction collected in a previous step was centrifuged in a refrigerated centrifuge (Sigma-202 MK, 10 min, 2000 *x g*) to separate the cellular part from the plasma. The latter (supernatant) was, then, collected and stored at -80 ºC, for IgE determination.

After a step of thawing of both BALF and plasma, samples were brought to room temperature, and IgE levels determined using a mouse immunoglobulin E (IgE) kit (RayBiotech, Norcross, GA, USA), following the indications provided by the supplier. A dilution of 1:100 was used for plasma, while BALF samples were used without dilution.

4.2.2.4.3. Lactate dehydrogenase (LDH) quantification

LDH release was quantified in BALF samples collected from mice. An adaptation of the protocol described in section 4.2.1.4 was carried out, as well as an adjustment of the LDH release percentages. The LDH release (%) was calculated using Equation 4.3:

$$LDH\ release\ = \frac{A}{CM} \times 100 \qquad \text{(Equation 4.3)}$$

where A is the absorbance obtained for the LDH release in the wells corresponding to the groups exposed to LBG (1x and 10x) and CM is the absorbance obtained for naïve animals (control group). The assay was performed in duplicate.

4.2.2.4.4. Total protein determination

The total protein levels were quantified in BALF samples collected for all groups using the Bradford assay (Bio-rad, Algés, Portugal), following an adaptation of the

protocol provided by the supplier. In brief, 80 µL of BAL fluid were put in a 96-well plate and 20 µL of Bradford reagent were added to each well. After an incubation period of 5 min under light protection, samples were analysed by spectrophotometry (Infinite M200, Tecan, Männedorf, Switzerland) at 595 nm. A calibration curve was performed using bovine serum albumin (BSA, 0-160 µg/mL) as standard.

4.2.2.4.5. Tissue index

Liver, spleen, lung, and kidneys were collected and weighed. The respective tissue index (%) was determined using Equation 4.4:

$$Tissue\ index\ = \sqrt{\frac{Organ\ weight}{Animal\ weight}} \times 100 \qquad \text{(Equation 4.4)}$$

The results obtained were further compared with the naïve group, used as control.

4.2.2.4.6. Histology

Lungs were weighed and stored in 50 mL tubes in a formalin solution (10%, v/v, Sigma-Aldrich, Germany). Afterwards, the respective tubes were sent to Instituto Nacional de Investigação Agrária e Veterinária, I.P. (INIAV, Lisbon, Portugal) for histological analysis.

4.2.2.5. Statistical analysis of *in vivo* data

Three ANOVA tests were performed on the data herein present: one-way ANOVA (Tukey and Dunnett's tests), two-way ANOVA (Dunnett's test) and the nested ANOVA (Dunnett's test) with the pairwise multiple comparison procedure were used to compare multiple groups with the naïve set. All analyses were run using GraphPad Prism® statistical program (GraphPad Software, version 9.4.0.673), and differences were considered significant at a level of $p < 0.05$.

4.3. Results and discussion

4.3.1. Biological risk assessment *in vitro*

4.3.1.1. Cell metabolic activity

The impact of materials in living systems is, most of the times, the necessary pathway to ascertain their safety regarding eventual use in further experimentation.

Moreover, the origin of the materials and the methods used for subsequent processing can also be a determining factor in safety assessments. For LBG, the scenario is not different, as the gums from three different suppliers show a macroscopic diversity that could impact living systems. LBG from Sigma-Aldrich® was tested before in MTT assays as a material envisaging a lung delivery application [219], but the method used for the preparation of microparticles varies significantly when compared with the present work. Herein, a stock solution of LBG (2 mg/mL) was prepared and dilutions with CCM were made to obtain concentrations ranging from 0.1 to 1 mg/mL. Figures 4.1, 4.2. and 4.3 show the cell viability obtained through the MTT assay upon exposure to the various samples of LBG. For the purpose of the work herein described, the guideline ISO 10993-5-2009 [285] was used as a reference, which considers toxicity to occur when cell viability lower than 70% is determined.

The analysis of the data evidenced two grand scenarios. The first one entails a time-dependent effect on cell viability, especially between short and long exposure times. For the commercial and purified forms of LBG from Sigma-Aldrich® and Industrial Farense®, the statistical differences are observed for higher concentrations (0.5 and 1.0 mg/mL, $p < 0.05$), which induced cell viability decrease. It was also observed for some of the commercial samples an increase of cell viability with time, which is possibly due to the presence of other compounds in the raw material samples that are afterwards eliminated during purification, and which have a role as nutrients.

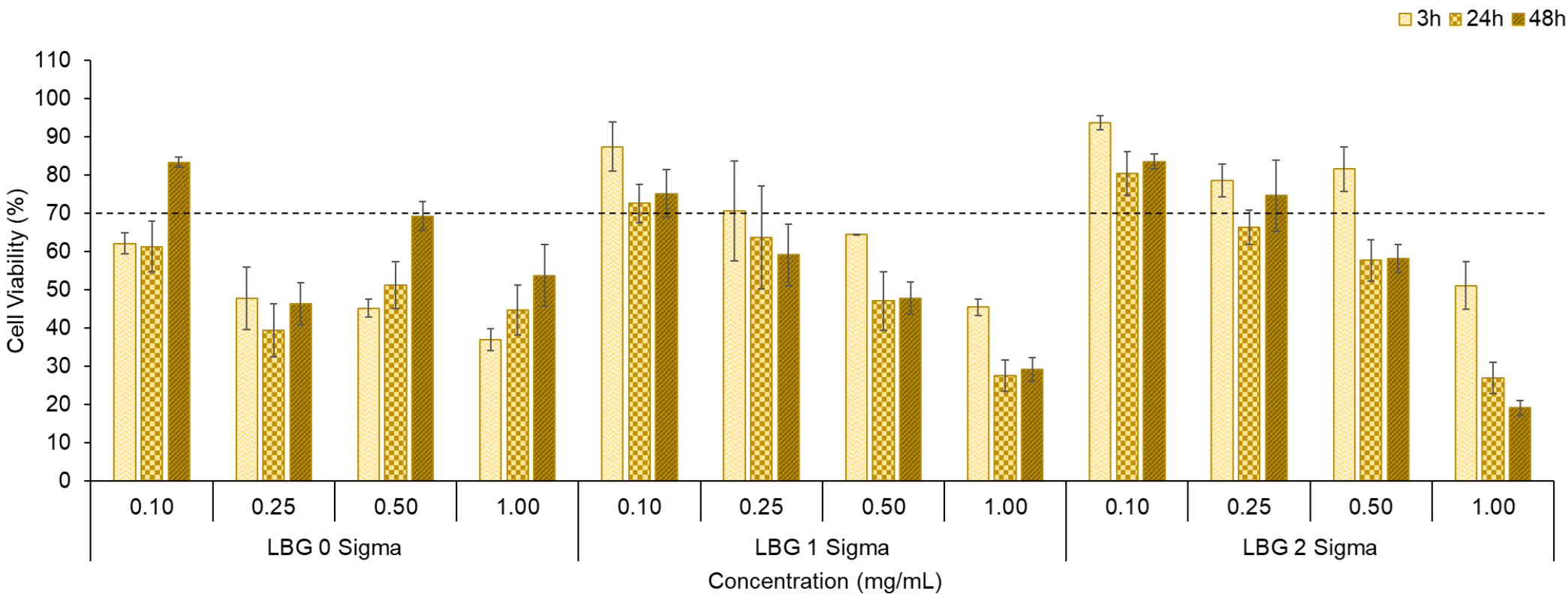

Figure 4.1 – A549 cell viability induced by (a) commercial locust bean gum (LBG 0), (b) purified locust bean gum (LBG 1) and (c) locust bean gum (LBG)-based microparticles (LBG 2) from Sigma-Aldrich® upon 3 h, 24 h and 48 h contact with cells (textured columns in yellow and brown: ●●●, Table B.IV in Annex B). Data represent mean ± SEM (n = 3).

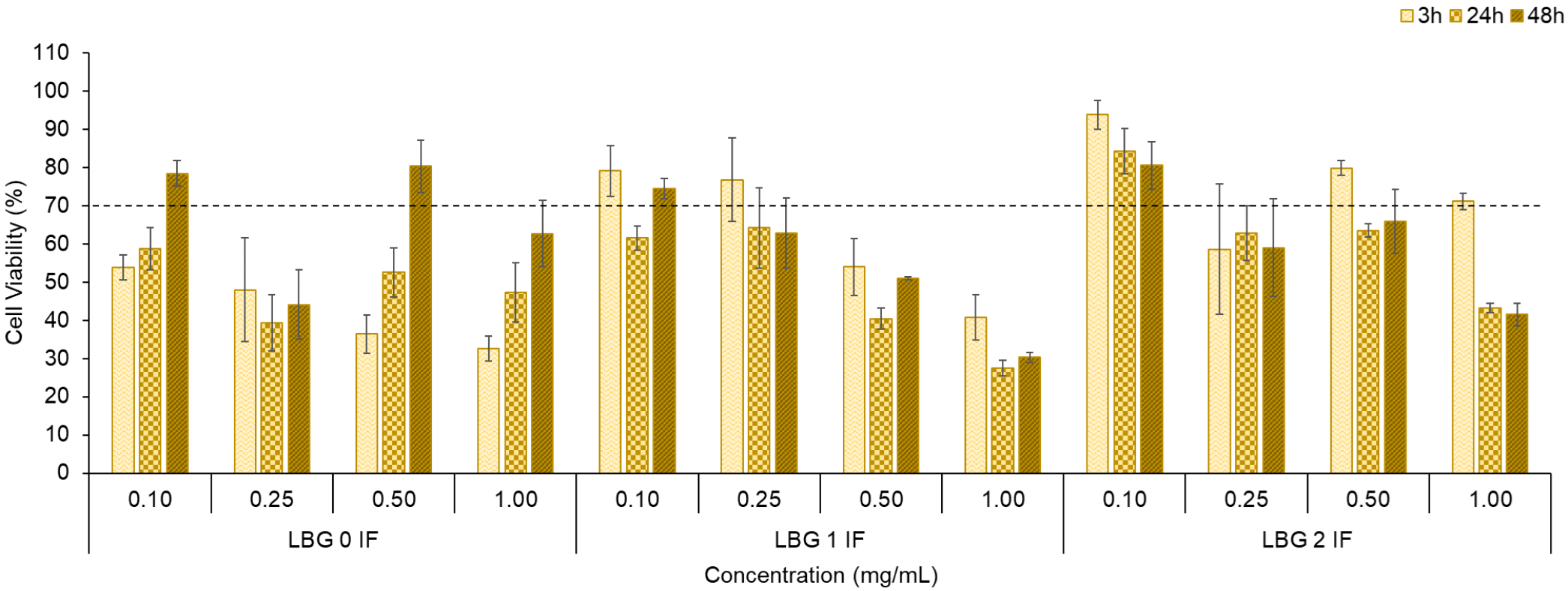

Figure 4.2 – A549 cell viability induced by (a) commercial locust bean gum (LBG 0), (b) purified locust bean gum (LBG 1) and (c) locust bean gum (LBG)-based microparticles (LBG 2) from Industrial Farense® (IF) upon 3 h, 24 h and 48 h contact with cells (textured columns in yellow and brown: ●●●, Table B.IV in Annex B). Data represent mean ± SEM (n = 3).

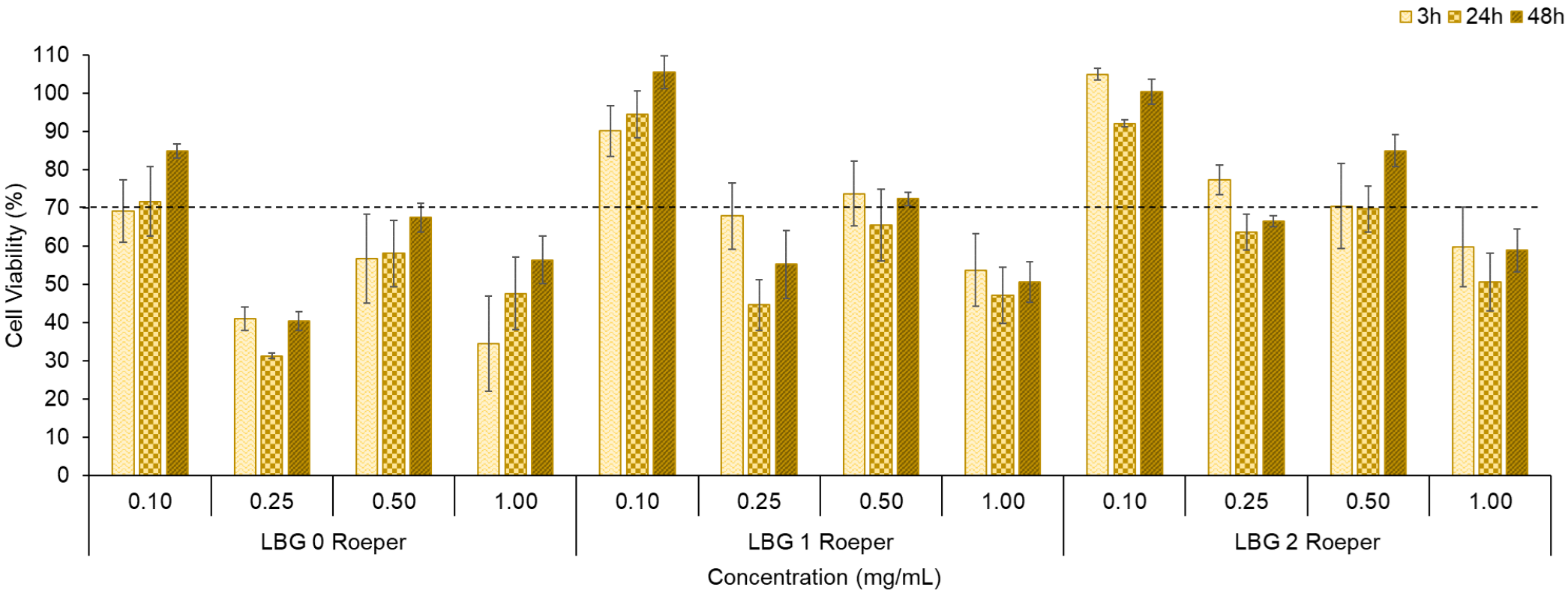

Figure 4.3 – A549 cell viability induced by (a) commercial locust bean gum (LBG 0), (b) purified locust bean gum (LBG 1) and (c) locust bean gum (LBG)-based microparticles (LBG 2) from C. E. Roeper® upon 3 h, 24 h and 48 h contact with cells (textured columns in yellow and brown: ●●●, Table B.IV in Annex B). Data represent mean ± SEM (n = 3).

The analysis of the MTT results further suggested a second scenario of a concentration-dependent effect. In fact, for all forms of LBG and the different suppliers, higher concentrations (0.5 and 1.0 mg/mL) generally resulted in lower cell viability ($p < 0.05$). The dissolution of LBG produces viscous solutions. At lower concentrations, the viscosity is reduced, having little impact on the access of cells to nutrients and gases available in the culture medium. However, higher LBG concentrations show a marked viscosity, which could possibility create a physical and viscous barrier, complicating the biological processes of the cells and resulting in reduced cell viability.

The maximal inhibitory concentration (IC_{50}) was calculated for the purified LBG and the LBG-based microparticles produced with polymers from Sigma-Aldrich® and Industrial Farense®, those displaying cell viability below 50%. The results are compiled in Table 4.1.

Table 4.1 – IC_{50} (mg/mL) calculated for different samples of locust bean gum (LBG) upon 24 h and 48 h contact with A549 cells.

	IC_{50} (mg/mL)			
Exposure time	**LBG 1 Sigma**	**LBG 2 Sigma**	**LBG 1 Industrial Farense**	**LBG 2 Industrial Farense**
24 h	0.3949	0.4953	0.3287	0.7592
48 h	0.3931	0.5046	0.4391	0.7457

LBG 1 indicates purified LBG; LBG 2 indicates microparticles

Despite some effect of the exposure time on the IC_{50} of purified LBG from Industrial Farense, the most important observation regarding IC_{50} values is the fact that the type of LBG sample being tested (purified - 1 or microparticle - 2) impacts on cell interaction. The processing of LBG to produce microparticles results in an increase of the IC_{50}, suggesting that cells might react better to a microcarrier rather than a purified form of the polymer. This observation can be justified with LBG characteristics. The form of purified LBG in both cases entails a more viscous dispersion compared with the microparticles, which hinder the access of cells to

oxygen and the nutrients contained in the CCM. In turn, due to further processing in the spray-dryer, LBG microparticles appeared to have lower viscosity in the dispersion, which benefits cells in their access to the components necessary to their growth, thus resulting in an increased IC_{50}. Specific tests on viscosity should however be performed to confirm these observations. Nonetheless, considering the area of the lung, the real concentration expected to be observed is closer to 0.1 mg/mL, and the obtained results are very promising at that concentration.

4.3.1.2. Cell membrane integrity

The impact of the LBG samples in cells was further complemented with the determination of the cytoplasmatic enzyme LDH released to the culture medium. This occurrence implies the disruption of the cell membrane and is, therefore, a sign of harm. The higher concentrations tested in the MTT assay (0.5 mg/mL and 1.0 mg/mL) were those assessed, and results are depicted in Figure 4.4.

A closer observation of the results reveals that, comparing the different samples at the same timepoint, only LBG microparticles produced with polymer from Sigma-Aldrich® at 1.0 mg/mL evidenced a statistically significant increase in the released LDH as compared with the control (cell culture medium; $p < 0.05$). This increase was of approximately 10% and was the maximum release observed in all tested conditions. Overall, the obtained results are thus considered quite amenable, with very low concentrations of LDH being detected.

The satisfactory results permitted the use of LBG-based microparticles in *in vivo* assays, which were performed with the expectation of having more information to support the application of the material in lung delivery. The results are discussed in the next section.

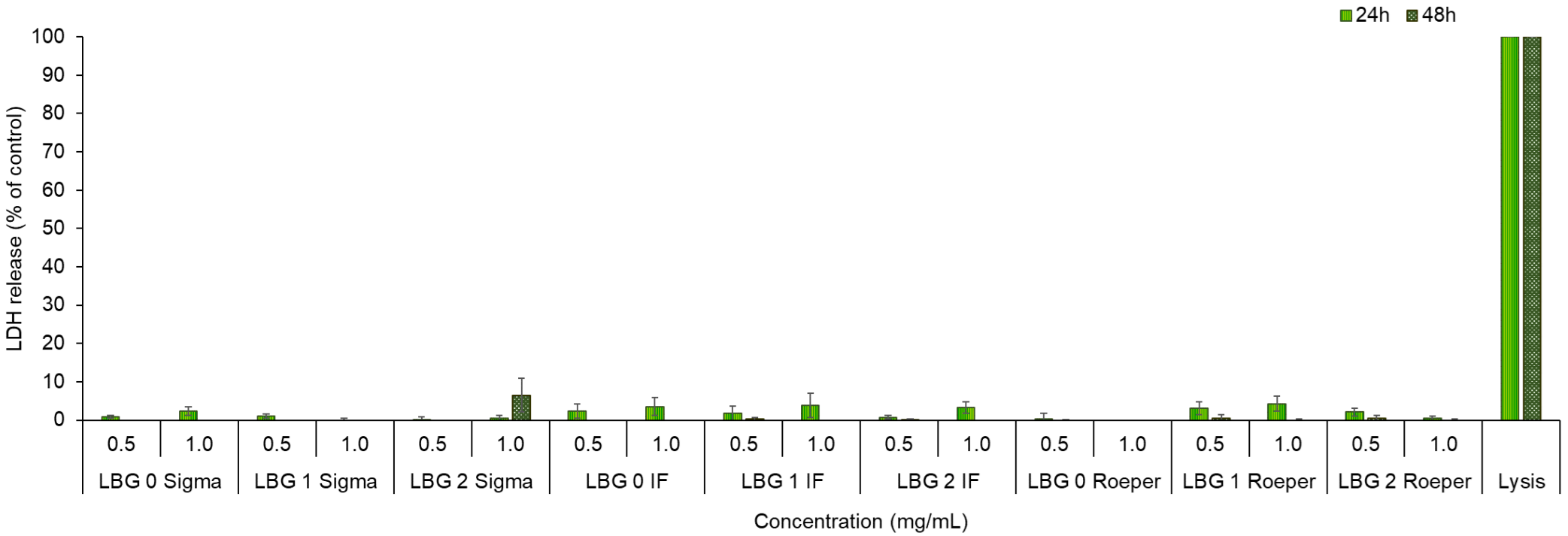

Figure 4.4 – Lactate dehydrogenase (LDH) released from A549 cells (textured columns in green: ●●) upon 24 h and 48 h exposure to different locust bean gum (LBG) concentrations corresponding to commercial (LBG 0), purified (LBG 1) and LBG-based microparticles (LBG 2) from different suppliers. Data represent mean ± SEM (n = 3).

4.3.2. Biological risk assessment *in vivo*

Many cellular events occur, in the human body, upon contact with foreign substances. These events are very important when inhalation is considered, as inflammation or structural changes in lung epithelia may be observed. Biosafety parameters are, thus, relevant in formulation development, their characterisation being, ultimately, essential for an envisaged use in therapy. Although, for the latter, data on the complete dosage form is required, excipients used in formulation also demand characterisation of their biological impact and, ultimately, of the toxicological profile. Similarly to drugs, excipients also interact with the human body, and this activity often remains to be fully understood and quantified. In this regard and considering that LBG is proposed herein as an excipient for lung delivery applications, safety parameters were studied *in vivo*. In brief, mice underwent the inhalation of LBG-based microparticles (polymer from Sigma-Aldrich®) composed only of the excipient, devoid of any drug, following an acute (single dose) or subacute (ten doses during two weeks) exposure. The animals were monitored for clinical signs of morbidity and, after sacrifice, BALF was performed and analysed, along with organs and serum, in order to evaluate toxicity biomarkers and allergic response.

4.3.2.1. Monitorisation of body weight

The body weight of mice exposed to ten doses of LBG microparticles was monitored every day, since the day of first dose administration until moments before their sacrifice and compared with naïve mice (Figure 4.5).

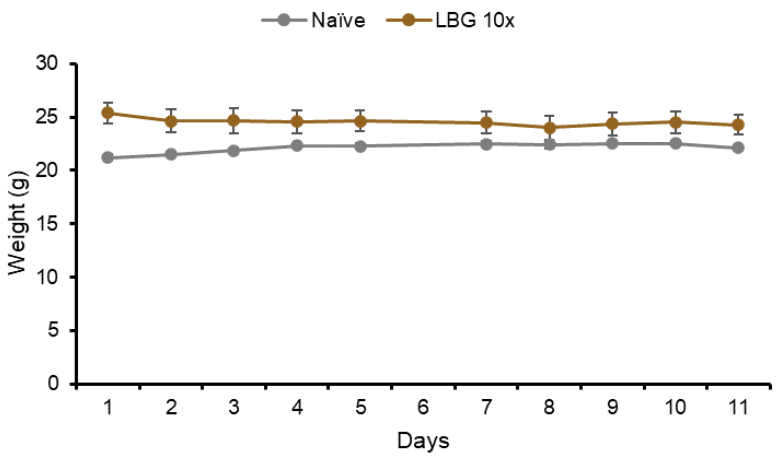

Figure 4.5 – Variation of mice body weight in the naïve group and in the mice exposed to ten doses of locust bean gum (LBG) microparticles (LBG 10x) (mean ± SD, n = 6).

The results revealed absence of major alterations on the weight of mice within the same group, for both groups, despite the inhalation of microparticles in one group. Some concerns were raised throughout the assay related to the weight of the mice. Due to the swelling properties of LBG [287,288], and the amount of powder that was to be inhaled, a concern arose pertaining to some of the powder entering the pharynx into the gastrointestinal tract of the mice, leading to an alteration of their overall weight. However, despite this concern, and even if the swallowing of LBG-based microparticles did occur, it did not have a measurable influence throughout the assay. Mice body weight was also assessed in the group receiving a single dose of LBG-based microparticles, before and after administration (data not shown), without significant alterations being observed.

4.3.2.2. Counting of differentiated leucocytes

White blood cells play a pivotal role in maintaining body homeostasis. The immune system is comprised of several types of cells, involved in both innate and adaptative immunity. Modifications of their normal numbers frequently indicate the occurrence of molecular events, such as inflammation or infection [289], which is helpful in the monitorisation of health conditions. A deeper study of the white blood cell population could, thus, provide some relevant data on the reactions to lung drug delivery approaches. As such, blood leucocytes from animals receiving LBG microparticles

were characterised and compared with naïve mice, and results are shown in Figure 4.6.

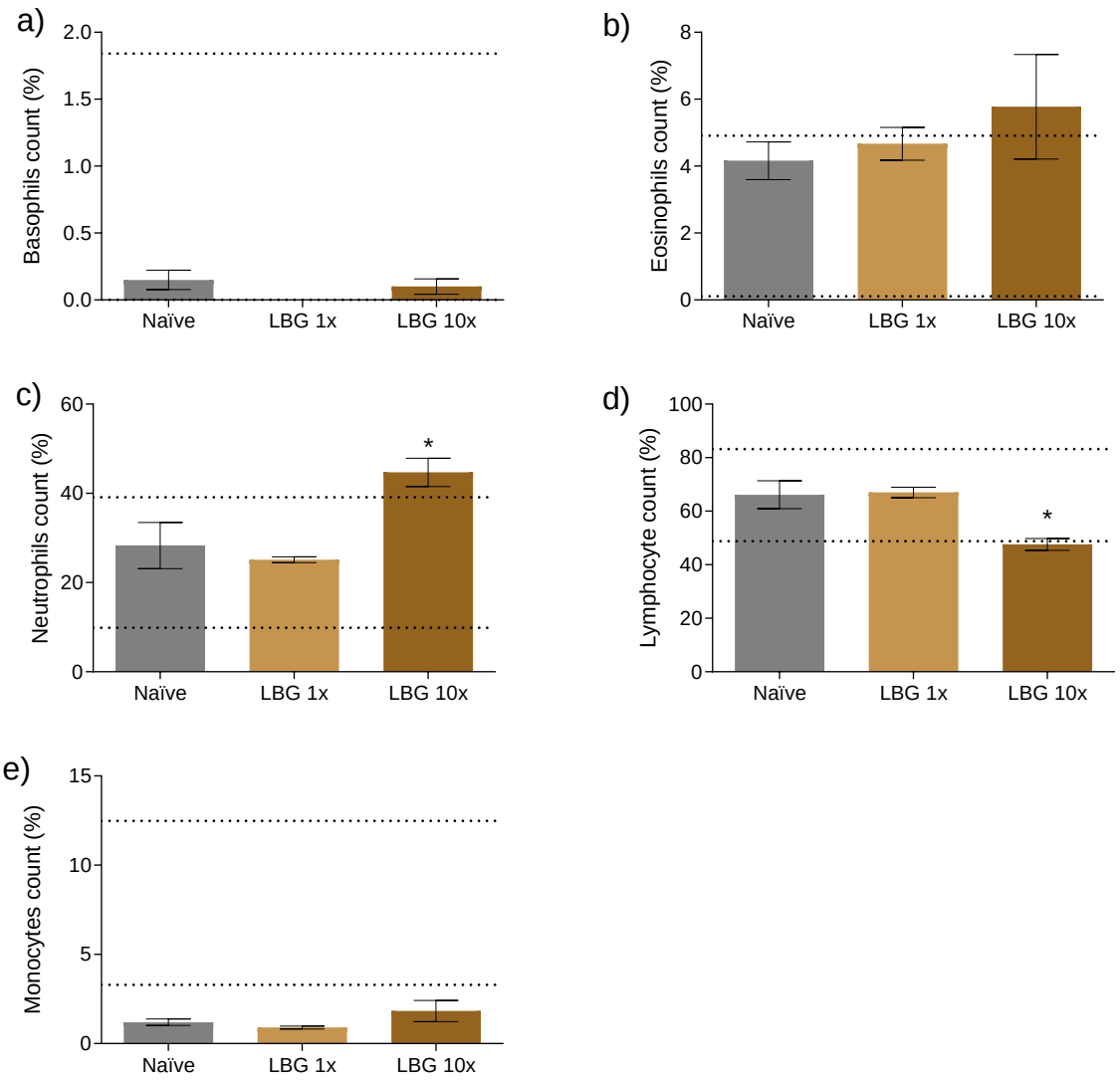

Figure 4.6 – Leucocyte count in mice blood: (a) Basophils, (b) Eosinophils, (c) Neutrophils, (d) Lymphocytes and (e) Monocytes. Dashed lines represent the reference intervals for each type of white blood cell (mean ± SEM, n = 6). Statistical significance comparing with control (naïve group) is indicated with an asterisk (*) for $p < 0.05$.

Basophils are the only type of white blood cell that is within the reference levels determined by Charles River Laboratories International [290], in all the tested groups and no statistical differences were found between the three groups. The case changes for eosinophils, which, much like neutrophiles, are associated with

inflammation and allergy reactions [291]. The eosinophil count was within the reference levels for the naïve group and the mice receiving a single dose of LBG microparticles. However, when the number of administrations increased to ten (administered over two weeks), eosinophil count overpassed the reference, showing a phenomenon of eosinophilia. Despite the initial thoughts of an inflammatory state occurring in the mice, that can only be assumed as a suggestion due to the lack of statistical significance and the standard deviation being large, in the latter group.

Neutrophils can also be associated with an allergy or an inflammatory episode in mice [292]. In fact, both naïve and the single dose administration groups had results within the reference interval [290]. However, for the group receiving ten doses, the results were above the higher reference level, with a statistically significant increase ($p < 0.05$) comparing with the naïve group. These results of neutrophilia can be associated with an inflammatory reaction, but more studies are required to confirm that and establish an eventual causative effect with the exposure to inhaled LBG microparticles.

With regards to lymphocytes, these cells surprisingly decreased below the reference levels for the group receiving ten doses. Lymphocytes may also be indicator of inflammation [293], being typically ‘called’ to inflamed tissues in a process termed ‘homing’ [294]. The detected lymphocytopenia might be explained by this ‘homing’, as lymphocytes may have possibly abandoned the blood circulation to concentrate in the inflamed tissue. As for the monocytes, their count was below the reference levels for every group analysed. No explanation was found for the effect so far but, importantly, monocyte levels did not change significantly after exposure to LBG microparticles [295].

Information regarding LBG being pro-inflammatory are scarce to non-existent, either as a polymeric dispersion or in a drug delivery platform. Literature reports the works of Chen *et al*, in which they tested the production of pro-inflammatory factors by both native LBG and its hydrolysed form. While the latter did not induce inflammation, native LBG did trigger the production of tumour necrosis factor (TNF)-α in RAW264.7 cells at several concentrations (0.05% to 0.2%) [296]. Upon analysis of leucocyte

counts, the results suggest that there is a possible inflammation that might not be associated with an infection. Further testing is required to understand its origin.

4.3.2.3. Immunoglobulin E (IgE) quantification

Besides inflammation, the potential of induction of an allergic reaction upon inhalation of LBG dry powder was considered relevant and was thus assessed. IgE antibodies were therefore quantified in plasma and BALF, as they are associated with the release of inflammatory mediators, among other roles [297,298]. Basal values of IgE in humans and mice are the lowest of all antibodies, and highly regulated [299,300]. The results obtained are shown in Figure 4.7.

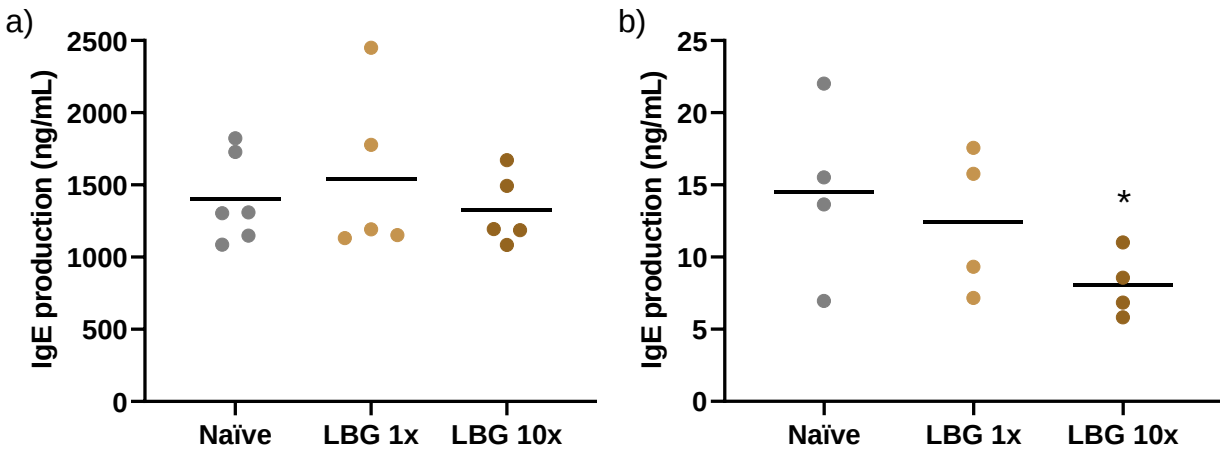

Figure 4.7 – IgE levels determined in a) plasma and b) bronchoalveolar lavage (BAL) samples of the mice from naïve and locust bean gum (LBG) groups receiving single dose administration (LBG 1x) and ten doses (LBG 10x) of LBG-based microparticles. Lines represent the mean IgE secretion expressed in ng/mL (plasma: n = 6; BAL: n = 4). Statistical significance comparing with control (naïve group) is indicated with an asterisk (*) as $p < 0.05$.

Mean values of IgE production of 1400 ng/mL, 1541 ng/mL, 1326 ng/mL for the naïve, single dose and ten-dose administration of LBG-based microparticles, respectively, were determined in plasma. No statistically significant differences were found between the groups, suggesting that no allergic reaction was initiated in the sequence of the inhalation of LBG microparticles. As for the IgE determined in BALF, much lower values were found compared with those determined in plasma [301],

corresponding to mean values of 14.54 ng/mL (Naïve), 11.59 ng/mL (LBG 1x) and 8.07 ng/mL (LBG 10x) were determined.

Only the group receiving multiple doses showed a statistically significant difference in the produced IgE, but it decreased to approximately the half. This effect might be another indication that no allergic reaction starts upon the administration of LBG-based microparticles. In fact, the decrease in the levels of this immunoglobulin leads to lower activation of the FcεRI receptor by cross-linking, a receptor with high affinity for IgE, thus inhibiting the activation of basophils and mast cells, leading to no cytokine release [302,303]. With less IgE, inactivated cells and no circulating cytokines, no allergic reaction takes place.

4.3.2.4. Lactate dehydrogenase (LDH) quantification

The quantification of LDH, a cytoplasmatic enzyme, is an important feature in characterising the cytotoxicity of a tested material. In fact, the release of LDH from cells refers to the loss of cell membrane integrity, thus indicating a process of toxicity, being more severe as the LDH release percentage increments [304,305]. In this study, this enzyme was quantified in BALF, and the results are depicted in Figure 4.8.

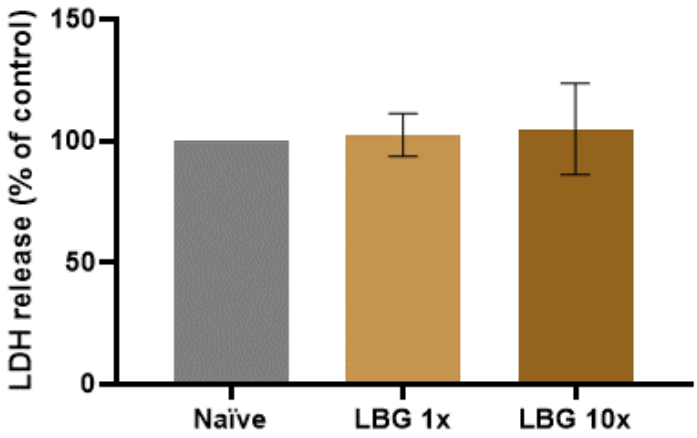

Figure 4.8 – Lactate dehydrogenase (LDH) quantified in BAL samples obtained from mice of naïve and LBG groups receiving a single dose administration (LBG 1x) and ten doses (LBG 10x) of LBG-based microparticles (mean ± SEM, n = 4).

As observed, the inhalation of LBG-based microparticles did not induce increased release of LDH in any of the tested groups, thus, suggesting that LBG does not induce toxicity upon delivery through inhalation.

4.3.2.5. Total protein quantification

The total protein was another parameter quantified in BALF samples for all three groups of mice. This assay is complementary to others herein described, as it helps understanding if there is an inflammatory event occurring in the animals or if lung cells maintain their integrity [306,307]. The results obtained are depicted in Figure 4.9.

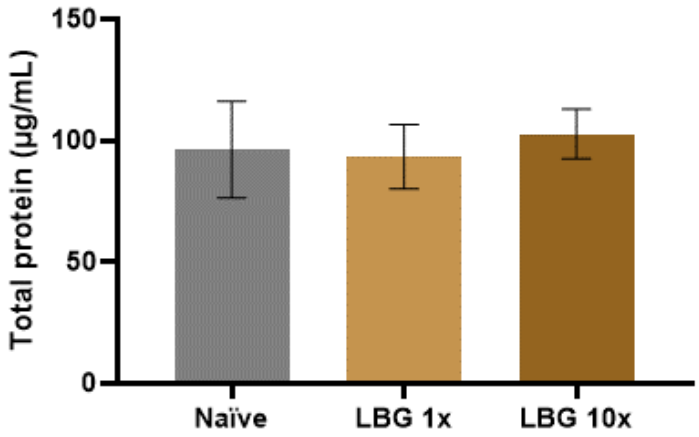

Figure 4.9 – Total protein quantification determined by Bradford assay, in BALF samples, extracted from mice in the three groups tested: naïve, single dose administration (1x) and ten dose administration (10x) of LBG-based microparticles (mean ± SEM, n = 4).

The results obtained for the total protein, in BAL, for all three groups were similar and around 100 µg/mL. No statistical difference was found between groups, thus the result providing another indication that the inhalation of LBG microparticles (LBG 1x and LBG 10x) did not induce an inflammatory process or lung cell disruption, as these events would cause an increase in the total amount of protein.

4.3.2.6. Tissue Index

The determination of the tissue index can also be an indicator of toxicity upon exposure to materials and, in this case, an excipient [308,309]. After the inhalation

period, mice were sacrificed and the organs of interest, such as liver, spleen, lungs, and kidneys, collected and weighed. Afterwards, tissue indexes were calculated, and compared with those obtained for the naïve group, which received no treatment. Results are shown in Table 4.2.

Table 4.2 – Tissue index for liver, spleen, lungs, and kidneys for naïve and treatment groups (LBG 1x: single dose administration; LBG 10x: administration of ten doses) receiving locust bean gum (LBG)-based microparticles (mean + SD, n = 6). Different letters mean different levels of significance for each parameter ($p < 0.05$).

	Liver (%)	**Spleen (%)**	**Lungs (%)**	**Kidneys (%)**
Naïve	22.6 ± 0.8^{a}	5.7 ± 0.2^{b}	8.6 ± 1.1^{c}	12.7 ± 0.3^{d}
LBG 1x	22.7 ± 1.1^{a}	5.9 ± 0.3^{b}	9.0 ± 0.9^{c}	12.8 ± 0.3^{d}
LBG 10x	22.5 ± 0.9^{a}	5.6 ± 0.1^{b}	8.4 ± 1.0^{c}	13.0 ± 0.4^{d}

Considering the results obtained for the treatment groups, by comparison with the naïve set, no statistical significance was detected. The organs of interest maintained their tissue index despite the administration of a dry powder formulation.

4.3.2.7. Histology

Both molecular events in cells and morphology of organs are most important when in an *in vivo* experiment. Through all the previous sections, data have been suggesting that no inflammation process is induced upon the inhalation of LBG microparticles, requiring further studies to determine if it indeed occurs. Histological analysis was performed on lung tissue obtained from animals of each group, to complement the observations described in previous sections. Results are depicted in Figure 4.10.

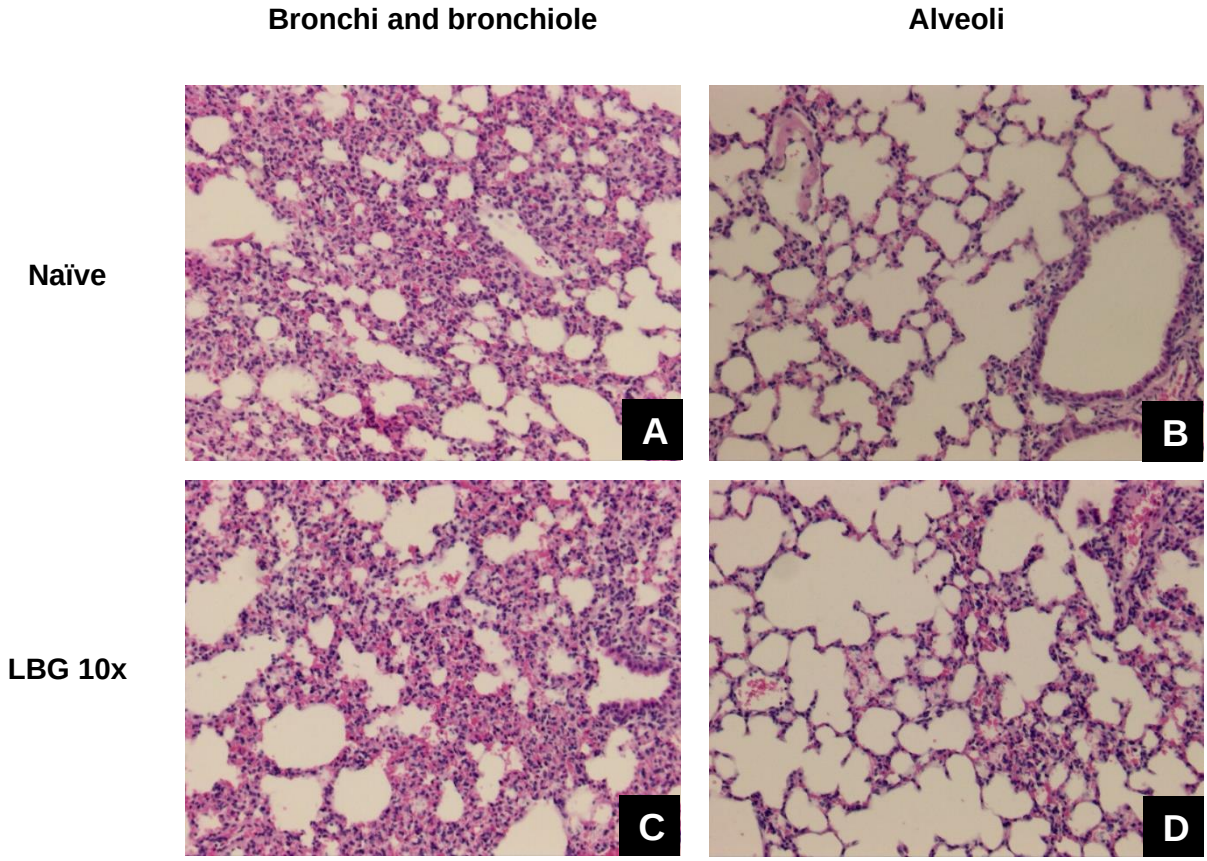

Figure 4.10 – Representative haematoxylin and eosin (H&E) stain lung histology sections (100x) of the bronchi and bronchioles (a, c) and alveoli (b, d) for the naïve group and the animals receiving ten doses of microparticles (LBG 10x).

Lung and bronchi were, in general, normal, with no cellular modifications worthy of note. However, in the images B and D of Figure 4.10, although variable between mice, there seems to occur an infiltration of mononucleated cells in both groups, naïve and the group that received the microparticles. These observations might suggest an infiltration of neutrophils despite the inhalation of LBG microparticles. This infiltration is common in lung injury scenarios [307,310,311] and in lung inflammation [312]. Moreover, the morphology images suggest the occurrence of some molecular event in the lungs of mice, but that cannot be attributed to the inhalation of LBG microparticles because it is also observed in naïve mice. Therefore, further testing would be required to clarify the observations.

In conclusion, the biological risk assessment of LBG herein presented and discussed evidenced a safety profile concerning the polysaccharide. *In vitro* assays provide good indications if a concentration closer to that expected to observe in the lung is considered. The *in vivo* assessment generally provided positive indications, although the occurrence of an eventual inflammatory event cannot be discarded, which should be clarified in subsequent tests. The data herein obtained are a valuable contribution for the event of proposing LBG as a possible excipient in lung delivery applications.

CHAPTER 5:

DEVELOPMENT OF A DEVICE WITH COMPUTER-ASSISTED DESIGN

The information contained in this chapter was partially included in the following patent:

Pontes, Jorge F.; Diogo, Hermínio P.; Conceição, Eusébio; Santos, Rui M.B.; Grenha, Ana. Portable Device to Study the Exposure of Cells to Dry Powders. World Intellectual Property Organization, application n.º PCT/IB2022/060464 (PT 117541), deposited on **31/10/2022** (patent pending).

This page was intentionally left in blank.

5.1. Introduction

In the first chapter, the applicability of the 3D printing at a laboratory scale [313] was discussed, and its use has become a reality. The implementation of 3D printing has followed a low pace, but it has seen great application in scientific experimentation through several methods [314-316]. Figure 5.1 highlights two, the fused deposition modelling [317] and the stereolithography [318] methods.

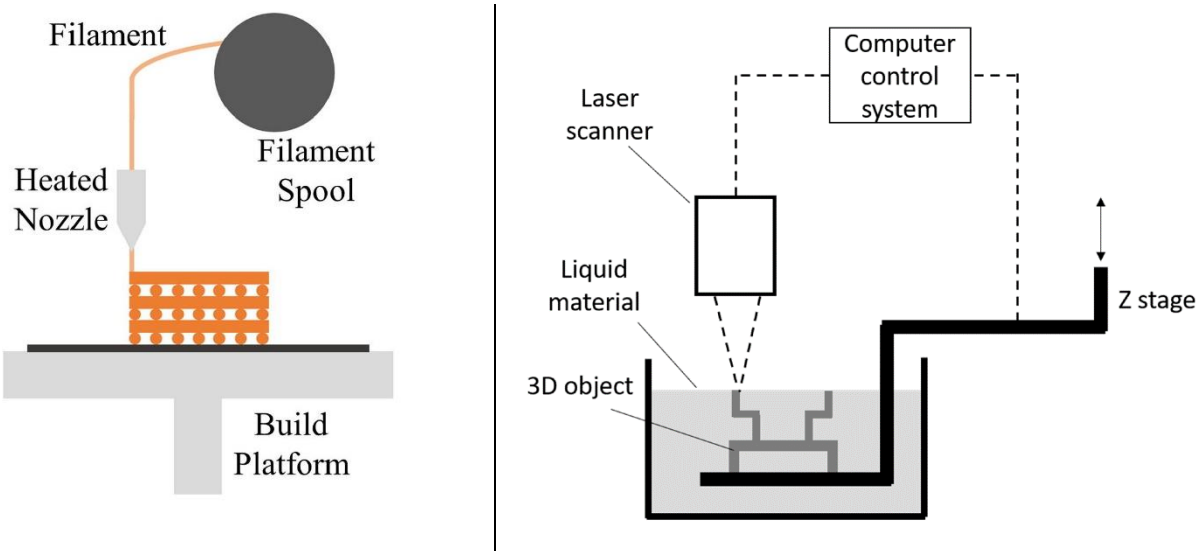

Figure 5.1 – Examples of two methods employed in 3D printing. On the left, the fused deposition modelling method is presented, where a filament is melted by a heated nozzle, and a piece is printed according with the spatial orientation contained in a computer-aided design file read by the 3D printer [317]. On the right, the stereolithography method relies on the hardening of a liquid resin upon incidence of an UV light at specific points of the 3D space contained in a computer-aided design file read by the 3D printer [318].

The easiness of their use, the prospect of idea modulation depending on the necessity and the low costs associated with the materials enable out-of-the-box solutions to day-by-day problems [319]. The areas of application are wide and lung drug delivery can also take benefit of its application [320-322], despite the latter being a niche group. Nowadays, lung diseases and the impact of environment and climate change in the respiratory systems grow in priority and importance [323]. Biorelevant *in vitro* assays are more important than ever, to establish better correlations and draw strong conclusions regarding the impact of aerosols and particles with the

many structures of the lung. In our research group, a need was identified to have a device enabling the insufflation of dry powders over cell cultures, exploring the said *in vitro* approaches. 3D printing was assumed as an adequate technique to obtain the idealised device in a cheap and independent manner.

5.2. Initial steps towards a design

The design and development of a device requires several steps, starting from an idea and conception until it can be made real. Despite the commercially available options, one of the objectives pertaining to this project was the development of a device that enables insufflation, concretely for lung-oriented *in vitro* assays. In fact, the marketed solutions with a similar objective, despite the shown usefulness, constitute an option that is often technically complex and expensive. This project aims at proposing an alternative and economically viable solution and Figure 5.2 depicts what is intended to achieve.

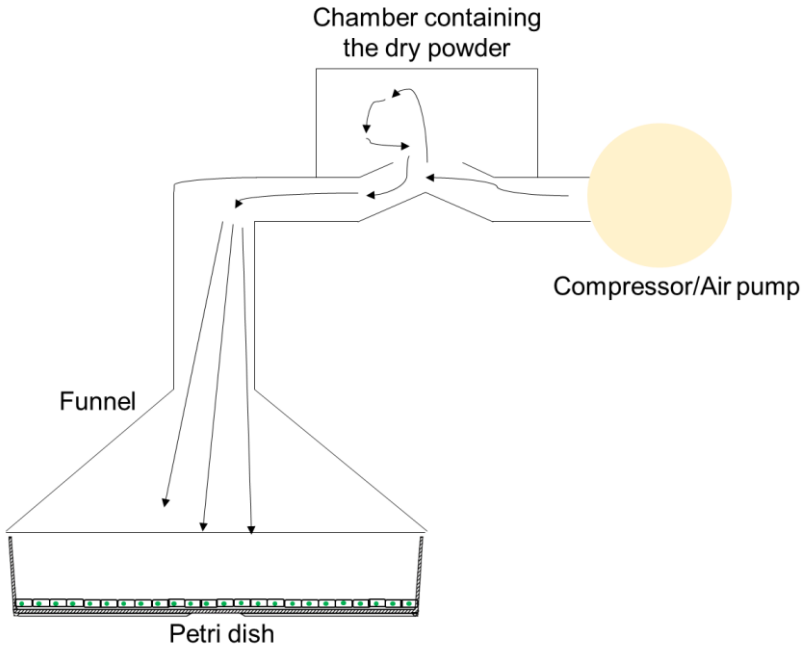

Figure 5.2 – Initial drawing of the concept for a device fitting a petri dish, expected to be the support for cell culture. The powder will be weighed and placed in the chamber, and air will be injected into the system with the help of an air pump. It is intended that the air enters the chamber and drags the powder down through the funnel, onto the petri dish.

The transformation of a drawing to an actual device required the translation of the idea into a project using AutoCAD (Autodesk, Inc., USA). Figure 5.3 shows the 3D digital model of the drawing in Figure 5.2.

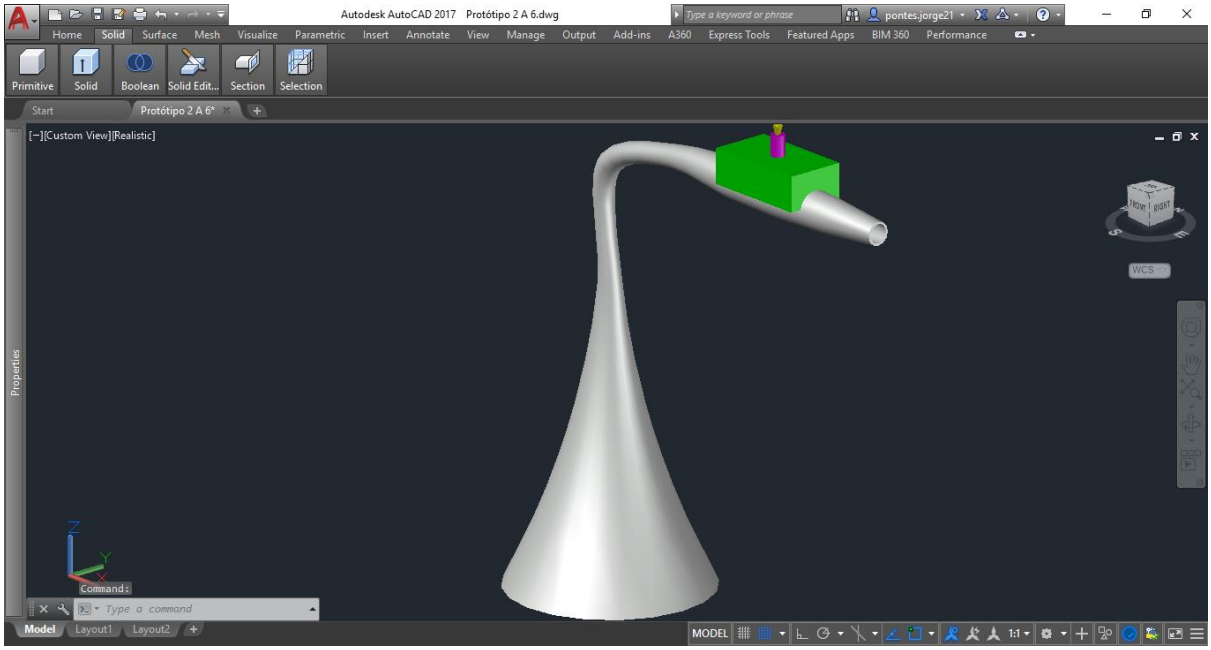

Figure 5.3 – First design of the device, with three major parts: the lower part represents the funnel, which will fit the cell support, and two top parts, one that is the entry point of air, and the green box will be the entry point of the dry powder.

Figure 5.3 depicts a first device containing a funnel intended to be placed on top of a plate/cell support. To achieve this, there is a tube that is the continuation of the funnel to the top, that will function as a connector and driver of the powder, that will be placed inside the green box. The extremity of this tube will be the point of entry of air, that will drag the powder from the green box to the plate/cell support. Although it seemed a robust idea, the design represented on Figure 5.2 and the model showed on Figure 5.3 was not 3D printable. Upon export of this file to another specific software, it was realised that the top part, with that curved design, would fall off during 3D printing. Adding supports to the design was considered, but that would increase the time and materials spent on the device printing. Considering this great limitation, an improvement of the drawing was performed.

5.3. Drawing upgrade to overcome printing limitations

Considering the rough sketch of Figure 5.1 and the limitations of the 3D printing process, adjustments were made to the original idea. A two-piece device was envisaged, comprising a main body (the funnel) and a structure that would be a smaller piece, a weighing head, that would function as a chamber for the dry powder. A new conceptual idea is depicted in Figure 5.4.

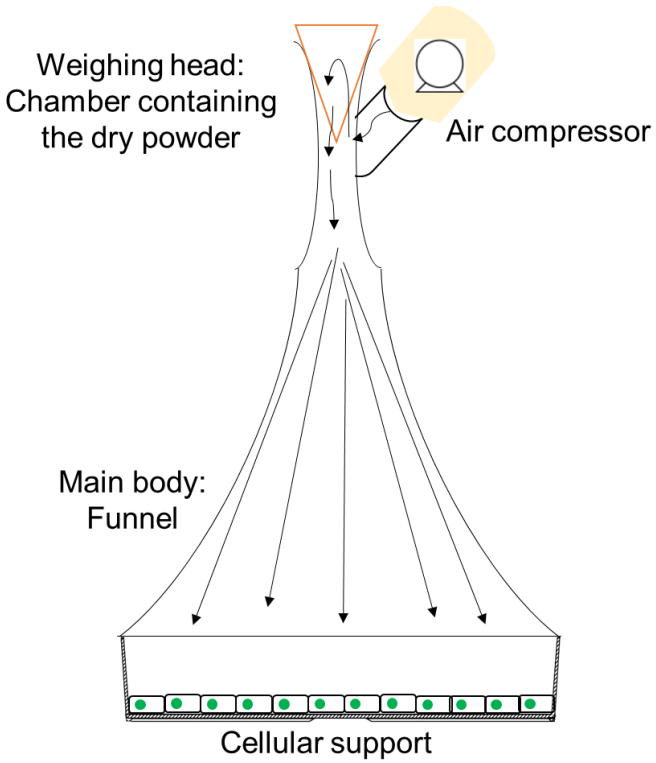

Figure 5.4 – Drawing of the device fitting a petri dish. The powder will be weighed and placed in the chamber (orange triangle), and air will be injected into the system with the help of an air pump. Due to the design of the path, the air, represented by the arrows, will drag the powder onto the funnel, and then to the cell support.

In this concept, it is thought that the powder would be weighed in the orange piece, and then put together with the main body and locked, to avoid leaks. Afterwards, air will be pumped through the entry point, dragging the powder down to the petri dish, where cells will be in culture. The depiction is for a petri dish, with a diameter of 35 mm, but the idea is to adapt the device to other cell supports (6-well and 12-well plates, for example). The 3D digital model of Figure 5.4 is depicted in Figure 5.5.

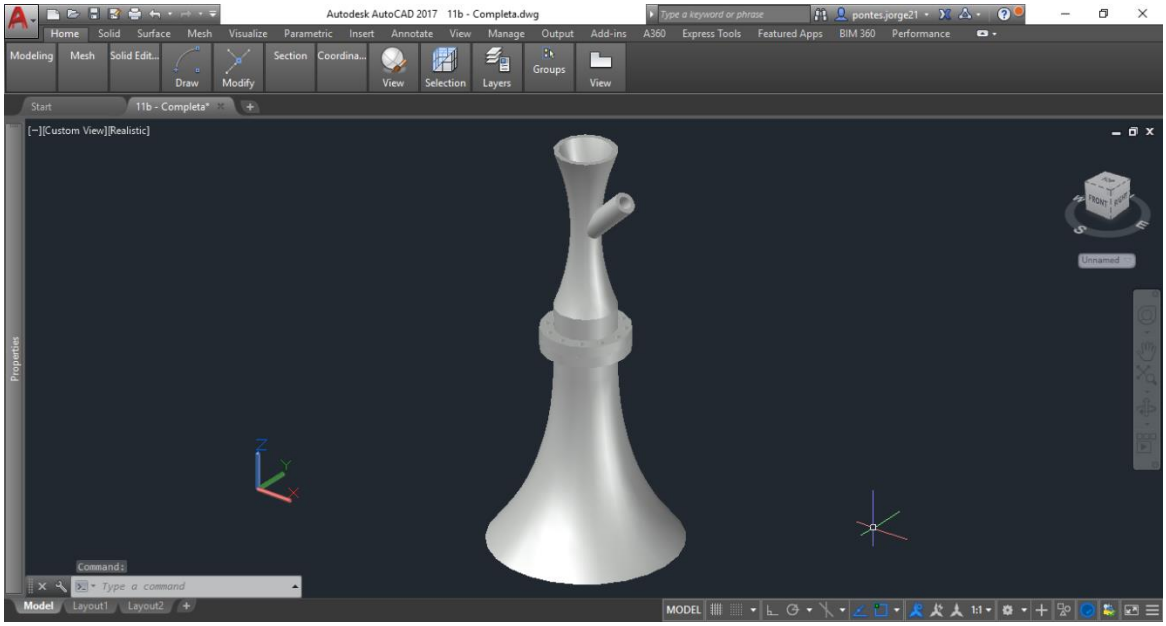

Figure 5.5 – Second design of the device, with two parts. The top part comprises a Venturi tube, with the entrance for the powder and the air. The bottom part, which can be interchangeable between different cell supports, is the funnel.

This second design presented itself as a great improvement from the first. On the one hand, it is completely vertical, thus printable. On the other hand, the possibility of having two separate parts enables its use on different cell supports. However, this second design had some limitations too. With two parts, the height of the device will need to be optimized and well thought out, otherwise it will not be practical. Additionally, it is constructed of two separate parts which, if not properly assembled before use, can lead to loss of powder. Moreover, the requirement of having two parts and then the need to use screws to tightly assemble the parts did not seem feasible. Although it had its advantages, there was a need to go towards a different kind of device. One possibility was the part of the funnel be one single part, which can be seen in Figure 5.6.

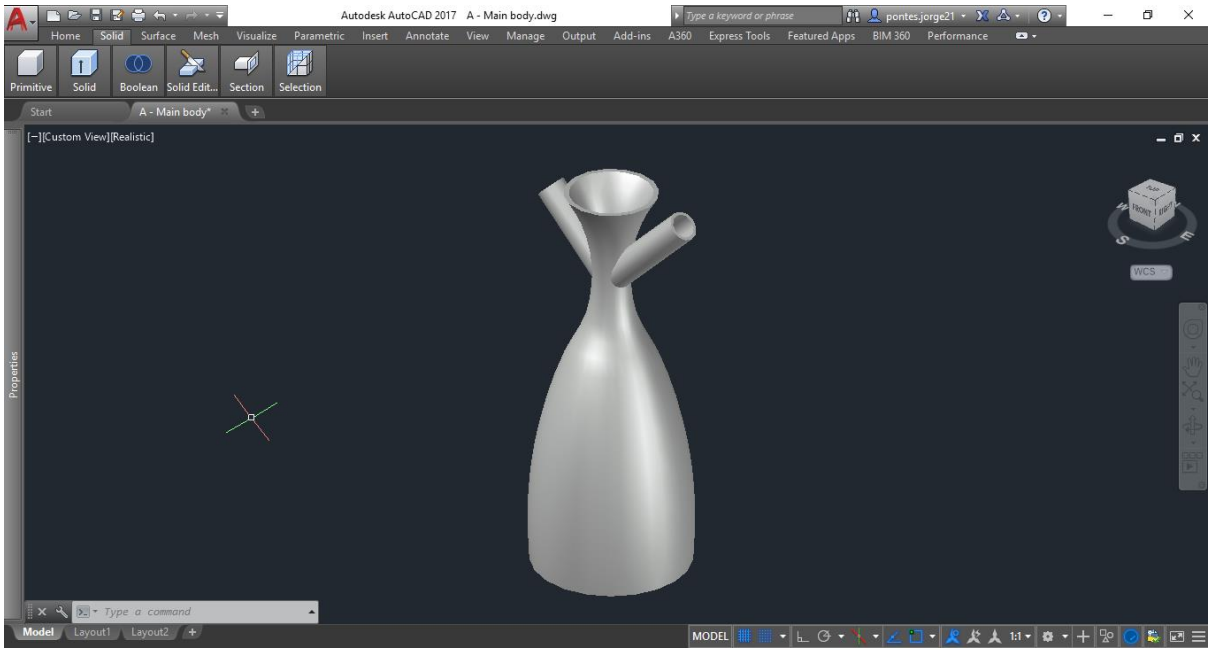

Figure 5.6 – Third design of the device, consisting of a single piece. The entry point for the air is one of the arms. The weighing head that will carry the powder will be placed on top.

The third design is a single piece. The funnel has a curvature of 18.81º, corresponding to the angular measure between the bottom and the point right after the Venturi tube. Initially, a theoretical angle of 18º was set, but due to the intended dimensions of the device, which should not surpass 10 cm, an adjustment was necessary. Even with a slight increase of the overture angle, the design is set to ensure a laminar flow [324], which provides the best dispersion of the powder. In fact, turbulent flow should be avoided in the design of a device, as it favours particle agglomeration [325]. There are two entry points: one for the air, right at the middle of the Venturi tube (one of the arms), and at the top, for the weighing head that will carry the powder, a drawing that can be seen in Figure 5.7. The second arm is purely aesthetic, and together they can anchor to lock the adapter with the powder in place if that need should arise.

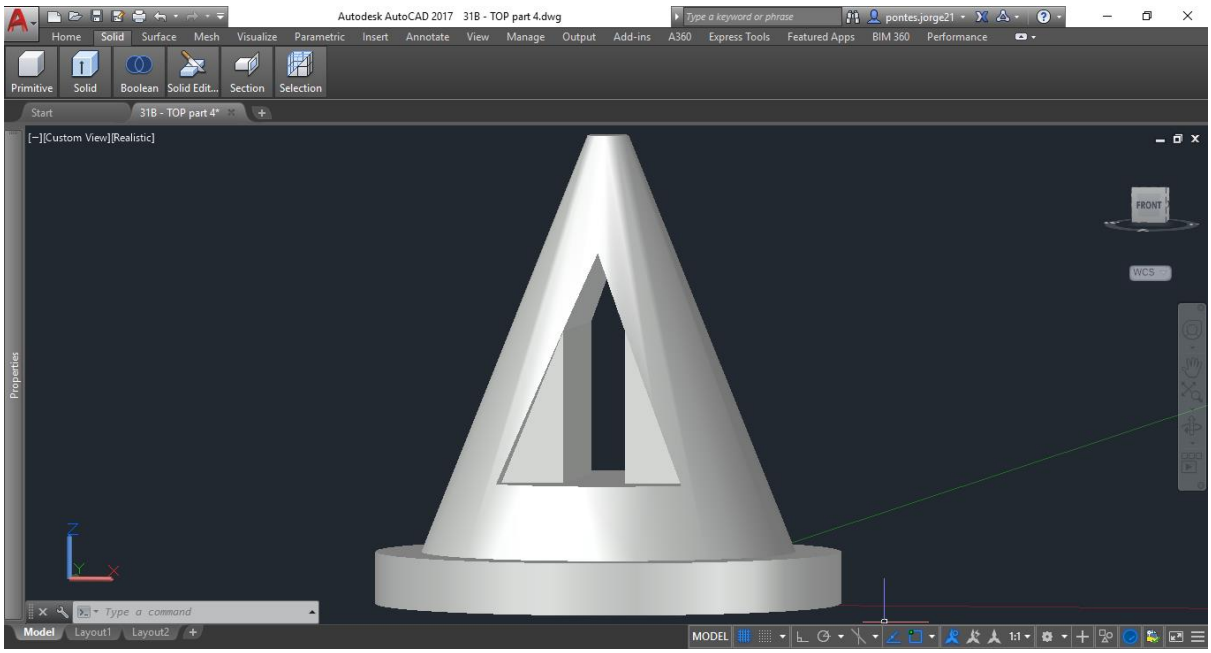

Figure 5.7 – The design of the adapter here presented upside down, in which the powder will be weighed. Besides this, two wedges were added to the design, to make this adapter printable, to work as a support upon printing.

This adapter is one of the most important parts of this device, as it will enable the weighing of the powder inside its structure. Afterwards, it will be inserted on the top of the device, and the air will drag the powder down. Considering the scale of the adapter, some limitations were noticed with the proposed design in Figure 5.7. The main limitation was the amount of powder that could be weighed, and the design itself, which needs to be functional to fulfil its purpose, but it also needs to be printable. Considering all these aspects, a new design for this weighing head can be seen in Figure 5.8.

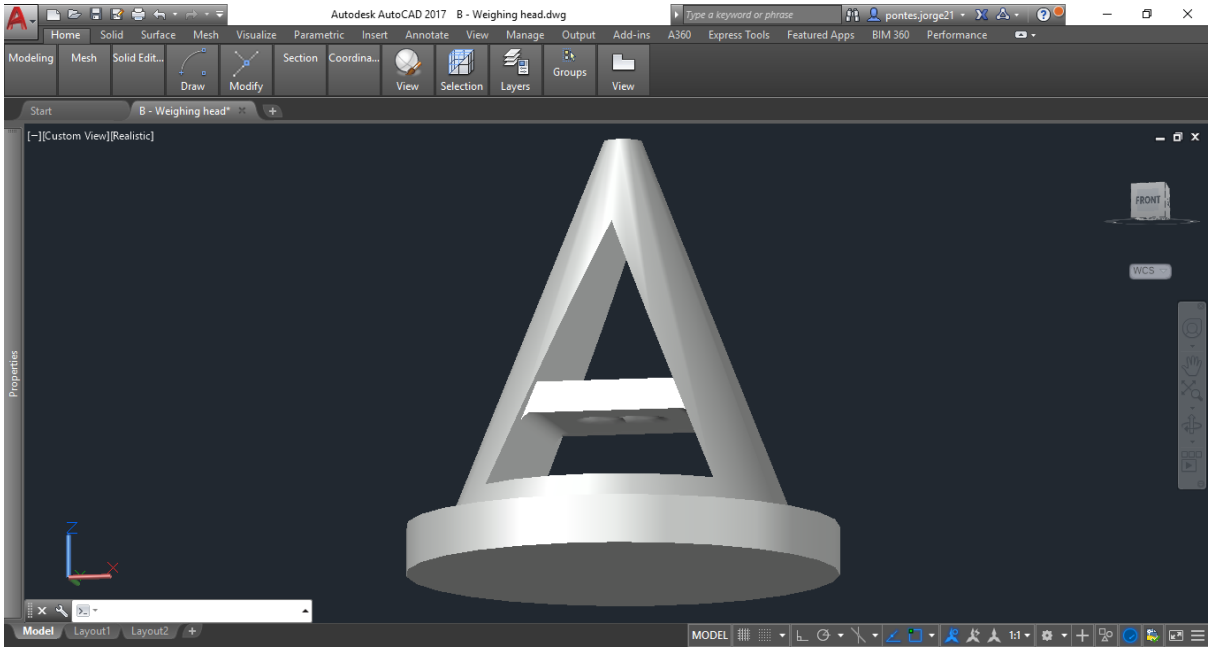

Figure 5.8 – The improved design of the adapter here presented upside down, with a platform for powder weighing. The curves in the margins maintain the adapter free of 90º angles, not promoting powder trapping upon insufflation.

The main structure was maintained from Figure 5.7, but the inside of the piece was changed. In this new proposal, a small platform was created at the middle, to ensure a stable area for the weighing of the powder. A smooth and slight depression on the middle of the platform was designed to have the powder set in a specific point, to not fall over. After some considerations and adjustments, a printable weighing head was achieved.

Upon completion of the final design of both the main body and the weighing head, the respective technical sheets were created. These documents present all measures and angles of the components of the device, so that it can be replicated further. The technical sheet for the main body is presented in Figure 5.9 and the one corresponding to the weighing head is presented in Figure 5.10.

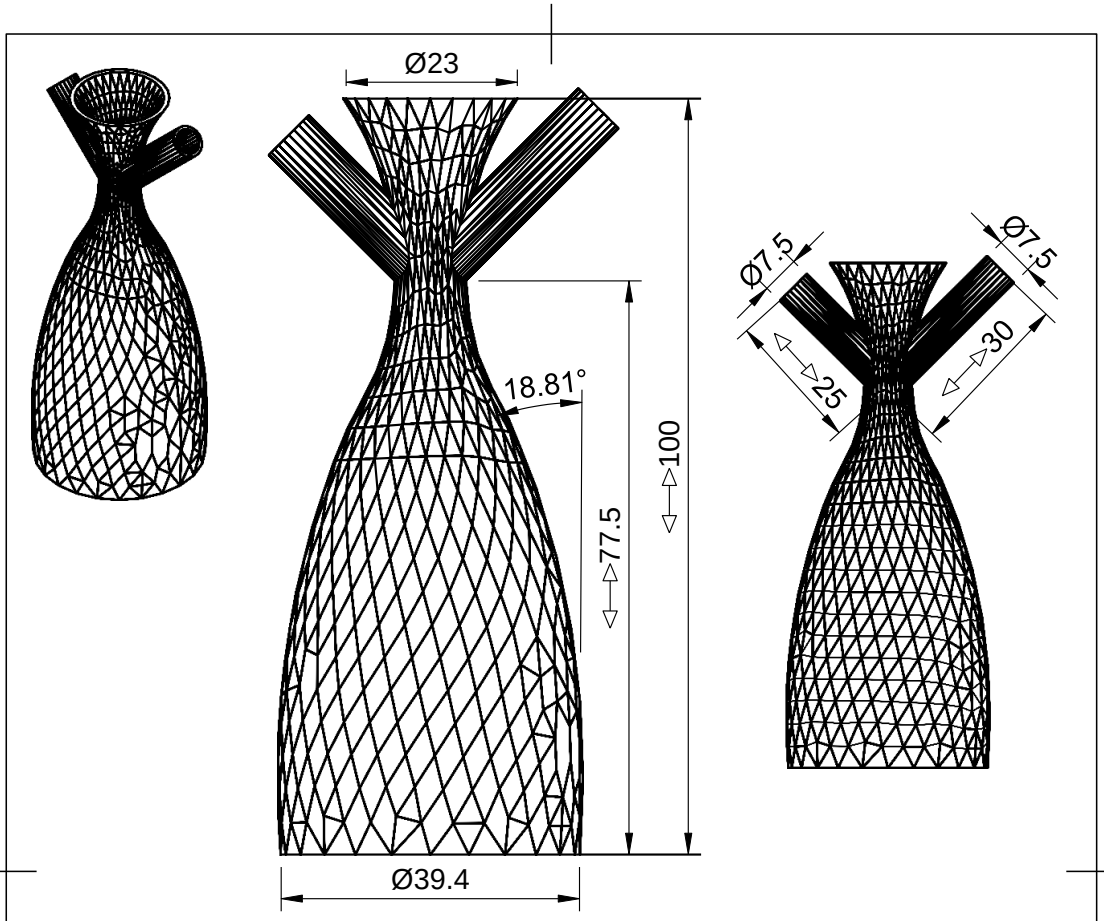

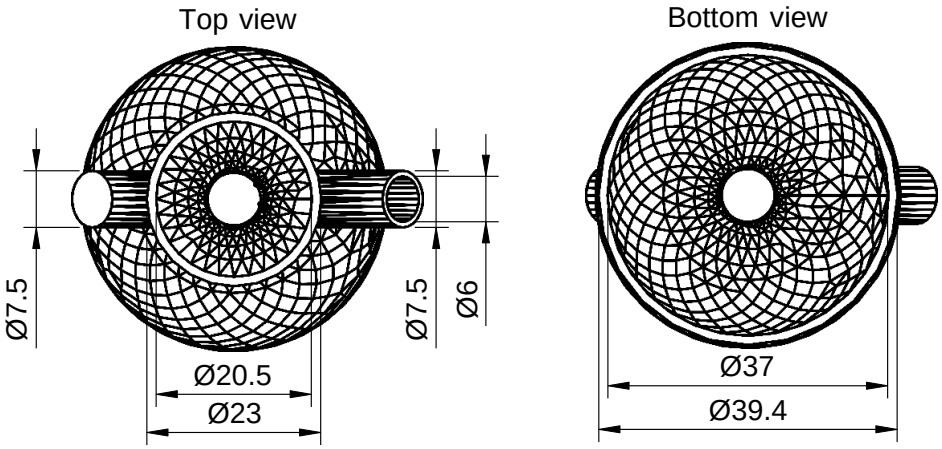

Dept.	Technical reference	Created by	Approved by
	DDLab2.22/001	Jorge Pontes 21-Apr-22	
All measures presented are in mm.		Document type: Technical sheet	Document status:
		Title: A-Main body: Funnel	DWG No.: 17F-BaseTOP+Air7.0
			Rev. / Date of issue / Sheet: 1/1

Figure 5.9 – Technical sheet for the main body of the built device.

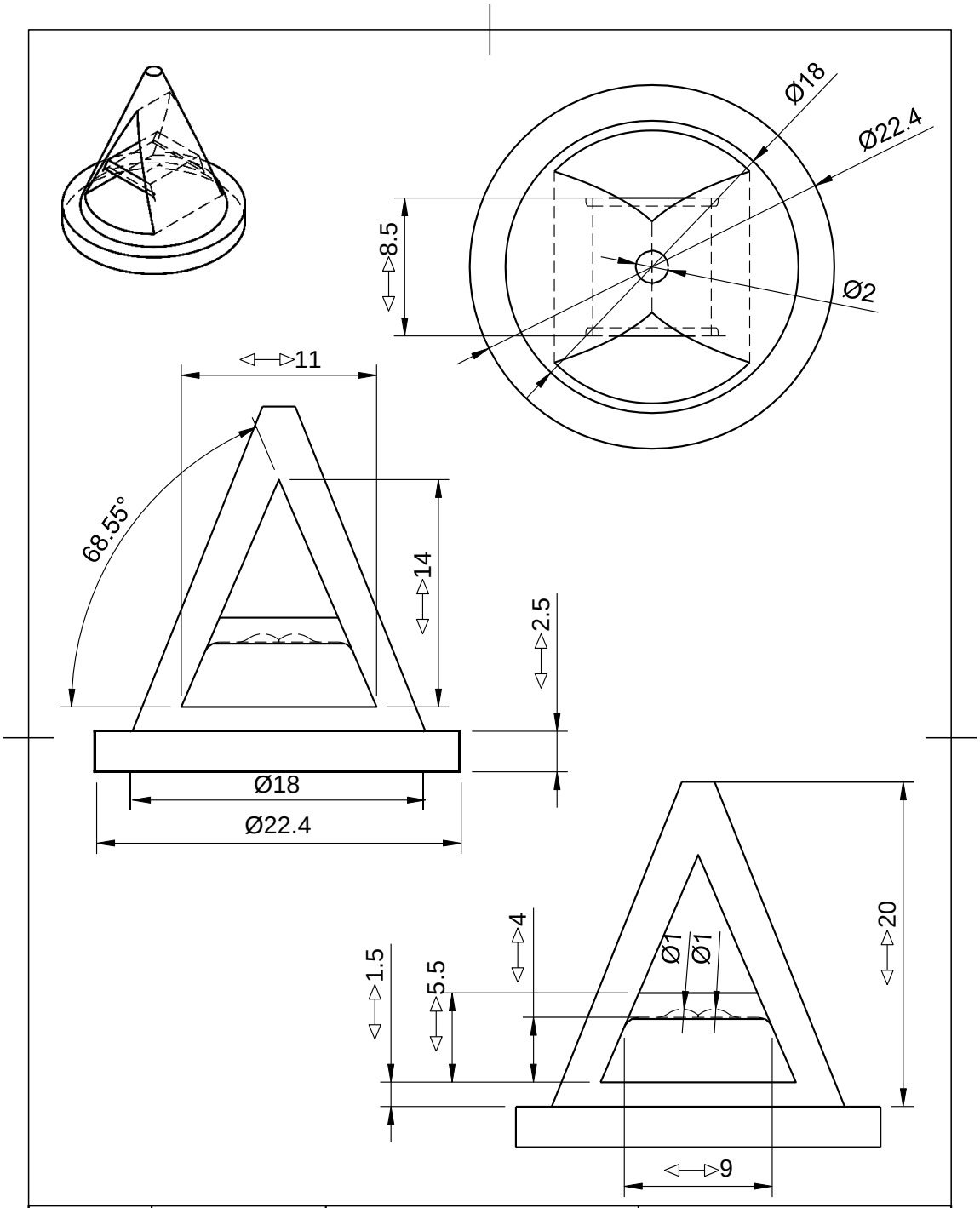

Dept.	Technical reference	Created by	Approved by
	DDLab2.22/002	Jorge Pontes 21-Apr-22	
All measures presented are in mm.		Document type: Technical sheet	Document status:
		Title: B - Weighing head	DWG No.: 42B - TOP part 9
			Rev. / Date of issue: 21-Apr-22 / Sheet: 1/1

Figure 5.10 – Technical sheet for the weighing head of the built device.

After achieving a structure design that could fulfil the intended objective, and after some further adjustments required by the 3D printing process, it was possible to obtain the device, as shown in Figure 5.11.

Figure 5.11 – The first 3D printed device. On the left, the device if fully assembled, and on the right, the two parts are separated, with the weighing chamber on the side.

A depiction of the weighing process is represented in Figure 5.12.

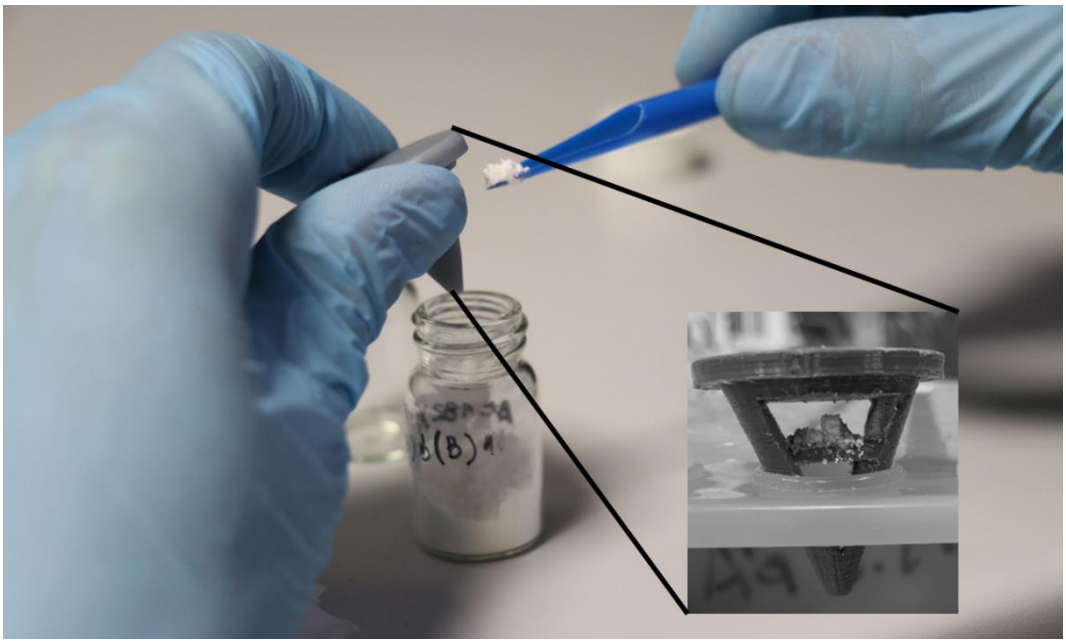

Figure 5.12 – The weighing chamber, the top part of the device, showcasing the platform in which the powder is weighed to be insufflated inside the device.

The first printed device was obtained by a fused deposition modelling method using an extrusion 3D printer, in which the polymer is melted and the device built layer-by-layer [326]. This process creates a rough surface which, upon powder insufflation may hinder its adequate dispersion, because the powder can be trapped in between the layers of the polymeric material. This can ultimately impact the amount of dry powder falling onto the petri dish on the bottom. A new version of the device was printed to address these concerns, using stereolithography as printing methodology, which uses UV light to harden a resin [318]. The new printed device is shown in Figure 5.13.

Figure 5.13 – New device printed by stereolithography using UV light and a washable resin.

For reading and analysis purposes of the remaining sections of this thesis, the device shown in Figure 5.11 will be known as “Device 1 – Brown” and the device shown in Figure 5.13 will be named as “Device 2 – Gray”.

The idea and the design herein presented resulted in a completely new, economically accessible, and easy to manipulate device for *in vitro* insufflation of dry powders. Furthermore, the work that was developed permitted the writing and submission of an international patent, currently under evaluation.

CHAPTER 6:

DOSIMETRY FOR DRY POWDER INSUFFLATION CHARACTERISATION

The information contained in this chapter was partially included in the following patent:

Pontes, Jorge F.; Diogo, Hermínio P.; Conceição, Eusébio; Santos, Rui M.B.; Grenha, Ana. Portable Device to Study the Exposure of Cells to Dry Powders. World Intellectual Property Organization, application n.º PCT/IB2022/060464 (PT 117541), deposited on **31/10/2022** (patent pending).

This page was intentionally left in blank.

6.1. Development of an insufflation method using Device 1

The next step on the development of the device would be to find the most adequate strategy to insufflate the powders. In brief, it is intended that the air pushes the powder resting in the platform, dragging it down in a homogenous spray over a petri dish. Initially, three different pumps were tested: 1) a lens dust blower, 2) a bicycle pump and 3) a syringe, which are depicted in Figure 6.1.

Figure 6.1 – First three pumps tested for the insufflation of powders with the device. From top to bottom: the lens blower (1), the bicycle pump (2) and a syringe (3).

The first pump tested, the lens blower, was the first idea due to its simplicity. However, this strategy was not adequate as the pumped air was constantly in reflux, which resulted in loss of powder. Moreover, the pump revealed ineffective in dispersing the weighed amount (5 mg). The following two pumps tested were also easy to find and to apply to what was envisaged. Moreover, they seemed to show enough force to pump air into the device without the reflux seen with the lens blower. However, both proved ineffective in dispersing the powder, ultimately because they could not generate a strong enough air flow. This led us to use a fourth and fifth pump, namely a garden sprayer and an air compressor (Figures 6.2 and 6.3).

Figure 6.2 – Garden sprayer used to pump air into the device, with the aim of dragging the powder to the petri dish in the bottom.

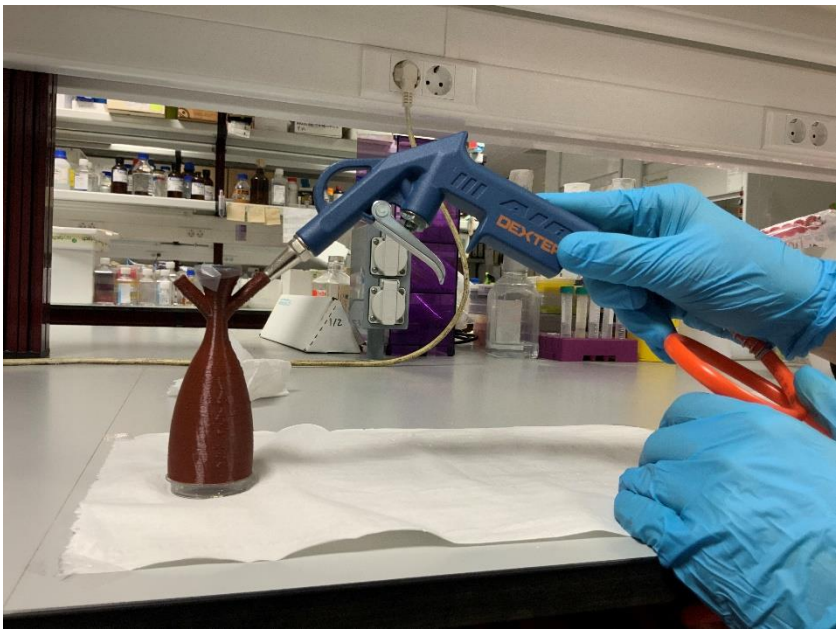

Figure 6.3 – Air compressor used to pump air into the device, with the aim of dragging the powder to the petri dish in the bottom.

The two pumps showed in Figures 6.2 and 6.3 were efficient on generating an air flow that had the necessary strength to drag the powder onto the petri dish that will be used as cell culture support. Both have a reservoir, which accumulates air, allowing a more controlled release of air with no reflux. At this point of the development, this seemed to be a reliable option to continue the studies, and a measure of dry powder insufflation was necessary to quantify the amount of dry powder reaching the cell support. Equation 6.1 was set, with the variable “yield of insufflation” being the quantifiable parameter that will further help with the analysis, as presented next:

$$Yield\ of\ insufflation\ (\%) = \frac{Amount\ of\ powder\ on\ petri\ dish}{Total\ amount\ of\ powder\ weighed} \times 100 \qquad \text{(Equation 6.1)}$$

The insufflation assays were conducted with the pumps shown in Figures 6.2 and 6.3 (garden sprayer and air compressor) using selected powders previously produced by the research group in the context of this and other works. The set of dry powders that was tested is described in Table 6.1, which further shows details related with the production of the microparticles by spray-drying.

Table 6.1 – Dry powder samples selected from microparticles previously produced by the research group. *indicates that the dry powder was not used in the assays described in this chapter

Dry powder (microparticles)	Concentration	Name	T_{inlet} (ºC)	T_{outlet} (ºC)	Aspirator (%)	Feed flow (mL/min)	Reference
LBG Sigma	1% (m/v)	LBG S	130	84 ± 2.4	100	0.90 ± 0.01	Section 3.3.2.1
LBG Industrial Farense*	1% (m/v)	LBG IF*	130	89 ± 7.6	100	0.78 ± 0.03	Section 3.3.2.1
LBG Roeper*	1% (m/v)	LBG R*	130	85 ± 1.7	100	0.82 ± 0.02	Section 3.3.2.1
LBG/INH/RFB	10/1/0.5 2% (m/v) + % w/w	LBG/INH/RFB	160	100 ± 2.0	85	0.7 ± 0.1	[220]
XG	1% (m/v)	XG	160	92 ± 0.5	75	1.37 ± 0.06	Not yet published
XG/Na	10/1 1% m/v + 0.1% w/w	XG-Na	180	108 ± 2.5	90	1.40 ± 0.07	
Hydrolysed XG*	-	HXG*	Intermediate powder, no optimisation performed. Data missing				
Starch/CRG	1% (m/v)	Starch/CRG 1%	Intermediate powder, no optimisation performed. Data missing				
Starch/CRG	2% (m/v) 80/20 % w/w	Starch/CRG 2%	170	110 ± 2.0	90	0.7 ± 0.1	[327]
CRG/Starch	2% (m/v)	CRG/Starch 2%	Intermediate powder, no optimisation performed. Data missing				
KGM	-	KGM	Intermediate powder, no optimisation performed. Data missing				
KGM/Leu	1.5/0.75 % m/v	KGM/Leu	170	104 ± 2.0	85	0.83 ± 0.01	[328]
KGM/Man	1.5/0.75 % m/v	KGM/Man	160	90 ± 3.0	90	0.79 ± 0.02	[328]
KGM/INH/RFB	10/1/1 1.5% m/v + % w/w	KGM/INH/RFB	170	102 ± 2.0	90	0.74 ± 0.05	[257]
DS	2% w/v	DS	115	54 ± 1.4	65	2.7 ± 0.1	[329]

LBG: locust bean gum, INH: isoniazid, RFB: rifabutin, XG: xanthan gum, Na: sodium, CRG: carrageenan, KGM: Konjac glucomannan, Leu: leucine, Man: mannitol, DS: dextran sulphate.

An initial approach regarding these insufflation tests required the knowledge of how these pumps worked and how to set the experimental protocol to enable comparisons. When the garden sprayer is completely full, it takes approximately 7 seconds to empty its reservoir, at a certain velocity, which was measured with a portable anemometer. Since the compressor's reservoir is much bigger, and after a pressure adjustment of the air output, the experimental protocol was set to last for 14 seconds, with a constant release of air at a velocity that was similar to the garden sprayer. This way, the contact of air with the dry powder was maximised, enabling its dispersion from the weighing head to the cell support. The results obtained are shown in Table 6.2.

Table 6.2 – Insufflation yields for the first assays with a garden sprayer and the air compressor. Some acronyms are as follows: LBG: locust bean gum, INH: isoniazid, RFB: rifabutin, XG: xanthan gum, Na: sodium, KGM: Konjac glucomannan, Leu: leucine, Man: mannitol, DS: dextran sulphate.

Powders	Garden sprayer (%)	Air compressor (%)
LBG S	3.4 ± 2.5	4.8 ± 1.8
LBG/INH/RFB	0.5 ± 0.3	3.3 ± 2.3
XG	7.3 ± 4.3	10.4 ± 6.8
XG-Na	15.1 ± 3.5	14.9 ± 8.8
KGM	1.7 ± 1.4	6.1 ± 4.4
KGM:Leu	1.7 ± 0.7	6.6 ± 2.2
KGM:Man	1.3 ± 0.4	1.8 ± 0.9
DS	11.1 ± 5.7	23.9 ± 10.6

The main limitation concerning the data shown in Table 6.2 is that the overall insufflation yields are low, regardless of the pump used. This drawback will be addressed in more detail in the following sections, and several optimisations will be explored to increase the results obtained in this first screening. Nevertheless, observations made with both pumps revealed higher yields for the assays where air compressor was used. In fact, a more thorough analysis of the assays indicated that the force of the air that comes out of the compressor and its more constant flow, seem to be the reasons behind the higher insufflation yields. Additionally, the garden

sprayer is not too practical, because there is a need to manually fill its reservoir every time it needs to be used, hindering assay reproducibility. Finally, the existence of a manometer on the compressor, allowing a more precise selection of an air outlet pressure, gives this pump an accuracy that the garden sprayer cannot compete with. Considering the data and the analysis herein, the pump chosen to continue the assays was the compressor. Moreover, although several powders with distinct aerodynamic features were used, this first approach aimed at choosing the best apparatus to better disperse the dry powders when using the developed device. A more systematic analysis focused on the aspect of the dry powders at a macroscopic level, for instance addressing their aggregation, will be performed in the next chapter.

The next step towards the exploration of the capabilities of the compressor involved testing several outlet air pressures, to determine the most adequate conditions. In the early tests, an outlet air pressure of 90 psi was used to achieve the same velocity of air, at a constant flow rate, to match the one of the garden sprayer. However, further testing using this outlet air pressure resulted in high losses of powder and a difficulty to control the stability of the device. Furthermore, the previous method relied on timing the seconds by which the insufflation assay would be performed. Despite having a continuous air stream coming out of the compressor, this method could result in imprecise doses after the assay was finished. Thus, these occurrences forced a change in the insufflation method.

The use of the compressor relies on three main aspects: the manometer that enables the choice of the outlet air pressure, a hose that directs the circulation of air from the reservoir and an air pistol that, upon activation, allows the air to come out. The activation of the air pistol is done by pressing a trigger, resulting in the release of air that can have different strengths depending on the pressure applied to it. Considering this, several tests were performed, where the most adequate number of trigger presses were tested (either 20 or 30), as well as their duration (either quicker or longer air streams). These tests revealed that for the powder to be efficiently dragged at quantifiable amounts, the air pistol would have to be triggered rapidly for 30 times. The three powders providing the higher yields (see Table 6.2) were

selected for these first assays, where a range of outlet air pressures between 30 and 60 psi were tested. The results can be seen in Figure 6.4.

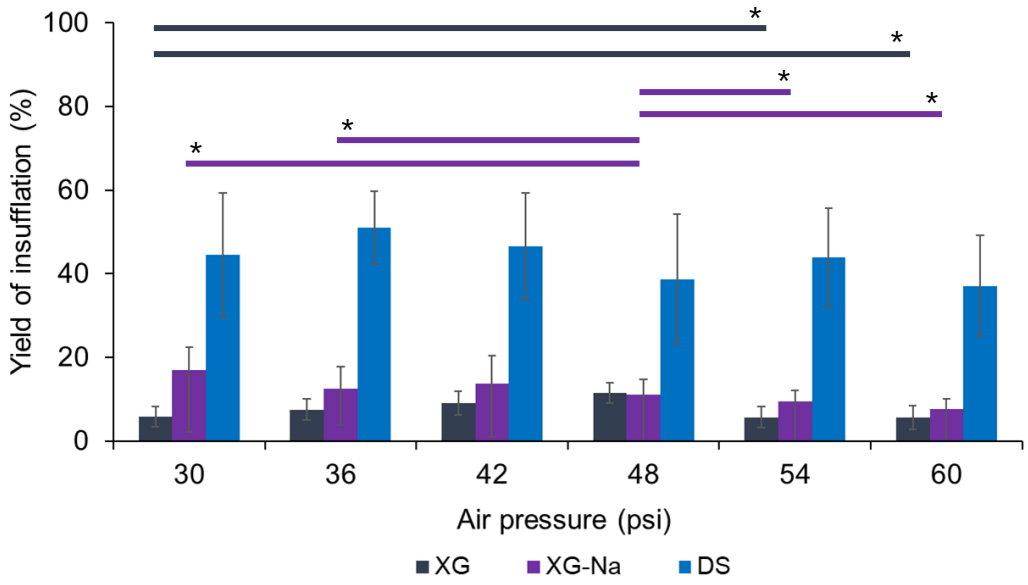

Figure 6.4 – Insufflation yields obtained with the Device 1 – Brown, for microparticles (MP) composed of xanthan gum (XG), xanthan gum/sodium chloride (XG-Na) and dextran sulphate (DS) (●●●, Table B.V in Annex B). Results are presented as mean ± SD, n = 10. Top bars indicate statistical differences ($p < 0.05$) with colours corresponding to those of the dry powder formulations.

The results shown in Figure 6.4 indicate that, overall, pressures of 36 and 42 psi are those maximising the yield of insufflation, though it depends on the dry powder used. Observations of tests performed at different air pressures indicated that it is possibly the macroscopic aspect of powders that impacts powder dispersion. In this regard, more than specifically characterised features of the dry powders, like geometric diameter, the results of yield of insufflation are mainly driven by their appearance to the naked eye. In fact, macroscopically, dextran sulphate (DS) microparticles occur as larger particles while xanthan gum (XG)-based powders have a smoother and finer appearance. DS microparticles might be more aggregated than XG and XG/sodium chloride (XG-Na) microparticles, which, under the conditions established for the assay, see a facilitated dispersion. Moreover, higher outlet pressures associated with finer powders (XG and XG-Na microparticles) can be linked to lower yields, as these dry powders tend to either escape or adhere to the main body of the

device. The yield of insufflation was, thus, suggested to depend on the particle/powder. Therefore, other polysaccharide-based microparticles with similar aspect between each other were tested, selecting the air pressures providing the best results in the previous assays (36 to 48 psi). Results are presented in Figure 6.5.

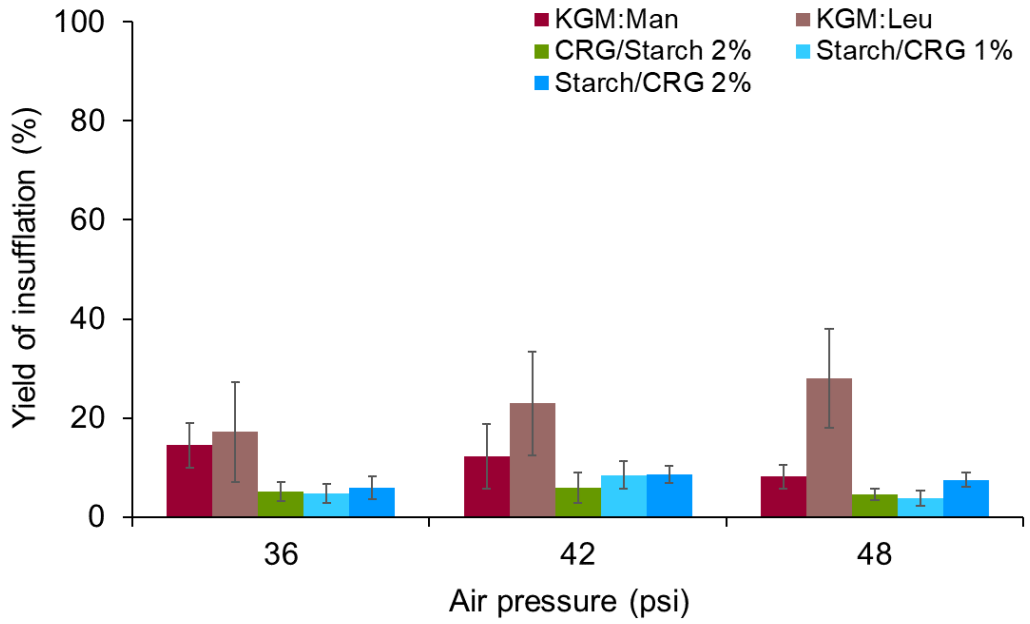

Figure 6.5 – Insufflation yields obtained with the Device 1 – Brown, for microparticles composed of konjac glucomannan with either mannitol or leucine (KGM:Man and KGM:Leu), starch and carrageenan (CRG) (●●●●●, Table B.V in Annex B). Results are presented as mean ± SD, n = 10, and differences were considered statistically significant when $p < 0.05$.

As said above, the powders tested in this set of insufflation assays had very similar appearance, being finer powders when compared to the assay resulting in Figure 6.4. The results suggested that microparticles prepared with konjac glucomannan (KGM) generally showed significantly higher yields ($p < 0.05$) than all other powders tested at the three selected outlet air pressures (36, 42 and 48 psi), independently of the used co-excipient. One other aspect that needs to be taken into consideration is that, when leucine (Leu) was used, dry powders tended to aggregate more during the insufflation assay, thus rendering higher yields. The contrary was observed when mannitol was used, as this powder did not aggregate as much during the tests,

which resulted in lower yields. The remaining dry powder formulations had yields that were similar between each other, and their behaviour similar upon testing. In conclusion, lower air pressures (36 and 42 psi) are suggested to be the most adequate to better disperse dry powders independently of their macroscopic appearance.

Further experiments were performed with the referred air pressures, testing other dry powders. In this regard and considering the aim of developing an LBG-based drug delivery platform, the dry powders described in Chapter 3 were tested (Tables 3.3, 3.4 and 3.5). In brief, dry powders produced with LBG from Sigma-Aldrich®, Industrial Farense® and C. E. Roeper®, at different inlet temperatures of the spray-drying equipment, were insufflated using Device 1. The aim focused on the assessment of the insufflation behaviour of the dry powders and results evidenced that the use of different T_{inlet} (see section 3.3.2.1) did not impact the obtained insufflation yields (Figures A.I, A.II and A.III, Annex A).

In all, the data herein shown and discussed allowed the development of a method to insufflate dry powders onto a petri dish using Device 1 – Brown. Despite the low insufflation yields obtained, the purpose for which the insufflation device was created was achieved and further optimisation will be addressed in the next chapter.

This page was intentionally left in blank.

CHAPTER 7:

QUARTZ CRYSTAL MICROBALANCE AND DRY POWDER INSUFFLATION: DETERMINATION OF DEPOSITION PROFILE AND CELL VIABILITY

The information contained in this chapter was partially included in the following publication:

Pontes, Jorge F.; Diogo, Hermínio P.; Conceição, Eusébio; Santos, Rui M.B.; Grenha, Ana. Portable Device to Study the Exposure of Cells to Dry Powders. World Intellectual Property Organization, application n.º PCT/IB2022/060464 (PT 117541), deposited on **31/10/2022** (patent pending).

This page was intentionally left in blank.

7.1. Introduction

The advancement of technology provides several improvements concerning analytical methods. One of these examples refers to the integration of electronics in respiratory delivery by means of piezoelectric sensors [330,331]. Piezoelectricity is a phenomenon first described in the late 19th century by Jacques and Pierre Curie, entailing the production of a proportional electric potential by the mechanical compression of specific crystals in certain directions [332]. Since then, the QCM was developed, and it has found applications in environmental sciences [333], medicine [334], and as a biosensor [335], among others [336]. The sensor within the QCM is comprised of a quartz crystal that is in between two gold electrodes [334] (Figure 7.1).

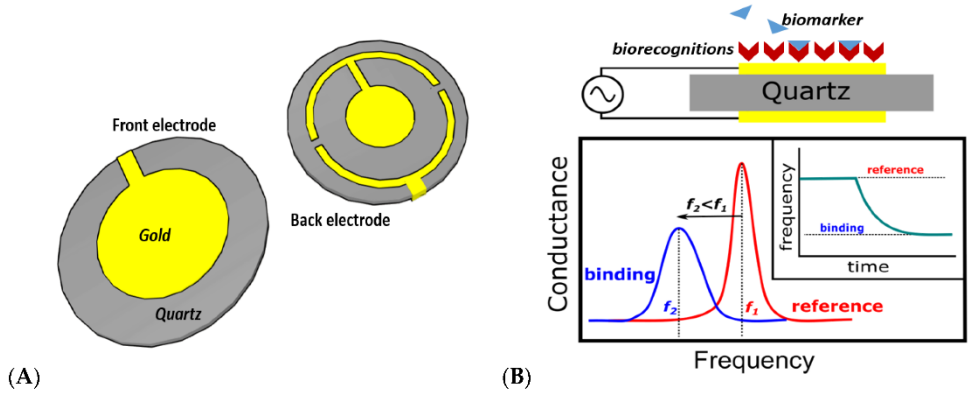

Figure 7.1 – Representative images of a QCM electrode (A) and a depiction of a circuit containing a QCM sensor with an example of a frequency decrease related to the binding of a biomarker (B). Adapted from [334].

When this sensor is connected to an oscillator and an electric current is applied, there is a mechanical deformation of the quartz crystal in two opposite directions, creating a wave propagating across the crystal. This wave is understood as a vibration frequency, that is highly sensitive to materials that deposit on top of the crystal. Sauerbrey described this phenomenon in 1959, stating that there is a change in the frequency of a vibrating quartz crystal when the deposition of materials occurs [337]. Additionally, it is this frequency change that allows the precise determination of the deposited mass of the materials tested. In this regard, due to the QCM sensitivity, it is possible to develop a QCM-based method for the detection of chiral molecules, as described elsewhere [338]. Furthermore, it is possible to use the QCM in immunology assays to characterise the binding mechanisms between antigens

and antibodies [339]. Another possible use of the QCM pertains to its use as a more precise balance by comparison with more conventional apparatus (technical and analytical laboratory weighing scales) [340-342]. By doing so, the QCM can also find a suitable usability in lung drug delivery, enabling testing of dry powders by insufflation.

The aim of this chapter is, thus, to use the QCM to develop an experimental method for the determination of the deposition profile of dry powders relying on their insufflation onto a quartz crystal. The resulting variation of frequency will allow the analysis of the dispersion pattern of the samples, which varies depending on the type, morphology and shape of the dry powders, herein comprised of polymeric microparticles.

7.2. Materials & Methods

7.2.1. Materials

LBG was obtained from three different suppliers, one was acquired from Sigma-Aldrich® and the other two were kind gifts from Industrial Farense® and C. E. Roeper®. Xanthan gum, D-mannitol (CAS n.º 69-65-8, MW = 182.17 g/mol), isoniazid (CAS n. º 54-85-3, ≥ 99.0% (TLC), MW = 137.14 g/mol), L-glutamine solution (200 mM), non-essential amino acids solution and penicillin/streptomycin (10000 units/mL, 10000 g/mL), trypsin-EDTA solution (2.5 g/L trypsin, 0.5 g/L EDTA), trypan blue solution (0.4%), thiazolyl blue tetrazolium bromide (MTT), sodium dodecyl sulphate (SDS), dimethylformamide (DMF), Triton-X 100, phosphate buffered saline (PBS) tablets pH 7.4, dimethyl sulfoxide (DMSO) were acquired from Sigma-Aldrich (Germany). Fetal bovine serum (FBS) was purchased from Gibco (Life Technologies, USA). Dulbecco's modified Eagle's media (DMEM) was acquired from BioConcept (Switzerland) and RPMI 1640 media from Lonza Group AG (Switzerland). Konjac glucomannan and RFB (CAS n. º 72559-06-9, 97.5%) were acquired from CHEMOS (Altdorf, Germany). Leucine was purchased from Panreac AppliChem (CAS n. º 61-90-5, MW = 131.18 g/mol, Germany), Ultrapure water (Milli-Q, Millipore, Watford, UK) was used throughout. All other chemicals were reagent grade.

7.2.2. Tested dry powders

Several dry powder formulations corresponding to microparticles produced by spray-drying were used throughout the work, which are described in detail in Table 6.1 of Chapter 6.

7.2.3. Data acquisition

Maxtek quartz crystals (5 MHz, Inficon) were used, which were previously coated with optically flat polished gold electrodes on both sides, and cleaned before use with absolute ethanol, ultrapure water and a piranha solution comprised of 3:1 mixture of sulphuric acid and 30% hydrogen peroxide for 15 min. Cleaned crystals were mounted on a kynar crystal holder (Maxtek CHT-100). The crystal holder was connected to a universal frequency counter (Agilent 53131A) through a phase-locked oscillator (Maxtek PLO-10i). The frequency counter was connected by GPIB to a computer running a data acquisition and control program developed in Keysight Visual Engineering Environment (VEE, Pro version 9.33, Agilent) for the real time acquisition of the QCM frequency.

7.2.4. Insufflation assays

Thirteen polysaccharide-based microparticles developed for lung applications, previously prepared by spray-drying (Buchi Mini Spray-Dryer, Buchi Labortechnik AG, Switzerland), were selected as model dry powders to test the device (Table 6.1). Before the assay, all parts of the device were weighed. Afterwards, 5 - 10 mg of dry powder were weighed in the weighing head, the device assembled and placed over the crystal holder (Maxtek CHT-100). The powder was aerosolized after blowing air into it (10 quick insufflations from an air compressor, Goldair), with an outlet pressure of the air compressor set at 30 psi. After conclusion of the assay, the parts of the device were weighed, the frequency data saved in an Excel file and images of the crystal and the device recorded after powder deposition.

7.2.5. Aerosol characterisation: deposition profile and yield of insufflation

7.2.5.1. Dry powders characterisation

The dry powders herein used were characterised regarding their morphology obtained by FESEM and their geometric size estimated as Feret’s diameter following the protocols detailed in section 3.3.1.5.

7.2.5.2. Aerodynamic diameter calculation

A theoretical aerodynamic diameter of the formulations, in µm, was calculated, whenever possible, according with Equation 1.1.

7.2.5.3. Dry powder deposition profile

The variation of the frequency was recorded in function of time between 0 and 300 seconds. The data generated allowed the drawing of a graph detailing the frequency change in different events along the assay: a first equilibrium, which establishes the baseline, a great frequency change when air and dry powder contact with the crystal and lastly, a second equilibrium, in which a new frequency is determined due to mass change.

7.2.5.4. Yield of insufflation

The amount of dry powder deposition was obtained, according with the simplified Sauerbrey equation [337] (Equation 7.1):

$$\Delta f = -C_f \times \Delta m \qquad \text{(Equation 7.1)}$$

in which, Δf represents the difference in frequency between the states with and without powder at a given point, C_f is the sensitivity factor of the crystal, in this case, 0.056 $Hz/ng/cm^2$ for a 5 MHz crystal at 20 ºC, and Δm is the change in mass per unit area (g/cm^2). Afterwards, a yield of insufflation was determined using Equation 6.1, which was adapted to consider the amount of powder on the crystal.

A qualitative correlation between powders was established, meaning that the highest yield obtained, recorded for LBG Sigma, will be assumed as the maximum (100%), and all the remaining will be calculated and adjusted considering this reference. This new parameter is called $degree\ of\ insufflation$ (Equation 7.2):

$$Degree\ of\ insufflation = \frac{Average\ yield\ of\ insufflation\ of\ powder\ Z}{Average\ yield\ of\ insufflation\ of\ LBG\ S} \qquad \text{(Equation 7.2)}$$

where “average yield of insufflation of powder Z” pertains to the average yield result of all other powders tested, except the LBG-based microparticles prepared with LBG from Sigma-Aldrich® at an inlet temperature of 130 ºC.

7.2.6. Cell culture

Human lung epithelial adenocarcinoma cells (A549) were provided by the American Type Culture Collection (ATCC, USA) and used in passages 24-30. Cells were cultured in flasks (75 cm^2), at 37 °C, in an incubator with 5% CO_2/95% humidified atmospheric air. Cell culture media (CCM) was Dulbecco’s modified Eagle’s medium (DMEM, BioConcept, Switzerland), supplemented with L-glutamine 200 mM (1%, v/v), non-essential amino acids (1%, v/v), penicillin/streptomycin at 1% (v/v) and FBS at 10% (v/v). CCM was exchanged two to three times weekly.

7.2.7. Metabolic activity test after insufflation

The metabolic activity of A549 cells after insufflation of LBG S powders was assessed. Cells were seeded in petri dishes with 35 mm of diameter (9.4 cm^2), at $3x10^5$ cells/plate and incubated overnight. The next day, CCM was removed, and both air and dry powders were insufflated onto the cultured cells for an exposure time of 3 h or 24 h. Afterwards, 500 µL of CCM without phenol red were added to the petri dishes to avoid desiccation of the cells. After the defined exposure time, the CCM and samples were removed, and replaced by 750 µL of a solution of MTT (5 mg/mL in PBS pH 7.4), which remained under incubation for 2 h. After that, 1.5 mL of DMSO were added to each plate to solubilise the formazan crystals. The absorbance was read by spectrophotometry (Infinite M200; Tecan, Austria) at 540 nm, with background correction at 640 nm. The cell viability was calculated using Equation 4.1.

7.2.8. Statistical evaluation

7.2.8.1. For insufflation assays

A one-way ANOVA (Dunnett’s test) with the pairwise multiple comparison procedure was used to compare the results obtained for the degree of insufflation of the different dry powders. A control set of data pertaining to the degree of insufflation of LBG-based microparticles from Sigma-Aldrich® was used for comparison. All

analyses were run using GraphPad Prism® statistical program (GraphPad Software, version 9.4.0.673), and differences were considered significant at a level of $p < 0.05$.

7.2.8.2. For cell viability assays

A two-tailed unpaired t-test was performed on the data pertaining to the cell viabilities obtained. Results were analysed in two different scenarios: (1) the influence of insufflation or either air or air plus dry powders and (2) the effect of time after insufflation. All analyses were run using GraphPad Prism® statistical program (GraphPad Software, version 9.4.0.673), and differences were considered significant at a level of $p < 0.05$.

7.3. Results and discussion

7.3.1. Acquisition program

The setup that was assembled to determine the deposition profile of all tested powders can be seen in Figure 7.2.

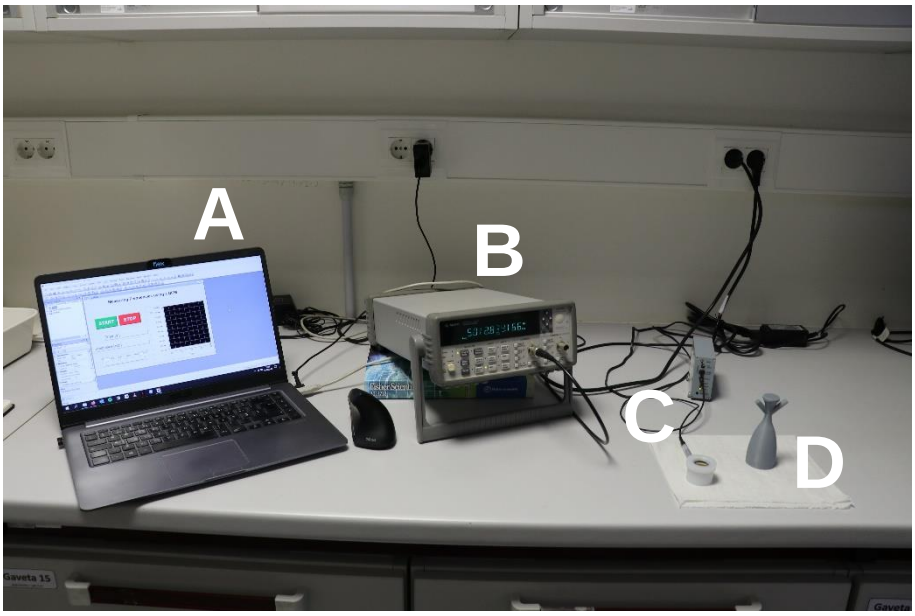

Figure 7.2 – Quartz Crystal Microabalance (QCM) setup. From left to right: computer with acquisition program (A), frequency counter (B), crystal holder and the oscillator behind (C), and the insufflation device (D). Photo credits: Chiu Chu (CCMAR).

The frequency counter is one of the crucial parts of the QCM setup, as it reads the oscillation frequency at any given time. For the assessment of the different

deposition profiles of the dry powders, it was required that all frequencies during the time of the assay were registered and saved for analysis. The frequency counter is from Agilent®, which also has available a program called Keysight Visual Engineering Environment (VEE). This software enables the design of a program that fulfils the aim of registering all frequencies. Figure 7.3 depicts its architecture.

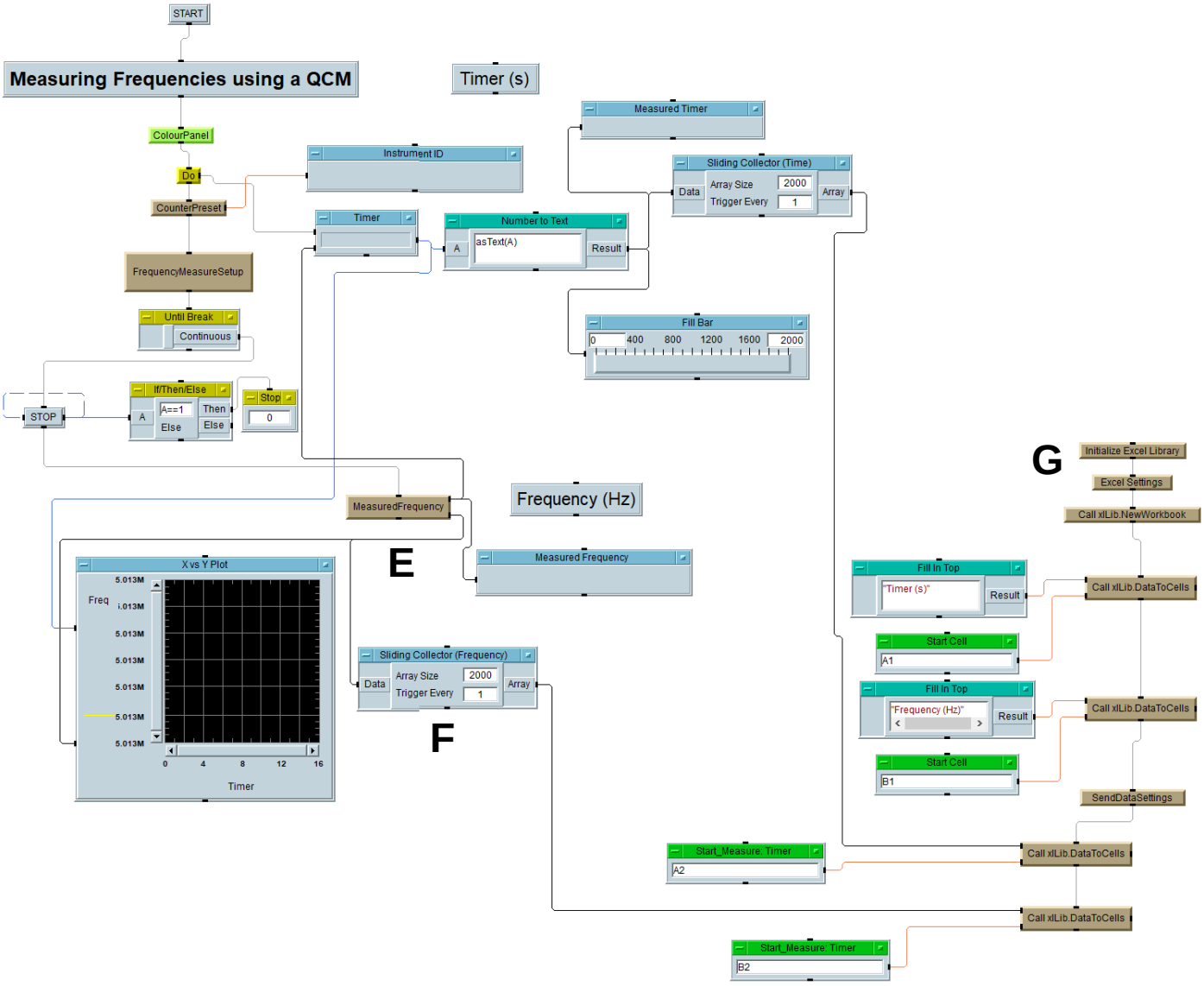

Figure 7.3 – Architecture of the program designed in Keysight Visual Engineering Environment for the detection of a frequency counter connected by GPIB responsible for reading and writing frequencies given by an oscillating Maxtek quartz crystal (see text).

The analysis will be discussed from the top left to the bottom right. After the start button, the program will call the frequency counter and reset it for a new set of measures, followed by a loop that enables a stop button. The program continues by connection to a box called “Measured Frequency” (E), which is the actual measure of the frequency in the counter, that will be recorded in a graph and registered in a “Sliding Collector” (F). Within the program, upon starting, memory is allocated to this array (depending on its size, set by the user), which not only will record the frequency but also the time that it was recorded. The measure of frequency in function of time will give a vector consisting of several results given as (x, y), meaning that it is translated in the form of $(time, frequency)$. These two parameters are, then, sent to a new Excel file (G), that is open every time a measure is started. The results concerning the variable $time$ will be in the column A, starting at line 2, and the variable $frequency$ will be in the column B, starting also at line 2[1]. After successfully completing the assay, the user must not forget to save the Excel file. Regrettably, this is one of the limitations of this program, as it doesn’t save the file automatically. If such a command were to be added, after a first $(time, frequency)$ measure, it would save the Excel file, an occurrence that was not desired. However, a fine amount of user input in this program is desirable, as it enables a finer control of the total number of measures it is required for the assay, as well as to manipulate the time interval between results, also called gate. Figure 7.4 displays the window that is presented to the user.

[1] One of the reasons why there was a need to group all measures in an array was because, if it wasn’t, measures would overwrite themselves, and it would not be possible to see an actual frequency change in the assays. That is the reason why, in the beginning, a pre-defined number of total measures must be considered, so that there are enough lines in the Excel to gather all the needed data.

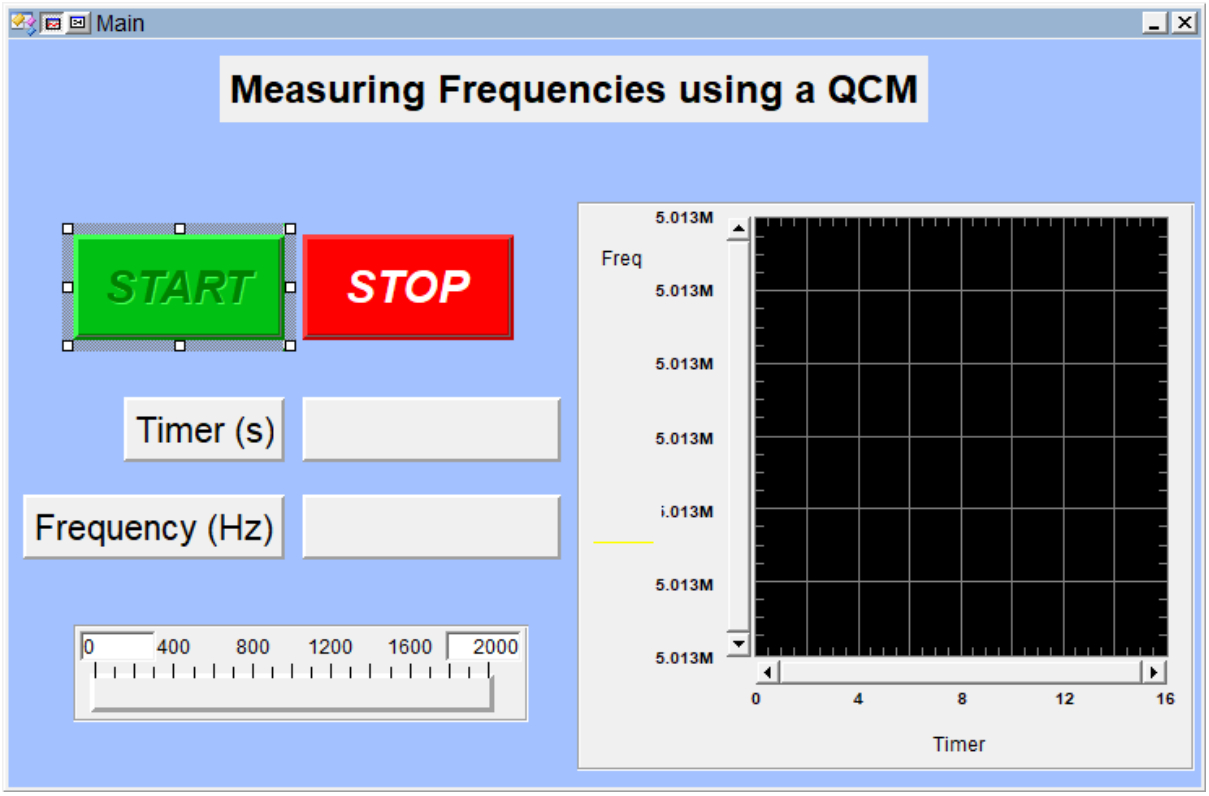

Figure 7.4 – Runtime version of the program designed in Keysight Visual Engineering Environment, with two buttons requiring user input (START/STOP). The values of frequency and time are shown below the START/STOP buttons, as well as a real-time graph of the variation of the frequency. A total measure count is also displayed in the form of a fill bar, below the frequency box.

One other box that it is considered useful in the user interface is the fill bar, that shows the total number of possible measures that run can allocate in the memory. It is a parameter highly dependent on the user needs, and an indication of the progression of the assay.

7.3.2. Insufflation assays

In Chapter 6, an insufflation protocol was established that required 30 quick trigger activations of the air pistol at an outlet air pressure of either 36 or 42 psi, so that the dry powder would be dragged towards the cell support. However, the first assays using the QCM evidenced its sensitivity towards the insufflations, thus further optimisation was required. A first approach relied on the determination of the adequate outlet air pressure, that was changed from 36 psi/42 psi to 30 psi, with the QCM responding favourably. Moreover, the team believed that the powder would be dragged with fewer activations of the air pistol. A new experimental setup was, thus, devised, in which the minimal number of required insufflations to be applied was assessed, ensuring at the same time the desired frequency change. The stop point would be when the frequency reached a new equilibrium, by having very subtle variations, thus ending the assay. This was tested several times, and the new protocol was set at 10 quick trigger activations of the air pistol (or insufflations) at an outlet air pressure of 30 psi, despite observations sugesting that the totality of the powder was dispersed after two or three insufflations. In fact, the reduced number of insufflations by comparison with the protocol in Chapter 6, simplified the experimentation and made it easier to apply.

Before using powders, the determination of QCM frequency variation in the sequence of air insufflation (control assay) was essential. These first assays were performed with both printed devices (Device 1 – Brown and Device 2- Gray), and the respective variations of frequency are shown in Figure 7.5.

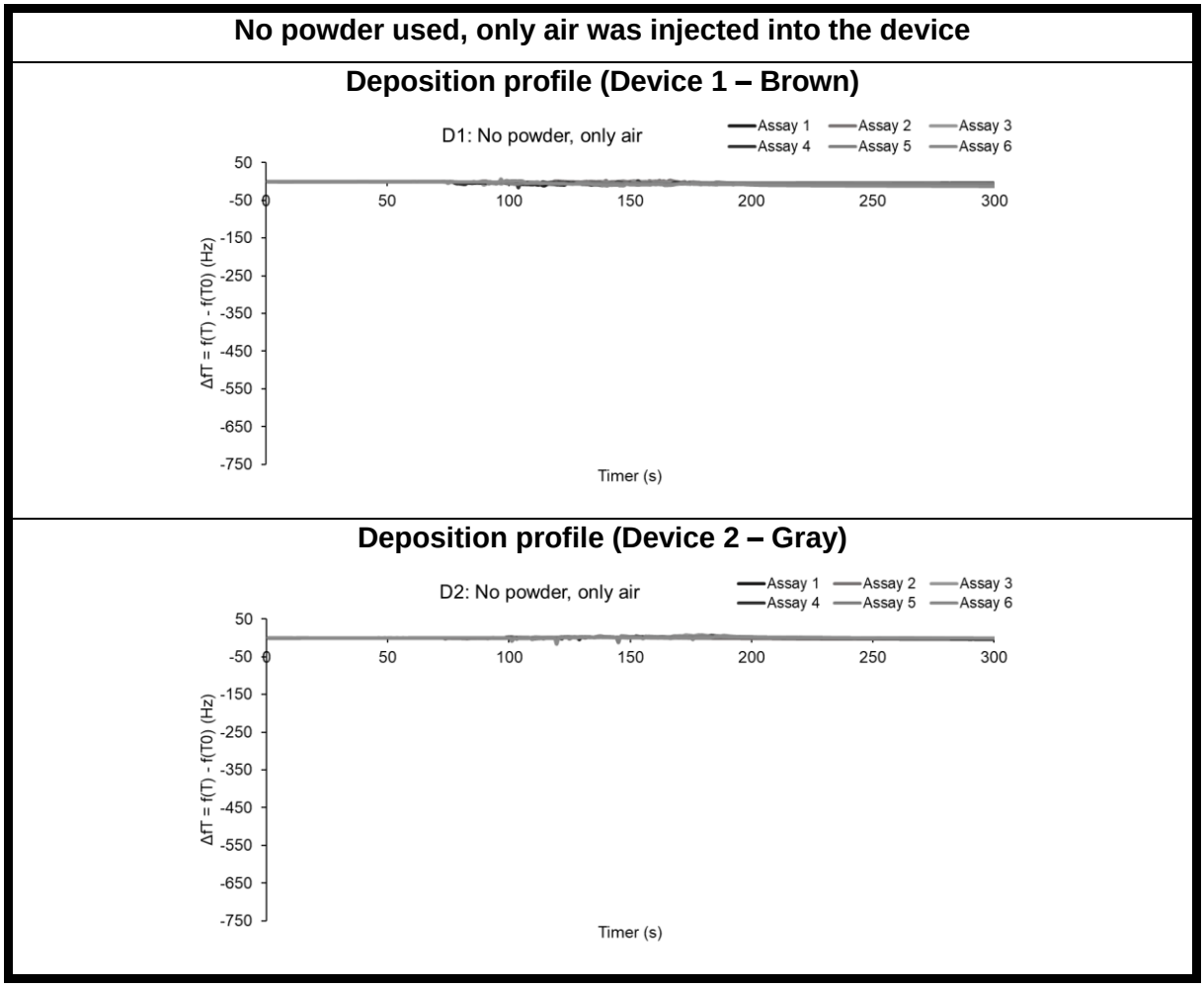

Figure 7.5 – Variation of frequency of the QCM upon insufflation of air into the device (no powder present). Results are presented as mean ± SD, n = 6.

The graphs shown in Figure 7.5 display a first frequency equilibrium, that started at time 0. Air started to be insufflated approximately 65 seconds after the beginning of the analysis. After that, the frequency returned to a value that was close to that recorded in the beginning of the run, which indicated that, when no powder is used, frequency does not change, even when the system is disturbed. Thirteen microparticle formulations comprised of a diverse set of polysaccharides were, then, selected to perform these assays. The selection was driven by different aerodynamic properties and morphology of the microparticles, which are expected to have an impact on the insufflation process. Furthermore, those differences would enable establishing correlations between the morphology and capacity to disperse. These results are compiled in the graphics, for both devices, in Figure 7.6 to Figure 7.18, with different powders having different colours (Table B.VI in Annex B).

Powder: Locust bean gum-based microparticles from Sigma-Aldrich (LBG S)

Feret's diameter: 3.95 ± 4.25 µm

Aerodynamic diameter: ≈1.94 µm*

Morphology

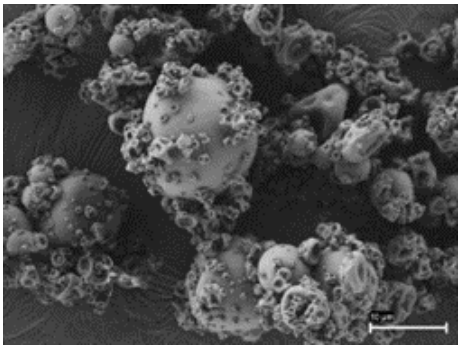

Appearance

Device 1: Deposition profile | Degree of insufflation: 100

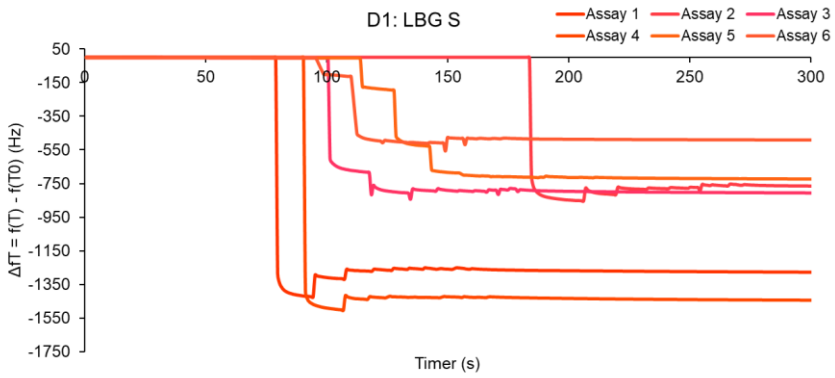

Device 2: Deposition profile | Degree of insufflation: 100

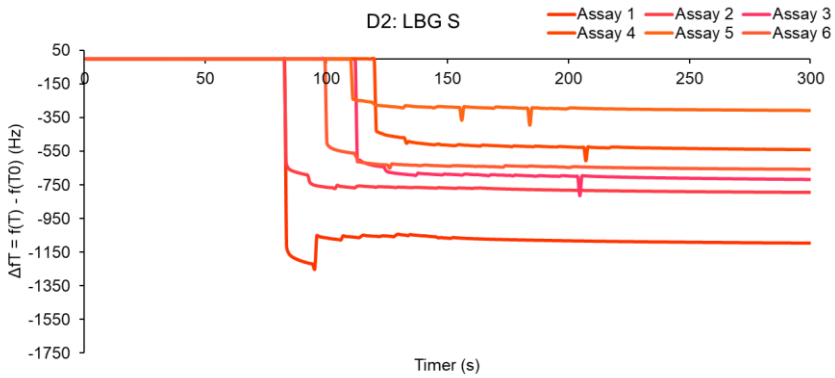

Figure 7.6 – Deposition profile and corresponding degree of insufflation for locust bean gum (LBG)-based microparticles produced with LBG from Sigma-Aldrich® (LBG S), obtained after assays with the device 1 and device 2. Powder appearance, microparticle morphology (scanning electron microscopy) and particle diameters (Feret and aerodynamic) are provided, when possible. Results are presented as mean ± SD, n = 6. *indicates theoretical calculation.

Powder: Locust bean gum-based microparticles from Industrial Farense (LBG IF)

Feret's diameter: 4.31 ± 4.39 µm	**Aerodynamic diameter:** ≈2.11 µm*
Morphology	**Appearance**

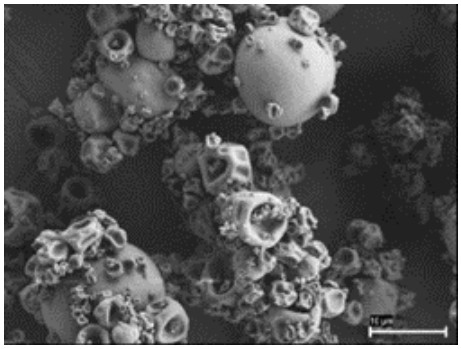

Device 1: Deposition profile | Degree of insufflation: 84.26 ± 22.77

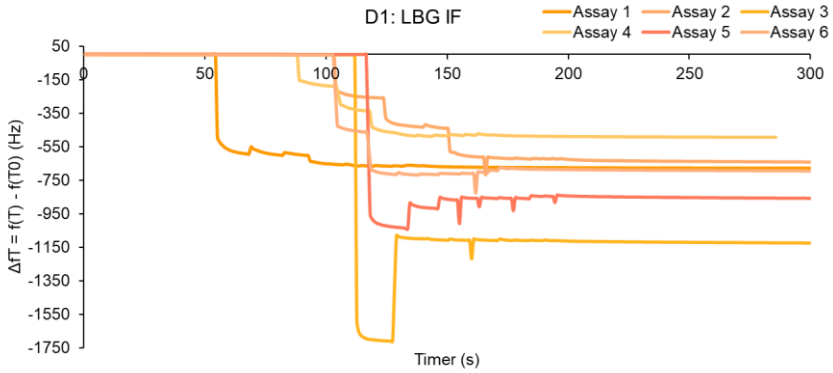

Device 2: Deposition profile | Degree of insufflation: 85.05 ± 35.47

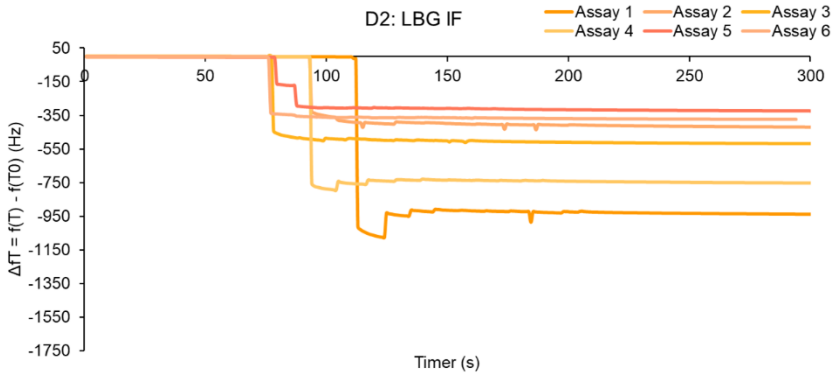

Figure 7.7 – Deposition profile and corresponding degree of insufflation for locust bean gum (LBG)-based microparticles produced with LBG from Industrial Farense® (LBG IF), obtained after assays with the device 1 and device 2. Powder appearance, microparticle morphology (scanning electron microscopy) and particle diameters (Feret and aerodynamic) are provided, when possible. Results are presented as mean ± SD, n = 6. *indicates theoretical calculation.

Powder: Locust bean gum-based microparticles from C. E. Roeper (LBG R)

Feret's diameter: 3.76 ± 4.54 µm

Aerodynamic diameter: ≈1.84 µm*

Morphology

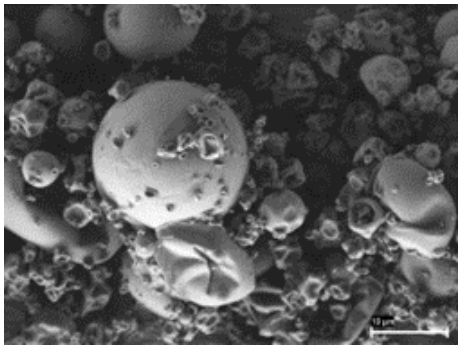

Appearance

Device 1: Deposition profile | Degree of insufflation: 96.59 ± 40.26

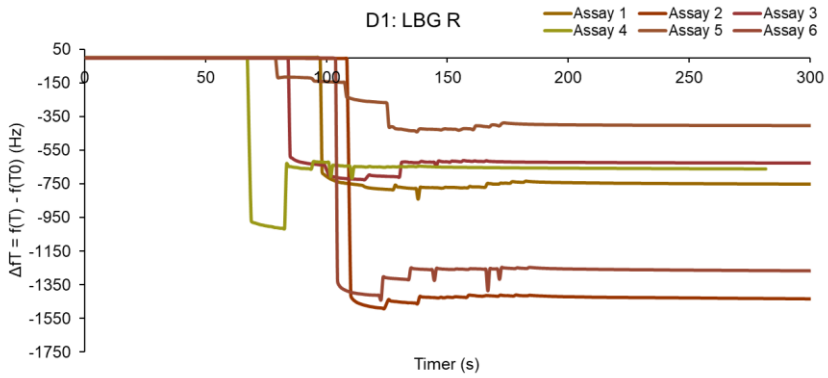

Device 2: Deposition profile | Degree of insufflation: 78.15 ± 31.85

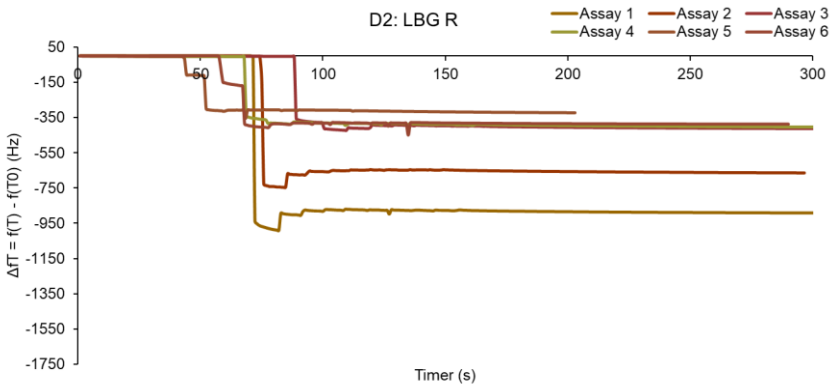

Figure 7.8 – Deposition profile and corresponding degree of insufflation for locust bean gum (LBG)-based microparticles produced with LBG from C. E. Roeper® (LBG R), obtained after assays with the device 1 and device 2. Powder appearance, microparticle morphology (scanning electron microscopy) and particle diameters (Feret and aerodynamic) are provided, when possible. Results are presented as mean ± SD, n = 6. *indicates theoretical calculation.

Powder: Xanthan gum-based microparticles (XG)

Feret's diameter: 2.46 ± 1.26 µm

Aerodynamic diameter: ≈1.41 µm*

Morphology

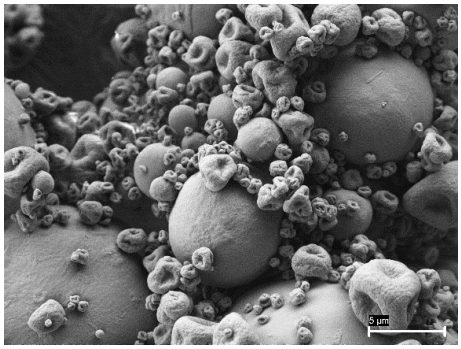

Appearance

Device 1: Deposition profile | Degree of insufflation: 40.13 ± 18.58

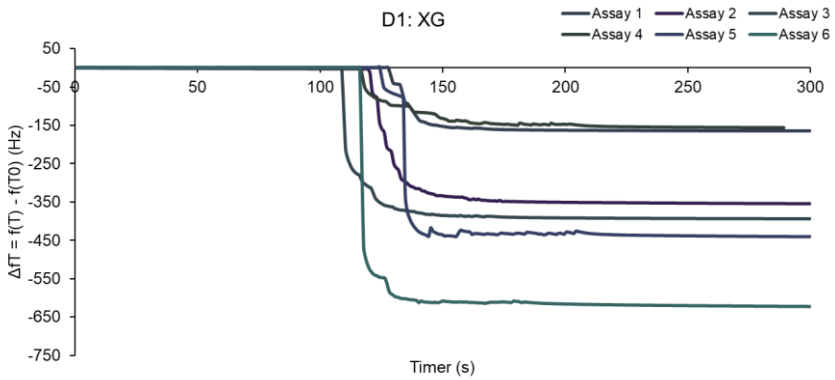

Device 2: Deposition profile | Degree of insufflation: 78.13 ± 6.00

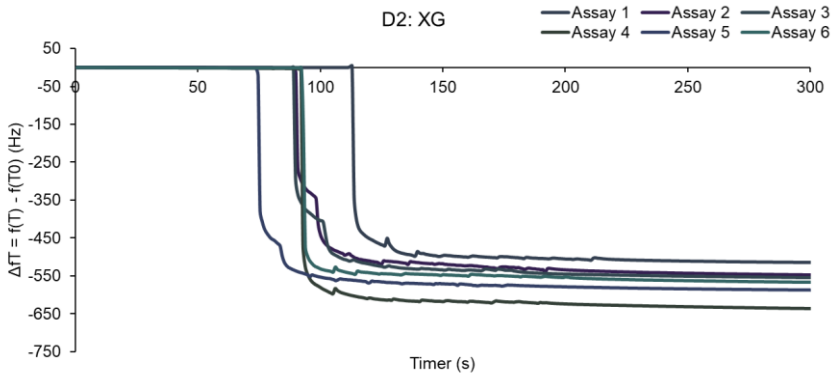

Figure 7.9 – Deposition profile and corresponding degree of insufflation for xanthan gum-based microparticles (XG), obtained after assays with the device 1 and device 2. Powder appearance, microparticle morphology (scanning electron microscopy) and particle diameters (Feret and aerodynamic) are provided, when possible. Results are presented as mean ± SD, n = 6. *indicates theoretical calculation.

Powder: Xanthan gum/sodium chloride-based microparticles (XG Na)

Feret's diameter: 2.38 ± 1.13 µm	**Aerodynamic diameter:** ≈1.37 µm*

Morphology

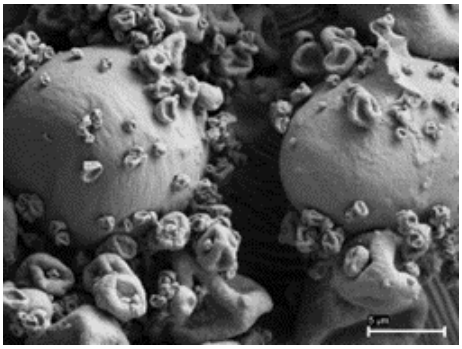

Appearance

Device 1: Deposition profile | Degree of insufflation: 37.66 ± 9.57

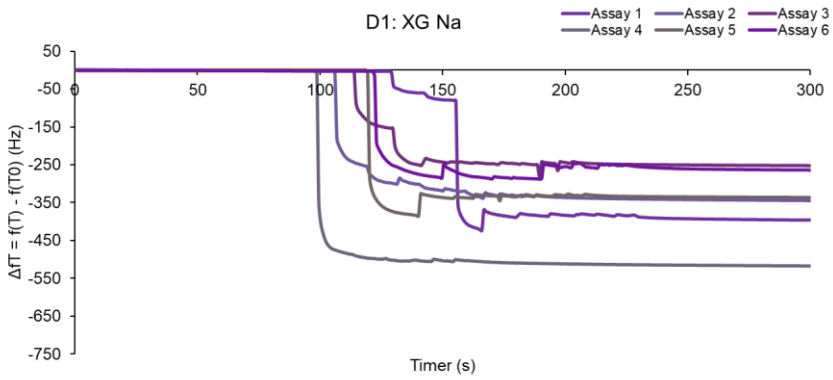

Device 2: Deposition profile | Degree of insufflation: 21.19 ± 5.33

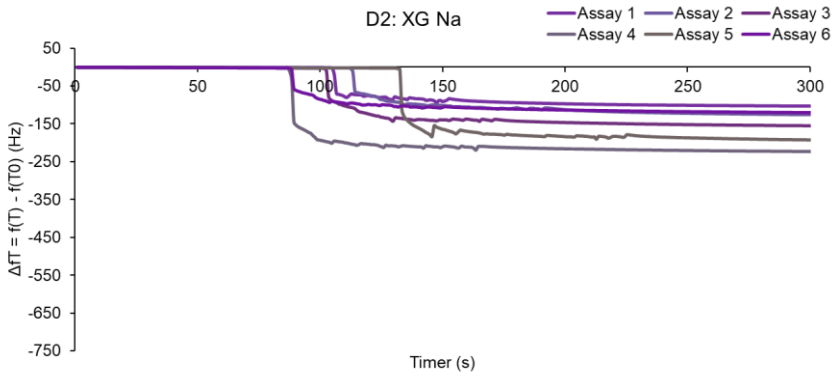

Figure 7.10 – Deposition profile and corresponding degree of insufflation for xanthan gum/sodium chloride-based microparticles (XG Na), obtained after assays with the device 1 and device 2. Powder appearance, microparticle morphology (scanning electron microscopy) and particle diameters (Feret and aerodynamic) are provided, when possible. Results are presented as mean ± SD, n = 6. *indicates theoretical calculation.

Powder: Hydrolysed xanthan gum-based microparticles (HXG)

Feret's diameter: -	**Aerodynamic diameter:** -
Morphology -	**Appearance** 

Device 1: Deposition profile | Degree of insufflation: 40.27 ± 6.02

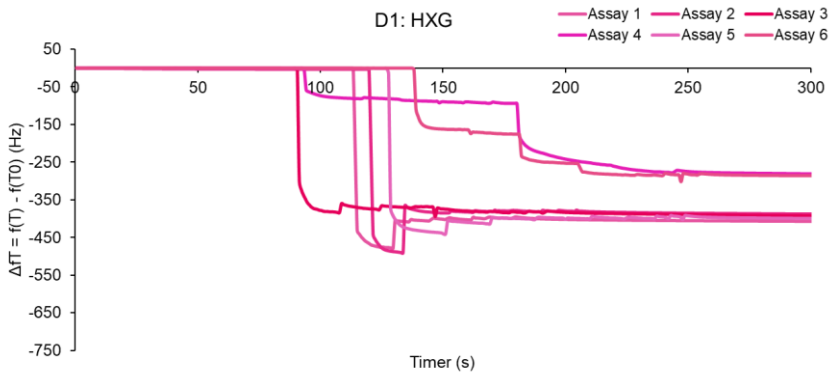

Device 2: Deposition profile | Degree of insufflation: 49.40 ± 5.40

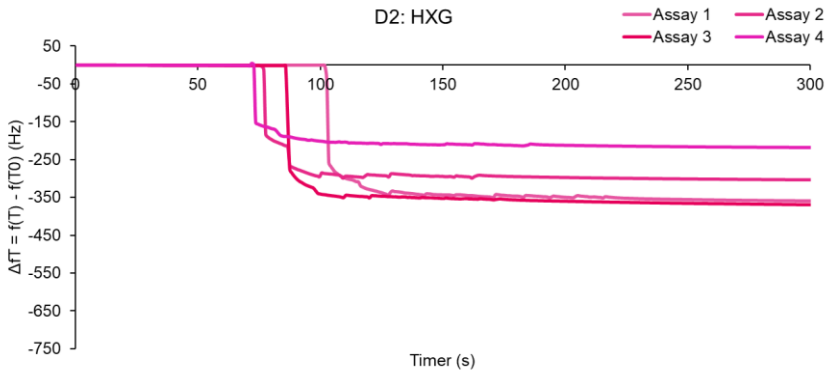

Figure 7.11 – Deposition profile and corresponding degree of insufflation for hydrolysed xanthan gum-based microparticles (HXG) obtained after assays with the two devices printed. Powder appearance is provided. Morphology and particle diameters (Feret and aerodynamic) were not determined. Results are presented as mean ± SD, n = 6 (Device 1) and n = 4 (Device 2).

Powder: Starch/carrageenan-based microparticles (Starch/CRG 1%)

Feret's diameter: -	**Aerodynamic diameter:** -
Morphology -	**Appearance** 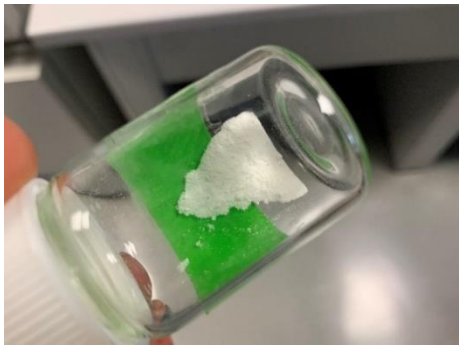

Device 1: Deposition profile | Degree of insufflation: 20.78 ± 2.99

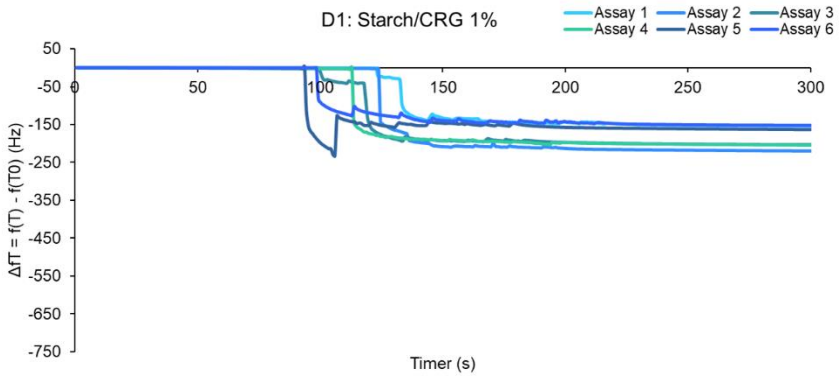

Device 2: Deposition profile | Degree of insufflation: 15.43 ± 4.12

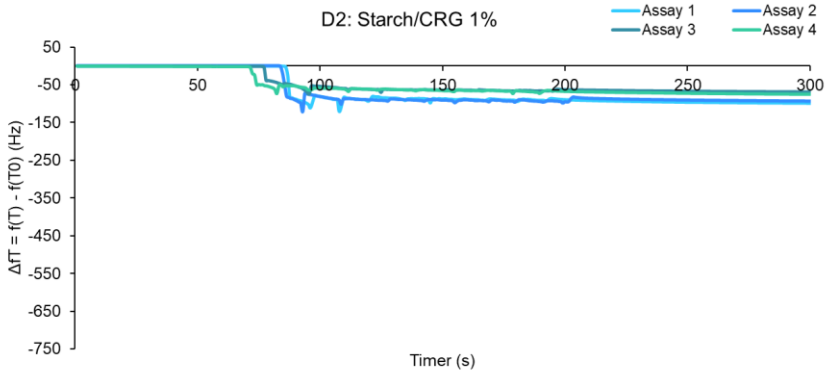

Figure 7.12 – Deposition profile and corresponding degree of insufflation for starch/carrageenan-based microparticles (Starch/CRG 1%) obtained after assays with the two devices printed. Powder appearance is provided. Morphology and particle diameters (Feret and aerodynamic) were not determined. Results are presented as mean ± SD, n = 6 (Device 1) and n = 4 (Device 2).

Powder: Starch/carrageenan-based microparticles (Starch/CRG 2%)

Feret's diameter: 1.69 ± 0.06 µm [327]	**Aerodynamic diameter:** ≈0.73 µm*

Morphology

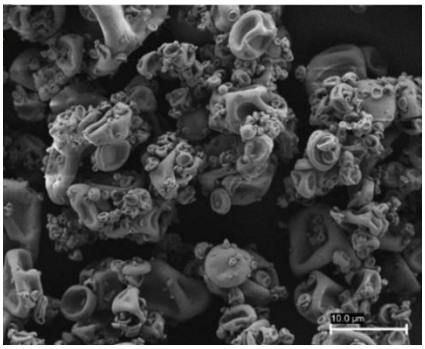

Appearance

Device 1: Deposition profile | Degree of insufflation: 20.41 ± 5.80

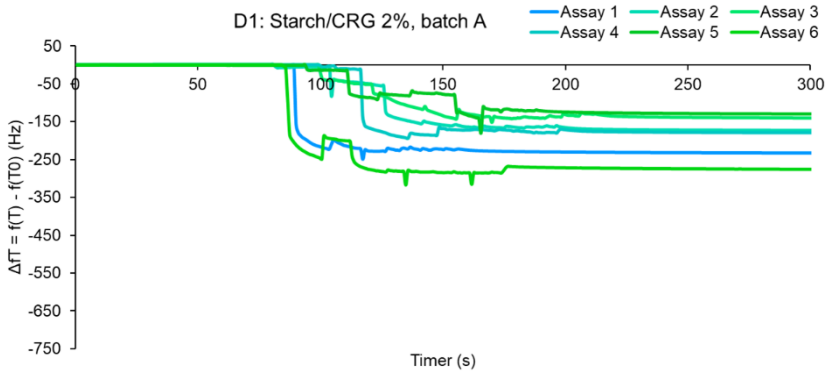

Device 2: Deposition profile | Degree of insufflation: 30.61 ± 5.25

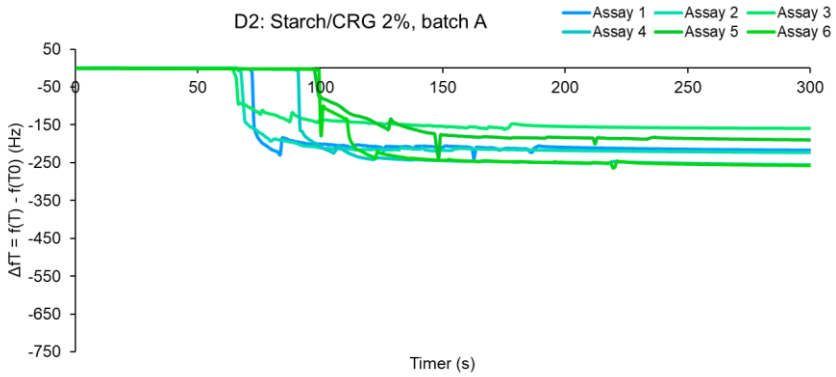

Figure 7.13 – Deposition profile and corresponding degree of insufflation for starch/carrageenan-based microparticles (Starch/CRG 2%, batch A) obtained after assays with the two devices printed. Powder appearance, microparticle morphology (scanning electron microscopy) and particle diameters (Feret and aerodynamic) are provided, when possible. Results are presented as mean ± SD, n = 6. *indicates theoretical calculation.

Powder: Carrageenan/starch-based microparticles (CRG/Starch 2%)

Feret's diameter: -	**Aerodynamic diameter:** -
Morphology -	**Appearance** 

Device 1: Deposition profile | Degree of insufflation: 18.77 ± 4.36

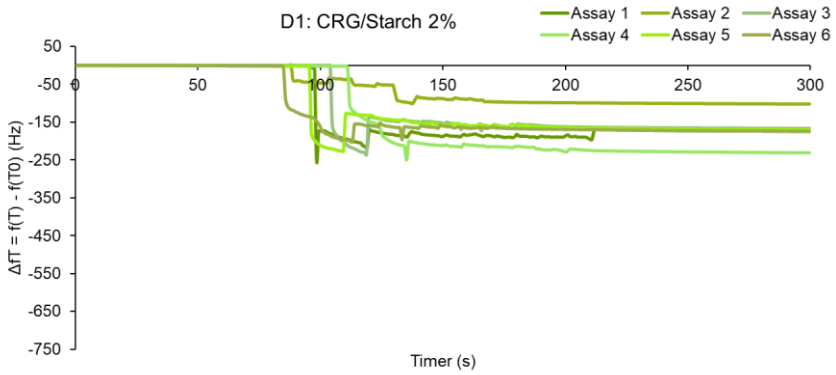

Device 2: Deposition profile | Degree of insufflation: 15.99 ± 2.03

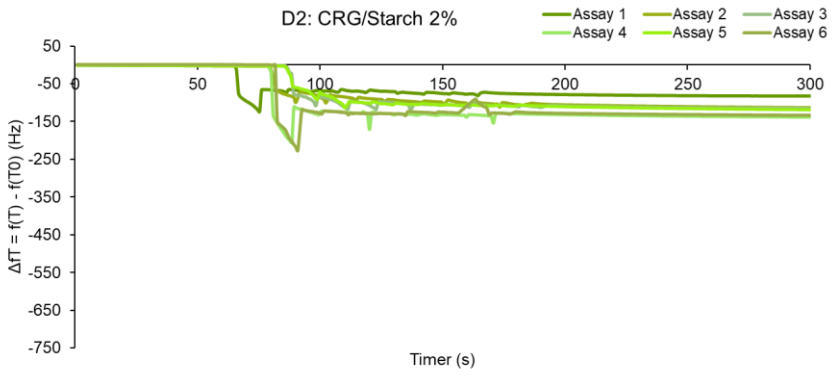

Figure 7.14 – Deposition profile and corresponding degree of insufflation for starch/carrageenan-based microparticles (Starch/CRG 1%) obtained after assays with the two devices printed. Powder appearance is provided. Morphology and particle diameters (Feret and aerodynamic) were not determined. Results are presented as mean ± SD, n = 6.

Powder: Konjac glucomannan/leucine-based microparticles (KGM/Leu)

Feret's diameter: 1.18 ± 0.75 µm [328]

Aerodynamic diameter: 1.40 ± 0.07 µm [328]

Morphology

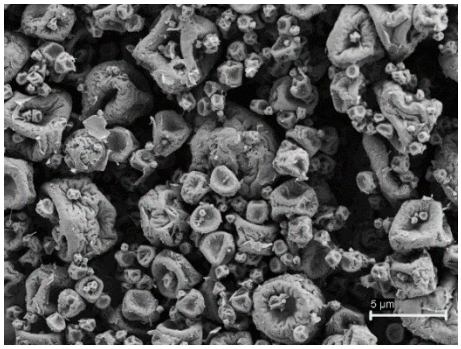

Appearance

Device 1: Deposition profile | Degree of insufflation: 13.67 ± 6.21

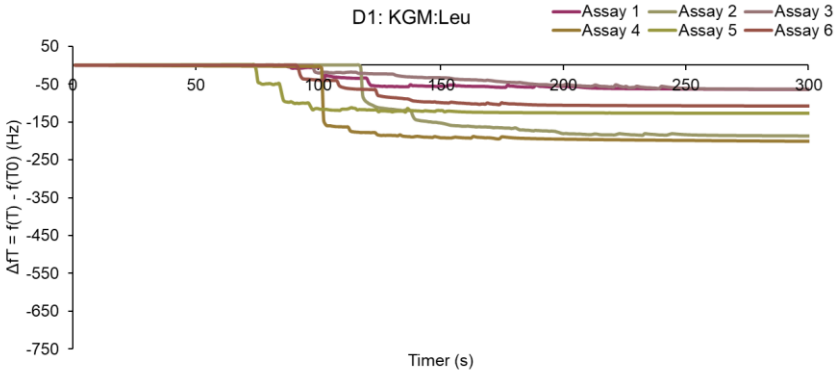

Device 2: Deposition profile | Degree of insufflation: 33.98 ± 8.26

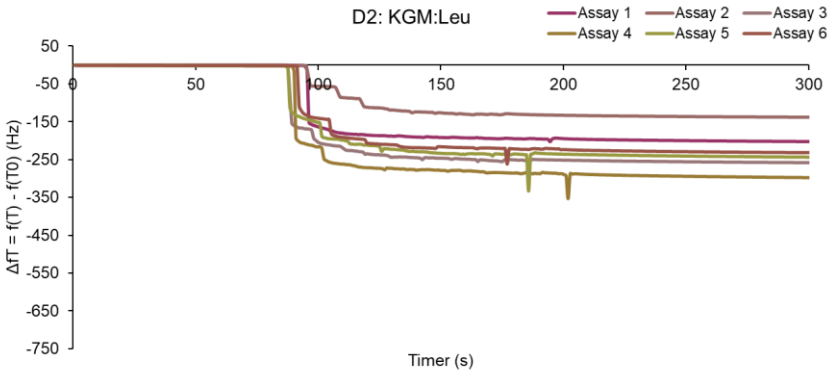

Figure 7.15 – Deposition profile and corresponding degree of insufflation for konjac glucomannan/leucine-based microparticles (KGM/Leu) obtained after assays with the two devices printed. Powder appearance, microparticle morphology (scanning electron microscopy) and particle diameters (Feret and aerodynamic) are provided, when possible. Results are presented as mean ± SD, n = 6.

Powder: Konjac glucomannan/mannitol-based microparticles (KGM/Man)

Feret's diameter: 1.44 ± 0.83 µm [328]

Aerodynamic diameter: 1.72 ± 0.03 µm [328]

Morphology

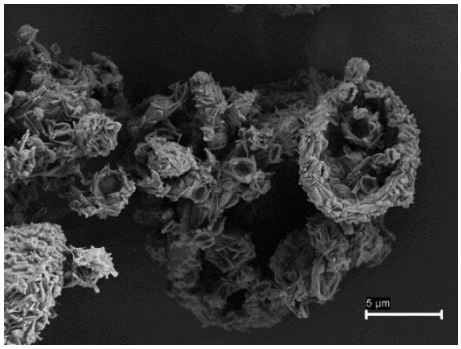

Appearance

Device 1: Deposition profile | Degree of insufflation: 11.19 ± 1.79

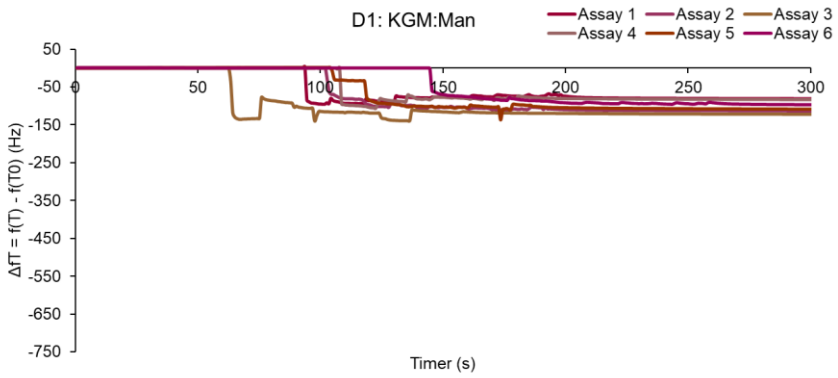

Device 2: Deposition profile | Degree of insufflation: 22.40 ± 4.72

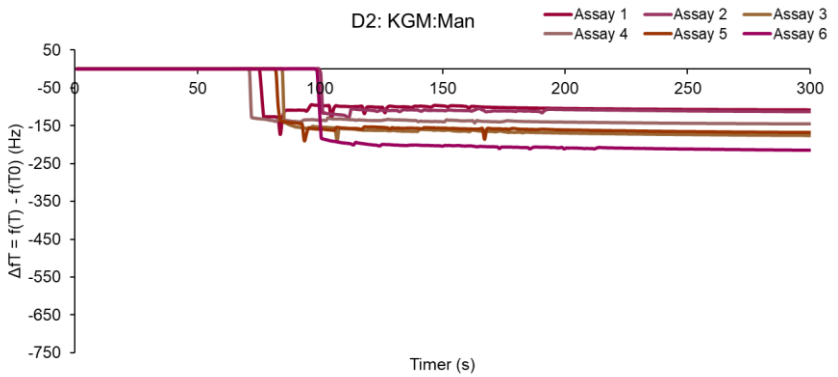

Figure 7.16 – Deposition profile and corresponding degree of insufflation for konjac glucomannan/mannitol-based microparticles (KGM/Man) obtained after assays with the two devices printed. Powder appearance, microparticle morphology (scanning electron microscopy) and particle diameters (Feret and aerodynamic) are provided, when possible. Results are presented as mean ± SD, n = 6.

Powder: Dextran sulphate-based microparticles (DS)

Feret's diameter: 1.91 ± 1.17 µm [329]

Aerodynamic diameter: 1.48 ± 0.02 µm [329]

Morphology

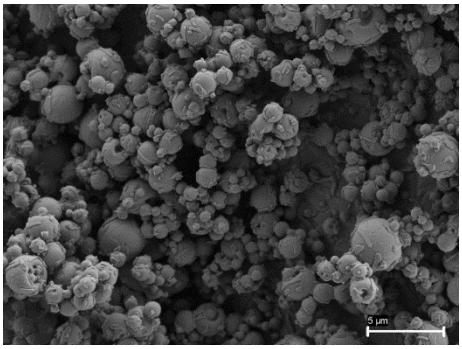

Appearance

Device 1: Deposition profile | Degree of insufflation: 8.07 ± 4.13

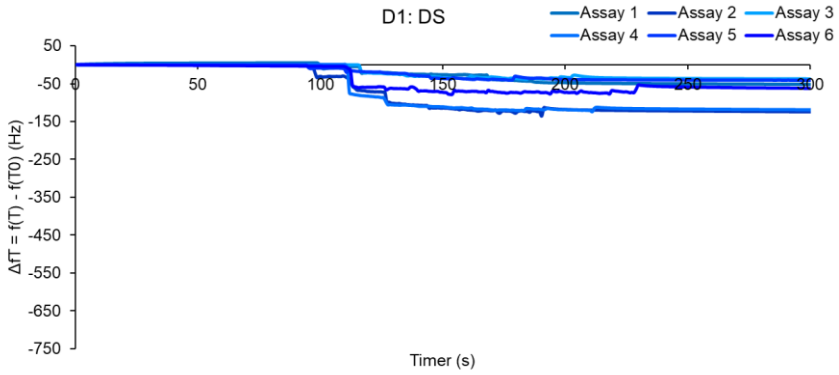

Device 2: Deposition profile | Degree of insufflation: 4.23 ± 1.44

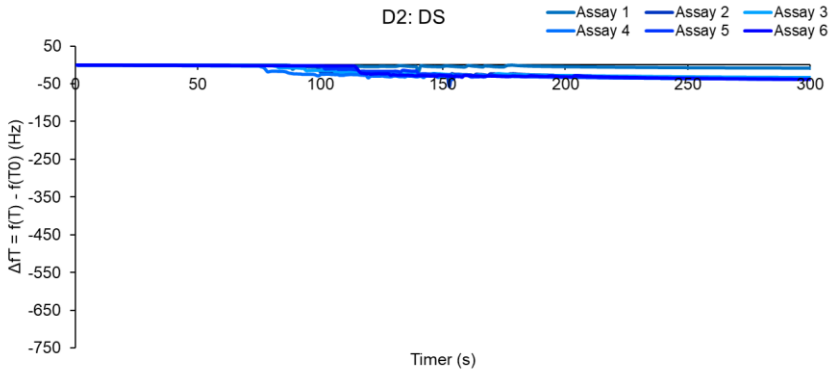

Figure 7.17 – Deposition profile and corresponding degree of insufflation for dextran sulphate-based microparticles (DS) obtained after assays with the two devices printed. Powder appearance, microparticle morphology (scanning electron microscopy) and particle diameters (Feret and aerodynamic) are provided, when possible. Results are presented as mean ± SD, n = 6.

Powder: Isoniazid and rifabutin-loaded konjac glucomannan microparticles (KGM/INH/RFB)

Feret's diameter: 2.06 ± 2.15 µm [260]

Aerodynamic diameter:
3.05 ± 0.05 µm (INH), 3.24 ± 0.09 µm (RFB) [260]

Morphology

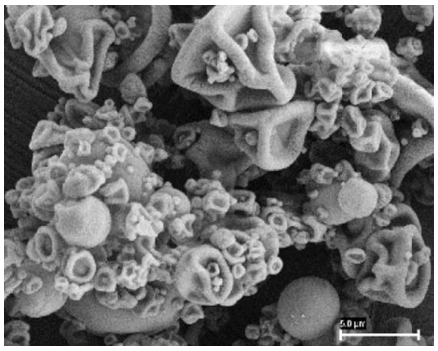

Appearance

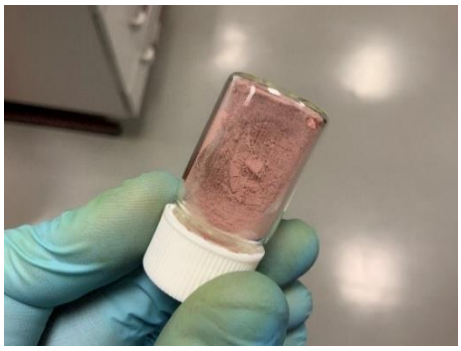

Device 1: Deposition profile | Degree of insufflation: 25.26 ± 3.82

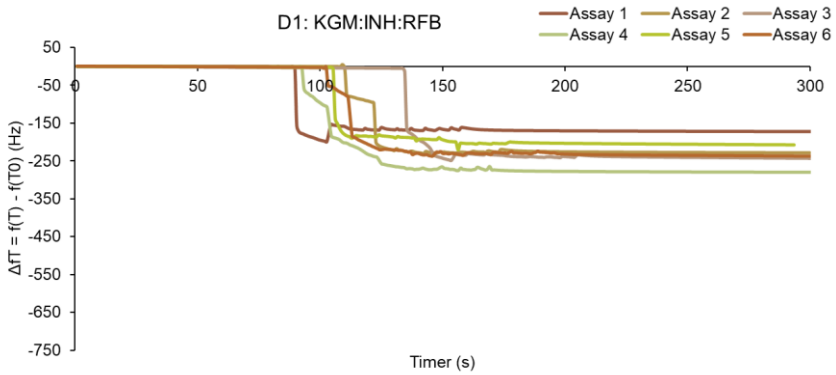

Device 2: Deposition profile | Degree of insufflation: 24.28 ± 8.51

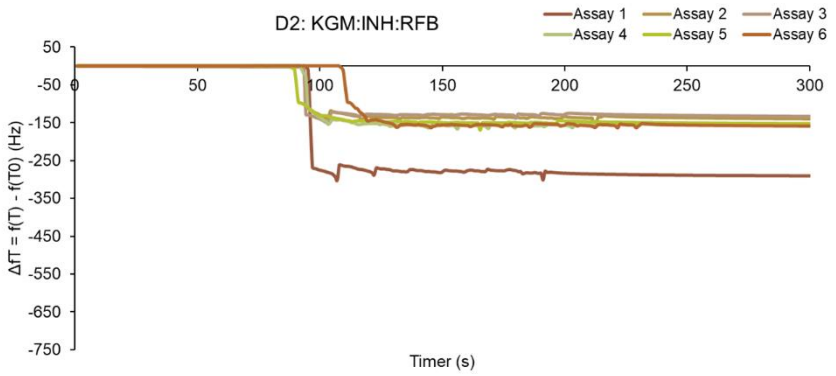

Figure 7.18 – Deposition profile and corresponding degree of insufflation for isoniazid and rifabutin-loaded konjac glucomannan microparticles (KGM/INH/RFB 10/1/1, %w/w) obtained after assays with the two devices printed. Powder appearance, microparticle morphology (scanning electron microscopy) and particle diameters (Feret and aerodynamic) are provided, when possible. Results are presented as mean ± SD, n = 6.

The QCM works based on a relaxation method. In brief, when the sensor is in equilibrium, but it is disrupted by an external force such as the insufflation of air, the frequency varies, and it only stabilises when this disruption ends. At this point, the QCM resonates to a new equilibrium, thus sensing the mass of dry powder that fell onto it, resulting in a new frequency result. Despite that, due to the nature of the QCM apparatus (see Figure 7.1), the crystal holder and the printed device are not completely tight, thus permitting powder escape, which hinders the results. Considering what was observed in all the assays performed, the evaluation of the deposition profile of all dry powders tested required a more qualitative approach, in which the best dry powder would be selected, and comparisons would be made in relation to this one. The concept of degree of insufflation was therefore established (Equation 7.2), thus enabling an easier correlation. The calculation of the degree of insufflation was performed considering as 100% degree of insufflation that of LBG-based microparticles produced with LBG from Sigma-Aldrich®. This was the dry powder showing the higher yield of insufflation, thus having the most fitting dispersion pattern. The degree of insufflation of all the other dry powders was calculated based on that assumption.

Table 7.1 – Degree of insufflation of several powders, and organisation of the best performances (ranking) according with the results. Results are presented as mean ± SD, n = 6 (exceptional situation of n = 4 indicated with an asterisk (*)).

Dry powders	Degree of insufflation		Ranking Device 1	Ranking Device 2
	Device 1	Device 2		
LBG S	100	100	LBG S	LBG S
LBG IF	84.26 ± 22.77	85.05 ± 35.47	LBG R	LBG IF
LBG R	96.59 ± 40.26	78.15 ± 31.85	LBG IF	LBG R
XG	40.13 ± 18.58	78.13 ± 6.00	HXG	XG
XG Na	37.66 ± 9.57	21.19 ± 5.33	XG	HXG
HXG	40.27 ± 6.02	49.40 ± 5.40*	XG Na	KGM:Leu
Starch/CRG 1%	20.78 ± 2.99	15.43 ± 4.12*	KGM:INH:RFB	Starch/CRG 2%
Starch/CRG 2%	20.41 ± 5.80	30.61 ± 5.25	Starch/CRG 1%	KGM:INH:RFB
CRG/Starch 2%	18.77 ± 4.36	15.99 ± 2.03	Starch/CRG 2%	KGM:Man
KGM:Leu	13.67 ± 6.21	33.98 ± 8.26	CRG/Starch 2%	XG Na
KGM:Man	11.19 ± 1.79	22.40 ± 4.72	KGM:Leu	CRG/Starch 2%
DS	8.07 ± 4.13	4.23 ± 1.44	KGM:Man	Starch/CRG 1%
KGM:INH:RFB	25.26 ± 3.82	24.28 ± 8.51	DS D	DS D

LBG: locust bean gum, XG: xanthan gum, Na: sodium, HXG: hydrolysed xanthan gum, CRG: carrageenan, KGM: Konjac glucomannan, Leu: leucine, Man: mannitol, DS: dextran sulphate, INH: isoniazid, RFB: rifabutin

The various measures of the degree of insufflation showed that all LBGs present a good deposition profile using any of the devices, when compared to the remaining powders. For Device 1, all other remaining powders evidenced a significantly different degree of insufflation ($p < 0.05$) when compared to the powders of LBG. A similar behaviour was found for Device 2, but in this case, the powder comprised of XG-based microparticles was also in the group showing the best performance. This means that, for Device 2, four powders showed similar degrees of insufflation, translating into statistically significant differences with all remaining powders ($p < 0.05$) except the microparticles prepared with the hydrolysed xanthan gum (HXG).

Further analysis of Table 7.16 and the corresponding deposition profile graphs of the various powders evidenced that it is possible to organise the samples in three

different dispersion categories: good, mediocre and bad. Examples of these deposition profiles are shown in Figure 7.5, with images of both the petri dish and the QCM crystal.

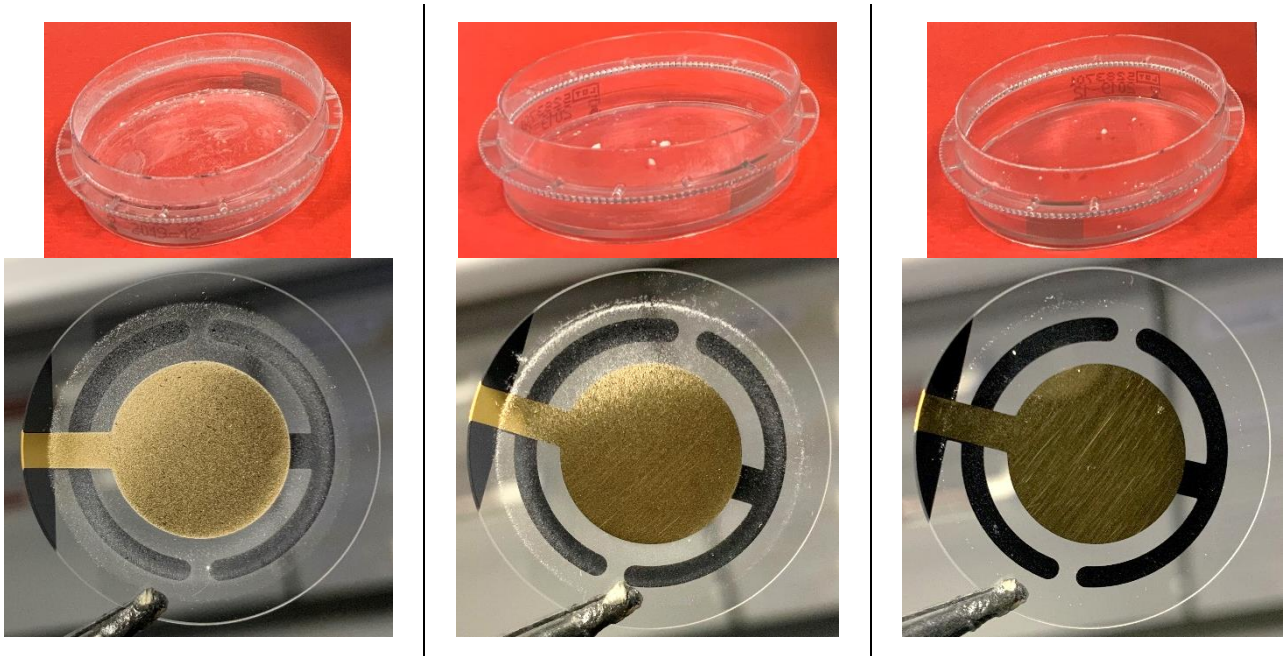

Figure 7.19 – Examples of deposition profiles in a petri dish and in the QCM (see text).

In brief, the left photographs in Figure 7.19 evidence a good powder dispersion, where the petri dish is covered by a homogeneous cloud of dry powder, as well as the QCM. The middle photographs represent a mediocre powder dispersion, where the petri dish has areas covered by dry powder and other areas where agglomerates are visible. The QCM evidences dry powder concentrated in one region of the crystal. The photographs on the right correspond to bad powder dispersions, where a few particles are seen spread on the petri dish and on the QCM. In these images, an area with dry powder homogenously dispersed is absent.

Considering the analysis herein and Figure 7.19, powders were reorganised depending on their deposition profiles, as shown in Table 7.2 and 7.3 for Device 1 and Device 2, respectively.

Table 7.2 – Categorisation of the dry powders in accordance with their deposition profile determined with Device 1, signalled by three distinct colours (●●●).

A good deposition profile (●)	A mediocre deposition profile (●)	A bad deposition profile (●)
LBG S	Starch/CRG 2%	KGM:Man
LBG IF	CRG/Starch 2%	DS
LBG R	Starch/CRG 1%	
XG	KGM:INH:RFB	
XG Na	KGM:Leu	
HXG		

LBG: locust bean gum, XG: xanthan gum, Na: sodium, HXG: hydrolysed xanthan gum, CRG: carrageenan, KGM: Konjac glucomannan, Leu: leucine, Man: mannitol, DS: dextran sulphate, INH: isoniazid, RFB: rifabutin

Table 7.3 – Categorisation of the dry powders in accordance with their deposition profile determined with Device 2, signalled by three distinct colours (●●●).

A good deposition profile (●)	A mediocre deposition profile (●)			A bad deposition profile (●)
LBG S	XG Na	HXG	Starch/CRG 2%	DS
LBG IF	CRG/Starch 2%	Starch/CRG 1%	KGM:INH:RFB	
LBG R	KGM:Leu	KGM:Man		
XG				

LBG: locust bean gum, XG: xanthan gum, Na: sodium, HXG: hydrolysed xanthan gum, CRG: carrageenan, KGM: Konjac glucomannan, Leu: leucine, Man: mannitol, DS: dextran sulphate, INH: isoniazid, RFB: rifabutin

The first conclusion that can be drawn is that the insufflation of dry powders was achieved successfully, despite the different aerodynamic parameters associated with it. If further comparisons are made, between control assays (insufflation of air) and the assays where powders were insufflated, the latter always causes a change in the frequency that is being recorded. Another point that is worthy of note is the process by which the devices were obtained. When a 3D printer with an extrusion tip was

used, the resulting device is layered. This causes imperfections, in the sense that there are interstices that enable the powder to be trapped. This occurrence leads to a deposition profile that resembles staging, as if one insufflation leads to a change in frequency, the second insufflation to an even greater change and so forth, until the new equilibrium is reached. This profile does not seem to occur when Device 2 is used. This device was prepared using a resin, which resulted in a smoother inner surface and the insufflation by stages was not verified. Additionally, with Device 2, the insufflation is more direct, meaning that, upon a burst of air, almost all the powder goes out of the weighing head platform, either onto to the QCM or it escapes. Despite that, the change in the frequency is always detected.

One particular powder, KGM:Man, was a challenging sample. It was expected that by having adequate aerodynamic parameters, it would have a good deposition profile. However, looking at the SEM photos of this dry powder, and despite the irregularity of the microparticles, there are mannitol crystals all over the surface of the carriers. One possibility of this occurrence is explained by the Peclet number and the surface enrichment [265]. Due to KGM being amorphous, upon drying of the droplet on the spray-drying, the velocity of drying is superior to the velocity of the diffusion of the solute. Along with the fact that KGM is a molecule larger than mannitol, which hinders its movements within the droplet, it will lead to the accumulation of mannitol on the outside limits of the droplet alongside KGM in a process called surface enrichment. This process is not observed when mannitol is spray-dried alone, and it distributes evenly within the liquid droplet as it dries in the drying chamber. As mannitol is crystalline, it will undergo a process of crystallisation upon drying, leading to the prismatic forms observed in the SEM photos, and that, in theory, will influence the insufflation of these powders. For the KGM:Man, it was observed that the deposition profile is either mediocre or bad, as the changes in frequency are less pronounced than in other powders.

One other possible conclusion from all gathered data (morphology, deposition profile, degree of insufflation, and aspect of the powders) is that a mixture of both spherical and irregular shaped particles favours insufflation in relation to only spherical particles. Completely spherical particles, as in the case of DS, lead to inadequate patterns of deposition, which is in accordance with what is generally

verified for dry powders. In fact, irregular shapes lead to better aerodynamic behaviours, as the surface area that contacts with air is higher than that of spherical particles [128].

One last analysis that can be performed relates to the geometric and aerodynamic diameters of the dry powders. The degree of insufflation was reorganised depending on the diameters, and results are presented in Table 7.4.

Table 7.4 – Categorisation of the dry powders by their geometric and aerodynamic diameters, from highest to lowest, when it is available. An indication of the deposition profile of the dry powders is signalled before their name (●●●, see Tables 7.2 and 7.3). *indicates theoretical calculation.

Deposition profile by geometric diameter (both devices)	Deposition profile by aerodynamic diameter (both devices)
● LBG IF (4.31 ± 4.39 µm)	● KGM:INH:RFB (3.05 ± 0.05 µm (INH), 3.24 ± 0.09 µm (RFB)) [260]
● LBG S (3.95 ± 4.25 µm)	● LBG IF (≈2.11 µm) *
● LBG R (3.76 ± 4.54 µm)	● LBG S (≈1.94 µm) *
● XG (2.46 ± 1.26 µm)	● LBG R (≈1.84 µm) *
●● XG Na (2.38 ± 1.13 µm)	●● KGM:Man (1.72 ± 0.03 µm) [328]
●● HXG (not determined)	● DS (1.48 ± 0.02 µm) [329]
● KGM:INH:RFB (2.06 ± 2.15 µm) [260]	● XG (≈1.41 µm) *
● DS (1.91 ± 1.17 µm) [329]	● KGM:Leu (1.40 ± 0.07 µm) [328]
● Starch/CRG 2% (1.69 ± 0.06 µm) [327]	●● XG Na (≈1.37 µm) *
● CRG/Starch 2% (not determined)	●● HXG (not determined)
● Starch/CRG 1% (not determined)	● Starch/CRG 2% (≈0.73 µm) *
●● KGM:Man (1.44 ± 0.83 µm) [328]	● CRG/Starch 2% (not determined)
● KGM:Leu (1.18 ± 0.75 µm) [328]	● Starch/CRG 1% (not determined)

LBG: locust bean gum, XG: xanthan gum, Na: sodium, HXG: hydrolysed xanthan gum, CRG: carrageenan, KGM: Konjac glucomannan, Leu: leucine, Man: mannitol, DS: dextran sulphate, INH: isoniazid, RFB: rifabutin

There is a tendency of having lower yields and worse deposition profiles with lower geometric diameters, apart from DS-based microparticles. In this case, the dry powder is comprised of larger particles, and, upon insufflation, there can be an increased number of particles dispersing and depositing in the QCM. This will impact the overall yield and degree of insufflation, creating an artificial deviation of the current tendency, not necessarily related to their insufflation properties.

In all, the inclusion of the QCM in the experimental setting herein described constitutes a more complete approach on the *in vitro* analysis of dry powders. Despite the analytical balances giving a quantitative result for powder reaching the petri dish (discussed in chapter 6), the QCM is more advantageous. The use of this technology permits following the insufflation process in detail through frequency change and describe the behaviour of the dry powder as well as its dispersion profile.

7.3.3. Cell viability upon insufflation

The determination of the impact of insufflation in cultured cells is the last section of this chapter. In line with the development of a device and of an optimised protocol for the study of dry powders, assays in which air and dry powders were insufflated onto cells were performed, and results can be observed in Figure 7.20.

LBG-based microparticles produced with the polymer from Sigma-Aldrich® (LBG S) were used and the assay devised to resemble the lung environment. In brief, cells were cultured in petri dishes, and cell culture medium removed prior to the insufflation of either air or dry powder. Afterwards, a small volume of cell culture medium (500 µL) was added to avoid cell desiccation, and 3h or 24 h exposure was allowed before cell viability was determined. Overall, as observed in Figure 7.20, the insufflation of air and of dry powders did not impact cell viability that resulted in a major cell death event. In fact, cell viabilities roughly above 70% were always determined, which indicates the absence of cytotoxic effect. Nevertheless, the insufflation of air, used herein as a control, induced a lower reduction in cell viability than the insufflation of microparticles. The first indication on the used method of insufflation and on the proper LBG microparticles corresponds to a safe profile.

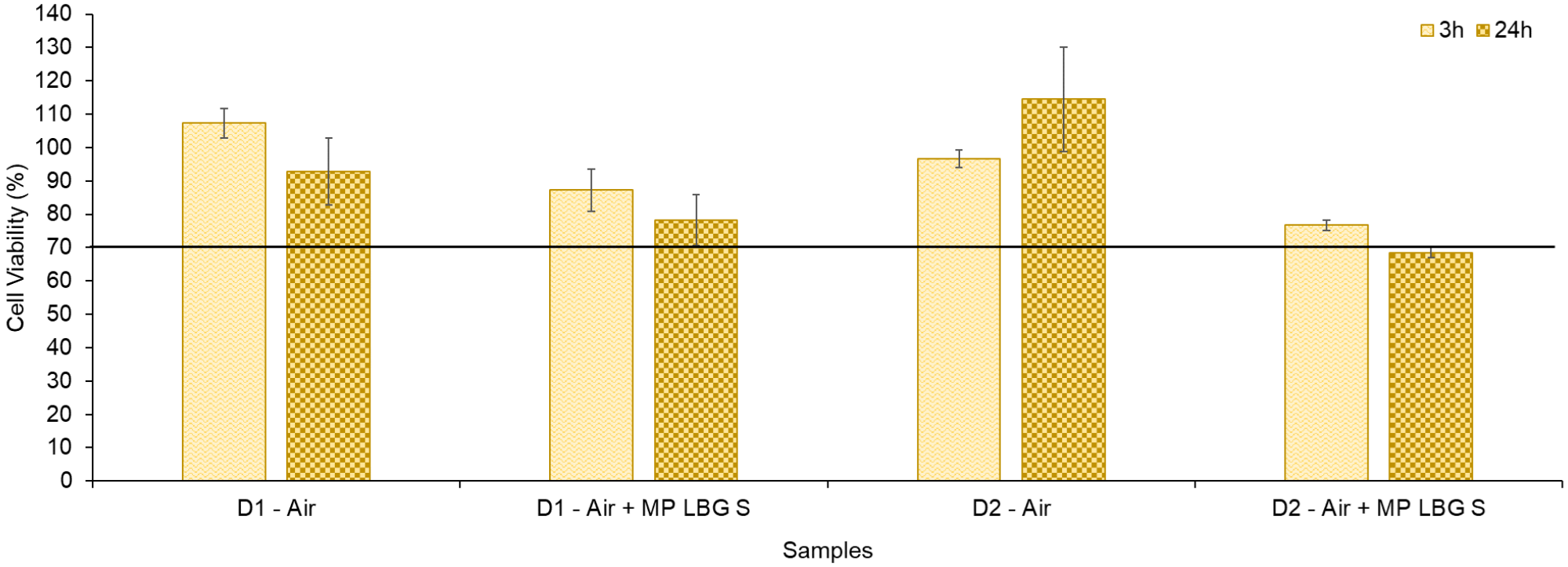

Figure 7.20 – Cell viability induced by the insufflation of air and of a mixture of air and a dry powder comprised of LBG-based microparticles, with the two prototypes of the device (D1 – brown and D2 – grey), upon 3 h and 24 h exposure of A549 cells (textured columns in yellow and brown: ●●). Data represent mean ± SEM (n = 3).

This chapter focused on the development of an experimental and reproducible method to qualitatively evaluate the dispersion of dry powders. The type, morphology and shape of the dry powders have important roles on the insufflation process, evidencing different capabilities on the formation of a cloud for further dispersion onto a cell support. Despite the insufflation not having an impact in cell viability, further testing is required to determine the real interaction between cells and dry powders, which can be attained using the QCM. In future assays, dry powders will be insufflated over cells seeded onto QCM crystals, aiming at quantifying the interactions. Nevertheless, the achievements herein discussed will be useful for earlier stages of inhalable formulation development, their optimisation, and the comprehension of their aerodynamic behaviour upon insufflation.

This page was intentionally left in blank.

CHAPTER 8:

GENERAL CONCLUSIONS AND FUTURE PERSPECTIVES

This page was intentionally left in blank.

The project described throughout this document focused on the development of a device that allows the delivery of dry powders onto cell surfaces, thus simulating more appropriately inhalation as a process. In this regard, the device was used to study the deposition profile of dry powders aimed at lung delivery. Furthermore, the project contributed with important information concerning excipients and formulations designed for lung delivery.

LBG was used in different approaches in the field of Pharmaceutical Technology that explored its use in applications other than the usual oral formulations. A sulphated derivative of the polysaccharide permitted the production of lipid nanocapsules by solvent displacement. Despite the versatility and stability of the carriers, conversion to dry powders suitable for inhalation purposes was unsuccessful.

The production of dry powders composed of LBG microparticles was successful when spray-drying was used as production methodology. LBG from three different suppliers was tested to produce the microparticles after purification. Selected microparticle formulations were thoroughly characterised using FTIR, DSC, TGA and HPSEC, and the results suggested that there is an impact of the temperature on LBG characteristics, in both the process of purification and in the preparation of microparticles. Future experiments could benefit from the assessment of LBG using Nuclear Magnetic Resonance (NMR), as this could provide information on degradation products, for instance. Additionally, the aerodynamic characterisation of microparticles should be performed, as well as rheology studies for further understanding of LBG behaviour.

A prototype for dry powder insufflation was designed and developed, using 3D printing methods for its production. It permits the homogenous dispersion of the insufflated powders over a petri dish and a QCM, and a more detailed study on how dry powders disperse over the supports. The device still requires further improvement, especially regarding the method for powder weighing. A company was recently subcontracted to provide advancements in the optimisation of the device. The intellectual property of the device is already protected, in the form of an international patent application that was recently submitted. In parallel, the impact of insufflation of air and of LBG-based microparticles was assessed, and it was

observed that both did not impact cell viability. In fact, cell viabilities roughly above 70% were always determined, which indicates the absence of cytotoxic effect.

Next stages of experimentation envisage the culture of cells over the crystal of QCM for an evaluation of particle/cell interaction upon insufflation of the dry powders. The inclusion of this technology in experimentation, especially concerning the *in vitro* analysis of dry powders, can provide more information and data in formulation development, further complementing analytical procedures and the strengthening of results and conclusions.

The project and data herein presented and discussed contributed to the advancement of inhalable LBG-based microparticles and proposed an alternative method for dry powder assessment at a laboratory scale. The novelty of the idea, its future applications, and the paths opened from the experimental approaches are certainly a valuable contribute to advancements in the state of the art of inhalation.

REFERENCES

1. Gea, J. The evolution of the human species: A long journey for the respiratory system. *Archivos de Bronconeumología ((English Edition))* **2008**, *44*, 263-270, doi:10.1016/s1579-2129(08)60042-7.

2. Coccia, M. Why do nations produce science advances and new technology? *Technology in Society* **2019**, *59*, doi:10.1016/j.techsoc.2019.03.007.

3. Rohr, J.R.; Civitello, D.J.; Halliday, F.W.; Hudson, P.J.; Lafferty, K.D.; Wood, C.L.; Mordecai, E.A. Towards common ground in the biodiversity-disease debate. *Nature Ecology & Evolution* **2020**, *4*, 24-33, doi:10.1038/s41559-019-1060-6.

4. Barabási, A.-L.; Gulbahce, N.; Loscalzo, J. Network medicine: A network-based approach to human disease. *Nature Reviews Genetics* **2011**, *12*, 56-68, doi:10.1038/nrg2918.

5. Herriges, M.; Morrisey, E.E. Lung development: Orchestrating the generation and regeneration of a complex organ. *Development* **2014**, *141*, 502-513, doi:10.1242/dev.098186.

6. Del Negro, C.A.; Funk, G.D.; Feldman, J.L. Breathing matters. *Nature Reviews Neuroscience* **2018**, *19*, 351-367, doi:10.1038/s41583-018-0003-6.

7. Weibel, E.R. Lung morphometry: The link between structure and function. *Cell and Tissue Research* **2017**, *367*, 413-426, doi:10.1007/s00441-016-2541-4.

8. Weibel, E.R. *Morphometry of the Human Lung*; Springer Berlin: Heidelberg, 1963; 10.1007/978-3-642-87553-3.

9. Deng, Q.; Deng, L.; Miao, Y.; Guo, X.; Li, Y. Particle deposition in the human lung: Health implications of particulate matter from different sources. *Environmental Research* **2019**, *169*, 237-245, doi:10.1016/j.envres.2018.11.014.

10. Varma, R.; Soleas, J.P.; Waddell, T.K.; Karoubi, G.; McGuigan, A.P. Current strategies and opportunities to manufacture cells for modeling human lungs. *Advanced Drug Delivery Reviews* **2020**, *161-162*, 90-109, doi:10.1016/j.addr.2020.08.005.

11. Iber, D. The control of lung branching morphogenesis. In *Cellular Networks in Development*, Elsevier: 2021; Vol. 143, pp. 205-237.

12. Nikolić, M.Z.; Sun, D.; Rawlins, E.L. Human lung development: Recent progress and new challenges. *Development* **2018**, *145*, doi:10.1242/dev.163485.

13. Yaqub, N.; Wayne, G.; Birchall, M.; Song, W. Recent advances in human respiratory epithelium models for drug discovery. *Biotechnology Advances* **2022**, *54*, 107832, doi:10.1016/j.biotechadv.2021.107832.

14. Hopwood, D.; Logan, K.R.; Bouchier, I.A. The electron microscopy of normal human oesophageal epithelium. *Virchows Archiv B Cell Pathology* **1978**, *26*, 345-358, doi:10.1007/BF02889561.

15. Rosekrans, S.L.; Baan, B.; Muncan, V.; van den Brink, G.R. Esophageal development and epithelial homeostasis. *American Journal of Physiology - Gastrointestinal and Liver Physiology* **2015**, *309*, G216-228, doi:10.1152/ajpgi.00088.2015.

16. McQualter, J.L. Endogenous lung stem cells for lung regeneration. *Expert Opinion on Biological Therapy* **2019**, *19*, 539-546, doi:10.1080/14712598.2019.1596256.

17. Bustamante-Marin, X.M.; Ostrowski, L.E. Cilia and mucociliary clearance. *Cold Spring Harbor Perspectives in Biology* **2017**, *9*, doi:10.1101/cshperspect.a028241.

18. Zuo, W.-L.; Shenoy, S.A.; Li, S.; O'Beirne, S.L.; Strulovici-Barel, Y.; Leopold, P.L.; Wang, G.; Staudt, M.R.; Walters, M.S.; Mason, C., et al. Ontogeny and biology of human small airway epithelial club cells. *American Journal of Respiratory and Critical Care Medicine* **2018**, *198*, 1375-1388, doi:10.1164/rccm.201710-2107OC.

19. Davis, C.W.; Dickey, B.F. Regulated airway goblet cell mucin secretion. *Annual Review of Physiology* **2008**, *70*, 487-512, doi:10.1146/annurev.physiol.70.113006.100638.

20. Liu, X.; Driskell, R.R.; Engelhardt, J.F. Chapter 3 - Airway Glandular Development and Stem Cells. In *Current Topics in Developmental Biology*, 2004; Vol. 64, pp. 33-56.

21. Foster, W.M. Mucociliary transport and cough in humans. *Pulmonary Pharmacology & Therapeutics* **2002**, *15*, 277-282, doi:10.1006/pupt.2002.0351.

22. Xu, J.; Yu, H.; Sun, X. Less is more: Rare pulmonary neuroendocrine cells function as critical sensors in lung. *Developmental Cell* **2020**, *55*, 123-132, doi:10.1016/j.devcel.2020.09.024.

23. Jones-Freeman, B.; Starkey, M.R. Bronchioalveolar stem cells in lung repair, regeneration and disease. *Journal of Pathology* **2020**, *252*, 219-226, doi:10.1002/path.5527.

24. Singh, L.; Bajaj, S.; Gadewar, M.; Verma, N.; Ansari, M.N.; Saeedan, A.S.; Kaithwas, G.; Singh, M. Modulation of host immune response is an alternative strategy to combat SARS-CoV-2 pathogenesis. *Frontiers in Immunology* **2021**, *12*, 660632, doi:10.3389/fimmu.2021.660632.

25. Williams, M.C. Alveolar type I cells: Molecular phenotype and development. *Annual Review of Physiology* **2003**, *65*, 669-695, doi:10.1146/annurev.physiol.65.092101.142446.

26. Yu, H.; Lin, Y.; Zhong, Y.; Guo, X.; Lin, Y.; Yang, S.; Liu, J.; Xie, X.; Sun, Y.; Wang, D., et al. Impaired AT2 to AT1 cell transition in PM2.5-induced mouse model of chronic obstructive pulmonary disease. *Respir Res* **2022**, *23*, 70, doi:10.1186/s12931-022-01996-w.

27. Hidalgo, A.; Garcia-Mouton, C.; Autilio, C.; Carravilla, P.; Orellana, G.; Islam, M.N.; Bhattacharya, J.; Bhattacharya, S.; Cruz, A.; Pérez-Gil, J. Pulmonary surfactant and drug delivery: Vehiculization, release and targeting of surfactant/tacrolimus formulations. *Journal of Controlled Release* **2021**, *329*, 205-222, doi:10.1016/j.jconrel.2020.11.042.

28. Mason, R.J. Biology of alveolar type II cells. *Respirology* **2006**, *11 Suppl*, S12-15, doi:10.1111/j.1440-1843.2006.00800.x.

29. Fröhlich, E.; Mercuri, A.; Wu, S.; Salar-Behzadi, S. Measurements of deposition, lung surface area and lung fluid for simulation of inhaled compounds. *Frontiers in Pharmacology* **2016**, *7*, 181, doi:10.3389/fphar.2016.00181.

30. Hou, F.; Xiao, K.; Tang, L.; Xie, L. Diversity of macrophages in lung homeostasis and diseases. *Frontiers in Immunology* **2021**, *12*, 753940, doi:10.3389/fimmu.2021.753940.

31. Sun, X.; Perl, A.-K.; Li, R.; Bell, S.M.; Sajti, E.; Kalinichenko, V.V.; Kalin, T.V.; Misra, R.S.; Deshmukh, H.; Clair, G., et al. A census of the lung: CellCards from LungMAP. *Developmental Cell* **2022**, *57*, 112-145 e112, doi:10.1016/j.devcel.2021.11.007.

32. Liu, G.; Summer, R. Cellular metabolism in lung health and disease. *Annual Review of Physiology* **2019**, *81*, 403-428, doi:10.1146/annurev-physiol-020518-114640.

33. Sanderson, M.J. Exploring lung physiology in health and disease with lung slices. *Pulmonary Pharmacology & Therapeutics* **2011**, *24*, 452-465, doi:10.1016/j.pupt.2011.05.001.

34. Schiller, H.B.; Montoro, D.T.; Simon, L.M.; Rawlins, E.L.; Meyer, K.B.; Strunz, M.; Vieira Braga, F.A.; Timens, W.; Koppelman, G.H.; Budinger, G.R.S., et al. The human lung cell atlas: A high-resolution reference map of the human lung in health and disease. *American Journal of Respiratory Cell and Molecular Biology* **2019**, *61*, 31-41, doi:10.1165/rcmb.2018-0416TR.

35. World Health Organization (WHO). Global Health Estimates 2020: Deaths by Cause, Age, Sex, by Country and by Region, 2000-2019. Availabe online: https://www.who.int/news-room/fact-sheets/detail/the-top-10-causes-of-death (accessed on August 27th, 2022).

36. World Health Organization (WHO). Global Health Estimates: Leading Causes of Death in Portugal, 2000-2019. Availabe online: https://www.who.int/data/gho/data/themes/mortality-and-global-health-estimates/ghe-leading-causes-of-death (accessed on August 27th, 2022).

37. Nainwal, N.; Sharma, Y.; Jakhmola, V. Dry powder inhalers of antitubercular drugs. *Tuberculosis* **2022**, *135*, 102228, doi:10.1016/j.tube.2022.102228.

38. Momin, M.A.M.; Tucker, I.G.; Das, S.C. High dose dry powder inhalers to overcome the challenges of tuberculosis treatment. *International Journal of Pharmaceutics* **2018**, *550*, 398-417, doi:10.1016/j.ijpharm.2018.08.061.

39. Asghar, A.; Imran, H.M.; Bano, N.; Maalik, S.; Mushtaq, S.; Hussain, A.; Varjani, S.; Aleya, L.; Iqbal, H.M.N.; Bilal, M. SARS-COV-2/COVID-19: Scenario, epidemiology, adaptive mutations, and environmental factors. *Environmental Science and Pollution Research* **2022**, 10.1007/s11356-022-22333-0, doi:10.1007/s11356-022-22333-0.

40. Han, Q.; Zheng, B.; Daines, L.; Sheikh, A. Long-term sequelae of COVID-19: A systematic review and meta-analysis of one-year follow-up studies on post-COVID symptoms. *Pathogens* **2022**, *11*, doi:10.3390/pathogens11020269.

41. World Health Organization (WHO). Global Tuberculosis Report 2021. Availabe online: https://www.who.int/teams/global-tuberculosis-programme/tb-reports/global-tuberculosis-report-2021 (accessed on August 31st, 2022).

42. Havasi, A.; Visan, S.; Cainap, C.; Cainap, S.S.; Mihaila, A.A.; Pop, L.-A. Influenza A, Influenza B, and SARS-CoV-2 similarities and differences - A focus on diagnosis. *Frontiers in Microbiology* **2022**, *13*, 908525, doi:10.3389/fmicb.2022.908525.

43. Waterer, G. What is pneumonia? *Breathe* **2021**, *17*, 210087, doi:10.1183/20734735.0087-2021.

44. Cilloniz, C.; Martin-Loeches, I.; Garcia-Vidal, C.; San Jose, A.; Torres, A. Microbial etiology of pneumonia: Epidemiology, diagnosis and resistance patterns. *International Journal of Molecular Sciences* **2016**, *17*, doi:10.3390/ijms17122120.

45. Colombo, G.L.; Di Matteo, S.; Martinotti, C.; Oselin, M.; Valentino, M.C.; Bruno, G.M.; Pitotti, C.; Menzella, F. Omalizumab and long-term quality of life outcomes in patients with moderate-to-severe allergic asthma: A systematic review. *Therapeutic Advances in Respiratory Disease* **2019**, *13*, 1753466619841350, doi:10.1177/1753466619841350.

46. Caimmi, D.; Marseglia, A.; Pieri, G.; Benzo, S.; Bosa, L.; Caimmi, S. Nose and lungs: One way, one disease. *Italian Journal of Pediatrics* **2012**, *38*, 60, doi:10.1186/1824-7288-38-60.

47. Yawn, B.P.; Mintz, M.L.; Doherty, D.E. GOLD in practice: Chronic obstructive pulmonary disease treatment and management in the primary care setting.

International Journal of Chronic Obstructive Pulmonary Disease **2021**, *16*, 289-299, doi:10.2147/COPD.S222664.

48. Patel, B.; Priefer, R. Impact of chronic obstructive pulmonary disease, lung infection, and/or inhaled corticosteroids use on potential risk of lung cancer. *Life Sciences* **2022**, *294*, 120374, doi:10.1016/j.lfs.2022.120374.

49. Kanwal, M.; Ding, X.-J.; Cao, Y. Familial risk for lung cancer. *Oncology Letters* **2017**, *13*, 535-542, doi:10.3892/ol.2016.5518.

50. Herbst, R.S.; Morgensztern, D.; Boshoff, C. The biology and management of non-small cell lung cancer. *Nature* **2018**, *553*, 446-454, doi:10.1038/nature25183.

51. Oronsky, B.; Reid, T.R.; Oronsky, A.; Carter, C.A. What's new in SCLC? A review. *Neoplasia* **2017**, *19*, 842-847, doi:10.1016/j.neo.2017.07.007.

52. Sabari, J.K.; Lok, B.H.; Laird, J.H.; Poirier, J.T.; Rudin, C.M. Unravelling the biology of SCLC: Implications for therapy. *Nature Reviews Clinical Oncology* **2017**, *14*, 549-561, doi:10.1038/nrclinonc.2017.71.

53. Yang, S.-R.; Schultheis, A.M.; Yu, H.; Mandelker, D.; Ladanyi, M.; Buttner, R. Precision medicine in non-small cell lung cancer: Current applications and future directions. *Seminars in Cancer Biology* **2022**, *84*, 184-198, doi:10.1016/j.semcancer.2020.07.009.

54. Testa, U.; Castelli, G.; Pelosi, E. Lung cancers: Molecular characterization, clonal heterogeneity and evolution, and cancer stem cells. *Cancers* **2018**, *10*, doi:10.3390/cancers10080248.

55. Passiglia, F.; Bertolaccini, L.; Del Re, M.; Facchinetti, F.; Ferrara, R.; Franchina, T.; Malapelle, U.; Menis, J.; Passaro, A.; Pilotto, S., et al. Diagnosis and treatment of early and locally advanced non-small-cell lung cancer: The 2019 AIOM (Italian Association of Medical Oncology) clinical practice guidelines. *Critical Reviews in Oncology/Hematology* **2020**, *148*, 102862, doi:10.1016/j.critrevonc.2019.102862.

56. Zlatanova, T.; Arabadjiev, J.; Kirova-Nedyalkova, G.; Nikova, D. Successful treatment with docetaxel plus nintedanib in a patient with lung adenocarcinoma and pulmonary fibrosis: A case report and literature review. *Frontiers in Oncology* **2022**, *12*, 907321, doi:10.3389/fonc.2022.907321.

57. Maher, T.M.; Wells, A.U.; Laurent, G.J. Idiopathic pulmonary fibrosis: Multiple causes and multiple mechanisms? *European Respiratory Journal* **2007**, *30*, 835-839, doi:10.1183/09031936.00069307.

58. Wei, Y.; Hou, J.; Lu, P.; Fu, L.; Wang, X.; Huang, Y.; Chen, L.; Lv, C. A near-infrared fluorescent probe was used to evaluate the role of histone deacetylase in pulmonary fibrosis cells and mice. *Sensors and Actuators B: Chemical* **2022**, *366*, doi:10.1016/j.snb.2022.132012.

59. Saluzzo, F.; Riberi, L.; Messore, B.; Lore, N.I.; Esposito, I.; Bignamini, E.; De Rose, V. CFTR modulator therapies: Potential impact on airway infections in cystic fibrosis. *Cells* **2022**, *11*, doi:10.3390/cells11071243.

60. Quispe, C.; Herrera-Bravo, J.; Khan, K.; Javed, Z.; Semwal, P.; Painuli, S.; Kamiloglu, S.; Martorell, M.; Calina, D.; Sharifi-Rad, J. Therapeutic applications of curcumin nanomedicine formulations in cystic fibrosis. *Progress in Biomaterials* **2022**, 10.1007/s40204-022-00198-3, doi:10.1007/s40204-022-00198-3.

61. Ong, V.; Mei, V.; Cao, L.; Lee, K.; Chung, E.J. Nanomedicine for cystic fibrosis. *SLAS Technology* **2019**, *24*, 169-180, doi:10.1177/2472630318824334.

62. Akkerman-Nijland, A.M.; Akkerman, O.W.; Grasmeijer, F.; Hagedoorn, P.; Frijlink, H.W.; Rottier, B.L.; Koppelman, G.H.; Touw, D.J. The pharmacokinetics of antibiotics in cystic fibrosis. *Expert Opinion on Drug Metabolism & Toxicology* **2021**, *17*, 53-68, doi:10.1080/17425255.2021.1836157.

63. Farinha, C.M.; Callebaut, I. Molecular mechanisms of cystic fibrosis - how mutations lead to misfunction and guide therapy. *Bioscience Reports* **2022**, *42*, doi:10.1042/BSR20212006.

64. De Boeck, K. Cystic fibrosis in the year 2020: A disease with a new face. *Acta Paediatrica* **2020**, *109*, 893-899, doi:10.1111/apa.15155.

65. Mercier, J.-C.; Foucaud, P. Modulateurs pharmacologiques du canal CFTR: Une révolution thérapeutique dans la mucoviscidose. *Bulletin de l'Académie Nationale de Médecine* **2022**, *206*, 775-786, doi:10.1016/j.banm.2022.01.027.

66. van Dorst, J.M.; Tam, R.Y.; Ooi, C.Y. What do we know about the microbiome in cystic fibrosis? Is there a role for probiotics and prebiotics? *Nutrients* **2022**, *14*, doi:10.3390/nu14030480.

67. Faber, S.C.; McCullough, S.D. Through the looking glass: *In vitro* models for inhalation toxicology and interindividual variability in the airway. *Applied In Vitro Toxicology* **2018**, *4*, 115-128, doi:10.1089/aivt.2018.0002.

68. Chingwaru, W.; Glashoff, R.H.; Vidmar, J.; Kapewangolo, P.; Sampson, S.L. Mammalian cell cultures as models for *Mycobacterium tuberculosis*-human immunodeficiency virus (HIV) interaction studies: A review. *Asian Pacific Journal of Tropical Medicine* **2016**, *9*, 832-838, doi:10.1016/j.apjtm.2016.07.002.

69. Primavessy, D.; Metz, J.; Schnur, S.; Schneider, M.; Lehr, C.-M.; Hittinger, M. Pulmonary *in vitro* instruments for the replacement of animal experiments. *European Journal of Pharmaceutics and Biopharmaceutics* **2021**, *168*, 62-75, doi:10.1016/j.ejpb.2021.08.005.

70. Tian, L.; Gao, J.; Garcia, I.M.; Chen, H.J.; Castaldi, A.; Chen, Y.-W. Human pluripotent stem cell-derived lung organoids: Potential applications in

development and disease modeling. *Wiley Interdisciplinary Reviews: Developmental Biology* **2021**, *10*, e399, doi:10.1002/wdev.399.

71. Huang, D.; Liu, T.; Liao, J.; Maharjan, S.; Xie, X.; Pérez, M.; Anaya, I.; Wang, S.; Tirado Mayer, A.; Kang, Z., et al. Reversed-engineered human alveolar lung-on-a-chip model. *Proceedings of the National Academy of Sciences of the United States of America* **2021**, *118*, doi:10.1073/pnas.2016146118.

72. Schubert, C.; van Langeveld, M.C.; Donoso, L.A. Innovations in 3D printing: A 3D overview from optics to organs. *British Journal of Ophthalmology* **2014**, *98*, 159-161, doi:10.1136/bjophthalmol-2013-304446.

73. Hull, C.W. Patent US4575330A: Apparatus for production of three-dimensional objects by stereolithography. US4575330A, March 11th, 1986.

74. Rayna, T.; Striukova, L. From rapid prototyping to home fabrication: How 3D printing is changing business model innovation. *Technological Forecasting and Social Change* **2016**, *102*, 214-224, doi:10.1016/j.techfore.2015.07.023.

75. Ngo, T.D.; Kashani, A.; Imbalzano, G.; Nguyen, K.T.Q.; Hui, D. Additive manufacturing (3D printing): A review of materials, methods, applications and challenges. *Composites Part B: Engineering* **2018**, *143*, 172-196, doi:10.1016/j.compositesb.2018.02.012.

76. Turner, B.N.; Strong, R.; Gold, S.A. A review of melt extrusion additive manufacturing processes: I. Process design and modeling. *Rapid Prototyping Journal* **2014**, *20*, 192-204, doi:10.1108/rpj-01-2013-0012.

77. Melchels, F.P.W.; Feijen, J.; Grijpma, D.W. A review on stereolithography and its applications in biomedical engineering. *Biomaterials* **2010**, *31*, 6121-6130, doi:10.1016/j.biomaterials.2010.04.050.

78. Minocchieri, S.; Burren, J.M.; Bachmann, M.A.; Stern, G.; Wildhaber, J.; Buob, S.; Schindel, R.; Kraemer, R.; Frey, U.P.; Nelle, M. Development of the premature infant nose throat-model (PrINT-Model): An upper airway replica of a premature neonate for the study of aerosol delivery. *Pediatric Research* **2008**, *64*, 141-146, doi:10.1203/PDR.0b013e318175dcfa.

79. Bücking, T.M.; Hill, E.R.; Robertson, J.L.; Maneas, E.; Plumb, A.A.; Nikitichev, D.I. From medical imaging data to 3D printed anatomical models. *PLoS One* **2017**, *12*, e0178540, doi:10.1371/journal.pone.0178540.

80. Wei, X.; Hindle, M.; Kaviratna, A.; Huynh, B.K.; Delvadia, R.R.; Sandell, D.; Byron, P.R. *In vitro* tests for aerosol deposition. VI: Realistic testing with different mouth-throat models and *in vitro-in vivo* correlations for a dry powder inhaler, metered dose inhaler, and soft mist inhaler. *Journal of Aerosol Medicine and Pulmonary Drug Delivery* **2018**, *31*, 358-371, doi:10.1089/jamp.2018.1454.

81. Mirza, A.A.; Robinson, T.E.; Gifford, K.; Guo, H.H. 3D printing and the cystic fibrosis lung. *Journal of Cystic Fibrosis* **2019**, *18*, 278-279, doi:10.1016/j.jcf.2018.09.004.

82. Zhang, Y.S.; Yue, K.; Aleman, J.; Moghaddam, K.M.; Bakht, S.M.; Yang, J.; Jia, W.; Dell'Erba, V.; Assawes, P.; Shin, S.R., et al. 3D bioprinting for tissue and organ fabrication. *Annals of Biomedical Engineering* **2017**, *45*, 148-163, doi:10.1007/s10439-016-1612-8.

83. Galliger, Z.; Vogt, C.D.; Panoskaltsis-Mortari, A. 3D bioprinting for lungs and hollow organs. *Translational Research* **2019**, *211*, 19-34, doi:10.1016/j.trsl.2019.05.001.

84. Derakhshanfar, S.; Mbeleck, R.; Xu, K.; Zhang, X.; Zhong, W.; Xing, M. 3D bioprinting for biomedical devices and tissue engineering: A review of recent trends and advances. *Bioactive Materials* **2018**, *3*, 144-156, doi:10.1016/j.bioactmat.2017.11.008.

85. Wang, Y.; Yuan, X.; Yao, B.; Zhu, S.; Zhu, P.; Huang, S. Tailoring bioinks of extrusion-based bioprinting for cutaneous wound healing. *Bioactive Materials* **2022**, *17*, 178-194, doi:10.1016/j.bioactmat.2022.01.024.

86. Lewis, A.; Koukoura, A.; Tsianos, G.-I.; Gargavanis, A.A.; Nielsen, A.A.; Vassiliadis, E. Organ donation in the US and Europe: The supply vs demand imbalance. *Transplantation Reviews* **2021**, *35*, 100585, doi:10.1016/j.trre.2020.100585.

87. Tetsuka, H.; Shin, S.R. Materials and technical innovations in 3D printing in biomedical applications. *Journal of Materials Chemistry B* **2020**, *8*, 2930-2950, doi:10.1039/d0tb00034e.

88. dos Santos, D.M.; Cardoso, R.M.; Migliorini, F.L.; Facure, M.H.M.; Mercante, L.A.; Mattoso, L.H.C.; Correa, D.S. Advances in 3D printed sensors for food analysis. *Trends in Analytical Chemistry* **2022**, *154*, doi:10.1016/j.trac.2022.116672.

89. Bock, S.; Rades, T.; Rantanen, J.; Scherliess, R. Additive manufacturing in respiratory sciences - Current applications and future prospects. *Advanced Drug Delivery Reviews* **2022**, *186*, 114341, doi:10.1016/j.addr.2022.114341.

90. Yilmaz, B.; Kara, B.Y. Mathematical surface function-based design and 3D printing of airway stents. *3D Printig in Medicine* **2022**, *8*, 24, doi:10.1186/s41205-022-00154-8.

91. de Boer, A.H.; Hagedoorn, P.; Grasmeijer, F. Dry powder inhalation, part 1: Ancient history and precursors to modern dry powder inhalers. *Expert Opinion on Drug Delivery* **2022**, 10.1080/17425247.2022.2112568, 1-12, doi:10.1080/17425247.2022.2112568.

92. Olschewski, H.; Seeger, W.; Grimminger, F. Physiologie und Pathophysiologie der pulmonalen Zirkulation. *Internist* **1999**, *40*, 696-709, doi:10.1007/s001080050391.

93. de Boer, A.H.; Hagedoorn, P.; Grasmeijer, F. Dry powder inhalation, part 2: The present and future. *Expert Opinion on Drug Delivery* **2022**,

10.1080/17425247.2022.2112570, 1-15, doi:10.1080/17425247.2022.2112570.

94. Mack, G.S. Pfizer dumps Exubera. *Nature Biotechnology* **2007**, *25*, 1331-1332, doi:10.1038/nbt1207-1331.

95. Pettus, J.; Santos Cavaiola, T.; Edelman, S.V. Recommendations for initiating use of Afrezza inhaled insulin in individuals with type 1 diabetes. *Diabetes Technology & Therapeutics* **2018**, *20*, 448-451, doi:10.1089/dia.2017.0463.

96. Pontes, J.F.; Grenha, A. Multifunctional nanocarriers for lung drug delivery. *Nanomaterials* **2020**, *10*, doi:10.3390/nano10020183.

97. Ahsan, F.; Rivas, I.P.; Khan, M.A.; Suárez, A.I.T. Targeting to macrophages: Role of physicochemical properties of particulate carriers—liposomes and microspheres—on the phagocytosis by macrophages. *Journal of Controlled Release* **2002**, *79*, 29-40, doi:10.1016/s0168-3659(01)00549-1.

98. Grenha, A.; Alves, A.; Guerreiro, F.; Pinho, J.; Simões, S.; José Almeida, A.; Manuela Gaspar, M. Inhalable locust bean gum microparticles co-associating isoniazid and rifabutin: Therapeutic assessment in a murine model of tuberculosis infection. *European Journal of Pharmaceutics and Biopharmaceutics* **2020**, *147*, 38-44, doi:10.1016/j.ejpb.2019.11.009.

99. Mehta, P.P.; Dhapte-Pawar, V.S. Novel and evolving therapies for COVID-19 related pulmonary complications. *American Journal of the Medical Sciences* **2021**, *361*, 557-566, doi:10.1016/j.amjms.2021.02.019.

100. Koszalka, P.; Subbarao, K.; Baz, M. Preclinical and clinical developments for combination treatment of influenza. *PLoS Pathogens* **2022**, *18*, e1010481, doi:10.1371/journal.ppat.1010481.

101. Masjedi, M.; Montahaei, T.; Sharafi, Z.; Jalali, A. Pulmonary vaccine delivery: An emerging strategy for vaccination and immunotherapy. *Journal of Drug Delivery Science and Technology* **2022**, *69*, doi:10.1016/j.jddst.2022.103184.

102. Mehanny, M.; Boese, A.; Bornamehr, B.; Hoppstädter, J.; Presser, V.; Kiemer, A.K.; Lehr, C.-M.; Fuhrmann, G. Spray-dried pneumococcal membrane vesicles are promising candidates for pulmonary immunization. *International Journal of Pharmaceutics* **2022**, *621*, 121794, doi:10.1016/j.ijpharm.2022.121794.

103. Mathis, B.J.; Kusumoto, M.; Zaboronok, A.; Hiramatsu, Y. Packaging and delivery of asthma therapeutics. *Pharmaceutics* **2021**, *14*, doi:10.3390/pharmaceutics14010092.

104. Elkomy, M.H.; El Menshawe, S.F.; Kharshoum, R.M.; Abdeltwab, A.M.; Hussein, R.R.S.; Hamad, D.S.; Alsalahat, I.; Aboud, H.M. Innovative pulmonary targeting of terbutaline sulfate-laded novasomes for non-invasive tackling of asthma: Statistical optimization and comparative *in vitro*/*in vivo* evaluation. *Drug Delivery* **2022**, *29*, 2058-2071, doi:10.1080/10717544.2022.2092236.

105. Alfahad, A.J.; Alzaydi, M.M.; Aldossary, A.M.; Alshehri, A.A.; Almughem, F.A.; Zaidan, N.M.; Tawfik, E.A. Current views in chronic obstructive pulmonary disease pathogenesis and management. *Saudi Pharmaceutical Journal* **2021**, *29*, 1361-1373, doi:10.1016/j.jsps.2021.10.008.

106. Virmani, T.; Kumar, G.; Virmani, R.; Sharma, A.; Pathak, K. Nanocarrier-based approaches to combat chronic obstructive pulmonary disease. *Nanomedicine* **2022**, 10.2217/nnm-2021-0403, doi:10.2217/nnm-2021-0403.

107. Emran, T.B.; Shahriar, A.; Mahmud, A.R.; Rahman, T.; Abir, M.H.; Siddiquee, M.F.-R.; Ahmed, H.; Rahman, N.; Nainu, F.; Wahyudin, E., et al. Multidrug resistance in cancer: Understanding molecular mechanisms, immunoprevention and therapeutic approaches. *Frontiers in Oncology* **2022**, *12*, 891652, doi:10.3389/fonc.2022.891652.

108. Hani, U.; M, Y.B.; Wahab, S.; Siddiqua, A.; Osmani, R.A.M.; Rahamathulla, M. A comprehensive review of current perspectives on novel drug delivery systems and approaches for lung cancer management. *Journal of Pharmaceutical Innovation* **2021**, 10.1007/s12247-021-09582-1, doi:10.1007/s12247-021-09582-1.

109. Liang, W.; Pan, H.W.; Vllasaliu, D.; Lam, J.K.W. Pulmonary delivery of biological drugs. *Pharmaceutics* **2020**, *12*, doi:10.3390/pharmaceutics12111025.

110. Ruigrok, M.J.R.; Frijlink, H.W.; Melgert, B.N.; Olinga, P.; Hinrichs, W.L.J. Gene therapy strategies for idiopathic pulmonary fibrosis: Recent advances, current challenges, and future directions. *Molecular Therapy: Methods & Clinical Development* **2021**, *20*, 483-496, doi:10.1016/j.omtm.2021.01.003.

111. Pramanik, S.; Mohanto, S.; Manne, R.; Rajendran, R.R.; Deepak, A.; Edapully, S.J.; Patil, T.; Katari, O. Nanoparticle-based drug delivery system: The magic bullet for the treatment of chronic pulmonary diseases. *Molecular Pharmaceutics* **2021**, *18*, 3671-3718, doi:10.1021/acs.molpharmaceut.1c00491.

112. Pailhoriès, H.; Herrmann, J.-L.; Velo-Suarez, L.; Lamoureux, C.; Beauruelle, C.; Burgel, P.-R.; Héry-Arnaud, G. Antibiotic resistance in chronic respiratory diseases: From susceptibility testing to the resistome. *European Respiratory Review* **2022**, *31*, doi:10.1183/16000617.0259-2021.

113. Majumder, J.; Minko, T. Targeted nanotherapeutics for respiratory diseases: Cancer, fibrosis, and coronavirus. *Advanced Therapeutics* **2021**, *4*, 2000203, doi:10.1002/adtp.202000203.

114. Ito, K. Inhaled antifungal therapy: Benefits, challenges, and clinical applications. *Expert Opinion on Drug Delivery* **2022**, *19*, 755-769, doi:10.1080/17425247.2022.2084530.

115. Brunaugh, A.D.; Sharma, S.; Smyth, H. Inhaled fixed-dose combination powders for the treatment of respiratory infections. *Expert Opinion on Drug Delivery* **2021**, *18*, 1101-1115, doi:10.1080/17425247.2021.1886074.

116. Xu, P.-Y.; Kankala, R.K.; Pan, Y.-J.; Yuan, H.; Wang, S.-B.; Chen, A.-Z. Overcoming multidrug resistance through inhalable siRNA nanoparticles-decorated porous microparticles based on supercritical fluid technology. *International Journal of Nanomedicine* **2018**, *13*, 4685-4698, doi:10.2147/IJN.S169399.

117. Mehta, P.; Kadam, S.; Pawar, A.; Bothiraja, C. Dendrimers for pulmonary delivery: Current perspectives and future challenges. *New Journal of Chemistry* **2019**, *43*, 8396-8409, doi:10.1039/c9nj01591d.

118. Lababidi, N.; Ofosu Kissi, E.; Elgaher, W.A.M.; Sigal, V.; Haupenthal, J.; Schwarz, B.C.; Hirsch, A.K.H.; Rades, T.; Schneider, M. Spray-drying of inhalable, multifunctional formulations for the treatment of biofilms formed in cystic fibrosis. *Journal of Controlled Release* **2019**, *314*, 62-71, doi:10.1016/j.jconrel.2019.10.038.

119. García-González, C.A.; Sosnik, A.; Kálmar, J.; De Marco, I.; Erkey, C.; Concheiro, A.; Alvarez-Lorenzo, C. Aerogels in drug delivery: From design to application. *Journal of Controlled Release* **2021**, *332*, 40-63, doi:10.1016/j.jconrel.2021.02.012.

120. Obaidat, R.M.; Tashtoush, B.M.; Bayan, M.F.; Al Bustami, R.T.; Alnaief, M. Drying using supercritical fluid technology as a potential method for preparation of chitosan aerogel microparticles. *AAPS PharmSciTech* **2015**, *16*, 1235-1244, doi:10.1208/s12249-015-0312-2.

121. McVey, M.J.; Maishan, M.; Blokland, K.E.C.; Bartlett, N.; Kuebler, W.M. Extracellular vesicles in lung health, disease, and therapy. *American Journal of Physiology - Lung Cellular and Molecular Physiology* **2019**, *316*, L977-L989, doi:10.1152/ajplung.00546.2018.

122. Zillen, D.; Beugeling, M.; Hinrichs, W.L.J.; Frijlink, H.W.; Grasmeijer, F. Natural and bioinspired excipients for dry powder inhalation formulations. *Current Opinion in Colloid & Interface Science* **2021**, *56*, doi:10.1016/j.cocis.2021.101497.

123. Kumbhar, P.; Manjappa, A.; Shah, R.; Jha, N.K.; Singh, S.K.; Dua, K.; Disouza, J.; Patravale, V. Inhalation delivery of repurposed drugs for lung cancer: Approaches, benefits and challenges. *Journal of Controlled Release* **2022**, *341*, 1-15, doi:10.1016/j.jconrel.2021.11.015.

124. Pasqua, E.; Hamblin, N.; Edwards, C.; Baker-Glenn, C.; Hurley, C. Developing inhaled drugs for respiratory diseases: A medicinal chemistry perspective. *Drug Discovery Today* **2022**, *27*, 134-150, doi:10.1016/j.drudis.2021.09.005.

125. Mekonnen, T.; Cai, X.; Burchell, C.; Gholizadeh, H.; Cheng, S. A review of upper airway physiology relevant to the delivery and deposition of inhalation aerosols. *Advanced Drug Delivery Reviews* **2022**, *191*, 114530, doi:10.1016/j.addr.2022.114530.

126. Nahar, K.; Gupta, N.; Gauvin, R.; Absar, S.; Patel, B.; Gupta, V.; Khademhosseini, A.; Ahsan, F. *In vitro*, *in vivo* and *ex vivo* models for studying particle deposition and drug absorption of inhaled pharmaceuticals. *European Journal of Pharmaceutical Sciences* **2013**, *49*, 805-818, doi:10.1016/j.ejps.2013.06.004.

127. Brewer, E.; Ramsland, A. Particle size determination by automated microscopical imaging analysis with comparison to laser diffraction. *Journal of Pharmaceutical Sciences* **1995**, *84*, 499-501, doi:10.1002/jps.2600840421.

128. Yaqoubi, S.; Chan, H.-K.; Nokhodchi, A.; Dastmalchi, S.; Alizadeh, A.A.; Barzegar-Jalali, M.; Adibkia, K.; Hamishehkar, H. A quantitative approach to predicting lung deposition profiles of pharmaceutical powder aerosols. *International Journal of Pharmaceutics* **2021**, *602*, 120568, doi:10.1016/j.ijpharm.2021.120568.

129. Gupta, A.; Pant, G.; Mitra, K.; Madan, J.; Chourasia, M.K.; Misra, A. Inhalable particles containing rapamycin for induction of autophagy in macrophages infected with *Mycobacterium tuberculosis*. *Molecular Pharmaceutics* **2014**, *11*, 1201-1207, doi:10.1021/mp4006563.

130. Chaurasiya, B.; Zhao, Y.-Y. Dry powder for pulmonary delivery: A comprehensive review. *Pharmaceutics* **2020**, *13*, doi:10.3390/pharmaceutics13010031.

131. Newman, S.P. 3.2. Fine Particle Fraction: The Good and the Bad. In *ISAM Textbook of Aerosol Medicine*.

132. Mitchell, J.P.; Nagel, M.W. Cascade impactors for the size characterization of aerosols from medical inhalers: Their uses and limitations. *Journal of Aerosol Medicine* **2003**, *16*, 341-377, doi:10.1089/089426803772455622.

133. 2.9.18. Preparations for inhalation: Aerodynamic Assessment of Fine Particles. In *European Pharmacopoeia*, 10th ed.; European Directorate for the Quality of Medicines & HealthCare of the Council of Europe (EDQM): Starsbourg, 2019.

134. Marple, V.A. History of impactors - The first 110 years. *Aerosol Science and Technology* **2004**, *38*, 247-292, doi:10.1080/02786820490424347.

135. Borghardt, J.M.; Kloft, C.; Sharma, A. Inhaled therapy in respiratory disease: The complex interplay of pulmonary kinetic processes. *Canadian Respiratory Journal* **2018**, *2018*, 2732017, doi:10.1155/2018/2732017.

136. Darquenne, C. Aerosol deposition in health and disease. *Journal of Aerosol Medicine and Pulmonary Drug Delivery* **2012**, *25*, 140-147, doi:10.1089/jamp.2011.0916.

137. Darquenne, C. Deposition mechanisms. *Journal of Aerosol Medicine and Pulmonary Drug Delivery* **2020**, *33*, 181-185, doi:10.1089/jamp.2020.29029.cd.

138. Sorino, C.; Negri, S.; Spanevello, A.; Visca, D.; Scichilone, N. Inhalation therapy devices for the treatment of obstructive lung diseases: The history of inhalers towards the ideal inhaler. *European Journal of Internal Medicine* **2020**, *75*, 15-18, doi:10.1016/j.ejim.2020.02.023.

139. Freedman, T. Medihaler® therapy for bronchial asthma; A new type of aerosol therapy. *Postgraduate Medicine* **1956**, *20*, 667-673, doi:10.1080/00325481.1956.11691366.

140. Lewis, D. Metered-dose inhalers: Actuators old and new. *Expert Opinion on Drug Delivery* **2007**, *4*, 235-245, doi:10.1517/17425247.4.3.235.

141. Steiropoulos, P.; Bakakos, P.; Hatziagorou, E.; Katsaounou, P.; Loukides, S.; Papaioannou, A.; Porpodis, K.; Samaras, K.; Tzouvelekis, A.; Kalafatakis, K., et al. The present and future of inhalation therapy for the management of obstructive airway diseases: Emphasis on pressurized metered-dose inhalers. *Pneumon* **2021**, 10.18332/pne/144614, 1-13, doi:10.18332/pne/144614.

142. Gleeson, P.K.; Feldman, S.; Apter, A.J. Controller inhalers: Overview of devices, instructions for use, errors, and interventions to improve technique. *The Journal of Allergy and Clinical Immunology: In Practice* **2020**, *8*, 2234-2242, doi:10.1016/j.jaip.2020.03.003.

143. Román-Rodríguez, M.; Metting, E.; Gacía-Pardo, M.; Kocks, J.; van der Molen, T. Wrong inhalation technique is associated to poor asthma clinical outcomes. Is there room for improvement? *Current Opinion in Pulmonary Medicine* **2019**, *25*, 18-26, doi:10.1097/MCP.0000000000000540.

144. Stein, S.W.; Sheth, P.; Hodson, P.D.; Myrdal, P.B. Advances in metered dose inhaler technology: Hardware development. *AAPS PharmSciTech* **2014**, *15*, 326-338, doi:10.1208/s12249-013-0062-y.

145. Jeswani, H.K.; Azapagic, A. Life cycle environmental impacts of inhalers. *Journal of Cleaner Production* **2019**, *237*, doi:10.1016/j.jclepro.2019.117733.

146. Fulford, B.; Mezzi, K.; Aumônier, S.; Finkbeiner, M. Carbon footprints and life cycle assessments of inhalers: A review of published evidence. *Sustainability* **2022**, *14*, doi:10.3390/su14127106.

147. Rogueda, P.; Lallement, A.; Traini, D.; Iliev, I.; Young, P.M. Twenty years of HFA pMDI patents: facts and perspectives. *Journal of Pharmacy and Pharmacology* **2012**, *64*, 1209-1216, doi:10.1111/j.2042-7158.2011.01387.x.

148. Sellers, W.F.S. Asthma pressurised metered dose inhaler performance: Propellant effect studies in delivery systems. *Allergy, Asthma & Clinical Immunology* **2017**, *13*, 30, doi:10.1186/s13223-017-0202-0.

149. Pernigotti, D.; Stonham, C.; Panigone, S.; Sandri, F.; Ferri, R.; Unal, Y.; Roche, N. Reducing carbon footprint of inhalers: Analysis of climate and clinical implications of different scenarios in five European countries. *BMJ Open Respiratory Research* **2021**, *8*, doi:10.1136/bmjresp-2021-001071.

150. Hargreaves, C.; Budgen, N.; Whiting, A.; Lachacz, K.; Sommerville, M.; Archbell, J.; Joshi, V. S60 A new medical propellant HFO-1234ze(E): Reducing the environmental impact of inhaled medicines. In Proceedings of 'The Day After Tomorrow' – Impact of the carbon footprint in lung health; pp. A38.32-A39.

151. Lavorini, F.; Chudek, J.; Gálffy, G.; Pallarés-Sanmartin, A.; Pelkonen, A.S.; Rytilä, P.; Syk, J.; Szilasi, M.; Tamási, L.; Xanthopoulos, A., et al. Switching to the dry-powder inhaler Easyhaler®: A narrative review of the evidence. *Pulmonary Therapy* **2021**, *7*, 409-427, doi:10.1007/s41030-021-00174-5.

152. Berkenfeld, K.; Lamprecht, A.; McConville, J.T. Devices for dry powder drug delivery to the lung. *AAPS PharmSciTech* **2015**, *16*, 479-490, doi:10.1208/s12249-015-0317-x.

153. ElKasabgy, N.A.; Adel, I.M.; Elmeligy, M.F. Respiratory tract: Structure and attractions for drug delivery using dry powder inhalers. *AAPS PharmSciTech* **2020**, *21*, 238, doi:10.1208/s12249-020-01757-2.

154. Lavorini, F.; Pistolesi, M.; Usmani, O.S. Recent advances in capsule-based dry powder inhaler technology. *Multidisciplinary Respiratory Medicine* **2017**, *12*, 11, doi:10.1186/s40248-017-0092-5.

155. Wang, J.; Kong, X.; Hu, L.; Hu, Y. Dry powder inhalers: A patent review. *Journal of Drug Delivery Science and Technology* **2022**, *74*, doi:10.1016/j.jddst.2022.103540.

156. Azouz, W.; Chrystyn, H. Clarifying the dilemmas about inhalation techniques for dry powder inhalers: Integrating science with clinical practice. *Primary Care Respiratory Journal* **2012**, *21*, 208-213, doi:10.4104/pcrj.2012.00010.

157. Ke, W.-R.; Chang, R.Y.K.; Chan, H.-K. Engineering the right formulation for enhanced drug delivery. *Advanced Drug Delivery Reviews* **2022**, *191*, 114561, doi:10.1016/j.addr.2022.114561.

158. Abiona, O.; Wyatt, D.; Koner, J.; Mohammed, A. The optimisation of carrier selection in dry powder inhaler formulation and the role of surface energetics. *Biomedicines* **2022**, *10*, doi:10.3390/biomedicines10112707.

159. Newman, B.; Babiskin, A.; Bielski, E.; Boc, S.; Dhapare, S.; Fang, L.; Feibus, K.; Kaviratna, A.; Li, B.V.; Luke, M.C., et al. Scientific and regulatory activities initiated by the U.S. Food and drug administration to foster approvals of generic dry powder inhalers: Bioequivalence perspective. *Advanced Drug Delivery Reviews* **2022**, *190*, 114526, doi:10.1016/j.addr.2022.114526.

160. 006/2018: Monitorização e Tratamento Para o Controlo da Asma na Criança, no Adolescente e no Adulto. Direção Geral de Saúde (DGS), Ed. 2018; p 46.

161. Daley-Yates, P.T.; Deans, A.; Mehta, R.; Sousa, A.R. Comparative clinical pharmacology of mometasone furoate, fluticasone propionate and fluticasone furoate. *Pulmonary Pharmacology & Therapeutics* **2022**, *77*, 102171, doi:10.1016/j.pupt.2022.102171.

162. Melani, A.S. Inhaler technique in asthma and COPD: Challenges and unmet knowledge that can contribute to suboptimal use in real life. *Expert Review in Clinical Pharmacology* **2021**, *14*, 991-1003, doi:10.1080/17512433.2021.1929922.

163. Bass, K.; Farkas, D.; Hassan, A.; Bonasera, S.; Hindle, M.; Longest, P.W. High-efficiency dry powder aerosol delivery to children: Review and application of new technologies. *Journal of Aerosol Science* **2021**, *153*, doi:10.1016/j.jaerosci.2020.105692.

164. Park, H.; Ha, E.-S.; Kim, M.-S. Surface modification strategies for high-dose dry powder inhalers. *Journal of Pharmaceutical Investigation* **2021**, *51*, 635-668, doi:10.1007/s40005-021-00529-9.

165. Wilkinson, A.J.K.; Braggins, R.; Steinbach, I.; Smith, J. Costs of switching to low global warming potential inhalers. An economic and carbon footprint analysis of NHS prescription data in England. *BMJ Open* **2019**, *9*, e028763, doi:10.1136/bmjopen-2018-028763.

166. Rospond, B.; Krakowska, A.; Muszyńska, B.; Opoka, W. The history, current state and perspectives of aerosol therapy. *Acta Pharmaceutica* **2022**, *72*, 225-243, doi:10.2478/acph-2022-0017.

167. Gaul, R.; Ramsey, J.M.; Heise, A.; Cryan, S.-A.; Greene, C.M. Chapter 6 - Nanotechnology approaches to pulmonary drug delivery. In *Design of Nanostructures for Versatile Therapeutic Applications*, 2018; 10.1016/b978-0-12-813667-6.00006-1pp. 221-253.

168. Thomas, B.; Pugalenthi, A. Currently available inhaled therapies in asthma and advances in drug delivery and devices. *Indian Journal of Pediatrics* **2022**, *89*, 387-394, doi:10.1007/s12098-021-03976-2.

169. Khairnar, S.V.; Jain, D.D.; Tambe, S.M.; Chavan, Y.R.; Amin, P.D. Nebulizer systems: A new frontier for therapeutics and targeted delivery. *Therapeutic Delivery* **2022**, *13*, 31-49, doi:10.4155/tde-2021-0070.

170. McCarthy, S.D.; Gonzalez, H.E.; Higgins, B.D. Future trends in nebulized therapies for pulmonary disease. *Journal of Personalized Medicine* **2020**, *10*, doi:10.3390/jpm10020037.

171. Coste, G. Les techniques d'aérosolthérapie par nébulisation. *Actualités Pharmaceutiques* **2019**, *58*, 49-53, doi:10.1016/j.actpha.2018.12.012.

172. Cataldo, D.; Hanon, S.; Peché, R.V.; Schuermans, D.J.; Degryse, J.M.; De Wulf, I.A.; Elinck, K.; Leys, M.H.; Rummens, P.L.; Derom, E. How to choose the right inhaler using a patient-centric approach? *Advances in Therapy* **2022**, *39*, 1149-1163, doi:10.1007/s12325-021-02034-9.

173. Iwanaga, T.; Tohda, Y.; Nakamura, S.; Suga, Y. The Respimat® soft mist inhaler: Implications of drug delivery characteristics for patients. *Clinical Drug Investigation* **2019**, *39*, 1021-1030, doi:10.1007/s40261-019-00835-z.

174. Dalby, R.N.; Eicher, J.; Zierenberg, B. Development of Respimat® Soft Mist™ Inhaler and its clinical utility in respiratory disorders. *Medical Devices: Evidence and Research* **2011**, *4*, 145-155, doi:10.2147/MDER.S7409.

175. Kilfeather, S.A.; Ponitz, H.H.; Beck, E.; Schmidt, P.; Lee, A.; Bowen, I.; Hesse, C. Improved delivery of ipratropium bromide/fenoterol from Respimat® Soft Mist Inhaler in patients with COPD. *Respiratory Medicine* **2004**, *98*, 387-397, doi:10.1016/j.rmed.2003.12.007.

176. Taube, C.; Bayer, V.; Zehendner, C.M.; Valipour, A. Assessment of patient experiences with Respimat® in everyday clinical practice. *Pulmonary Therapy* **2020**, *6*, 371-380, doi:10.1007/s41030-020-00127-4.

177. Hochrainer, D.; Holz, H.; Kreher, C.; Scaffidi, L.; Spallek, M.; Wachtel, H. Comparison of the aerosol velocity and spray duration of Respimat Soft Mist inhaler and pressurized metered dose inhalers. *Journal of Aerosol Medicine* **2005**, *18*, 273-282, doi:10.1089/jam.2005.18.273.

178. Wachtel, H.; Kattenbeck, S.; Dunne, S.; Disse, B. The Respimat® development story: Patient-centered innovation. *Pulmonary Therapy* **2017**, *3*, 19-30, doi:10.1007/s41030-017-0040-8.

179. Velaga, S.P.; Djuris, J.; Cvijic, S.; Rozou, S.; Russo, P.; Colombo, G.; Rossi, A. Dry powder inhalers: An overview of the *in vitro* dissolution methodologies and their correlation with the biopharmaceutical aspects of the drug products. *European Journal of Pharmaceutical Sciences* **2018**, *113*, 18-28, doi:10.1016/j.ejps.2017.09.002.

180. Ince, L.M.; Pariollaud, M.; Gibbs, J.E. Lung physiology and defense. *Current Opinion in Physiology* **2018**, *5*, 9-15, doi:10.1016/j.cophys.2018.04.005.

181. Klein, W.; Codd, J.R. Breathing and locomotion: Comparative anatomy, morphology and function. *Respiratory Physiology & Neurobiology* **2010**, *173 Suppl*, S26-32, doi:10.1016/j.resp.2010.04.019.

182. Lynch, H.N.; Goodman, J.E.; Bachman, A.N. Lung physiology and controlled exposure study design. *Journal of Pharmacological and Toxicological Methods* **2021**, *112*, 107106, doi:10.1016/j.vascn.2021.107106.

183. Steelant, B.; Seys, S.F.; Boeckxstaens, G.; Akdis, C.A.; Ceuppens, J.L.; Hellings, P.W. Restoring airway epithelial barrier dysfunction: A new therapeutic challenge in allergic airway disease. *Rhinology* **2016**, *54*, 195-205, doi:10.4193/Rhino15.376.

184. Meldrum, O.W.; Chotirmall, S.H. Mucus, microbiomes and pulmonary disease. *Biomedicines* **2021**, *9*, doi:10.3390/biomedicines9060675.

185. Newman, S.P. Drug delivery to the lungs: Challenges and opportunities. *Therapeutic Delivery* **2017**, *8*, 647-661, doi:10.4155/tde-2017-0037.

186. Mercer, P.F.; Abbott-Banner, K.; Adcock, I.M.; Knowles, R.G. Translational models of lung disease. *Clin Sci (Lond)* **2015**, *128*, 235-256, doi:10.1042/CS20140373.

187. European Comission. Directive 2010/63/EU of the European Parliament and of the Council of 22 September 2010 on the protection of animals used for scientific purposes. Official Journal of the European Union: 2010.

188. Arnesdotter, E.; Rogiers, V.; Vanhaecke, T.; Vinken, M. An overview of current practices for regulatory risk assessment with lessons learnt from cosmetics in the European Union. *Critical Reviews in Toxicology* **2021**, *51*, 395-417, doi:10.1080/10408444.2021.1931027.

189. PennCentury™. Dry Powder Insufflator™ for Mouse. Availabe online: https://penncentury.com/products/dry-powder-devices/dry-powder-insufflator-dp-4m/model-dp-4m/ (accessed on 17/08/2022).

190. Sung, J.C.; Padilla, D.J.; Garcia-Contreras, L.; Verberkmoes, J.L.; Durbin, D.; Peloquin, C.A.; Elbert, K.J.; Hickey, A.J.; Edwards, D.A. Formulation and pharmacokinetics of self-assembled rifampicin nanoparticle systems for pulmonary delivery. *Pharmaceutical Research* **2009**, *26*, 1847-1855, doi:10.1007/s11095-009-9894-2.

191. Roa, W.H.; Azarmi, S.; Al-Hallak, M.H.D.K.; Finlay, W.H.; Magliocco, A.M.; Lobenberg, R. Inhalable nanoparticles, a non-invasive approach to treat lung cancer in a mouse model. *Journal of Controlled Release* **2011**, *150*, 49-55, doi:10.1016/j.jconrel.2010.10.035.

192. Cingolani, E.; Alqahtani, S.; Sadler, R.C.; Prime, D.; Stolnik, S.; Bosquillon, C. *In vitro* investigation on the impact of airway mucus on drug dissolution and absorption at the air-epithelium interface in the lungs. *European Journal of Pharmaceutics and Biopharmaceutics* **2019**, *141*, 210-220, doi:10.1016/j.ejpb.2019.05.022.

193. Cunha, L.; Rodrigues, S.; Rosa da Costa, A.M.; Faleiro, L.; Buttini, F.; Grenha, A. Inhalable chitosan microparticles for simultaneous delivery of isoniazid and rifabutin in lung tuberculosis treatment. *Drug Development and Industrial Pharmacy* **2019**, *45*, 1313-1320, doi:10.1080/03639045.2019.1608231.

194. Gumaste, A.; Fleming, S.; Chan, P. Patent WO 2011/003022 A1: Laboratory Animal Pulmonary Dosing Device. 2010.

195. Pharma, A. PADA: Powder Administration Device for Animals. Availabe online: https://www.aptar.com/products/pharmaceutical/pada-starter-kit-for-pre-clinical-pulmonary-research-in-mice/ (accessed on August 15th, 2022).

196. Gaspar, D.P.; Gaspar, M.M.; Eleutério, C.V.; Grenha, A.; Blanco, M.; Goncalves, L.M.D.; Taboada, P.; Almeida, A.J.; Remuñán-Lopez, C.

Microencapsulated solid lipid nanoparticles as a hybrid platform for pulmonary antibiotic delivery. *Molecular Pharmaceutics* **2017**, *14*, 2977-2990, doi:10.1021/acs.molpharmaceut.7b00169.

197. Tonnis, W.F.; Bagerman, M.; Weij, M.; Sjollema, J.; Frijlink, H.W.; Hinrichs, W.L.J.; de Boer, A.H. A novel aerosol generator for homogenous distribution of powder over the lungs after pulmonary administration to small laboratory animals. *European Journal of Pharmaceutics and Biopharmaceutics* **2014**, *88*, 1056-1063, doi:10.1016/j.ejpb.2014.10.011.

198. Cidem, A.; Bradbury, P.; Traini, D.; Ong, H.X. Modifying and integrating *in vitro* and *ex vivo* respiratory models for inhalation drug screening. *Frontiers in Bioengineering and Biotechnology* **2020**, *8*, 581995, doi:10.3389/fbioe.2020.581995.

199. Viana, F.; O'Kane, C.M.; Schroeder, G.N. Precision-cut lung slices: A powerful *ex vivo* model to investigate respiratory infectious diseases. *Molecular Microbiology* **2022**, *117*, 578-588, doi:10.1111/mmi.14817.

200. Dimou, P.; Trivedi, S.; Liousia, M.; D'Souza, R.R.; Klampatsa, A. Precision-cut tumor slices (PCTS) as an *ex vivo* model in immunotherapy research. *Antibodies* **2022**, *11*, doi:10.3390/antib11020026.

201. Liu, G.; Betts, C.; Cunoosamy, D.M.; Åberg, P.M.; Hornberg, J.J.; Sivars, K.B.; Cohen, T.S. Use of precision cut lung slices as a translational model for the study of lung biology. *Respiratory Research* **2019**, *20*, 162, doi:10.1186/s12931-019-1131-x.

202. Schremmer, C.; Steinritz, D.; Gudermann, T.; Beech, D.J.; Dietrich, A. An *ex vivo* perfused ventilated murine lung model suggests lack of acute pulmonary toxicity of the potential novel anticancer agent (-)-englerin A. *Archives of Toxicology* **2022**, *96*, 1055-1063, doi:10.1007/s00204-022-03235-z.

203. Baldassi, D.; Gabold, B.; Merkel, O. Air-liquid interface cultures of the healthy and diseased human respiratory tract: Promises, challenges and future directions. *Advanced NanoBiomed Research* **2021**, *1*, doi:10.1002/anbr.202000111.

204. Tang, X.-Y.; Wu, S.; Wang, D.; Chu, C.; Hong, Y.; Tao, M.; Hu, H.; Xu, M.; Guo, X.; Liu, Y. Human organoids in basic research and clinical applications. *Signal Transduction and Targeted Therapy* **2022**, *7*, 168, doi:10.1038/s41392-022-01024-9.

205. Baptista, D.; Moreira Teixeira, L.; Barata, D.; Tahmasebi Birgani, Z.; King, J.; van Riet, S.; Pasman, T.; Poot, A.A.; Stamatialis, D.; Rottier, R.J., et al. 3D lung-on-chip model based on biomimetically microcurved culture membranes. *ACS Biomaterials Science & Engineering* **2022**, *8*, 2684-2699, doi:10.1021/acsbiomaterials.1c01463.

206. Haghi, M.; Traini, D.; Bebawy, M.; Young, P.M. Deposition, diffusion and transport mechanism of dry powder microparticulate salbutamol, at the

respiratory epithelia. *Molecular Pharmaceutics* **2012**, *9*, 1717-1726, doi:10.1021/mp200620m.

207. Guénette, J.; Breznan, D.; Thomson, E.M. Establishing an air-liquid interface exposure system for exposure of lung cells to gases. *Inhalation Toxicology* **2022**, *34*, 80-89, doi:10.1080/08958378.2022.2039332.

208. Jung, D.J.; Shin, T.H.; Kim, M.; Sung, C.O.; Jang, S.J.; Jeong, G.S. A one-stop microfluidic-based lung cancer organoid culture platform for testing drug sensitivity. *Lab on a Chip* **2019**, *19*, 2854-2865, doi:10.1039/c9lc00496c.

209. Campillo, N.; Oliveira, V.R.; da Palma, R.K. Alveolus lung-on-a-chip platform: A proposal. *Chemosensors* **2021**, *9*, doi:10.3390/chemosensors9090248.

210. Hein, S.; Bur, M.; Kolb, T.; Muellinger, B.; Schaefer, U.F.; Lehr, C.-M. The Pharmaceutical Aerosol Deposition Device on Cell Cultures (PADDOCC) *in vitro* system: Design and experimental protocol. *Alternatives to Laboratory Animals* **2010**, *38*, 285-295, doi:10.1177/026119291003800408.

211. Hein, S.; Bur, M.; Schaefer, U.F.; Lehr, C.-M. A new Pharmaceutical Aerosol Deposition Device on Cell Cultures (PADDOCC) to evaluate pulmonary drug absorption for metered dose dry powder formulations. *European Journal of Pharmaceutics and Biopharmaceutics* **2011**, *77*, 132-138, doi:10.1016/j.ejpb.2010.10.003.

212. Paur, H.-R.; Waescher, T.; Muelhopt, S. Patent WO 2008/116540 A1: Device for Measuring Superfine Particle Masses. 2008.

213. Lim, H.J.; Saha, T.; Tey, B.T.; Tan, W.S.; Ooi, C.W. Quartz crystal microbalance-based biosensors as rapid diagnostic devices for infectious diseases. *Biosensors and Bioelectronics* **2020**, *168*, 112513, doi:10.1016/j.bios.2020.112513.

214. Jandas, P.J.; Prabakaran, K.; Luo, J.; Holaday M. G., D. Effective utilization of quartz crystal microbalance as a tool for biosensing applications. *Sensors and Actuators A: Physical* **2021**, *331*, doi:10.1016/j.sna.2021.113020.

215. Lenz, A.G.; Karg, E.; Lentner, B.; Dittrich, V.; Brandenberger, C.; Rothen-Rutishauser, B.; Schulz, H.; Ferron, G.A.; Schmid, O. A dose-controlled system for air-liquid interface cell exposure and application to zinc oxide nanoparticles. *Particle and Fibre Toxicology* **2009**, *6*, 32, doi:10.1186/1743-8977-6-32.

216. Mülhopt, S.; Diabaté, S.; Krebs, T.; Weiss, C.; Paur, H.R. Lung toxicity determination by *in vitro* exposure at the air liquid interface with an integrated online dose measurement. *Journal of Physics: Conference Series* **2009**, *170*, doi:10.1088/1742-6596/170/1/012008.

217. Metz, J.; Knoth, K.; Groß, H.; Lehr, C.-M.; Stäbler, C.; Bock, U.; Hittinger, M. Combining MucilAir™ and Vitrocell® Powder Chamber for the *in vitro*

evaluation of nasal ointments in the context of aerosolized pollen. *Pharmaceutics* **2018**, *10*, doi:10.3390/pharmaceutics10020056.

218. Asai, A.; Okuda, T.; Yamauchi, T.; Sugiura, Y.; Okamoto, H. Safety evaluation of dry powder formulations by direct dispersion onto air-liquid interface cultured cell layer. *Biological & Pharmaceutical Bulletin* **2016**, *39*, 368-377, doi:10.1248/bpb.b15-00791.

219. Alves, A.D.; Cavaco, J.S.; Guerreiro, F.; Lourenco, J.P.; Rosa da Costa, A.M.; Grenha, A. Inhalable antitubercular therapy mediated by locust bean gum microparticles. *Molecules* **2016**, *21*, 702, doi:10.3390/molecules21060702.

220. Rodrigues, S.; Alves, A.D.; Cavaco, J.S.; Pontes, J.F.; Guerreiro, F.; Rosa da Costa, A.M.; Buttini, F.; Grenha, A. Dual antibiotherapy of tuberculosis mediated by inhalable locust bean gum microparticles. *International Journal of Pharmaceutics* **2017**, *529*, 433-441, doi:10.1016/j.ijpharm.2017.06.088.

221. Cunha, L.; Rodrigues, S.; Rosa da Costa, A.M.; Faleiro, M.L.; Buttini, F.; Grenha, A. Inhalable fucoidan microparticles combining two antitubercular drugs with potential application in pulmonary tuberculosis therapy. *Polymers* **2018**, *10*, 636, doi:10.3390/polym10060636.

222. Hoppentocht, M.; Hoste, C.; Hagedoorn, P.; Frijlink, H.W.; de Boer, A.H. *In vitro* evaluation of the DP-4M PennCentury™ insufflator. *European Journal of Pharmaceutics and Biopharmaceutics* **2014**, *88*, 153-159, doi:10.1016/j.ejpb.2014.06.014.

223. Chaurasiya, B.; Zhou, M.; Tu, J.; Sun, C. Design and validation of a simple device for insufflation of dry powders in a mice model. *European Journal of Pharmaceutical Sciences* **2018**, *123*, 495-501, doi:10.1016/j.ejps.2018.08.010.

224. Ebi, K.L.; Frumkin, H.; Hess, J.J. Protecting and promoting population health in the context of climate and other global environmental changes. *Anthropocene* **2017**, *19*, 1-12, doi:10.1016/j.ancene.2017.07.001.

225. Tellier, R.; Li, Y.; Cowling, B.J.; Tang, J.W. Recognition of aerosol transmission of infectious agents: A commentary. *BMC Infectious Diseases* **2019**, *19*, 101, doi:10.1186/s12879-019-3707-y.

226. Manibusan, S.; Mainelis, G. Passive bioaerosol samplers: A complementary tool for bioaerosol research. A review. *Journal of Aerosol Science* **2022**, *163*, doi:10.1016/j.jaerosci.2022.105992.

227. Nair, A.N.; Anand, P.; George, A.; Mondal, N. A review of strategies and their effectiveness in reducing indoor airborne transmission and improving indoor air quality. *Environmental Research* **2022**, *213*, 113579, doi:10.1016/j.envres.2022.113579.

228. Richards, F.; Kodjamanova, P.; Chen, X.; Li, N.; Atanasov, P.; Bennetts, L.; Patterson, B.J.; Yektashenas, B.; Mesa-Frias, M.; Tronczynski, K., et al.

Economic burden of COVID-19: A systematic review. *ClinicoEconomics and Outcomes Research* **2022**, *14*, 293-307, doi:10.2147/CEOR.S338225.

229. Sokhi, R.S.; Moussiopoulos, N.; Baklanov, A.; Bartzis, J.; Coll, I.; Finardi, S.; Friedrich, R.; Geels, C.; Grönholm, T.; Halenka, T., et al. Advances in air quality research – Current and emerging challenges. *Atmospheric Chemistry and Physics* **2022**, *22*, 4615-4703, doi:10.5194/acp-22-4615-2022.

230. Meghji, J.; Mortimer, K.; Agusti, A.; Allwood, B.W.; Asher, I.; Bateman, E.D.; Bissell, K.; Bolton, C.E.; Bush, A.; Celli, B., et al. Improving lung health in low-income and middle-income countries: from challenges to solutions. *The Lancet* **2021**, *397*, 928-940, doi:10.1016/s0140-6736(21)00458-x.

231. Schneider, J.P.; Hegermann, J.; Wrede, C. Volume electron microscopy: Analyzing the lung. *Histochemistry and Cell Biology* **2021**, *155*, 241-260, doi:10.1007/s00418-020-01916-3.

232. Whittington, R.; Regnér, P.; Angwin, D.; Johnson, G.; Scholes, K. Chapter 4 - Resources and Capabilities Analysis. In *Exploring Strategy (Text and Cases)*, 12th ed.; Pearson Education Limited: United Kingdom, 2020.

233. Scholten, W.; Franssen, T.P.; van Drooge, L.; de Rijcke, S.; Hessels, L.K. Funding for few, anticipation among all: Effects of excellence funding on academic research groups. *Science and Public Policy* **2021**, *48*, 265-275, doi:10.1093/scipol/scab018.

234. Rahman, J.; Quodbach, J. Versatility on demand - The case for semi-solid micro-extrusion in pharmaceutics. *Advanced Drug Delivery Reviews* **2021**, *172*, 104-126, doi:10.1016/j.addr.2021.02.013.

235. Charan, G.R.S.; Haque, M.A.; Mohanty, D.; Bakshi, V. Review on recent advances in drug development by using 3D printing technology. *Pharmaceutical Chemistry Journal* **2022**, *56*, 270-276, doi:10.1007/s11094-022-02630-1.

236. Food and Drug Administration (FDA). Inactive Ingredients Database. Availabe online: https://www.fda.gov/drugs/drug-approvals-and-databases/inactive-ingredients-database-download (accessed on August 20th, 2022).

237. Meunier, L.; Garthoff, J.A.; Schaafsma, A.; Krul, L.; Schrijver, J.; van Goudoever, J.B.; Speijers, G.; Vandenplas, Y. Locust bean gum safety in neonates and young infants: An integrated review of the toxicological database and clinical evidence. *Regulatory Toxicology and Pharmacology* **2014**, *70*, 155-169, doi:10.1016/j.yrtph.2014.06.023.

238. Yadav, H.; Maiti, S. Research progress in galactomannan-based nanomaterials: Synthesis and application. *International Journal of Biological Macromolecules* **2020**, *163*, 2113-2126, doi:10.1016/j.ijbiomac.2020.09.062.

239. García-Ochoa, F.; Casas, J.A. Viscosity of locust bean (*Ceratonia siliqua*) gum solutions. *Journal of the Science of Food and Agriculture* **1992**, *59*, 97-100, doi:10.1002/jsfa.2740590114.

240. Prajapati, V.D.; Jani, G.K.; Moradiya, N.G.; Randeria, N.P.; Nagar, B.J. Locust bean gum: A versatile biopolymer. *Carbohydrate Polymers* **2013**, *94*, 814-821, doi:10.1016/j.carbpol.2013.01.086.

241. Braz, L.; Grenha, A.; Corvo, M.C.; Lourenco, J.P.; Ferreira, D.; Sarmento, B.; Rosa da Costa, A.M. Synthesis and characterization of locust bean gum derivatives and their application in the production of nanoparticles. *Carbohydrate Polymers* **2018**, *181*, 974-985, doi:10.1016/j.carbpol.2017.11.052.

242. Lipinski, C.A.; Lombardo, F.; Dominy, B.W.; Feeney, P.J. Experimental and computational approaches to estimate solubility and permeability in drug discovery and development settings. *Advanced Drug Delivery Reviews* **2001**, *46*, 3-26, doi:10.1016/s0169-409x(00)00129-0.

243. Lipinski, C.A. Lead- and drug-like compounds: The rule-of-five revolution. *Drug Discovery Today: Technologies* **2004**, *1*, 337-341, doi:10.1016/j.ddtec.2004.11.007.

244. Amidon, G.L.; Lennernäs, H.; Shah, V.P.; Crison, J.R. A theoretical basis for a biopharmaceutic drug classification: The correlation of *in vitro* drug product dissolution and *in vivo* bioavailability. *Pharmaceutical Research* **1995**, *12*, 413-420, doi:10.1023/A:1016212804288.

245. Braz, L.; Grenha, A.; Ferreira, D.; Rosa da Costa, A.M.; Gamazo, C.; Sarmento, B. Chitosan/sulfated locust bean gum nanoparticles: *In vitro* and *in vivo* evaluation towards an application in oral immunization. *International Journal of Biological Macromolecules* **2017**, *96*, 786-797, doi:10.1016/j.ijbiomac.2016.12.076.

246. Lollo, G.; Hervella, P.; Calvo, P.; Aviles, P.; Guillen, M.J.; Garcia-Fuentes, M.; Alonso, M.J.; Torres, D. Enhanced *in vivo* therapeutic efficacy of plitidepsin-loaded nanocapsules decorated with a new poly-aminoacid-PEG derivative. *International Journal of Pharmaceutics* **2015**, *483*, 212-219, doi:10.1016/j.ijpharm.2015.02.028.

247. Lollo, G.; Gonzalez-Paredes, A.; Garcia-Fuentes, M.; Calvo, P.; Torres, D.; Alonso, M.J. Polyarginine nanocapsules as a potential oral peptide delivery carrier. *Journal of Pharmaceutical Sciences* **2017**, *106*, 611-618, doi:10.1016/j.xphs.2016.09.029.

248. Rosso, A.; Lollo, G.; Chevalier, Y.; Troung, N.; Bordes, C.; Bourgeois, S.; Maniti, O.; Granjon, T.; Dugas, P.-Y.; Urbaniak, S., et al. Development and structural characterization of a novel nanoemulsion for oral drug delivery. *Colloids and Surfaces A: Physicochemical and Engineering Aspects* **2020**, 10.1016/j.colsurfa.2020.124614, doi:10.1016/j.colsurfa.2020.124614.

249. Schick, C. Differential scanning calorimetry (DSC) of semicrystalline polymers. *Analytical and Bioanalytical Chemistry* **2009**, *395*, 1589-1611, doi:10.1007/s00216-009-3169-y.

250. Saadatkhah, N.; Carillo Garcia, A.; Ackermann, S.; Leclerc, P.; Latifi, M.; Samih, S.; Patience, G.S.; Chaouki, J. Experimental methods in chemical engineering: Thermogravimetric analysis - TGA. *The Canadian Journal of Chemical Engineering* **2019**, *98*, 34-43, doi:10.1002/cjce.23673.

251. de Paula Rigoletto, T.; Silva, C.L.; Santana, M.H.A.; Rosada, R.S.; de la Torre, L.G. Effects of extrusion, lipid concentration and purity on physico-chemical and biological properties of cationic liposomes for gene vaccine applications. *Journal of Microencapsulation* **2012**, *29*, 759-769, doi:10.3109/02652048.2012.686530.

252. Upadhyay, T.K.; Fatima, N.; Sharma, D.; Saravanakumar, V.; Sharma, R. Preparation and characterization of beta-glucan particles containing a payload of nanoembedded rifabutin for enhanced targeted delivery to macrophages. *EXCLI Journal* **2017**, *16*, 210-228, doi:10.17179/excli2016-804.

253. Gaspar, D.P.; Faria, V.; Gonçalves, L.M.D.; Taboada, P.; Remuñán-López, C.; Almeida, A.J. Rifabutin-loaded solid lipid nanoparticles for inhaled antitubercular therapy: Physicochemical and *in vitro* studies. *International Journal of Pharmaceutics* **2016**, *497*, 199-209, doi:10.1016/j.ijpharm.2015.11.050.

254. Kumar, M.; Bishnoi, R.S.; Shukla, A.K.; Jain, C.P. Development and optimization of drug-loaded nanoemulsion system by phase inversion temperature (PIT) method using Box-Behnken design. *Drug Development and Industrial Pharmacy* **2021**, *47*, 977-989, doi:10.1080/03639045.2021.1957920.

255. Weerapol, Y.; Manmuan, S.; Chaothanaphat, N.; Limmatvapirat, S.; Sirirak, J.; Tamdee, P.; Tubtimsri, S. New approach for preparing solid lipid nanoparticles with volatile oil-loaded quercetin using the phase-inversion temperature method. *Pharmaceutics* **2022**, *14*, doi:10.3390/pharmaceutics14101984.

256. Kuntsche, J.; Horst, J.C.; Bunjes, H. Cryogenic transmission electron microscopy (cryo-TEM) for studying the morphology of colloidal drug delivery systems. *International Journal of Pharmaceutics* **2011**, *417*, 120-137, doi:10.1016/j.ijpharm.2011.02.001.

257. Guerreiro, F.; Pontes, J.F.; Rosa da Costa, A.M.; Grenha, A. Spray-drying of konjac glucomannan to produce microparticles for an application as antitubercular drug carriers. *Powder Technology* **2019**, *342*, 246-252, doi:10.1016/j.powtec.2018.09.068.

258. Littringer, E.M.; Noisternig, M.F.; Mescher, A.; Schroettner, H.; Walzel, P.; Griesser, U.J.; Urbanetz, N.A. The morphology and various densities of spray dried mannitol. *Powder Technology* **2013**, *246*, 193-200, doi:10.1016/j.powtec.2013.05.004.

259. Cunha, L.; Rosa da Costa, A.M.; Lourenco, J.P.; Buttini, F.; Grenha, A. Spray-dried fucoidan microparticles for pulmonary delivery of antitubercular drugs.

Journal of Microencapsulation **2018**, *35*, 392-405, doi:10.1080/02652048.2018.1513089.

260. Guerreiro, F.; Swedrowska, M.; Patel, R.; Flórez-Fernández, N.; Dolores Torres, M.; Rosa da Costa, A.M.; Forbes, B.; Grenha, A. Engineering of konjac glucomannan into respirable microparticles for delivery of antitubercular drugs. *International Journal of Pharmaceutics* **2021**, 10.1016/j.ijpharm.2021.120731, 120731, doi:10.1016/j.ijpharm.2021.120731.

261. Zhang, G.; Maladen, M.D.; Hamaker, B.R. Detection of a novel three component complex consisting of starch, protein, and free fatty acids. *Journal of Agricultural and Food Chemistry* **2003**, *51*, 2801-2805, doi:10.1021/jf030035t.

262. Gómez-Ordóñez, E.; Jiménez-Escrig, A.; Rupérez, P. Molecular weight distribution of polysaccharides from edible seaweeds by high-performance size-exclusion chromatography (HPSEC). *Talanta* **2012**, *93*, 153-159, doi:10.1016/j.talanta.2012.01.067.

263. Zhou, Q.; Cabaniss, S.E.; Maurice, P.A. Considerations in the use of high-pressure size exclusion chromatography (HPSEC) for determining molecular weights of aquatic humic substances. *Water Research* **2000**, *34*, 3505-3514, doi:10.1016/s0043-1354(00)00115-9.

264. Lopes da Silva, J.A.; Gonçalves, M.P. Studies on a purification method for locust bean gum by precipitation with isopropanol. *Food Hydrocolloids* **1990**, *4*, 277-287, doi:10.1016/s0268-005x(09)80204-x.

265. Vehring, R. Pharmaceutical particle engineering *via* spray drying. *Pharmaceutical Research* **2008**, *25*, 999-1022, doi:10.1007/s11095-007-9475-1.

266. Ordoubadi, M.; Gregson, F.K.A.; Wang, H.; Nicholas, M.; Gracin, S.; Lechuga-Ballesteros, D.; Reid, J.P.; Finlay, W.H.; Vehring, R. On the particle formation of leucine in spray drying of inhalable microparticles. *International Journal of Pharmaceutics* **2020**, 10.1016/j.ijpharm.2020.120102, 120102, doi:10.1016/j.ijpharm.2020.120102.

267. Maas, S.G.; Schaldach, G.; Littringer, E.M.; Mescher, A.; Griesser, U.J.; Braun, D.E.; Walzel, P.E.; Urbanetz, N.A. The impact of spray drying outlet temperature on the particle morphology of mannitol. *Powder Technology* **2011**, *213*, 27-35, doi:10.1016/j.powtec.2011.06.024.

268. Lozinsky, V.I.; Damshkaln, L.G.; Brown, R.; Norton, I.T. Study of cryostructuring of polymer systems. XIX. On the nature of intermolecular links in the cryogels of locust bean gum. *Polymer International* **2000**, *49*, 1434-1443, doi:10.1002/1097-0126(200011)49:11%3C1434::AID-PI525%3E3.0.CO;2-F.

269. Kaity, S.; Isaac, J.; Kumar, P.M.; Bose, A.; Wong, T.W.; Ghosh, A. Microwave assisted synthesis of acrylamide grafted locust bean gum and its application

in drug delivery. *Carbohydrate Polymers* **2013**, *98*, 1083-1094, doi:10.1016/j.carbpol.2013.07.037.

270. Kaity, S.; Isaac, J.; Ghosh, A. Interpenetrating polymer network of locust bean gum-poly (vinyl alcohol) for controlled release drug delivery. *Carbohydrate Polymers* **2013**, *94*, 456-467, doi:10.1016/j.carbpol.2013.01.070.

271. Jana, S.; Sen, K.K. Chitosan - Locust bean gum interpenetrating polymeric network nanocomposites for delivery of aceclofenac. *International Journal of Biological Macromolecules* **2017**, *102*, 878-884, doi:10.1016/j.ijbiomac.2017.04.097.

272. Jian, H.-L.; Lin, X.-J.; Zhang, W.-A.; Zhang, W.-M.; Sun, D.-F.; Jiang, J.-X. Characterization of fractional precipitation behavior of galactomannan gums with ethanol and isopropanol. *Food Hydrocolloids* **2014**, *40*, 115-121, doi:10.1016/j.foodhyd.2014.02.012.

273. Kök, M.S.; Hill, S.E.; Mitchell, J.R. Viscosity of galactomannans during high temperature processing: influence of degradation and solubilisation. *Food Hydrocolloids* **1999**, *13*, 535-542, doi:10.1016/s0268-005x(99)00040-5.

274. Wu, Y.; Cui, W.; Eskin, N.A.M.; Goff, H.D. An investigation of four commercial galactomannans on their emulsion and rheological properties. *Food Research International* **2009**, *42*, 1141-1146, doi:10.1016/j.foodres.2009.05.015.

275. Pollard, M.A.; Kelly, R.; Fischer, P.A.; Windhab, E.J.; Eder, B.; Amadò, R. Investigation of molecular weight distribution of LBG galactomannan for flours prepared from individual seeds, mixtures, and commercial samples. *Food Hydrocolloids* **2008**, *22*, 1596-1606, doi:10.1016/j.foodhyd.2007.11.004.

276. Lazaridou, A.; Biliaderis, C.G.; Izydorczyk, M.S. Structural characteristics and rheological properties of locust bean galactomannans: a comparison of samples from different carob tree populations. *Journal of the Science of Food and Agriculture* **2001**, *81*, 68-75, doi:10.1002/1097-0010(20010101)81:1<68::Aid-jsfa780>3.0.Co;2-g.

277. Fagerson, I.S. Thermal degradation of carbohydrates - A review. *Journal of Agricultural and Food Chemistry* **2002**, *17*, 747-750, doi:10.1021/jf60164a019.

278. Fidan, H.; Stankov, S.; Petkova, N.; Petkova, Z.; Iliev, A.; Stoyanova, M.; Ivanova, T.; Zhelyazkov, N.; Ibrahim, S.; Stoyanova, A., et al. Evaluation of chemical composition, antioxidant potential and functional properties of carob (*Ceratonia siliqua* L.) seeds. *Journal of Food Science and Technology* **2020**, *57*, 2404-2413, doi:10.1007/s13197-020-04274-z.

279. Maier, H.; Anderson, M.; Karl, C.; Magnuson, K.; Whistler, R.L. Chapter 8 - Guar, Locust Bean, Tara, and Fenugreek Gums. In *Industrial Gums*, 1993; 10.1016/b978-0-08-092654-4.50012-7pp. 181-226.

280. Pollard, M.; Kelly, R.; Wahl, C.; Fischer, P.; Windhab, E.; Eder, B.; Amado, R. Investigation of equilibrium solubility of a carob galactomannan. *Food Hydrocolloids* **2007**, *21*, 683-692, doi:10.1016/j.foodhyd.2006.08.010.

281. Rizzo, V.; Tomaselli, F.; Gentile, A.; La Malfa, S.; Maccarone, E. Rheological properties and sugar composition of locust bean gum from different carob varieties (*Ceratonia siliqua* L.). *Journal of Agricultural and Food Chemistry* **2004**, *52*, 7925-7930, doi:10.1021/jf0494332.

282. Li, T.; Liu, R.; Zhang, C.; Meng, F.; Wang, L. Developing a green film from locust bean gum/carboxycellulose nanocrystal for fruit preservation. *Future Foods* **2021**, *4*, doi:10.1016/j.fufo.2021.100072.

283. Rogers, M.A.; Roos, Y.H.; Goff, H.D. Structural heterogeneity and its effect on the glass transition in sucrose solutions containing protein and polysaccharide. *Food Hydrocolloids* **2006**, *20*, 774-779, doi:10.1016/j.foodhyd.2005.07.006.

284. Červenka, L.; Stępień, A.; Frühbauerová, M.; Velichová, H.; Witczak, M. Thermodynamic properties and glass transition temperature of roasted and unroasted carob (*Ceratonia siliqua* L.) powder. *Food Chemistry* **2019**, *300*, 125208, doi:10.1016/j.foodchem.2019.125208.

285. International Organization for Standardization (ISO). ISO 10993-5-2009: Biological evaluation of medical devices - Part 5: Tests for *in vitro* cytotoxicity. International Organization for Standardization (ISO): Switzerland, 2009; Vol. ISO 10993-5:2009(E).

286. Van Hoecke, L.; Job, E.R.; Saelens, X.; Roose, K. Bronchoalveolar lavage of murine lungs to analyze inflammatory cell infiltration. *Journal of Visualized Experiments* **2017**, 10.3791/55398, doi:10.3791/55398.

287. Dionisio, M.; Grenha, A. Locust bean gum: Exploring its potential for biopharmaceutical applications. *Journal of Phamacy and Bioallied Sciences* **2012**, *4*, 175-185, doi:10.4103/0975-7406.99013.

288. Kawamura, Y. *Carob bean gum - Chemical and Technical Assessment*; Joint FAO/WHO Expert Committee on Food Additives: 2016.

289. Guo, H.; Ahn, S.; Zhang, L. Benzene-associated immunosuppression and chronic inflammation in humans: a systematic review. *Occupational & Environmental Medicine* **2020**, 10.1136/oemed-2020-106517, doi:10.1136/oemed-2020-106517.

290. Charles River Laboratories International. BALB/C Mouse Hematology, North American Colonies: January 2008 - December 2012. **2012**.

291. Lee, L.-Y.; Hew, G.S.Y.; Mehta, M.; Shukla, S.D.; Satija, S.; Khurana, N.; Anand, K.; Dureja, H.; Singh, S.K.; Mishra, V., et al. Targeting eosinophils in respiratory diseases: Biological axis, emerging therapeutics and treatment modalities. *Life Sciences* **2021**, *267*, doi:10.1016/j.lfs.2020.118973.

292. Ding, L.; Yang, J.; Zhang, C.; Zhang, X.; Gao, P. Neutrophils modulate fibrogenesis in chronic pulmonary diseases. *Frontiers in Medicine* **2021**, *8*, 616200, doi:10.3389/fmed.2021.616200.

293. Gilmore, N.; Mohile, S.; Lei, L.; Culakova, E.; Mohamed, M.; Magnuson, A.; Loh, K.P.; Maggiore, R.; Belcher, E.; Conlin, A., et al. The longitudinal relationship between immune cell profiles and frailty in patients with breast cancer receiving chemotherapy. *Breast Cancer Research* **2021**, *23*, 19, doi:10.1186/s13058-021-01388-w.

294. Sakai, Y.; Kobayashi, M. Lymphocyte 'homing' and chronic inflammation. *Pathology International* **2015**, *65*, 344-354, doi:10.1111/pin.12294.

295. Auffray, C.; Sieweke, M.H.; Geissmann, F. Blood monocytes: Development, heterogeneity, and relationship with dendritic cells. *Annual Review of Immunology* **2009**, *27*, 669-692, doi:10.1146/annurev.immunol.021908.132557.

296. Chen, W.-L.; Chen, H.-L.; Guo, G.-W.; Huang, Y.-C.; Chen, C.-Y.; Tsai, Y.; Huang, K.-F.; Yang, C.-H. Locust bean gum galactomannan hydrolyzed by thermostable β-D-mannanase may reduce the secretion of pro-inflammatory factors and the release of granule constituents. *International Journal of Biological Macromolecules* **2018**, *114*, 181-186, doi:10.1016/j.ijbiomac.2018.03.097.

297. Kelly, B.T.; Grayson, M.H. Immunoglobulin E, what is it good for? *Annals of Allergy, Asthma & Immunology* **2016**, *116*, 183-187, doi:10.1016/j.anai.2015.10.026.

298. Haniuda, K.; Kitamura, D. Multi-faceted regulation of IgE production and humoral memory formation. *Allergology International* **2021**, *70*, 163-168, doi:10.1016/j.alit.2020.11.002.

299. Wu, L.C.; Zarrin, A.A. The production and regulation of IgE by the immune system. *Nature Reviews Immunology* **2014**, *14*, 247-259, doi:10.1038/nri3632.

300. Hnasko, R.M. Chapter 1 - The Biochemical Properties of Antibodies and Their Fragments. In *ELISA, Methods and Protocols*, Springer: New York, 2015; 10.1007/978-1-4939-2742-5_1.

301. Patel, K.K.; Anderson, E.; Salva, P.S.; Webley, W.C. The prevalence and identity of *Chlamydia*-specific IgE in children with asthma and other chronic respiratory symptoms. *Respiratory Research* **2012**, *13*, 32, doi:10.1186/1465-9921-13-32.

302. Infuhr, D.; Crameri, R.; Lamers, R.; Achatz, G. Molecular and cellular targets of anti-IgE antibodies. *Allergy* **2005**, *60*, 977-985, doi:10.1111/j.1398-9995.2005.00832.x.

303. Nguyen, T.-H.T.; Casale, T.B. Immune modulation for treatment of allergic disease. *Immunological Reviews* **2011**, *242*, 258-271, doi:10.1111/j.1600-065X.2011.01034.x.

304. Tzankova, V.; Aluani, D.; Yordanov, Y.; Valoti, M.; Frosini, M.; Spassova, I.; Kovacheva, D.; Tzankov, B. *In vitro* toxicity evaluation of lomefloxacin-loaded

MCM-41 mesoporous silica nanoparticles. *Drug and Chemical Toxicology* **2021**, *44*, 238-249, doi:10.1080/01480545.2019.1571503.

305. Fotakis, G.; Timbrell, J.A. *In vitro* cytotoxicity assays: Comparison of LDH, neutral red, MTT and protein assay in hepatoma cell lines following exposure to cadmium chloride. *Toxicology Letters* **2006**, *160*, 171-177, doi:10.1016/j.toxlet.2005.07.001.

306. Flemming, J.; Hudson, B.; Rand, T.G. Comparison of inflammatory and cytotoxic lung responses in mice after intratracheal exposure to spores of two different *Stachybotrys chartarum* strains. *Toxicological Sciences* **2004**, *78*, 267-275, doi:10.1093/toxsci/kfh064.

307. Sunil, V.R.; Vayas, K.N.; Abramova, E.V.; Rancourt, R.; Cervelli, J.A.; Malaviya, R.; Goedken, M.; Venosa, A.; Gow, A.J.; Laskin, J.D., et al. Lung injury, oxidative stress and fibrosis in mice following exposure to nitrogen mustard. *Toxicology and Applied Pharmacology* **2020**, *387*, doi:10.1016/j.taap.2019.114798.

308. Michael, B.; Yano, B.; Sellers, R.S.; Perry, R.; Morton, D.; Roome, N.; Johnson, J.K.; Schafer, K.; Pitsch, S. Evaluation of organ weights for rodent and non-rodent toxicity studies: a review of regulatory guidelines and a survey of current practices. *Toxicologic Pathology* **2007**, *35*, 742-750, doi:10.1080/01926230701595292.

309. Sellers, R.S.; Morton, D.; Michael, B.; Roome, N.; Johnson, J.K.; Yano, B.L.; Perry, R.; Schafer, K. Society of Toxicologic Pathology Position Paper: organ weight recommendations for toxicology studies. *Toxicology Pathology* **2007**, *35*, 751-755, doi:10.1080/01926230701595300.

310. Johansson, C.; Kirsebom, F.C.M. Neutrophils in respiratory viral infections. *Mucosal Immunology* **2021**, 10.1038/s41385-021-00397-4, doi:10.1038/s41385-021-00397-4.

311. Lax, S.; Wilson, M.R.; Takata, M.; Thickett, D.R. Using a non-invasive assessment of lung injury in a murine model of acute lung injury. *BMJ Open Respiratory Research* **2014**, *1*, e000014, doi:10.1136/bmjresp-2013-000014.

312. Cho, H.-Y.; Gladwell, W.; Yamamoto, M.; Kleeberger, S.R. Exacerbated airway toxicity of environmental oxidant ozone in mice deficient in *Nrf2*. *Oxidative Medicine and Cellular Longevity* **2013**, *2013*, 254069, doi:10.1155/2013/254069.

313. Saggiomo, V. A 3D printer in the lab: Not only a toy. *Advanced Science* **2022**, 10.1002/advs.202202610, e2202610, doi:10.1002/advs.202202610.

314. Andreadis, I.I.; Gioumouxouzis, C.I.; Eleftheriadis, G.K.; Fatouros, D.G. The advent of a new era in digital healthcare: A role for 3D printing technologies in drug manufacturing? *Pharmaceutics* **2022**, *14*, doi:10.3390/pharmaceutics14030609.

315. Su, M.; Song, Y. Printable smart materials and devices: Strategies and applications. *Chemical Reviews* **2022**, *122*, 5144-5164, doi:10.1021/acs.chemrev.1c00303.

316. Ambrosi, A.; Bonanni, A. How 3D printing can boost advances in analytical and bioanalytical chemistry. *Microchimica Acta* **2021**, *188*, 265, doi:10.1007/s00604-021-04901-2.

317. Borandeh, S.; van Bochove, B.; Teotia, A.; Seppälä, J. Polymeric drug delivery systems by additive manufacturing. *Advanced Drug Delivery Reviews* **2021**, *173*, 349-373, doi:10.1016/j.addr.2021.03.022.

318. Huang, J.; Qin, Q.; Wang, J. A review of stereolithography: Processes and systems. *Processes* **2020**, *8*, doi:10.3390/pr8091138.

319. Ford, S.; Despeisse, M. Additive manufacturing and sustainability: An exploratory study of the advantages and challenges. *Journal of Cleaner Production* **2016**, *137*, 1573-1587, doi:10.1016/j.jclepro.2016.04.150.

320. Haque, S.; Md, S.; Whittaker, M.; Kaminskas, L.M. The applications of 3D printing in pulmonary drug delivery and treatment of respiratory disorders. *Current Pharmaceutical Design* **2018**, *24*, 5072-5080, doi:10.2174/1381612825666181206123414.

321. Peterman, E.L.; Kolewe, E.L.; Fromen, C.A. Evaluating regional pulmonary deposition using patient-specific 3D printed lung models. *Journal of Visualized Experiments* **2020**, 10.3791/61706, doi:10.3791/61706.

322. Barreiro Carpio, M.; Dabaghi, M.; Ungureanu, J.; Kolb, M.R.; Hirota, J.A.; Moran-Mirabal, J.M. 3D bioprinting strategies, challenges, and opportunities to model the lung tissue microenvironment and its function. *Frontiers in Bioengineering and Biotechnology* **2021**, *9*, 773511, doi:10.3389/fbioe.2021.773511.

323. Mirsaeidi, M.; Motahari, H.; Taghizadeh Khamesi, M.; Sharifi, A.; Campos, M.; Schraufnagel, D.E. Climate change and respiratory infections. *Annals of the American Thoracic Society* **2016**, *13*, 1223-1230, doi:10.1513/AnnalsATS.201511-729PS.

324. Singh, G.; Tang, P.; Cheng, S.; Chan, H.-K.; Kourmatzis, A. From laminar to turbulent flow in a dry powder inhaler: The effect of simple design modifications. *International Journal of Pharmaceutics* **2022**, *616*, 121556, doi:10.1016/j.ijpharm.2022.121556.

325. Afkhami, M.; Hassanpour, A.; Fairweather, M. Effect of Reynolds number on particle interaction and agglomeration in turbulent channel flow. *Powder Technology* **2019**, *343*, 908-920, doi:10.1016/j.powtec.2018.11.041.

326. Jiménez, M.; Romero, L.; Domínguez, I.A.; Espinosa, M.d.M.; Domínguez, M. Additive manufacturing technologies: An overview about 3D printing methods and future prospects. *Complexity* **2019**, *2019*, 1-30, doi:10.1155/2019/9656938.

327. Rodrigues, S.; Cunha, L.; Rico, J.; Rosa da Costa, A.M.; Almeida, A.J.; Faleiro, M.L.; Buttini, F.; Grenha, A. Carrageenan from red algae: An application in the development of inhalable tuberculosis therapy targeting the macrophages. *Drug Delivery and Translational Research* **2020**, *10*, 1675-1687, doi:10.1007/s13346-020-00799-0.

328. Guerreiro, F. Spray-dried polysaccharide microparticles aimed at pulmonary delivery of antitubercular drugs. Master thesis, Universidade do Algarve, Portugal, 2015.

329. Musacchio, F.; Grenha, A. Dextran sulfate microparticles encapsulating isoniazid and/or rifabutin as carriers for pulmonary tuberculosis therapy. *Journal of Aerosol Medicine and Pulmonary Drug Delivery* **2017**, *30*, A20, doi:10.1089/jamp.2017.ab02.abstracts.

330. Shih, C.-H.; Lin, Y.-J.; Lee, K.-F.; Chien, P.-Y.; Drake, P. Real-time electronic nose based pathogen detection for respiratory intensive care patients. *Sensors and Actuators B: Chemical* **2010**, *148*, 153-157, doi:10.1016/j.snb.2010.04.025.

331. Lukman Hekiem, N.L.; Md Ralib, A.A.; Mat Hattar, M.A.b.; B. Ahmad, F.; Nordin, A.N.; Rahim, R.A.; Za'bah, N.F. Advanced vapour sensing materials: Existing and latent to acoustic wave sensors for VOCs detection as the potential exhaled breath biomarkers for lung cancer. *Sensors and Actuators A: Physical* **2021**, *329*, doi:10.1016/j.sna.2021.112792.

332. Curie, J.; Curie, P. Développement par compression de l'électricité polaire dans les cristaux hémièdres à faces inclinées. *Comptes Rendus de l'Académie des Sciences de Paris* **1880**, *3*, 90-93, doi:10.3406/bulmi.1880.1564.

333. Roshani, M.M.; Rostaminikoo, E.; Joonaki, E.; Mirzaalian Dastjerdi, A.; Najafi, B.; Taghikhani, V.; Hassanpouryouzband, A. Applications of the quartz crystal microbalance in energy and environmental sciences: From flow assurance to nanotechnology. *Fuel* **2022**, *313*, doi:10.1016/j.fuel.2021.122998.

334. Prabowo, B.A.; Cabral, P.D.; Freitas, P.; Fernandes, E. The challenges of developing biosensors for clinical assessment: A review. *Chemosensors* **2021**, *9*, doi:10.3390/chemosensors9110299.

335. Wang, D.-B.; Cui, M.-M.; Li, M.; Zhang, X.-E. Biosensors for the detection of *Bacillus anthracis*. *Accounts of Chemical Research* **2021**, *54*, 4451-4461, doi:10.1021/acs.accounts.1c00407.

336. P J, J.; Prabakaran, K.; Luo, J.; M G, D.H. Effective utilization of quartz crystal microbalance as a tool for biosensing applications. *Sensors and Actuators A: Physical* **2021**, *331*, doi:10.1016/j.sna.2021.113020.

337. Sauerbrey, G. Verwendung von Schwingquarzen zur Wägung dünner Schichten und zur Mikrowägung. *Zeitschrift für Physik* **1959**, *155*, 206-222, doi:10.1007/bf01337937.

338. Ma, Y.; Xiao, X.; Ji, Q. Design of surface nanostructures for chirality sensing based on quartz crystal microbalance. *Beilstein Journal of Nanotechnology* **2022**, *13*, 1201-1219, doi:10.3762/bjnano.13.100.

339. Pohanka, M. Overview of piezoelectric biosensors, immunosensors and DNA sensors and their applications. *Materials* **2018**, *11*, doi:10.3390/ma11030448.

340. Mecea, V.M. From Quartz Crystal Microbalance to fundamental principles of mass measurements. *Analytical Letters* **2005**, *38*, 753-767, doi:10.1081/al-200056171.

341. Mecea, V.M. Is quartz crystal microbalance really a mass sensor? *Sensors and Actuators A: Physical* **2006**, *128*, 270-277, doi:10.1016/j.sna.2006.01.023.

342. Huang, X.; Chen, Q.; Pan, W.; Yao, Y. Advances in the mass sensitivity distribution of Quartz Crystal Microbalances: A review. *Sensors* **2022**, *22*, doi:10.3390/s22145112.

This page was intentionally left in blank.

Annex A – Device 1 as a testing platform for locust bean gum (LBG)-based microparticles

Device 1 – Brown was employed in the dosimetry assays to ascertain the impact of inlet temperature of spray-drying in the insufflation of locust bean gum (LBG)-based microparticles, focusing on two chosen outlet air pressures: 36 and 42 psi. Figure A.I presents the results for the powders produced with LBG from Sigma-Aldrich®.

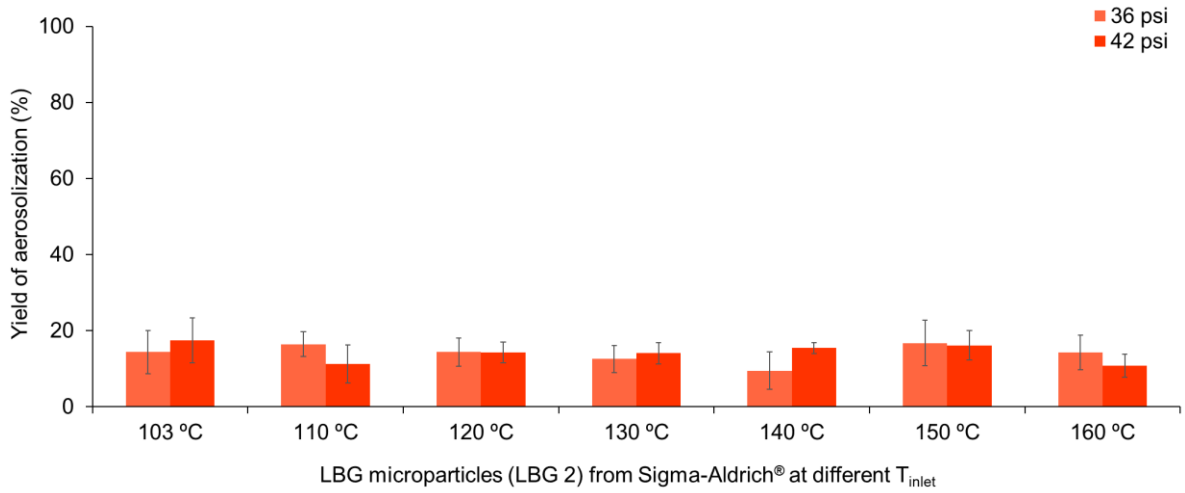

Figure A.I – Insufflation yields obtained with the Device 1 – Brown for microparticles composed of purified locust bean gum from Sigma-Aldrich® (●●, Table B.V in Annex B). Results are presented as mean ± SD, n = 10, and differences were considered statistically significant when $p < 0.05$.

The analysis continued with microparticles produced by spray-drying from Industrial Farense®, and results are presented in Figure A.II.

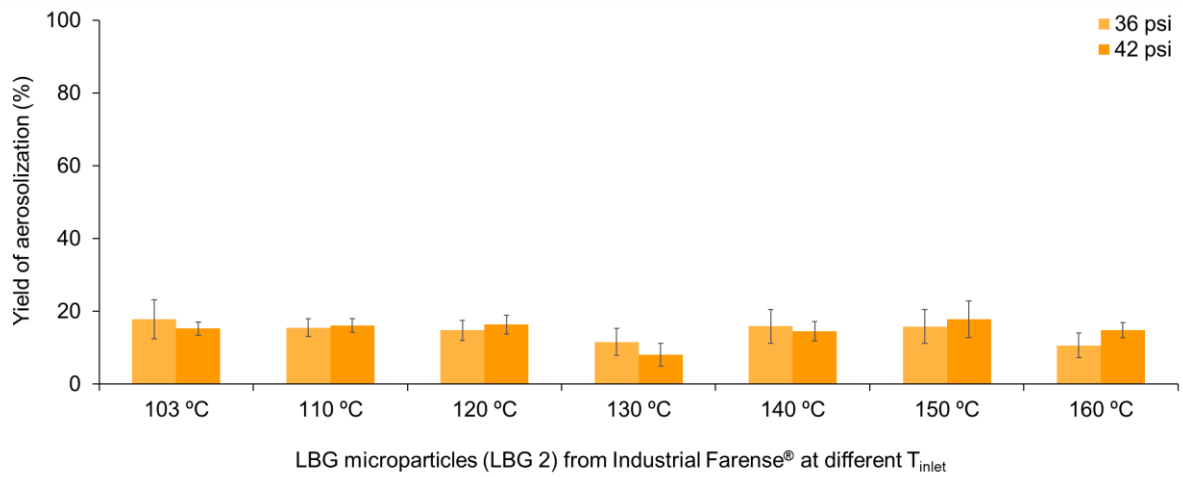

Figure A.II – Insufflation yields obtained with the Device 1 – Brown for microparticles composed of purified locust bean gum from Industrial Farense® (●●, Table B.V in Annex B). Results are presented as mean ± SD, n = 10, and differences were considered statistically significant when $p < 0.05$.

Finally, the microparticles prepared with purified LBG from C. E: Roeper were tested, and the results are shown in Figure A.III.

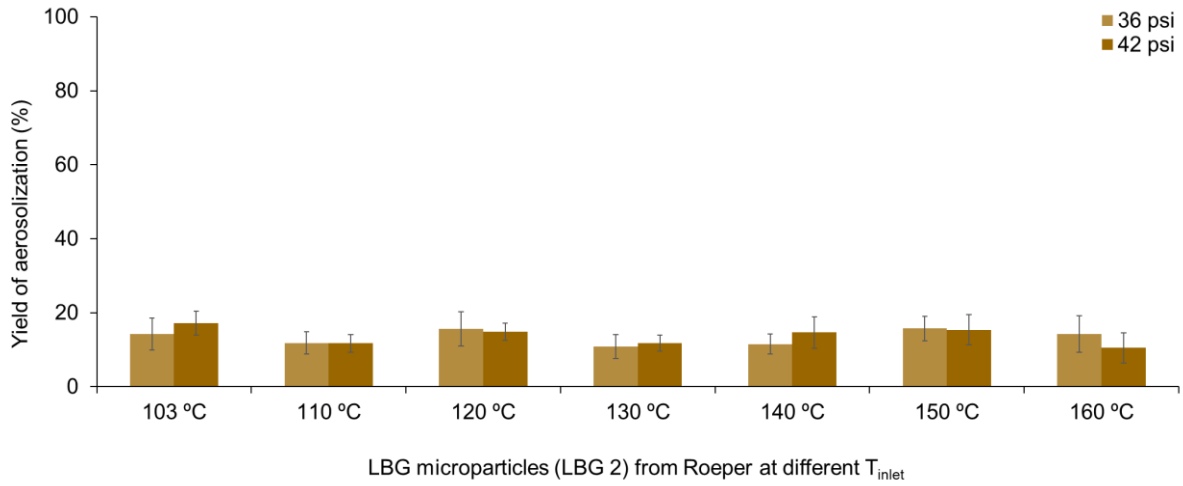

Figure A.III – Insufflation yields obtained with the Device 1 – Brown for microparticles composed of purified locust bean gum from C. E. Roeper® (●●, Table B.V in Annex B). Results are presented as mean ± SD, n = 10, and differences were considered statistically significant when $p < 0.05$.

Annex B – Colour palette on this document

Table B.I – Colour palette for the graphs concerning the lipid nanocapsules components and the thermogravimetric analysis (TGA) presented in Chapter 3.

Samples	Hexadecimal code
LBG Su	#CC00CC
DOTAP	#008080
LNC	#003366
RFB	#CC0066

Table B.II – Colour palette for the graphs concerning lipid nanoparticle formulations presented in Chapter 3.

Samples	Hexadecimal code		
	Size	**PdI**	**ζ-potential**
LBG Su/DOTAP 0.2/0.05	#7030A0		
LBG Su/DOTAP 0.5/0.05	#4772B9		
LBG Su/DOTAP 0.2/0.1	#C00000		
LBG Su/DOTAP 0.5/0.1	#FF33CC		

Table B.III – Colour palette for the graphs concerning FTIR spectra, HPSEC and TGA graphs for all LBG samples in Chapter 3.

Samples	Hexadecimal code
LBG S	#FF3300
LBG IF	#FF9900
LBG R	#996600

Table B.IV – Colour and texture palette for the graphs concerning cell viability (%, MTT) and LDH release (% of control) presented in Chapter 4.

Samples	MTT			LDH	
	3h	**24h**	**48h**	**24h**	**48h**
LBG S (0, 1, 2)	#FFD966 (main) + #FFF2CC (background) Texture: 	#BF9000 (main) + #FFE699 (background) Texture: 	#7F6000 (main) + #BF9000 (background) Texture: 	#99CC00 (main) + #009900 (background) Texture: 	#385723 (main) + #E2F0D9 (background) Texture: 
LBG IF (0, 1, 2)					
LBG R (0, 1, 2)					

Table B.V – Colour palette for the graphs concerning the initial insufflation assays in Chapter 6.

Samples	Hexadecimal code
XG	#333F50
XG Na	#7030A0
DS	#0070C0
KGM/Man	#990033
KGM/Leu	#996966
CRG/Starch 2%	#669900
Starch/CRG 1%	#33CCFF
Starch/CRG 2%	#0099FF
LBG S	36 psi: #FF3300 + 25% transparency; 42 psi: #FF3300
LBG IF	36 psi: #FF9900 + 25% transparency; 42 psi: #FF9900
LBG R	36 psi: #996600 + 25% transparency; 42 psi: #996600

Table B.VI – Colour palette for the graphs presented in Chapter 7.

Samples	Hexadecimal code					
	Assay 1	**Assay 2**	**Assay 3**	**Assay 4**	**Assay 5**	**Assay 6**
No powder	#181717	#767171	#969696	#333333	#808080	#8A8A8A
LBG S	#FF3300	#FF3D46	#FF3364	#FF4700	#FF6514	#FF5B32
LBG IF	#FF9900	#FFAA69	#FFB41E	#FFC864	#FF785A	#FFAF7D
LBG R	#996600	#993400	#993434	#999834	#99522D	#994632
XG	#333F50	#331E50	#334650	#333F37	#333F64	#336464
XG Na	#7630A0	#705AA0	#70307D	#70647D	#706464	#7014A0
HXG	#E654A0	#E62887	#E6005A	#E61EB4	#E664B9	#E64B86
Starch/CRG 1%	#33CCFF	#338EFF	#338EA5	#33CCA0	#3364A0	#3364FF
Starch/CRG 2%	#0099FF	#00DCB4	#00E86E	#00C8C3	#00C825	#00D714
CRG/Starch 2%	#669900	#99AF14	#99BE82	#99E664	#99F010	#99AD47
KGM/Leu	#993366	#996966	#997677	#997B35	#999941	#995347
KGM/Man	#990033	#993360	#996533	#996565	#993300	#99005A
DS	#0070C0	#0034C0	#00A2FF	#0070FF	#0034FF	#0000FF
KGM/INH/RFB	#9A5A40	#B5964B	#B5967D	#B5C37D	#B5C32D	#B5692D